NEW APPLICATIONS OF THERMOLUMINESCENCE

Debabrata Banerjee

Ph. D. Thesis
September 1996

Guj. Unl. Library
T2168

Physical Research Laboratory
Ahmedabad 380 009
India

NEW APPLICATIONS OF THERMOLUMINESCENCE

A Thesis Submitted to Gujarat University

for

TH
2168

THE DEGREE OF DOCTOR OF PHILOSOPHY
IN
PHYSICS

by

Debabrata Banerjee

PHYSICAL RESEARCH LABORATORY
AHMEDABAD 380 009
INDIA

SEPTEMBER 1996

CERTIFICATE

I hereby declare that the work presented in this thesis is original and has not formed the basis for the award of any degree or diploma by any University or Institution.

D Banerjee

Debabrata Banerjee

Certified by:

N Bhandari

Prof. N. Bhandari
Physical Research Laboratory
Ahmedabad 380 009, India.

To
Ma, Baba, Pishemoshai, Pishimoni
and
Thakuma

Contents

Acknowledgements v

List of Figures vii

List of Tables xi

1 Introduction 1

1.1 Luminescence 2

1.2 Thermoluminescence Dating 3

1.3 Paleodose Determination for heated objects 6

1.4 Paleodose Determination for sediments 7

1.5 Annual Dose Determination 9

1.5.1 Measurement Techniques 10

1.6 Infra-red Stimulated Luminescence Dating 11

1.7 Error estimation 13

1.8 Scope of the present thesis 13

2 Dating of Paleoseişmic/Neotectonic Events : A review 15

2.1 Introduction to Paleoseismology 15

2.2 Review of earlier work on dating of paleoseismic and faulting events . . . 16

3 Dating of Paleoseismic/Neotectonic Events : Thermoluminescence dating of fault gouges 22

3.1 Introduction 22

3.2 The thermoluminescence method 23

3.3 Description of fault gouge sites 23

3.4 Previous studies on Zeroing of the ESR/TL signals in fault gouges 25

3.5 Zeroing : Present Studies 27

3.5.1 Grain Size Dependence of TL ages (Fault gouges) 27

3.5.2 Fault Gouge Paleodoses 31

3.5.3 Mechanoluminescence Studies 31

3.5.4 Mineralogical studies 33

3.5.5 Summary of results concerning zeroing of the luminescence signal during faulting 36

3.6 Stability of the TL signal : Determination of trap parameters and mean life estimation 37

3.7 Anomalous Fading Studies 40

3.8 Results of TL Dating of fault gouges 40

4 Chronology of Paleoseismic/Neotectonic Events : Luminescence dating of seismites, river terraces and soils developed on colluvium 44

4.1 Luminescence Dating of Seismites : Zeroing of the Luminescence signal . 45

4.2 Geological Setting of seismites 46

4.3 Sedimentological Characteristics 47

4.4 Climatic Attributes 48

4.5 Experimental Details 48

4.6 Results and Discussion 50

4.7 Luminescence dating of river terraces and soils developed on colluvium . 52

4.8 Experimental Techniques 53

4.9 Results and Discussion 53

5 Thermoluminescence and Infra-red Stimulated Luminescence dating of Pedogenic Carbonates **55**

5.1 Introduction 55

5.2 Dating of Pedogenic Carbonates: Earlier work 57

5.3 The Luminescence dating method 59

5.4 Methodological Aspects of the luminescence dating method 62

5.4.1 Dosimetric changes due to loss of ^{238}U and/or ^{232}Th 62

5.4.2 The interpretation of luminescence ages for multiple carbonate precipitation events in a single profile 63

5.4.3 Estimation of errors 64

5.5 Samples and procedures 65

5.5.1 Luminescence Measurements 65

5.5.2 X-ray Diffraction Studies 67

5.6 Results and Discussion 68

6 Thermoluminescence and Infra-Red Stimulated Luminescence dating of alluvial sediments **71**

6.1 Introduction 71

6.1.1 Alluvial sediments in Paleoclimatology 71

6.1.2 Earlier studies on zeroing of the luminescence signals of water-borne sediments 72

6.1.3 Present Studies 76

6.2 Experimental Techniques 76

6.3 Results and Discussion 78

7 Conclusions **81**

7.1 Summary of Results 81

7.1.1 Dating of Neotectonic/Paleoseismic Events 82

7.1.2 Dating of Climate related sequences 84

7.2 Future Studies 86
7.2.1 Dating of Neotectonic/Paleoseismic Events 86
7.2.2 Dating of Climate related sequences 88

Bibliography 90

Appendices 104

Acknowledgements

First and foremost, I express my heartfelt thanks to Prof. Ashok Kumar Singhvi and Prof. Narendra Bhandari and Dr. Kanchan Pande, for their support, encouragement and valuable advice throughout the thesis work and in the making of this manuscript. Prof. Singhvi's good-humoured nature provided a congenial working environment in the luminescence laboratory. Kanchan's role has been more of a friend rather than a vigilant co-supervisor over the past four years. I also thank Kanchan and Navin for sharing their field expertise during sample collection.

I thank Prof. K.S. Valdiya for sharing his profound knowledge on Himalayan Tectonics and for extending all possible help to myself and Kanchan during our stay in Nainital. I also thank Profs. S. Krishnaswami, K.S.V. Nambi, G. Wagner, S.N. Rajaguru, B.L.K. Somayajulu, J.N. Goswami, S.K. Tandon, M. Krebetschek, R.K. Pant, S.K. Bhattacharya, R. Ramesh, P.N. Shukla, M. Chougankar, J.N. Desai, R.Sridharan, N.N. Rao, A. Jayaraman, T. Chandrasekhar, N.M. Ashok, B.G. AnandaRao, M.M. Sarin, R.P.Dhir and P. Sharma for their interest, encouragement during the thesis and critical appraisal of the present work.

I am also obliged to Dr. V. Gogte for performing mineralogical analyses on my samples and allowing me to visit his laboratory at Pune, Drs. T.N. Bagati, R.K. Mohindra for providing the seismite samples for luminescence dating, Dr. B.P. Chandra for consenting to my Jabalpur visit and utilization of the Mechanoluminescence facility at Rani Durgavati University, Jabalpur, Dr. M. Krebetschek and T. Trautman in procuring TL spectra and Dr. M.A. Courty for valuable dicussions on the luminescence ages of Ghaggar and Chautang flood-plain deposits presented in this thesis.

The help received from Navin, Ramaswamy, Aniruddha, Raju, Manish, Ramachandran, Somesh, Anil, Cecilia, Ansu, Santhanam, Ratan, Siva, Nandakumar and Kishankumar is gratefully acknowledged.

I thank all my friends (and any probable enemies!) in PRL (especially my batch-mates Poulose, Watson, Sandeep, Abhijit, Shibu, Anshu and Prashant) for providing cheerful company.

I thank Mr. Pandian and Mr. Pranav (the electronic 'whiz-kids') for troubleshooting during many an occasion in the last four years.

I am grateful to the members of the PRL Library Staff for providing an excellent service.

I acknowledge Shanti and Sundar Bhavsar for drafting the figures, D.R. Ranpura for photographs and K.R. Nambiar for typing the thesis chapters at a 'supersonic' speed.

Finally I thank Ma, Baba, Bablu and Shonamoni for their concern over my well-being and for their affection, understanding and support.

List of Publications

1. Singhvi, A.K., **Banerjee, D.**, Rajaguru, S.N. and Kishan, K.V.S. (1994). Luminescence Chronology of a fossil dune at Budha Pushkar, Thar Desert: Paleoenvironmental and Paleochronological implications, Current Science, 66, 10, 770-773.

2. Singhvi, A.K., **Banerjee, D.**, Pande, K., Gogte, V. and Valdiya, K.S. (1994). Luminescence Studies of Neotectonic events in South-Central Kumaun Himalaya: A Feasibility Study, Quaternary Geochronology, 13, 595-600.

3. Singhvi, A.K., **Banerjee, D.**, Rajaguru, S.N., Ramesh, R. and Gogte, V. (1996). A Luminescence Method for Dating "Dirty" Pedogenic Carbonates for Paleoenvironmental Reconstruction, Earth and Planetary Sciences, 139 (1-2), 321-332.

4. **Banerjee, D.**, Singhvi, A.K., Mohindra, R.K. and Bagati, T.N., Luminescence Chronology of seismites at Sumdo (Spiti Valley) near Kaurik-Chango Fault, Northwestern Himalaya: Its bearing on cyclicity of regional paleoseismic events, communicated to Geology.

List of Figures

Chapter 1

Fig. 1.1. Explanation of luminescence (TL, OSL) processes in terms of the band theory of solids. The symbols L and T indicate hole traps and electron traps respectively. E denotes the activation energy, which for minerals such as quartz, K-feldspars ranges from $\sim 0.7-2$ eV.

Fig. 1.2. Energy level representation of the IRSL process (after Hutt et al., 1988).

Chapter 2

Fig. 2.1. Locations sampled for Paleoseismological/Neotectonic studies. The hatched squares representing Dehradun and Spiti are shown in detail in figs. 3.2 and 4.2; Nainital is presented in figs. 3.1 and 4.6.

Chapter 3

Fig. 3.1. Locations of fault gouges and host rocks sampled for luminescence dating in Nainital and its vicinities.

Fig. 3.2. Location map of Mohand Thrust, Dehradun. Fault gouges MOH-1 and MOH-2 were collected from Mohand Thrust for TL and IRSL dating (modified after Valdiya, 1990).

Fig. 3.3. Dependence of TL ages on mean grain size for fault gouges TLV-1 and TLV-3.

Fig. 3.4. Dependence of TL ages on mean grain size for fault gouges KU93-1, MOH-1.

Fig. 3.5. A Schematic diagram of the experimental arrangement used for measurement of Mechanoluminescence in crystals. This facility is available at the Physics Department, Jabalpur University.

Fig. 3.6. Variation of ML intensity with applied pressure for fault gouge TLV-3 and host rock TLV-2.

Fig. 3.7a. A plot of ln (TL Intensity) vs (Temperature)$^{-1}$ for fault gouge KU93-1. E is the activation energy.

Fig. 3.7b. Variation of activation energy with glow curve temperature for the fault gouge KU93-1.

Fig. 3.8a. A plot of ln (TL Intensity) vs (Temperature)$^{-1}$ for fault gouge KU93-2.

Fig. 3.8b. Variation of activation energy with glow curve temperature for fault gouge KU93-2.

Fig. 3.9. Anomalous fading test for fault gouge TLV-3.

Fig. 3.10. Anomalous fading test for sample KU93-8.

Fig. 3.11. TL glow and growth curve for fault gouge TLV-1 (4-11 μm). P indicates the paleodose.

Fig. 3.12. TL glow and growth curves for fault gouge KU93-7.

Fig. 3.13. IRSL growth curve and shine plateau for fault gouge MOH-1. P indicates the paleodose.

Fig. 3.14. Age plateaus for fault gouge TLV-1.

Fig. 3.15. Age plateaus for fault gouge KU93-1.

Chapter 4

Fig. 4.1a. IRSL bleaching curve for a typical seismite. The IRSL intensity is reduced to $\sim$ 8% of its initial value after exposure to natural sunlight filtered through a 4 mm transparent window glass for $\sim$ 10 minutes.

Fig. 4.1b. Decay of IRSL with time for a typical seismite on exposure to light emitting diodes (LED) emitting at 880 $\pm$ 80 nm. Comparison with Fig 4.1a shows that diode exposure for $\sim$ 200 seconds in equivalent to an exposure of $\sim$ 600 seconds of natural sunlight filtered through window glass in reducing the IRSL intensity to 8% of its initial value.

Fig. 4.2a. Index map showing general tectonic trend in the northwestern Himalaya and location of the study area.

Fig. 4.2b. Geological map around Sumdo (after Mohindra and Bagati, 1996).

Fig. 4.2c. Cross-section along A-B

Fig. 4.3. Composite lithostratigraphic column showing deformed zones (S_1-S_8) and facies variation in Sumdo area. Note the location of samples analyzed for dating.

Fig. 4.4. Grain size distributions for the seismites. MZ, SKI and GI indicate mean size, sorting index and skewness of the distributions.

Fig. 4.5a. IRSL shine-down curves for K-feldspar extracts from sample, L-2.

Fig. 4.5b. IRSL growth curve for L-2.

Fig. 4.5c. IRSL shine plateau for L-2.

Fig. 4.6. Location map showing uplifted river terraces sites around Nainital where samples were collected for luminescence dating (modified after Valdiya, 1990).

Fig. 4.7. TL glow curve, growth curve and equivalent dose plateau for a typical buried soil, KU91-1.

Fig. 4.8a. IRSL growth curve and b. shine plateau for a typical river terrace, TLV-8. The IRSL analysis was done using 75-106 μm K-feldspars.

Chapter 5

Fig. 5.1. Schematic representation of basic principles involved in luminescence dating of a carbonate. The symbols used have been explained in the text.

Fig. 5.2. Locality map of North-west India. Pedogenic carbonate sites sampled for luminescence dating are presented in the diagram (modified after Kar, 1995). Khudala was only sampled for aeolian sands (results are discussed elsewhere).

Fig. 5.3a. Glow curves for quartz separates from a typical host sand, PSH 92-2. SL and SS represent bleaching times of 700 and 30 minutes under the natural sun.

Fig. 5.3b. Glow curves for quartz separates from a typical calcrete, CAL-4. SL and SS represent bleaching times of 700 and 30 minutes under the natural sun.

Fig. 5.4a. Total Bleach growth curve for quartz separates from PSH 92-2.

Fig. 5.4b. Total Bleach growth curve for quartz separates from CAL-4.

Fig. 5.5a. TL growth curve for K-feldspar extracts from host sand JAL-II/2S.

Fig. 5.5b. TL paleodose plateau from JAL-II/2S.

Fig. 5.6. IRSL shinedown curves for K-feldspar separates from the carbonate JAL-II/2C.

Fig. 5.7a. IRSL growth curve for K-feldspar separates from carbonate JAL-II/2C.

Fig. 5.7b. IRSL shine plateau for JAL-II/2C.

Fig. 5.8a. IRSL growth curve for K-feldspar extracts from host sand TL-13S.

Fig. 5.8b. IRSL growth curve for K-feldspar extracts from carbonate TR-13C.

Fig. 5.9. Stratigraphy, TL ages, Carbon and Oxygen isotopic data for carbonates from Budha Pushkar, Thar Desert.

Chapter 6

Fig. 6.1. Effect of sunlight exposure on OSL and TL signals of quartz and feldspars. Optical signal is for 1 second after laser is switched on (10 mW/cm^2: Quartz; 15mW/cm^2: feldspar). The 514 nm was the exciting wavelength (after Godfrey-Smith et al., 1988).

Fig. 6.2. Locality map of North-west India showing Chautang and Ghaggar flood plain sites sampled for luminescence dating.

Fig. 6.3. Stratigraphic summary of Ghaggar, Chautang and South Chautang flood plain sections. ^{14}C and IRSL ages on various units sampled for luminescence dating are also provided.

Fig. 6.4. IRSL shinedown curved for K-feldspar extracts from the sample CNF-16.

Fig. 6.5a. IRSL growth curve for K-feldspar extracts from the sample CNF-16.

Fig. 6.5b. IRSL shine plateau for sample CNF-16.

Fig. 6.6a. IRSL growth curve for K-feldspar extracts from the sample CNF-13.

Fig. 6.6b. IRSL shine plateau for sample CNF-13.

Appendix A

Fig. A.1. Schematic of TL measurement system.

Fig. A.2. Schematic of IRSL measurement system.

Appendix B

Fig. B.1. TL Emission spectra for fault gouge TLV-3, shown as a contour map.

Fig. B.2. TL Emission spectra for host rock, KU93-5.

Fig. B.3. TL Emission spectra for host rock, KU93-6.

Fig. B.4. TL Emission spectra for quartz extracts from CNF-6.

Fig. B.5. TL Emission spectra for quartz extracts from KD-8.

Fig. B.6. TL Emission spectra for alkali feldspar extracts from JAL-I/1.

Fig. B.7. TL Emission spectra for alkali feldspar extracts from JAL-I/17.

List of Tables

Chapter 3

Table 3.1. Grain-Size Dependence of luminescence ages.

Table 3.2. Illite Hb_{rel} values for fault gouges and host rocks.

Table 3.3. Chlorite peak ratios and inferred thermal excursions for fault gouges and host rocks.

Table 3.4. Activation energies, frequency factor and lifetimes for fault gouges and host rocks.

Table 3.5. Radioactivity data for fault gouges and host rocks.

Table 3.6. Luminescence dating results for fault gouges and host rocks.

Chapter 4

Table 4.1. Mineralogical data for the seismites L-1, L-2, L-3 and L-4 analysed for luminescence dating.

Table 4.2. Luminescence dating results for seismites from Spiti Valley, Himachal Pradesh, India.

Table 4.3. Radioactivity data for soils developed on colluvial debris and terrace sediments.

Table 4.4. Luminescence dating results for soils developed on colluvium and sediments from river terraces.

Chapter 5

Table 5.1. Radionuclide data for carbonates and host sands from Thar Desert.

Table 5.2a. β dose fraction from potassium to quartz extracts from host sands and calcretes.

Table 5.2b. Fraction of annual alpha and beta dose from potassium to K-feldspars within host sands and calcretes.

Table 5.3. Thermoluminescence data, ^{14}C ages and stable isotopic values for carbonates from Budha Pushkar, Thar Desert, India.

Table 5.4a. IRSL dating results for carbonates and host sands from Amarsar, Thar Desert, India.

Table 5.4b. IRSL dating results for carbonates and host sands from Chamu, Thar Desert, India.

Table 5.5. Luminescence data for carbonates and host sands from Jalore, Thar Desert.

Chapter 6

Table 6.1. Results of TL dating of alluvial and aeolian sands from Ghaggar and Chautang flood plains, Haryana, India.

Table 6.2. IRSL dating results for alluvial and aeolian sands from Ghaggar and Chautang flood plains, Haryana, India.

Table 6.3. Comparison of IRSL, ^{14}C and FSE-TL ages for flood plain deposits from Southern Chautang, Haryana.

Chapter 1

Introduction

The suggestion of Daniels et al., (1953) that thermoluminescence (TL) could be used for geological and archaeological age evaluation provided a stimulus for basic research on the methodology and applications of TL dating (Aitken et al., 1964, Mejdahl, 1969). By the seventies, the method was fully established as a reliable method for dating pottery and was also extended to sediments baked by lava flows. During the mid seventies, Huntley, Johnson and Wintle's studies on ocean sediment cores provided evidence for an increase in TL signal with depth which suggested that solar exposure causes resetting of the TL signal for unheated sediments. This was followed by the development of various sediment dating TL techniques (Wintle and Huntley, 1982; Singhvi et al., 1982; Proszynska, 1983; Debenham and Walton, 1983) and their application to date various types of deposits, e.g., loess, marine sediments, dune sands, soils, lake sediments, fluvial sands, glacial dust, colluvium etc. With the advent of optically stimulated luminescence (OSL) dating and infra-red stimulated luminescence (IRSL) dating techniques in the late 1980s, reliable dating of poorly bleached sediments (sediments having received a short pre-depositional sun-exposure) is now achievable. The luminescence methods have the potential to revolutionize Quaternary Geochronology as they can be used for dating a variety of earth surface processes and sediments that were conventionally considered undatable and have

a dating range of 1 – $\geq$ 200 ka which is complementary to the radiocarbon, U-series and paleomagnetic dating methods. Secondly, the luminescence methods involve analysis of minerals constituting the sediments, thereby circumventing problems associated with sample-strata correlations. Finally, luminescence ages do not require calibration as is necessary in radiocarbon dating. The present thesis aimed at developing thermoluminescence and infra-red stimulated luminescence dating techniques for providing a chronology of important geological processes, viz., neotectonic/paleoseismic events, carbonate formation and alluvial deposition periods. Dating of neotectonic/paleoseismic events is important for evaluating the seismic risks associated with a particular region and in predicting when major earthquakes (magnitude > 6) are likely to occur in the future (Khattri, 1996). Pedogenic carbonate formation and alluvium depositional events are good indicators of climate, notably the precipitation : carbonates primarily occur in arid zones of the world with an annual precipitation of < 400-600 mm (Cooke et al., 1993) whereas large alluvial deposition generally represents higher rainfall (Nanson et al., 1992). As conventional radiometric methods have often been found to be inapplicable and occasionally unreliable, the present thesis explored the possibilities of utilizing thermoluminescence and infra-red stimulated luminescence dating methods for dating these events. This chapter gives a brief description of luminescence dating techniques and outlines the contents of the following chapters of the present thesis. For an exhaustive review of the luminescence processes and dating techniques, the reader is referred to Aitken (1985), Singhvi and Wagner (1985), Berger (1988), Aitken (1992), Aitken (1994).

1.1 Luminescence

The emission of light (excluding black-body radiation) from a substance subsequent to its excitation by ionizing radiations is called luminescence. The stimulated luminescence process can be explained in terms of the band theory of solids (Fig. 1.1). Exposure to

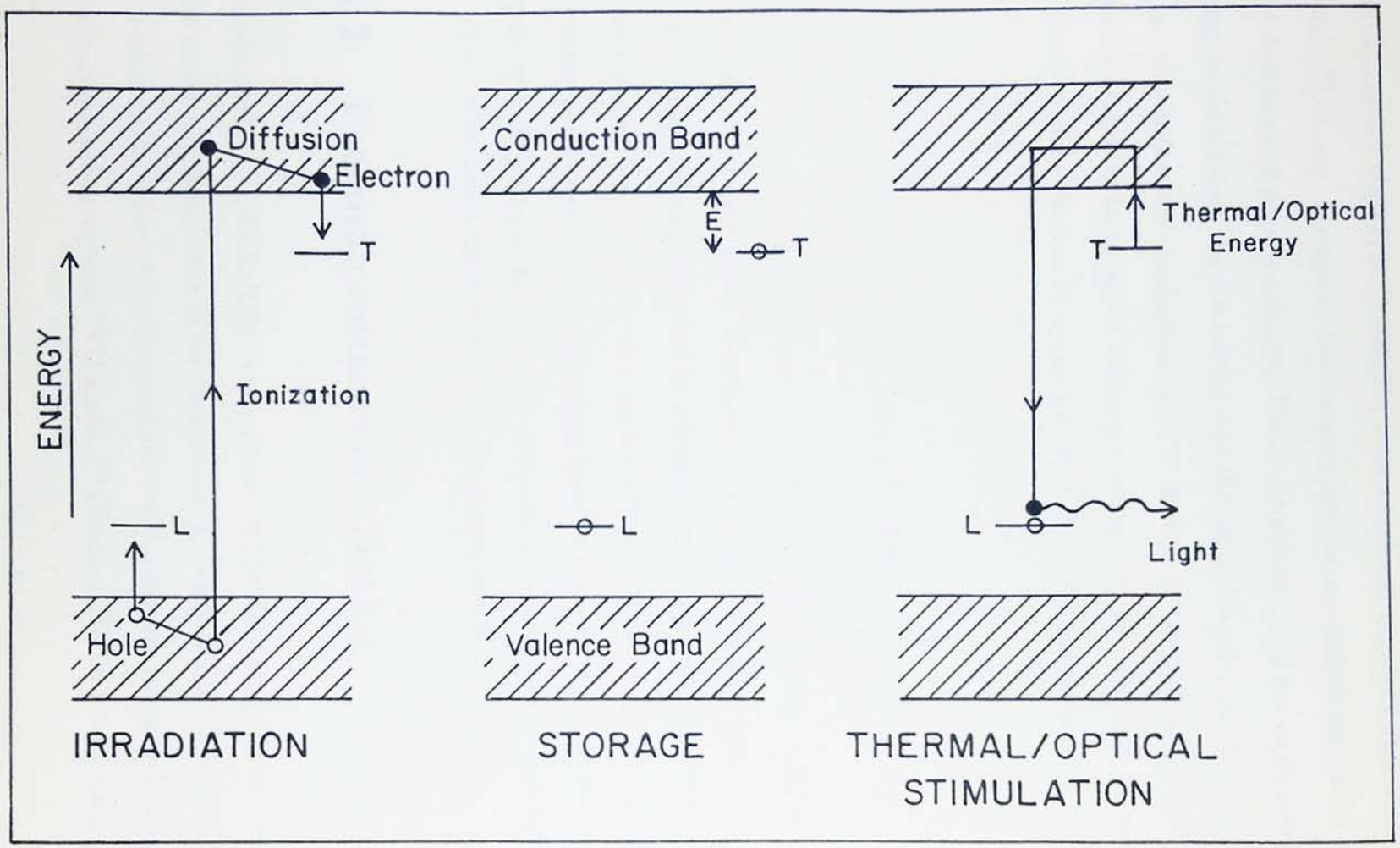


Fig. 1.1. Explanation of luminescence (TL, OSL) processes in terms of the band theory of solids. The symbols L and T indicate hole traps and electron traps respectively. E denotes the activation energy, which for minerals such as quartz, K-feldspars ranges from $\sim$ 0.7–2 eV.

ionising radiations create many free electrons and holes in the crystal. Most of these free charges recombine instantaneously. A small fraction of these charges get trapped at lattice defect sites (viz., vacancies, interstitial and impurity atoms etc.) within the crystal. Thus, e.g., a negative ion vacancy acts as an electron trap since there exists a local deficiency of negative charge. The electron/hole traps are represented as localized energy levels between the conduction and the valence bands. For an electron, the depth of the trap below the conduction band is defined as the activation energy (E). If the electron attempts to escape s times per second, in the simplest approximation, the lifetime (τ) of an electron in a trap (of depth E) at the temperature T can be expressed as

$$\tau = s^{-1} \cdot e^{E/kT} \tag{1.1}$$

s is called as the frequency factor. The electronic lifetimes at room temperature can vary from 10^{-4} to 10^{9} years. Eventually, the trapped charges (electrons/holes) may absorb thermal/optical energy and be released into the conduction/valence band. Some of these charges may recombine at a luminescence centre to emit light. Different kinds of luminescence processes exist depending upon on the source of stimulation viz., thermoluminescence (heat energy), optically stimulated luminescence (visible light energy) and infra-red stimulated luminescence (infra-red light energy).

1.2 Thermoluminescence Dating

Luminescence (TL/IRSL/OSL) can only be used for dating particular events which reset the acquired luminescence of the luminescent minerals comprising the sample to zero or a negligibly low value. After the resetting event, exposure to natural radioactivity (α, β, γ radiations primarily from ^{238}U series, ^{232}Th series, ^{40}K and cosmic rays) builds up the

thermoluminescence level of the minerals constituting the sample. On excavation, the thermoluminescence level of a sample is a measure of the radiation dose absorbed by the minerals since the resetting/zeroing event and can be expressed in terms of the annual dose received by the constituent minerals of the sample and the time since the zeroing event. The expression for the thermoluminescence age can be derived in the following way (Aitken, 1985). If L is the total thermoluminescence acquired during antiquity, then

$$L = L_\alpha + L_l \quad . \tag{1.2}$$

where L_α and L_l are thermoluminescence components arising from the alpha and the lightly ionising radiations (beta, gamma, cosmic rays) respectively. In the simplest approximation, for the linear region of the growth curve,

$$L_\alpha = D_\alpha \chi_\alpha A \ ; \ L_l = \chi_l (D_l A - I) \tag{1.3}$$

χ_α and χ_l are TL sensitivities for alpha and lightly ionising radiations (beta, gamma, cosmic rays). D_α and D_l are annual dose components for alpha and lightly ionising radiations (beta, gamma, cosmic rays). I is the supralinearity intercept which arises because of competition for detrapped charges by traps which don't give rise to thermoluminescence (Chen and Bowman, 1978). This term is missing in the expression for L_α since supralinearity is absent for alpha particles. This is because the dose deposited by alpha-particles lies in a very narrow cylindrical track (diameter ~ 0.1 μm) so that TL produced by each new alpha-particle is independent of the existing number of tracks (Aitken, 1985).

$$L = A(D_\alpha \chi_\alpha + D_l \chi_l) - \chi_l I \tag{1.4}$$

Thus, the expression for the age is

$$A = \frac{L/\chi_l + I}{D_a \chi_a/\chi_l + D_l} \tag{1.5}$$

Now, defining L/χ_l as Q, the equivalent dose and χ_α / χ_l as a, we get

$$A = \frac{Q + I}{aD_\alpha + D_l} = \frac{P}{aD_\alpha + D_l} \tag{1.6}$$

where a is the alpha-efficiency factor and P stands for paleodose and is the total radiation dose received by the sample since the last zeroing event. Since D_l has 3 components viz., D_β, D_γ and D_{cosmic}, the age equation can be rewritten as

$$A = \frac{P}{aD_\alpha + D_\beta + D_\gamma + D_{cosmic}} \tag{1.7}$$

Even though this derivation involves some assumptions regarding the nature of the TL growth curve, equation 1.7 is the general expression for TL age.

Since the α-particles are much more ionizing than β or γ radiations and deposit their energies in narrow tracks, TL traps within these tracks get quickly saturated. Therefore, the alpha-particles are less efficient in producing TL compared to beta-particles/gamma-rays. The alpha-efficiency factor a is determined using the relation

$$a = \frac{\beta}{13 \cdot S \cdot y} \tag{1.8}$$

where S is the alpha-irradiation source strength in μm^{-2} min^{-1}, β is the beta dose in Grays which induces the same TL level as y minutes of alpha dose. This formulation

was first given by Aitken and Bowman (1975). Thus, the determination of the thermoluminescence age involves the evaluation of the paleodose, the annual dose components and the alpha-efficiency factor.

TL dating can be used for dating three types of events, viz., (i) the most recent heating event; (ii) the event of crystallisation and (iii) the most recent sun-bleaching event. The present thesis concerns dating of events represented by class (i) and (iii). The following sections describe procedures for estimating the paleodoses in these instances.

1.3 Paleodose Determination for heated objects

The paleodose is given by the expression P = Q + I where Q is the equivalent radiation dose that induces the TL level equal to that of a natural sample and I is the supralinearity intercept. The additive dose method (Aitken, 1985) is generally used for estimating Q and I. In this method, identical sub-portions of the sample are used to measure the natural thermoluminescence ('first glow') and natural plus artificial thermoluminescence. After normalization, the thermoluminescence intensities are plotted versus radiation dose (at a particular temperature) to form the growth curve. Extrapolation of the growth curve to the X-axis gives the value of Q, the equivalent dose. To find the supralinearity intercept, a second-glow growth curve is constructed by giving various beta doses to different portions used for determining natural thermoluminescence intensities and plotting the resulting TL ('second glow') intensities with radiation dose. The intercept on the X-axis gives the value of the supralinearity intercept. However, this procedure for finding I is only valid if no change in TL sensitivity occurs between the first glow and second glow. Subsequently, equivalent doses and supralinearity intercepts are evaluated at various temperatures and a plot of paleodose with temperature is constructed. However, in fine-grain dating, the a-value is also evaluated at various temperatures and TL ages are plotted with temperature. A paleodose/age plateau with

temperature in the 250–400°C region suggests that the TL signal in this temperature region has probably remained stable over the sample's geological history.

1.4 Paleodose Determination for sediments

Whereas during heating the sample's thermoluminescence gets completely zeroed, there exists a residual level of thermoluminescence (I_o) even after a long duration of sun exposure (few days). Thus, the natural TL of a sediment sample (I_{nat}) consists of two components, I_o, the remnant TL on deposition and I_d, the TL acquired by the sample after deposition :

$$I_{nat} = I_o + I_d$$

In terms of dose units, this equation can be written as $P = P_o + Q$ the paleodose and Q is the equivalent dose (dose acquired by the sediment sample since deposition). Thus, the age equation taken the form

$$A = \frac{Q}{aD_\alpha + D_\beta + D_\gamma + D_{cosmic}} \tag{1.9}$$

Various methods can be used for determining Q. In the **total bleach technique** (Singhvi et al., 1982), a variant of the additive dose technique, it is assumed that the sediments were bleached for a long period of time ($\sim$ few days). The value of P is determined as in the additive dose technique. To find P_o, some sub-portions of the sample are exposed to natural sunlight for > 6 hours whose thermoluminescence output gives the value of I_o. If R is defined as I_o / I_{nat}, then

$$Q = P(1 - R) \tag{1.10}$$

The total bleach method has been successful in dating sediments such as loess and dune sands. The **regeneration methods** (Proszynska, 1983; Debenham and Walton, 1983) have also been used for dating well bleached samples. Various sub-portions of the samples are sunbleached for > 6 hours and then given beta doses to construct a regeneration growth curve. The natural intensity (I_{nat}) is projected onto this curve to find the value of Q. This method is valid only if the sensitivity of the sample remains unaltered on sunbleaching.

Both the methods described above are utilized for dating well bleached sediments. However, for sediments exposed to sunlight for very short periods (e.g. water-borne sediments), one needs to resort to the **partial bleach method** (Wintle and Huntley, 1980). In this method, glow curves of some portions are measured after artificial irradiation, while another set of portions are given a short sun-bleach after irradiation before measurement. The intersection point of the two curves (N + beta, N + beta + S) gives the equivalent dose value. This method assumes that bleaching removes a given fraction of the bleachable TL. However, in reality, this assumption may not be satisfied, especially for samples exhibiting second order kinetic behaviour. Also, since the method involves extrapolation of two growth curves and relies on subtraction of two quantities, it is generally inapplicable for samples having natural TL in the saturation region (Aitken, 1985). Errors on Q values will also be larger in comparison to the regeneration and total bleach methods. To ensure that the laboratory bleaching time has not exceeded the bleaching time before deposition, it is generally recommended that Q be determined for various bleaching times to check for a plateau in Q.

1.5 Annual Dose Determination

The annual dose components can be estimated by measuring the concentrations of potassium, uranium and thorium (K, U and Th) in the sample. These elemental concentrations are used along with the 'infinite matrix' assumption to evaluate the annual dose. In the 'infinite matrix' approach, it is assumed that in a volume with dimensions greater than the range of the α, β, γ radiations and cosmic rays, conservation of energy will imply that the rate of energy absorbed per unit mass is equal to the rate of energy emitted per unit mass provided that radioactivity per unit mass and the absorption coefficient per unit mass is constant over the sample volume. The latter assumption may not be always satisfied. For e.g., in case of quartz inclusions in pottery, the clay matrix essentially supplies all the radioactivity whereas quartz, whose TL sensitivity is at least an order of magnitude higher than the clay matrix is mostly free of radioactivity. This leads to an inhomogeneity in alpha dose which calls for the use of fine-grain/quartz exclusion technique (Aitken, 1985) for age determination. The mineral inclusions such as zircon, apatite, K-feldspar also result in inhomogeneity of another kind. Inhomogeneity effects also arise when water is present inside the soil/sherd/sediment matrix. This occurs because compared to pottery/sediment constituents, water's absorption coefficient per unit mass is higher by approximately 50% for alpha particles, 25% for beta particles and 14% for gamma radiation (Zimmerman, 1971). Thus, correction factors need to be applied to the annual dose components. In this thesis, Zimmerman's correction formulae (1971) were used to estimate the 'wet' annual dose components.

The evaluation of annual dose by the 'infinite matrix' approach and the TL age equation assume that the radionuclides ^{238}U, ^{232}Th and their daughters are in equilibrium and no change in K concentration occurs since the 'zeroing event', thus ensuring that the annual dose remains constant. However, disequilibrium in the ^{238}U and ^{232}Th series can occur in certain situations. U, Th, Ra can be leached out by percolating ground

waters, especially in coarse-grain deposits due to their greater permeability compared to fine grained deposits (Berger, 1988). Disequilibrium can also occur in stalagmitic calcite, where uranium is incorporated into calcium carbonate at formation without thorium. Radon loss (especially ^{222}Rn with a half life of 3.8 days) can also cause disequilibrium in the decay series. Berger (1988) suggested that this loss is probably most important for waterlaid deposits exposed to changing water tables or conducive to percolation. Recent studies by Prescott and Hutton (1995) on sediments from various sites in Australia indicate that sites exposed to wet conditions are most susceptible to disequilibrium effects. Prescott and Hutton (1995) obtained little or no evidence for disequilibrium in aeolian dune systems.

1.5.1 Measurement Techniques

Various techniques exist for determination of the annual dose components. For a detailed review of these techniques, the reader is referred to Aitken (1985).

In this thesis, the uranium and thorium concentrations were determined using the thick source alpha counting technique. Samples were crushed and then kept on top of a ZnS scintillation screen (diameter 42 mm) placed on top of a photomultiplier tube. Each alpha particle produces scintillations which is registered as an electrical pulse at the anode of the PMT after amplification and is then counted by the Daybreak 582 alpha counter. The major advantages in using this technique are: (i) sensitivity to alphas being much larger than beta/gamma radiation and (ii) its low cost. The background count-rates were typically $\sim$ 0.05–0.3 counts/ks for a counting area of 13.85 cm^2.

The estimation of potassium was made using a 3′ x 3′ well type NaI (Tl) scintillator coupled to pre-amplifier and linear amplifiers and a multi-channel analyser. A small

energy window around 1.46 MeV was used. For some samples, the potassium concentrations determined by gamma-ray spectrometry were compared with those obtained in situ using the 4-channel Portable Gamma-ray Spectrometer (Aitken 1985) and atomic absorption spectrometry (AAS). Potassium concentrations determined using these various techniques were found to be consistent within errors (5%). The cosmic-ray dose was assumed to be 150 μGy/a (Prescott and Stephan (1982)).

1.6 Infra-red Stimulated Luminescence Dating

In thermoluminescence dating of sediments, a major difficulty arises in the evaluation of the I_o and therefore in estimating Q. This occurs because heating the samples releases electrons from both the light sensitive traps and the light insensitive traps. In nature, bleaching due to sunlight only evicts electrons from the light sensitive traps. This can be replicated in the laboratory if light energy is utilized for stimulating the sample. In a classic paper, Huntley et al., (1985) reported on the application of monochromatic green laser light to reset a rapidly bleachable optically stimulated luminescence. An argon ion laser was used for excitation of the sample. The PMT was heavily filtered to differentiate between the excitation and emission wavelengths (blue/violet). In an attempt at dating sedimentary deposits using OSL, Huntley et al., (1985) found that the luminescence signal increased with depth in two geological sequences spanning 0–700 ka (South-east Australian beach dunes) and 0–6 ka (British Columbian soil horizons). The additive dose method was used to evaluate the paleodose. As mentioned above, the stimulation signal could rapidly bleach the luminescence signal.

The OSL dating technique is advantageous in comparison to its TL counterpart in the following ways : (i) a negligibly low post-bleaching residual signal ($I_o \sim 0$) which makes it feasible to date poorly bleached sediments, (ii) no requirement of heating means that experiments can be performed rapidly and simply and with improvement in S/N

ratio, (iii) avoidance of spurious TL and thermal quenching processes and accessibility to electrons residing in deep traps. Also, since the method involves no heating, there exists a possibility of dating minerals (e.g. organic compounds, gypsum) which undergo a phase change on heating.

In 1988, Hutt et al., reported the presence of a strong resonance in the stimulation spectrum of K-feldspars in the region 750−1000 nm. This infra-red stimulated luminescence (IRSL) was eventually used for dating sediments. In comparison to Green Light Stimulated Luminescence (GLSL), IRSL is better suited for dating because of : (i) availability of a large wavelength band for detection resulting in enhanced sensitivity; (ii) faster bleaching, so a lower I_o and (iii) its cheaper costs (Aitken, 1994). Hutt et al., (1988) have proposed a model to explain the IRSL mechanism (Fig. 1.2): electrons are raised to excited states under IR stimulation and then arrive at the conduction band on absorbing thermal energy from lattice vibrations. Some of them recombine with holes at recombination centres to emit infra-red stimulated luminescence. IRSL is thus strongly dependent upon temperature.

In IRSL dating, the paleodose is usually determined by the additive dose method or the regeneration method. Aitken and Xie (1992) recommend the use of the subtraction technique where the value of the IRSL intensity after a long time-interval ($\sim$ 200 s) is subtracted from all IRSL intensities for an aliquot. This eliminates signals from scattered IR, PMT dark count and any 'hard-to-bleach' component which remained unbleached on deposition. The light intensity of a short IR exposure (short-shine) of 0.5 or 1 second is used to normalize the IRSL intensities (natural normalization) obtained on exposure for a longer time interval (shine-down $\sim$ 12 s). Shine-down curves (plots of IRSL intensity with diode exposure time) for aliquots with different amounts of artificial irradiation are constructed. Growth curves (plots of IRSL intensity with radiation dose at a particular exposure time) are then utilized for calculating paleodoses at each shine

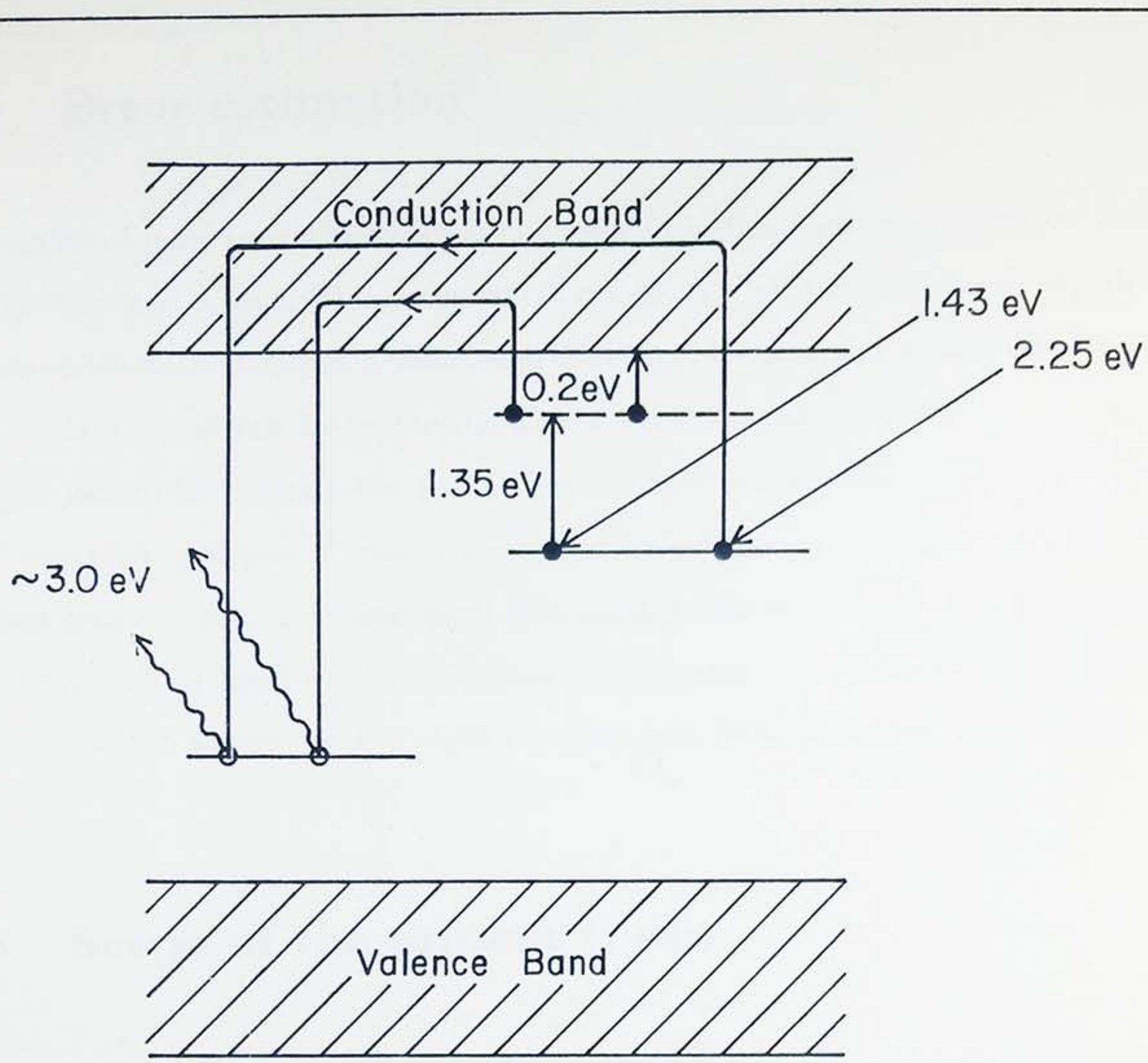


Fig. 1.2: Energy level representation of the IRSL process (after Hutt et al., 1988)

time. The paleodoses are then plotted against shine time and a shine-down plateau is a good indication of efficient zeroing of the IRSL signal at deposition (Aitken, 1994).

1.7 Error estimation

Estimation of error in luminescence ages presented in this thesis was based on Aitken (1985). The total error in TL age consists of two parts : (i) random errors in estimation of paleodose/equivalent dose, a-value, supralinearity intercept and annual dose and (ii) systematic errors arising due to uncertainties in α and β source, α counter and potassium analyser calibrations, parameters used in converting U and Th concentrations to annual dose components, degree of radon escape and uncertainty in the water content. The random errors in paleodose/equivalent dose mostly arise from curve fitting. Counting statistics (in alpha counting and potassium determination) and variation in scintillation efficiency of ZnS screens used in alpha counting contribute to random errors in annual dose.

1.8 Scope of the present thesis

The present thesis explored TL and IRSL dating's potential for providing chronology to geologically significant processes viz., neotectonic/paleoseismic events, carbonate formation and alluvium deposition epochs. A review of earlier work carried out to date neotectonic/paleoseismic events is provided in Chapter 2.

Absolute dating of fault gouges using luminescence methodology has been attempted for the first time. Chapter 3 begins with a brief review on earlier work related to zeroing of the ESR/TL signal during faulting. Next, the attempts made in the present thesis to test the validity of the assumption of 'zeroing' of the luminescence signal during

faulting are described. Tests on the stability of the TL signal are also reported. Chapter 3 concludes with a chronology of faulting events in the Lesser Himalaya and discussion on the implications of TL ages.

A luminescence method of dating seismites is presented in Chapter 4. Luminescence ages on seismites from Spiti Valley, Himachal Pradesh, soils developed on colluvium and uplifted river terraces are presented along with the implications of the luminescence ages in a regional context.

After a brief introduction to pedogenic carbonates, chapter 5 proposes a new luminescence method for dating pedogenic carbonates. Application of this method for dating carbonates from various sites in Thar Desert is also discussed.

Chapter 6 reports TL and IRSL ages of alluvium from Chautang and Ghaggar flood plains, Haryana, and discusses their paleoclimatic implications.

Chapter 7 summarizes the work carried out in the present thesis and analyses the possibilities of future research work.

Chapter 2

Dating of Paleoseismic/Neotectonic Events : A review

2.1 Introduction to Paleoseismology

Earthquakes are one of the most catastrophic and devastating natural hazards experienced by our planet. In the United States, devastating earthquakes in Alaska (1964) and in Southern California (1971) created awareness amongst the non-scientific community about the need for research in paleoseismology. In India, the Himalayan arc (Fig 2.1) comprising a boundary between the Eurasian and the Indian plate represents a zone of strong seismic activity. Four great earthquakes, the 1897 Shillong earthquake, the 1905 Kangra earthquake, the 1934 Bihar earthquake and the 1953 Assam earthquakes have all taken place in the last century. The Uttarkashi earthquake (magnitude 6.5) of 1991 claimed over 1500 lives. Therefore, it becomes important to understand the mechanisms responsible for producing such catastrophic earthquakes and their repeat frequency. This can only be possible if one understands the past behaviour of 'seismogenic' faults to predict their future behaviour (Crone, 1987). During the last three decades, a new discipline viz., paleoseismology has emerged which deals with the evaluation of age, magnitude and repeat frequency of past earthquakes. These studies are also

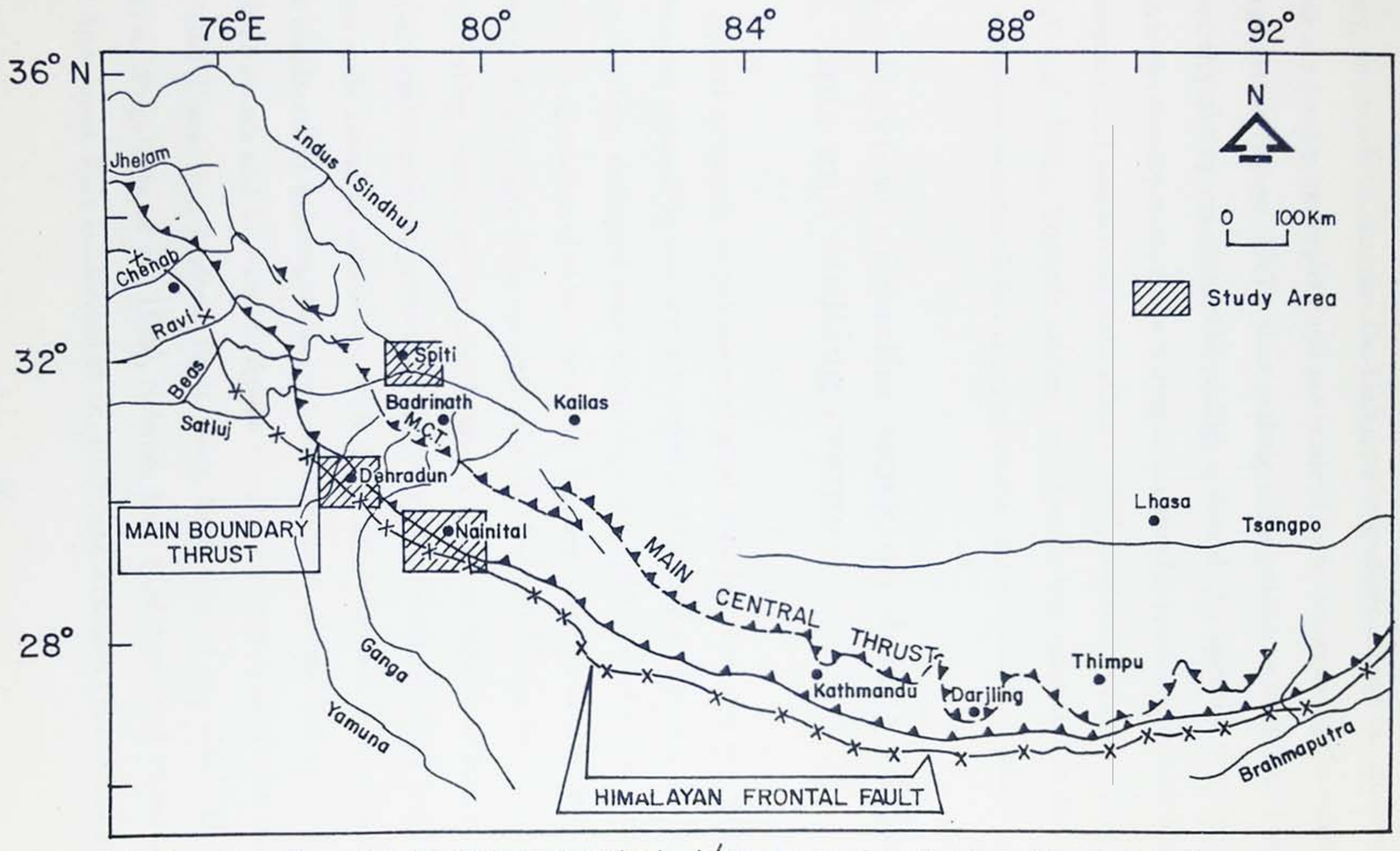


Fig. 2.1: Location Sampled for Paleoseismological/Neotectonic studies. The hatched squares representing Dehradun and Spiti are shown in detail in figs. 3.2 and 4.2; Nainital is presented in figs. 3.1 and 4.6.

significant for modelling stress accumulation and release patterns along plate boundaries. To establish a chronology of paleoearthquakes extending beyond the eighteenth century, one needs to examine the historical or geological records. However, historical records are mostly incomplete and are inadequate in determining the repeat frequency of large events (Crone, 1987), thus making it important to study the imprints of the paleoearthquake by examining the geological record. An essential pre-requisite for such efforts is the development of new dating techniques for providing reliable age controls on paleoseismic and neotectonic data (Crone, 1987; Radakrishna and Ramaseshan, 1992; Vittori et al., 1991). Towards this end, an attempt was made in this thesis to develop new luminescence methods for dating paleoseismic/neotectonic events.

2.2 Review of earlier work on dating of paleoseismic and faulting events

The general approach to paleoseismological work has been the inspection of geological features created by recent earthquakes and faulting events (e.g. fault scarps, folds, surface faulting, deformed sedimentary deposits, uplifted river and marine terraces) followed by examination of older geomorphic features in the vicinity of their modern counterparts. Chronology of paleoearthquakes is then established by radiometric/trapped charge dating techniques. In what follows, a review of various techniques used for dating paleoearthquakes is presented. Radiocarbon ages on charcoal, wood and organics within soils found in association with deformed sediments, liquefaction features and peat displaced by paleoearthquakes have been used to establish a chronology of paleoseismic events and to estimate repeat frequency of earthquakes with magnitudes > 6 in Pallet Creek, San Andreas Fault (Sieh, 1978; Sieh et al., 1989), El Asnam Fault, Algeria (Meghraoui et al., 1988), Salerno, Italy (Calderoni and Petrone, 1993), Central Apennines, Italy (Calderoni et al., 1990) and Arkansas (Tuttle and Schweig, 1995).

Sieh et al., (1989) provide evidence for at least nine paleoearthquakes during the last two millenia and estimated the average time interval between paleoearthquakes to be $\sim$ 160 years. Tuttle and Schweig's (1995) results suggest that prehistoric earthquakes of magnitude $\geq$ 6.4 took place at Blytheville, Arkansas in the past 6000 years. In Salerno, radiocarbon age brackets were assigned by Calderoni and Petrone (1993) for four large paleoearthquakes, viz., 3.4-2.8 ka BP, 4.4-3.4 ka BP, 6.8-4.3 ka BP and $>$ 6.8 ka. Meghraoui et al., (1988) presented age brackets for eight major paleoearthquakes during the last seven thousand years in El Asnam, Algeria. The average return period of the paleoearthquakes (magnitude $>$ 7) was estimated to be $\sim$ 720 years. However, during a cluster of seismic events, the repeat period reduces to 300-500 years.

Paleoearthquakes have also been dated using ^{14}C dating on mollusc and gastropod shells from seismically uplifted marine terraces in Corinth, Greece (Vita Finzi and King, 1985). The ages obtained were in the range 30,000-42,000 BP. However, these ages are perhaps underestimates of the actual paleoearthquake events. AMS ages on the uncontaminated part of partially recrystallized shells were 41 $\pm$ 2.7 ka BP and $>$ 42 ka BP in comparison with conventional radiocarbon ages of 31 $\pm$ 7 ka BP and 32 $\pm$ 7 ka BP respectively.

The growth of karst speleothems deviates from the original direction during large magnitude paleoearthquakes. Radiocarbon ages on carbonate minerals (travertine, alabaster) within karst speleothems have been used to indicate a $\sim$ 500 year BP paleoseismic event in Grotta del Cervo, Italy (Postpischl et al., 1991). U/Th ages from Grotta del Cervo show that seismic activity took place during the periods 350-150 ka, 110-90 ka and 40-30 ka and $<$ 5 ka ago.

Several problems are inherent in the above studies. These are basically related with the choice of proper sample for dating and with the ^{14}C method. Difficulties can occur in collecting stratigraphically undisturbed samples (Waterbolk, 1983), thus making

it impossible to associate the dated sample with the paleoseismic event. ^{14}C dating of carbonates such as shells and speleothems is problematic due to post depositional recrystallisation and incorporation of modern/dead carbon. Even for organic materials such as peat, different organic fractions from the same sample have given different ages, raising doubts on the validity of using peat for radiocarbon dating (Shore et al., 1995). The assumption that all datable materials have the same initial ^{14}C concentration as NBS oxalic acid standard/preindustrial atmospheric CO_2 may not be true. This is termed as the 'reservoir effect' and necessary corrections need to be made (Geyh and Schleicher, 1990) to determine the true ^{14}C age. Radiocarbon ages greater than $\sim$ 30 ka cannot be calibrated using coral data/dendrochronology. Moreover, despite the arrival of AMS dating, the technique is limited to dating samples younger than $\sim$ 50 ka.

K-Ar dating on the clay mineral fractions (e.g. illite, smectite) of fault gouges was attempted to estimate the time of faulting in New Hampshire, U.S.A. (Lyons and Snellenburg, 1971) and in Austria (Kralik et al., 1987). Kralik et al., (1987) suggested that clay formation took place along the Pailwand Fault and the Kreuzeck Fault during early Cretaceous and Tertiary. These K-Ar ages are minimum ages of faulting due to the time difference between the clay mineralisation and the faulting events. It must also be borne in mind that due to the finer size of these clay fractions, greater loss of radiogenic argon may occur leading to an erroneous age (Lyons and Snellenburg, 1971). Addition of ^{40}Ar into minerals by processes other than in situ decay of ^{40}K after faulting can also create problems in dating.

To determine ages of paleoseismic events, Ivanovich et al., (1983) dated mollusc shells from seismically uplifted beaches in Persian Gulf using the $^{230}Th/^{234}U$ method. The ages obtained were in the range 11.3–2 ka. The $^{230}Th/^{234}U$ method was also used by Edwards et al., (1988) to determine ages (6160 $\pm$ 25 years, 263 $\pm$ 5 years, 180 $\pm$ 5 years, 121 $\pm$ 4 years, 56 $\pm$ 5 years and 19 $\pm$ 3 years) on emerged corals from coseismically

uplifted marine terraces in Santo and Malekula Islands, Vanatu. This technique is however restricted to pure aragonitic/calcitic samples. It is also uncertain whether the technique will be applicable to older samples. Also, the closed system approximation may not always be satisfied for molluscs (Geyh and Schleicher, 1990). In another study by Eyal et al., (1992), uranium minerals, carnotite and tyayamunite which crystallised along fault planes and were subsequently deformed during faulting in Neger, Israel have been dated by the Th/U method to determine the time of faulting. These ages ranging from 123 to 19 ka were determined assuming that carnotites are closed chemically after faulting.

Fission track dating has been applied to date hydrothermal epidotes from fault planes in Sinai Peninsula, Israel (Bar et al., 1974). The epidote ages (32-11 Ma) represent faulting events if they were created during/immediately after faulting. Recently, cosmogenic isotopes such as in situ produced cosmogenic ^{10}Be in quartz from gneisses exposed on alluvial surfaces misaligned by faulting in Gobi-Altai, Western Mongolia have been used to derive minimum ages ($\sim$ 80-60 ka) of faulting and an upper limit ($\sim$ 1.2 mm/year) to the slip-rate along the fault (Ritz et al., 1995). However, Ritz et al., (1995) assumed (i) no loss of cosmogenic nuclides by erosion and (ii) very little production of ^{10}Be during transport, burial and reworking of material. Violation of these assumptions can cause systematic age deviations.

Wallace (1977) and Bucknam and Anderson (1979) demonstrated the relationship between height of a fault scarp, its slope angle and the age of fault scarps from Western Utah and Nevada, U.S.A. The slope angle was observed to be directly proportional to the logarithm of the scarp height and decreases with the age of the fault scarp for scarps of a given height. This technique can be used to obtain relative ages (between several thousand years and several hundred thousand years) of faulting but is subject to measurement and modelling errors.

Dendrochronology and lichenometry have also been applied to date past earthquakes. It has been suggested that tree ring widths show an anomalous change (increase/decrease) after an earthquake (Jacoby, 1987). However, variations in ring widths also occur due to climatic changes, e.g. drought (Jacoby, 1987) and hence a unique association may not be possible. Coseismic rockfall events in Sierra Nevada, California have been dated by lichenometry (Bull, 1996) to estimate the ages of past earthquakes in the past 1300 years (magnitude $\sim$ 7) along the southern San Andreas Fault.

ESR ages of faulting ($\sim$ 70 ka) were first reported by Ikeya et al., (1982) on quartz grains from Atotsugawa Fault gouge and latter confirmed by Tanaka (1990). Lee and Schwarz (1994) used the ESR techniques to determine ages of faulting along the San Gabriel Fault zone. Their ages imply tectonic activity along the San Gabriel Fault zone at three periods during the Pleistocene, viz., 382-310 ka, 246-212 ka and 177-124 ka. The ESR ages exhibited temporal and spatial clustering. Host rocks gave an age of 1173 $\pm$ 130 ka. However, the applicability of the ESR technique to fault gouges younger than 100 ka remains to be demonstrated. Also, Grun has stated that none of the ESR ages reported (until 1992) have been confirmed by independent age estimates (Grun, 1992).

The first attempts to date paleoearthquakes using thermoluminescence dating were by Forman et al., (1989; 1991) and McCalpin and Forman (1991). Forman et al., (1989) excavated trenches across fault scarps from the American Fork segment of the Wasatch Fault zone. Buried soils interposed between colluvium, faulted loess and sag pond deposits exposed in the trenches were used for TL dating. Equivalent doses evaluated using different methods agreed within 2σ. ^{14}C ages on carbonized wood and organic matter within buried soils were concordant with TL ages and show that three major faulting episodes occurred at 5.3 $\pm$ 0.3 ka, 2.6 $\pm$ 0.3 ka and 0.5 $\pm$ 0.2 ka ago.

An extension of this work was reported by Forman et al., (1991) who excavated

trenches across fault scarps in the Weber segment of the Wasatch Fault zone. TL dating was performed on colluvial wash facies deposited against fault scarps. TL ages were generally consistent with ^{14}C ages on charcoal and organic matter and were used by Forman et al., (1991) to constrain the timing of three major paleoearthquakes between 4.5-3.5 ka, 3.2-2.5 ka and 1.4-1.0 ka. Additionally, McCalpin and Forman (1991) report TL ages on lacustrine deposits and colluvium from fault scarp trenches in Bonneville delta surface, Utah. A radiocarbon age on gastropod shell was also available. The correlation of regional ^{14}C chronology with local Quaternary deposits and the TL ages constrain the timing of two paleoearthquakes between 15.5-13 ka and 7-4 ka.

Thus, in the summer of 1992 when work on this thesis commenced, only a few papers existed in the literature on TL dating of paleoearthquakes. No attempts had been made to date fault gouges/seismites using luminescence dating techniques. Since 1992, Hutton et al., (1994) have reported TL ages on aeolian sands from lake deposits adjacent to Roopena fault scarp near Tennant Creek, Australia. They concluded that this area had not experienced major paleoearthquakes during the last 50 ka.

Chapter 3

Dating of Paleoseismic/Neotectonic Events : Thermoluminescence dating of fault gouges

3.1 Introduction

Traditionally, faults are defined as fractures or a zone of fractures along which relative movement between opposite rock masses has taken place. This movement leads to damage and erosion of the opposing surfaces, a process that is known as wear. Existence of a hardness contrast between opposing materials causes abrasive wear which under brittle conditions results in fracture and formation of loose clayey material known as fault gouge (Scholz, 1990). Since most earthquakes are caused by slip along pre-existing faults, it is important to develop methods for dating fault gouges for determining the paleoseismic/neotectonic history of a fault. The various earlier attempts to date fault gouges have been described in Chapter 2. After Ikeya's pioneering attempt (Ikeya et al., 1982) using ESR dating, it seemed appropriate to develop the thermoluminescence method for dating fault gouges. This chapter describes a thermoluminescence method for dating fault gouges, experiments performed to examine the validity of the assumptions involving TL dating and application to some faults in the Himalaya.

3.2 The thermoluminescence method

The thermoluminescence method of dating fault gouges is based on the premise that during faulting, the TL signals of minerals constituting the fault gouge are reset due to frictional heating and cataclastic deformation. Subsequently, the TL signal builds up due to irradiation by ambient natural radioactivity (U, Th, K) such that at the time of sample excavation, the faulting age is given by the expression:

$$\text{Age} = \frac{\text{Paleodose}}{\text{AnnualDose}} \tag{3.1}$$

Thus, in order to find the TL faulting age, it is necessary to determine the paleodose and annual dose. The TL age represents the most recent, climactic movement occurring in the fault zone. The thermoluminescence technique offers additional advantages in comparison to other radiometric techniques because of the following factors: (a) ubiquity of gouge in fault zones in comparison to organic and shelly materials; (b) association of the dated sample to the neotectonic event; (c) a large dating range of $\sim 1 - \geq 200$ ka and (d) no requirement of calibration of the TL ages. For evaluating the reliability of TL ages, several experiments were conducted in the present studies to test basic assumptions involved in age determination. For these studies, fault gouges were collected from the seismically active Himalayan belt. A brief description of these sites is given below.

3.3 Description of fault gouge sites

Geophysical and structural studies suggest that seismicity in the Himalaya is related to movements along three major longitudinal thrusts/faults, (Fig. 2.1) viz., the Himalayan Frontal Fault (HFF), the Main Boundary Thrust (MBT) and the Main Central Thrust (MCT). These thrusts divide the Himalaya into three lithotectonic zones which are

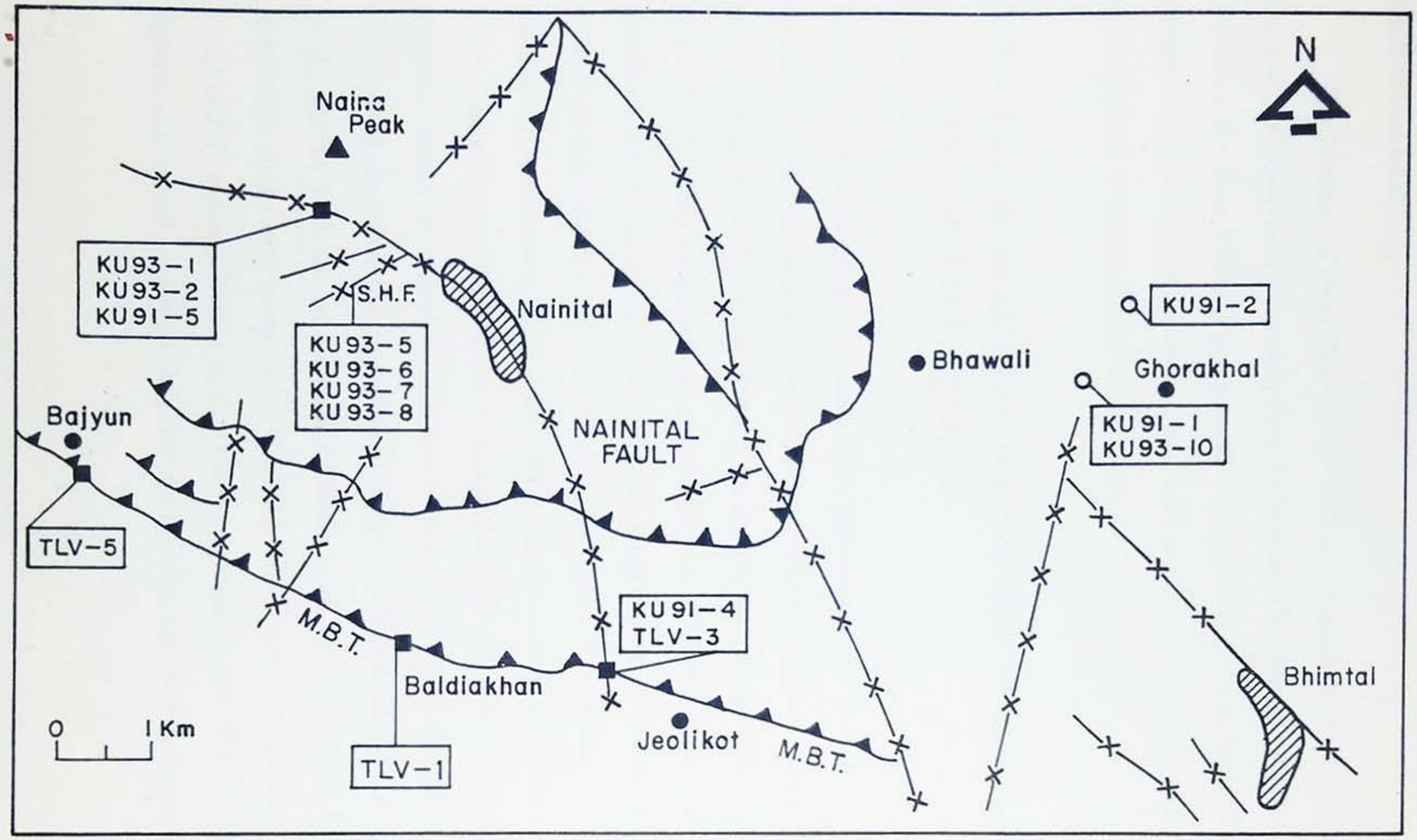
further dissected (Valdiya, 1976) by numerous transverse faults. After movements ceased along the Indus Suture Zone, the continued movement of the Indian plate has resulted in the breaking up of the Indian crust along MCT, MBT and HFF (Valdiya, 1992). Fault gouges for TL/IRSL dating were collected from Main Boundary Thrust (in the Nainital region), Sleepy Hollow Fault, Nainital Fault (Fig. 3.1) and Mohand Thrust (Fig. 3.2). A brief description of these sites is provided below.

The Main Boundary Thrust

The Main Boundary Thrust (Fig. 2.1; Fig. 3.1) is a chain of steeply inclined thrusts which divide the outer Himalayan Siwalik belt from the older, mature, recently rejuvenated Lesser Himalaya (Valdiya, 1992). Various types of evidences have been provided by Valdiya (1984; 1992) to indicate neotectonic activity along the MBT: (a) presence of wide valleys comprising cones and fans of landslide debris, (b) unpaired fluvial terraces overlapped by landslide debris, (c) upliftment and offsets of stream terraces, (d) evolution of sharp scarps, (e) warping and fitting of rocks/sediments and (f) geodetic measurements (Ansari et al., 1976).

Nainital Fault; Sleepy Hollow Fault

The Nainital Fault (Fig. 3.1) extends from Jeolikot through the Naini Lake to Kunjakharak in the north. It divides the deformed synclinal Nainital Massif into two parts. The Naini Peak was uplifted along the Nainital Fault relative to the Deopatta Peak in the south (Valdiya, 1988). This ventrical movement is suggested to be rotational (dip-slip and strike-slip) and caused blocking of a stream thus forming the Naini Lake (Pande, 1974; Valdiya, 1981). Displacement of river terraces and fans, abandonment of old channels, reversal and blocking of drainage are other indicators of neotectonism (Valdiya, 1988). Recent landslides and rockfalls including the 1880 and 1898 events have reduced the dimension of the lake.



M.B.T. = Main Boundary Thrust
S.H.F. = Sleep Hollow Fault

■ Fault Gouge
○ Terrace

Fig. 3.1: Location of fault gouges and host rocks in Nainital and its vicinities collected for TL dating.

The Sleepy Hollow Fault is antithetic to the Nainital Fault and is defined by vertical scarps and a straight steep slope demarcating Sleepy Hollow (Valdiya, 1988).

Mohand Thrust

The Mohand Thrust Zone (Fig. 3.2) is sympathetic to the Himalayan Frontal Fault and is located ~ 25 km away from Dehradun. Geodetic measurements at Dehradun show that the Dun Valley is being uplifted at a rate of ~ 1mm/year (Rajal et al., 1986). Presence of scarps, slickenslides in the fault zone, displacement and warping of rocks and unpaired terraces indicate neotectonism.

3.4 Previous studies on Zeroing of the ESR/TL signals in fault gouges

The dating of fault gouges is based upon the assumption that the thermoluminescence signal is completely zeroed during faulting. Many attempts have been made by ESR geochronologists to determine criteria for complete zeroing of the ESR signal. Fukuchi et al., (1985; 1986) suggested the use of different ESR centres in quartz having different stabilities for resetting (OHC, Ge, Al, E′ centres) to determine the faulting age. Thermal annealing experiments (Fukuchi et al., 1986) show that while Al and E′ centres are completely reset above 350°C, the OHC and Ge centre are reset only above 400°C. Thus, Fukuchi noted that if the ESR ages for different centres turned out to be same, resetting would be complete. However, Ikeya et al., (1982) suggest that hydrostatic stress could also erase the geological ESR signal during faulting. Experiments by Buhay et al., (1988) indicate an appreciable decrease in the paleodoses for all ESR centres mentioned above with pressure (~ 60 MPa). The OH centre was most affected, followed by Al and Ti centres. Buhay et al., (1988) advocate the use of various grain-sizes for age determination and suggested that the presence of a age plateau below a certain threshold

11045

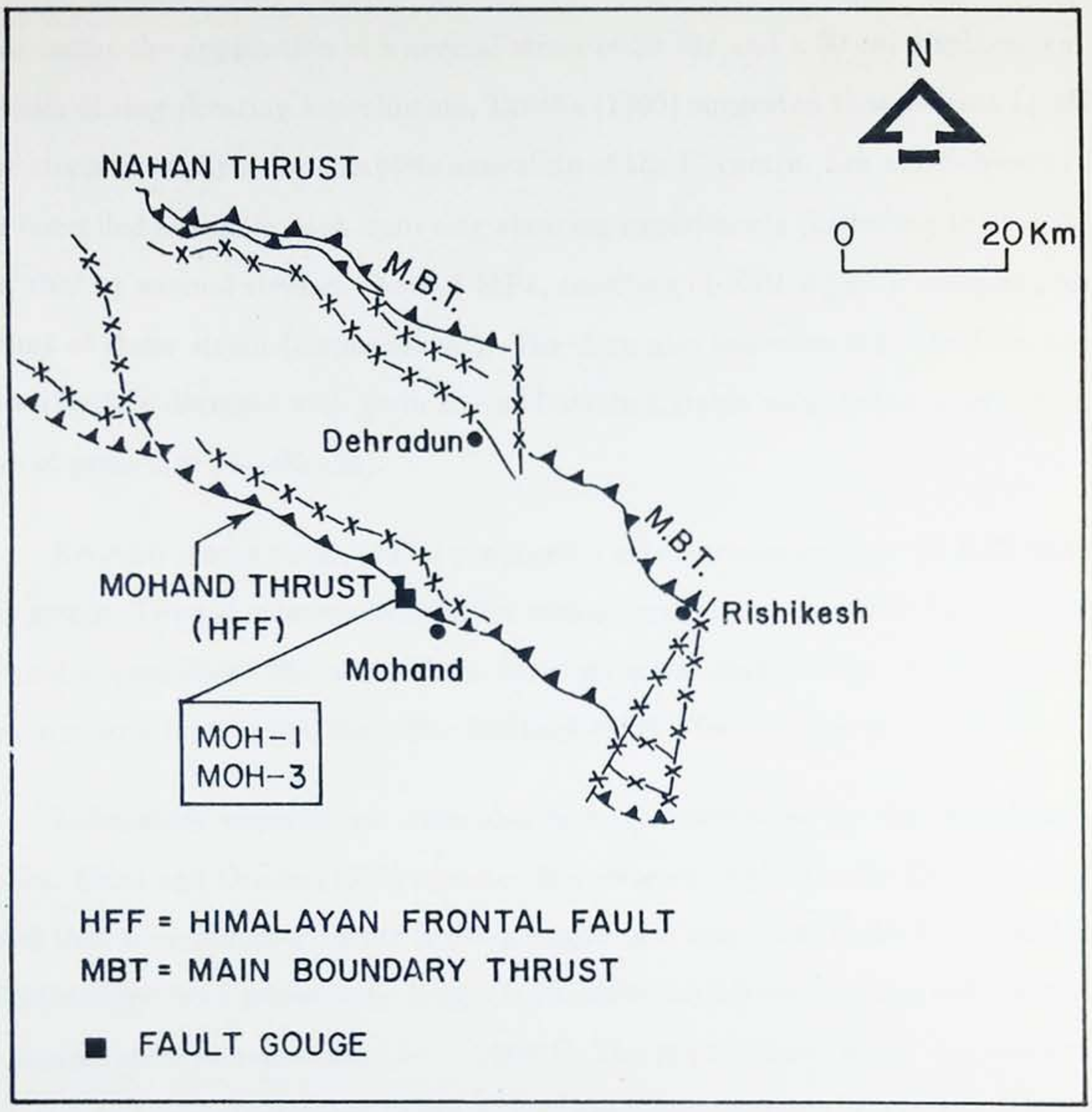


Fig. 3.2: Locations map of Mohand Thrust, Dehradun. Fault gouges MOH-1 and MOH-3 were collected from Mohand Thrust for TL and IRSL dating (modified after Valdiya, 1990).

value of grain size indicated complete resetting of the ESR signal.

Ariyama's (1985) experiments showed complete annealing of defects in quartz grains under the application of a normal stress of 20 bar and a 50 cm displacement. On the basis of ring-shearing experiments, Tanaka (1990) suggested that at least 11 MPa of shear stress is required for complete annealing of the E′ centre. Lee and Schwarz (1994) have compiled available data from ring shearing experiments (including their own) and show that at normal stresses above 4 MPa, resetting of ESR signal is complete for any amount of shear strain (displacement). The data also indicates that the ESR ages for various centres decrease with grain size and attain a stable value below a certain critical value of grain size ($\sim$ 100 μm).

Recently, Ikeya et al., (1995) proposed a new isochron method for ESR dating of fault gouge. The paleodoses obtained for various grain sizes are plotted as a function of external annual dose. The slope of the curve gives the isochron age. Application of this technique to a fault gouge from Mt. Rokko yielded a faulting age of $\sim$ 100 ka.

Laboratory experiments have also been complemented by theoretical and field studies. Scott and Drever (1953) reported the presence of glass in the Himalaya and suggested that temperatures during faulting might have been 1000°C. McKenzie and Brune (1972) studied heat generation along a fault plane during earthquakes and showed that the temperature increase could be $\sim$ 1000°C. The melting zone width was estimated to be 2 mm to 1 cm. Tuefel and Logan (1978) measured temperatures at the asperities of a saw-cut sample during triaxial compression tests on Tennessee Sandstone. The maximum temperature attained was $>$ 1000°C. Pseudotachylites, dark, glassy rocks having an appearance similar to but an origin different from glassy basaltic rocks (tachylytes) have been reported penetrating into fractures and fault planes. The temperature of pseudotachylyte formation has been estimated to be 1000°C on the basis of their chemical

compositions (Sibson, 1975, 1977). Measurements of friction induced thermoluminescence have been reported by Suzuki and Kennedy (1991). In another study, Hase et al., (1983) compared thermoluminescence intensities of quartz grains from clayey zone and host rocks in the Atotsugawa Fault and Adera Fault. Host rocks were found to emit more luminescence than clayey material. Shearing experiments carried out by Hase et al., (1983) indicate reduction in TL intensity of quartz grains on the application of normal stress.

3.5 Zeroing : Present Studies

3.5.1 Grain Size Dependence of TL ages (Fault gouges)

Previous studies on the variation of ESR ages with grain size (Lee and Schwarz, 1994; Buhay et al., 1988) have shown that the ESR signals of grains smaller than a certain critical size will be zeroed completely. Larger grains will retain some relic ESR signal which results in the evaluation of an erroneous age. To observe whether the fault gouge TL ages exhibited a similar or a disparate trend, TL ages were evaluated on various grain sizes.

Experimental Techniques involved in TL dating of fault gouges

The fault gouges were taken from spots approximately 0.5−1 m behind the exposed surface and were pretreated with 1N HCl (for removing carbonates) and 30% H_2O_2 (for removing the organic fraction). These samples were then subdivided into coarse (> 106 μm) and fine fractions (< 106 μm) from which the 4−11 μm fraction was extracted after a deflocculation with 0.01 N Na-oxalate followed by Stokes separation and deposition onto aluminium discs. The coarse fraction was dry sieved for obtaining various grain size fractions and deposited onto stainless steel discs using Silkospray. Although

the 420–500 μm grain size fraction was also sieved for various samples, it could not be used for TL analysis due to loss (> 50%) of sample grains while transferring the discs from the sample holder to the beta source. Even small movements (tilting the disc by a few degrees) led to grain loss within a few hours of deposition onto stainless steel discs. This grain loss was probably due to absorption of oil (Silkospray) by the fault gouge grains. For host rocks, a 2 mm layer from the surface was removed by sawing with a water cooled diamond wheel. This was done because of possible exposure to sunlight of the outer surface. Subsequently, they were gently crushed and treated with 1N HCl, 30% H_2O_2 and dry sieved to obtain the 106–150 μm fraction.

The TL analysis was done with the optics channel comprising a Schott UG-11 filter and a Chance Pilkington HA-3 filter coupled to an EMI 9635QA PMT and a photon counting system. Daybreak fused silica neutral density filters were used for brighter samples. The heating rate used was 2°C/s for coarse fractions and 5°C/s for the fine (4–11 μm) fractions. The 4–11 μm fractions were preheated to 220°C for one minute. No preheating was done on the other (> 11μm) fractions so as to minimize grain loss. The beta irradiations were carried out using a 25 mCi $^{90}Sr/^{90}Y$ beta source. Alpha irradiations were carried out using a six seater 0.22 mCi ^{241}Am vacuum alpha irradiation system (Singhvi and Aitken, 1978). The equivalent dose for the fault gouges was obtained using the additive dose method. A supralinearity correction was also determined by constructing the second glow growth curve. This correction was added onto the equivalent dose to obtain the total paleodose. Due to the build-up effect (Aitken, 1985), the average dose received by coarser grains is higher than that received by a layer of fine grains (4–11 μm). Multiplicative factors computed for grains of various thicknesses by Wintle and Aitken (1977) were used in the present studies.

Grains of different sizes will receive varying amounts of annual dose due to differing extents of attenuation (Aitken, 1985). The attenuation factors presented in Mejdahl

(1979) were used in estimating the annual dose for the fault gouges.

In the dose-rate analysis, thick source ZnS (Ag) alpha counting was used and the ^{238}U and ^{232}Th series were assumed to have equal alpha activity. The potassium concentration was determined using NaI(Tl) gamma spectrometry. An a-value was also used for coarse grains since the sample originates from a fine-grained shale which is assumed to have a uniform spatial distribution of alpha activity.

Results and Discussion

Figures 3.3, 3.4 and Table 3.1 presents the fault gouge TL ages for different grain-size fractions. The results suggest that TL ages attain a constant value (within errors) below a certain critical grain size (c_ϕ), thus indicating complete resetting of the TL signal of the smaller grains during faulting. For fault gouges from the Nainital Fault and Mohand Thrust, the critical grain size (c_ϕ) is ~ 360 μm and ~ 340 μm respectively. For the Main Boundary Thrust, TL ages for various grain sizes below 420 μm agree within experimental errors. As mentioned above, TL ages could not be determined on 420–500 μm fraction or higher grain size fractions. The data suggests that c_ϕ for MBT is probably > 420 μm. These observations can be explained as follows : During faulting, the maximum build up of stress occurs around defects (point defects, dislocations or surfaces) present within grains. These stresses give rise to microcracks which combine to form intra- and inter-grain fractures (Scholz, 1990). These effects are strongest where grains impinge upon each other leading to the development of large stresses (Kranz, 1983). The fraction of grain volume experiencing such high stresses increases with decreasing grain size (since intra-grain boundaries comprise a small part of the grain volume). So, it is likely that the TL signals of smaller grains will be completely zeroed whereas those of larger grains will be partially reset.

Frictional heating while strain energy is being dissipated during faulting has also

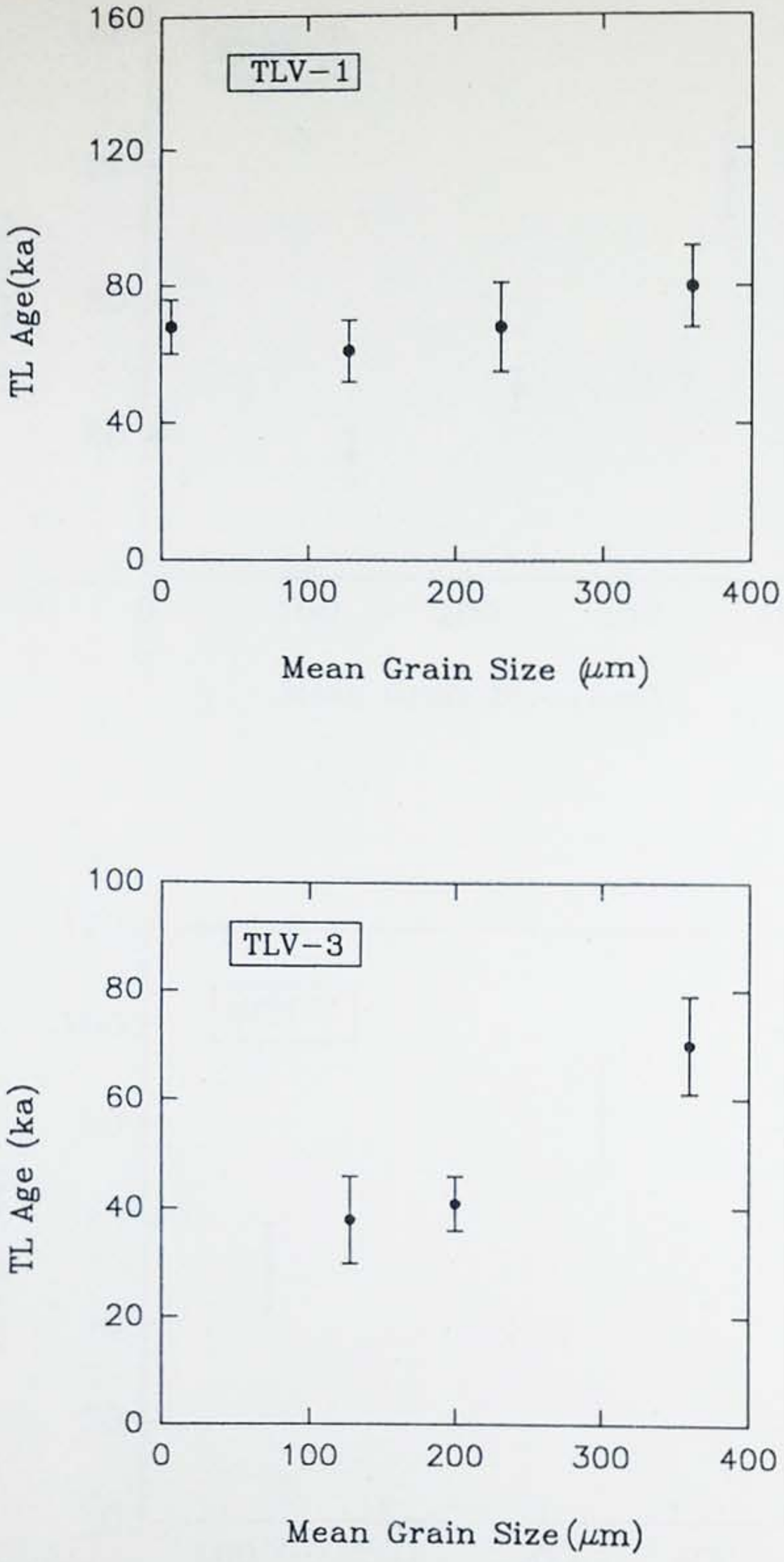
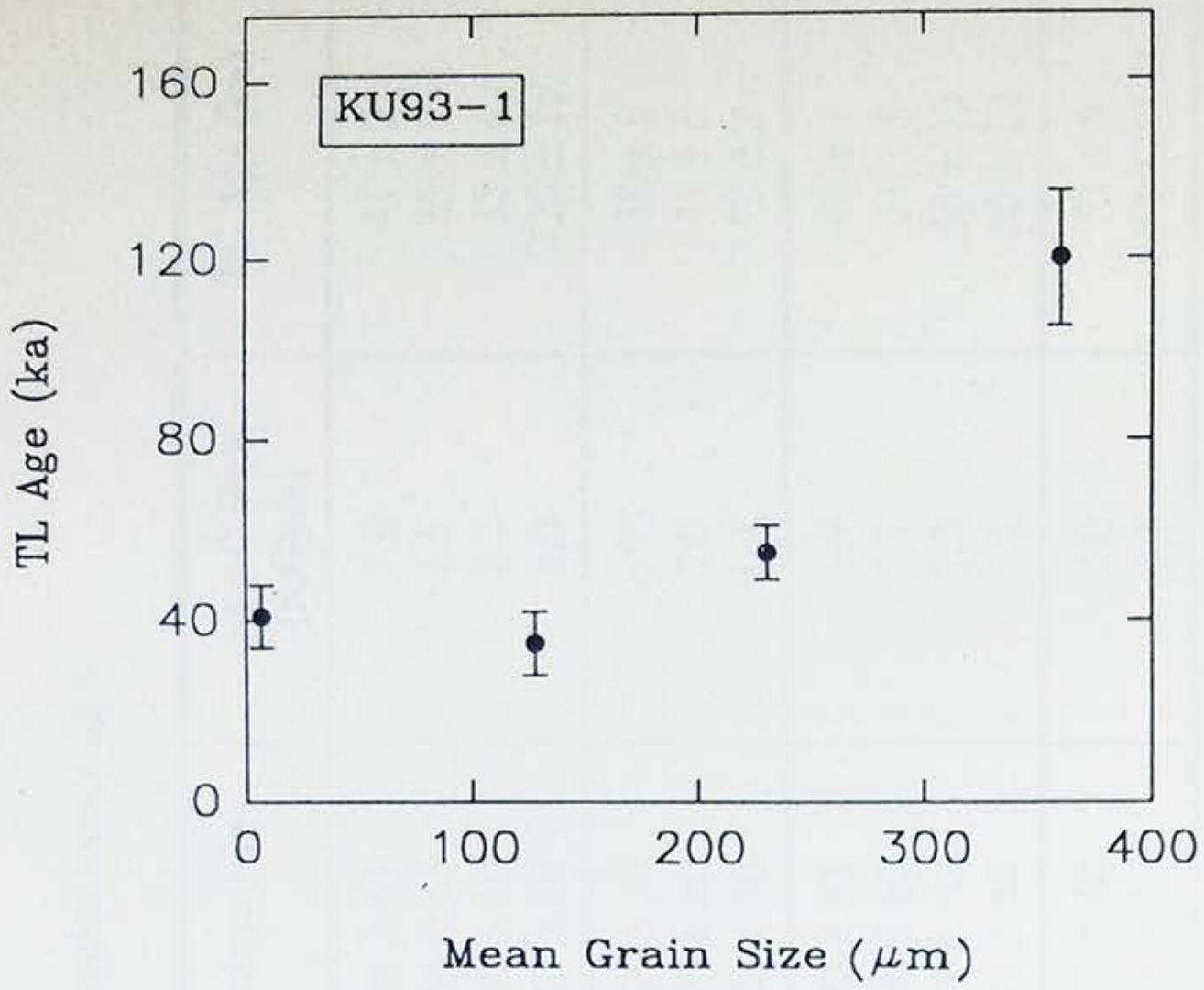


Fig. 3.3: Dependence of TL ages on mean grain size for fault gouges TLV−1 and TLV−3.



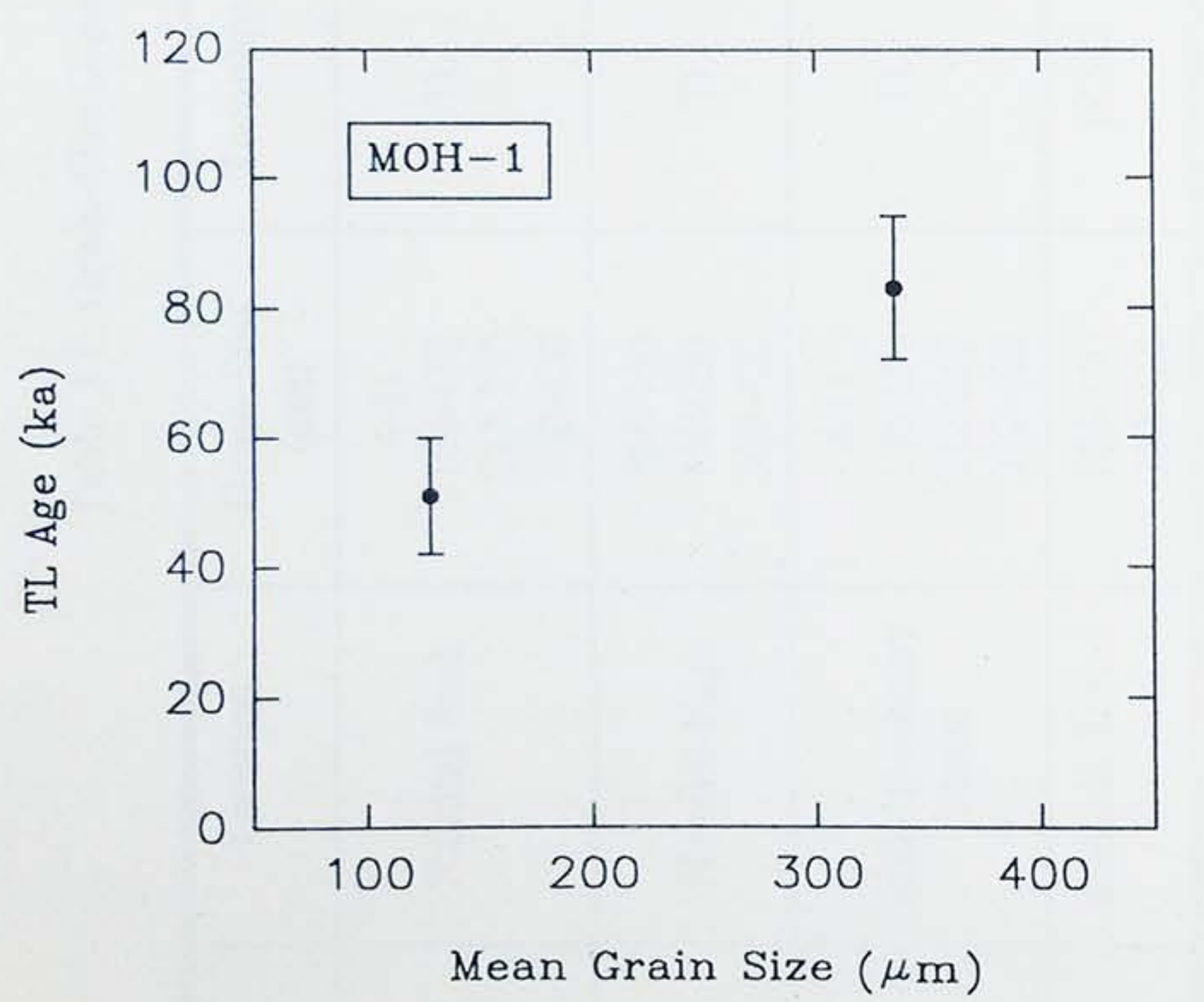


Fig. 3.4: Dependence of TL ages on mean grain size for fault gouges KU93−1 and MOH−1

Table 3.1: Grain-Size Dependence of luminescence ages

Sample	Location	Grain Size (μm)	Technique	Paleodose (Gy)	Annual Dose (mGy/a)	TL Age (ka)
KU93-1	Nainital Fault	4-11	TL	308 ± 61	7.6	41 ± 7
KU93-1		106-150		224 ± 45	6.5	35 ± 7
KU93-1		212-250		339 ± 20	6.2	55 ± 6
KU93-1		300-420		710 ± 68	6.0	120 ± 15
KU91-4	Nainital Fault	106-150	TL	264 ± 39	6.95	38 ± 8
TLV-3#		150-250		290 ± 30	7.0	41 ± 5
TLV-3#		300-420		473 ± 50	6.8	70 ± 9
TLV-1	Main Boundary Thrust	4-11	TL	542 ± 33	7.9	68 ± 8
TLV-1		106-150		468 ± 65	7.7	61 ± 9
TLV-1		212-250		495 ± 114	7.3	68 ± 13
TLV-1		300-420		571 ± 68	7.1	80 ± 12
MOH-1	Mohand Thrust	106-150	IRSL	202 ± 40	4.0	51 ± 9
MOH-1		250-420		258 ± 35	3.1	83 ± 11

TLV-3 was collected from approximately the same location as KU91-4

been suggested as a zeroing mechanism (Lee and Schwarz, 1994). This local heating effect will be maximum around the grain boundaries where stress concentration is maximum. Thus, a zone will exist around the grain boundaries where the TL signals of the grains is likely to be completely zeroed. This model can again explain the grain-size dependence of TL ages.

Bulk heating of the fault gouge has also been proposed as a method of zeroing the ESR/TL signal of fault gouges (Fukuchi, 1989; 1992). However, this model doesn't agree with the present observations. The timescales of thermal conduction for a spherical region of radius a can be estimated using the expression

$$\tau = \frac{a^2}{k\pi^2} \tag{3.2}$$

where k is the thermal diffusivity, τ is the characteristic time (in seconds) for heat conduction (Carslaw and Jaeger, 1959). Thus, using a typical value of 10^{-6} m^2/sec for thermal diffusivity (k), the characteristic time τ is $\sim 10^5$ a^2. The characteristic time of heat conduction for 1000 μm and 100 μm grains is 0.1 second and 10^{-3} respectively. Thus, grains of size 1000 μm will be in thermal equilibrium with 100 μm grains within $\sim$ 0.1 second. This implies that if bulk heating is responsible for zeroing of TL signals, the 300–420 μm TL age should be identical to TL ages for size ranges < 300 μm within experimental errors. This is not in accordance with our experimental observations, thus indicating that bulk heating of the fault gouge is unlikely to occur during faulting.

The critical grain size value for MBT fault gouges is greater than Nainital Fault or Mohand Thrust fault gouges probably because greater stress energy was available during faulting at the MBT. This is a reasonable assumption considering that MBT is the major fault system in this region. Movements along MBT and MCT have been suggested to be greater and faster since the frontal ranges related to them have acquired

greater heights and ruggedness (Valdiya, 1992).

3.5.2 Fault Gouge Paleodoses

The low value of paleodoses ($\sim$ 200–500 Gy) for fault gouges (Table 3.6) originating from Pliocene and older rocks of the Siwaliks and the concordance of faulting ages (40 $\pm$ 5 ka and 43 $\pm$ 4 ka) for fault gouges derived from rocks of different age and depositional environment is indicative of a definite TL resetting event. TL intensities of host rocks are upto two orders of magnitude higher compared to fault gouges, suggesting that complete resetting of the geological TL signal occurred during faulting.

3.5.3 Mechanoluminescence Studies

Luminescence induced during the mechanical deformation of solids is called mechanoluminescence (ML). Various materials exhibit mechanoluminescence, e.g., organic and inorganic crystals, amorphous solids, glasses, minerals etc. Most of these material emit ML during their fracture, but some (e.g. coloured alkali halides, alkaline earth oxides and some rubbers) exhibit ML in their elastic and plastic regions. In X-ray or gamma-ray irradiated alkali halide crystals, ML excitation takes place during the movement of dislocations. In the dislocation annihilation model, annihilation of dislocations of opposite sign may produce a high temperature locally, which results in luminescence emission as in thermoluminescence (Chandra, 1984). Since the zeroing of the TL signal can occur due to development of stresses during faulting, it was considered that ascertaining the dependence of ML of fault gouges with applied pressure could provide a useful compliment to the present studies. These studies were carried out by the author at the Department of Physics, Rani Durgavati University, Jabalpur. The dependence of TL with applied pressure could not be investigated due to logistical problems (a working TL experimental setup being unavailable at that time at the Department of Physics, Rani

Durgavati University, Jabalpur).

Experimental technique

The sieved fault gouges and host rocks were mechanically deformed and the ML intensity was measured using the experimental set up shown in Fig. 3.5. A load of mass 800 grams was dropped from different heights for striking the sample at different impact velocities and therefore at different applied pressures. The sample was placed on a transparent lucite plate inside a sample holder below the guiding cylinder. An RCA 931A photomultiplier tube connected to a phosphorescent screen oscilloscope (Scientific 203) placed below the transparent lucite plate was used for measuring luminescence. The response time of the PMT is $\sim 5\mu s$ and suits measurements of ML pulses of a few milliseconds duration.

For ML measurements, the sample was wrapped in thin aluminium foil and fixed on lucite plate with an adhesive tape. Lucite does not emit any luminescence under application of pressure. The aluminium foil reflects light and avoids dispersal of sample fragments when the load hits the sample. The rise and decay times of ML at different applied pressures were recorded by tracing the ML pulse appearing on the screen of the oscilloscope. The impact velocity was estimated as $(2gh)^{1/2}$ where g is the acceleration due to gravity and h is the distance of fall. The applied pressure σ is then computed using the expression

$$\sigma = \mathsf{M}\frac{(2gh)^{1/2}}{t_c A} \tag{3.3}$$

where M is the mass of load, A is the area of sample and t_c is the interaction time. However, this method for estimating the applied pressure is only an approximate one, and thus the pressure values are not absolute. The width of the ML pulse was assumed

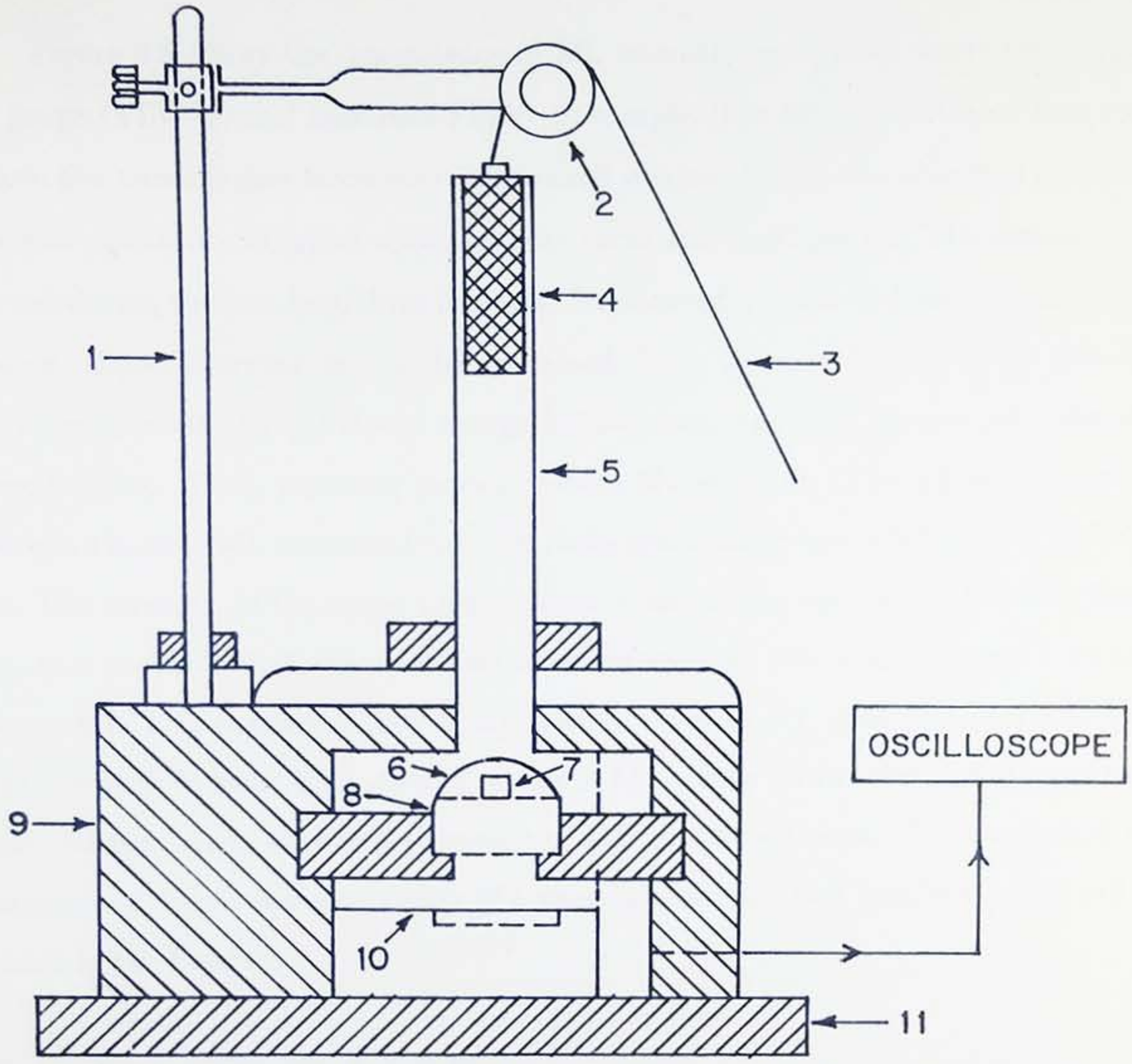


Fig. 3.5: (Available at Physics Dept., Jabalpur University)
Schematic diagram of the experimental arrangement used for measurement of ML in crystals.
(1–Stand, 2–Pulley, 3–Wire, 4–Load, 5– Guiding cylinder, 6–Aluminium foil, 7–Crystal, 8–Transparent lucite plate, 9–Wooden block, 10–PMT, 11–Iron base mounted on a table)

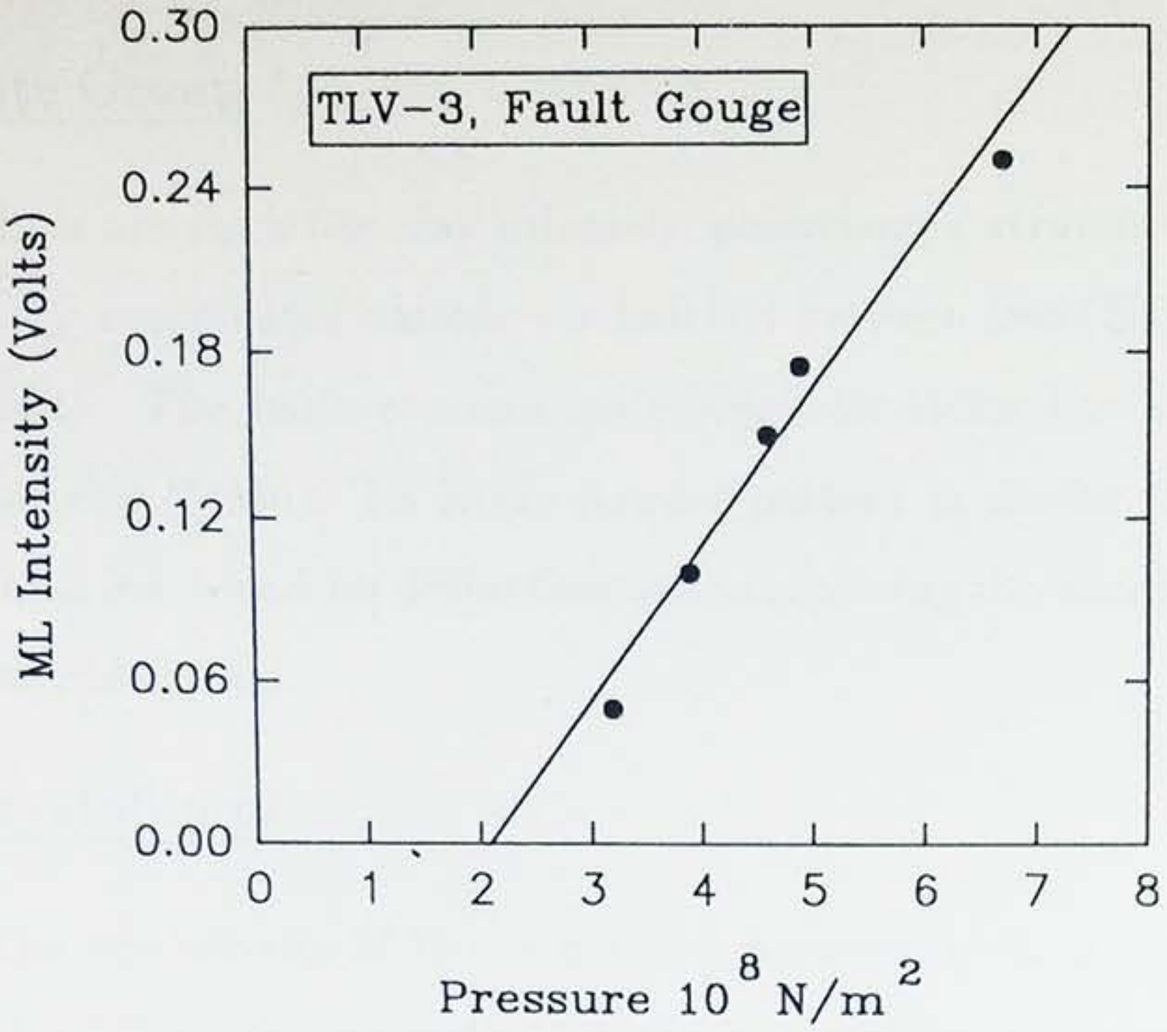
to be the interaction time. Typical interaction times were estimated to be $\sim$ 0.4–0.6 milliseconds.

Results and Discussion

Figure 3.6 shows the dependence of ML intensity on applied stress for a typical fault gouge (TLV–3) and host rock (TLV–2) sample. The ML intensities of host rocks are upto five times higher in comparison to fault gouges. It was also observed that if the mass was repeatedly dropped onto the host rocks and fault gouges, ML emission was observed during the first two/three impacts. Subsequent impacts did not give rise to ML emission. These observations can be explained if one assumes (i) host rocks have not been recently reset and (ii) stored energy in host rocks and fault gouges gets liberated during faulting. Thus, repeated impacts reduce ML emission. The minimum pressure required to initiate ML emission from host rocks and fault gouges was found to be $\sim$ 200 MPa. The strength of the upper crustal rocks is also of the same order (Scholz, 1990). Thus, it is probable that seismic events of magnitudes >6 will release energy from host rocks as ML. It is suggested that a comparative study of ML from host rock and fault gouge can provide some indication of release of ML energy during the formation of fault gouge. Further study on the dependence of ML growth with radiation dose could not be attempted due to non availability of a gamma source for bulk irradiation but will be pursued in the future.

3.5.4 Mineralogical studies

The minerals illite and chlorite were used for a possible determination of thermal excursions experienced by the fault gouges and host rocks. The basic premise in this study was that the structure of the minerals illite and chlorite undergoes changes on heating and thus thermal excursions during faulting should be discernible.



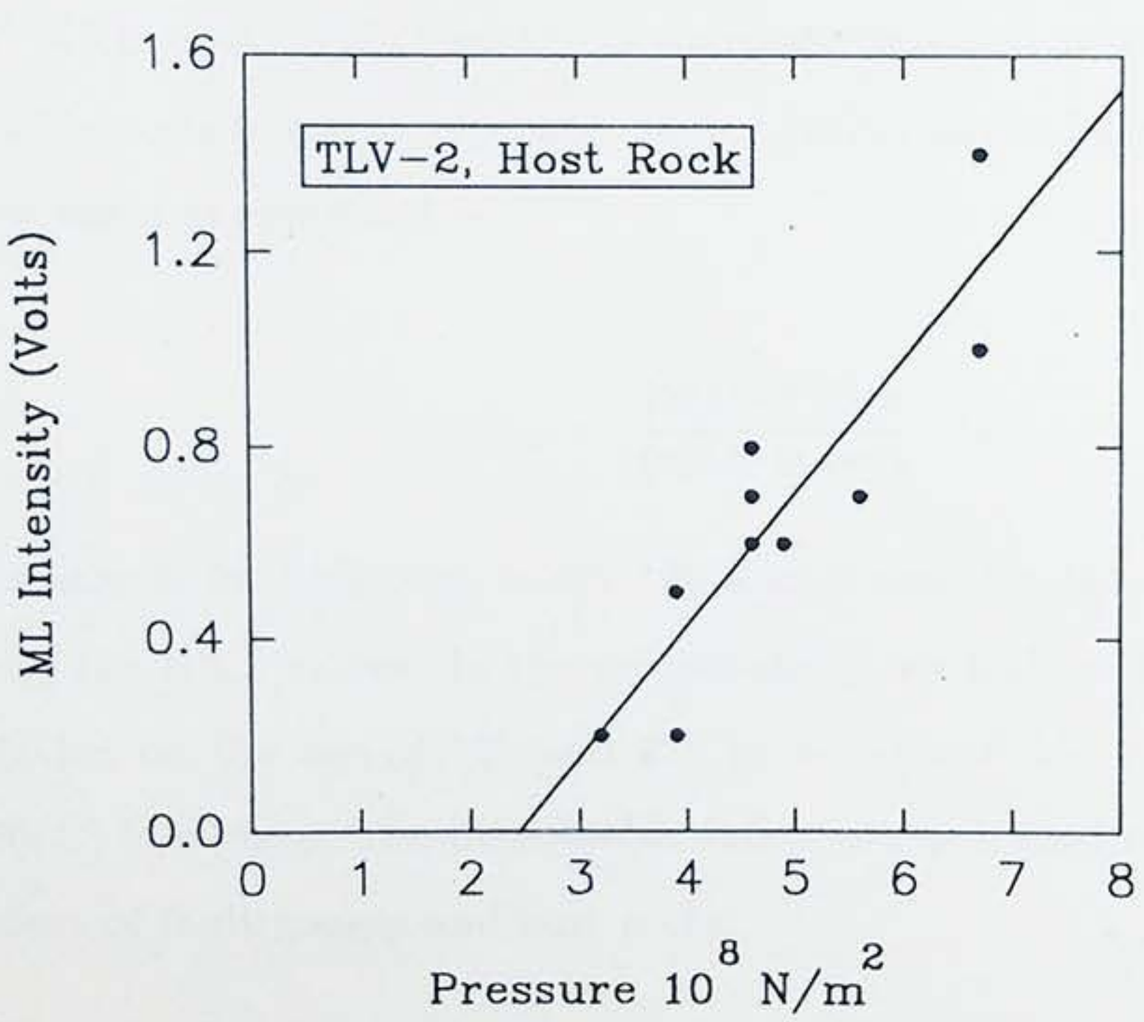


Fig. 3.6: Variation of ML Intensity with applied pressure for fault gouge TLV–3 and host rock TLV–2.

The Illite Group

Illites are mica-like clay minerals, possessing a structure consisting of planes of octahedrally coordinated cations sandwiched between two (Si, Al)O_4 tetrahedra (Deer et al., 1962). The most common polymorph for illites has a disordered one layered monoclinic cell (1 Md). Its X-ray powder pattern is similar to that of a mica except that it has a few broad hk diffraction bands replacing the sharp hkl reflections given by a well-ordered crystal.

Illite crystallinity

The crystallinity of illite signifies a parameter which measures the nature of 10 A° (001) XRD (X-ray diffraction) peak. On heating, illite loses interlayer water and adsorbs potassium. A rearrangement of ions occurs as potassium gets fixed in the interlayer positions. This phenomenon manifests itself in the increasing sharpness of the 10 A° XRD peak. This increase in sharpness was first used by Weaver (1960) as a measure of low-grade metamorphism. Weber (1972) devised a new crystallinity index : the Weber index is expressed as

$$\mathsf{Hb_{rel}} = \frac{\mathsf{Hb(10A°)illite}}{\mathsf{Hb(4A°)quartz}} \cdot 100 \tag{3.4}$$

where Hb stands for half peak width. Quartz is used for better interlaboratory comparisons of the Hb_{rel} values. In the present study, we utilized Blenkinsop's (1988) recommendation on the use of 149 and 378 as upper and lower value of the anchizone (200–370°C) boundary. The illite Weber index was also used to determine the heating temperature of fault gouges and host rocks.

The Chlorite Group

The chlorite structure is made of sheets of alternating talc-like and brucite-like

octahedral sheets. In most chlorites, Al, Fe^{2+} and Fe^{3+} substitute for Mg in octahedral sites both in the talc and brucite sheets and Al replaces Si in the tetrahedral sites (Deer et al., 1962). Various members of the group differ in the amount of substitution and the manner in which successive octahedral and tetrahedral layers are stacked along the c axis. X-ray diffractograms of chlorite suggest that the 14 A° peak becomes sharper from the non-metamorphic zone (very low grade) to the epimetamorphic zone (low grade). This shows that the lattice structure becomes more well defined with increasing temperatures (Wybrecht et al., 1985).

Chlorite Peak Ratio Method

Gogte (pers. commn.) has demonstrated that the XRD (X-ray diffraction) patterns of chlorite bearing clays exhibited a change in the ratio of the areas of 7.1 A° to 14.2 A° peaks with increasing temperatures. For temperatures between 0–250°C and 250–400°C, the ratios were found to be 1.6 ± 0.2 and 2.0 ± 0.1 respectively. Between 400–500°C, the ratio sharply approached zero. Minerals of the chlorite facies get transformed into chlorite schists and sericite at these temperatures (Dunoyer de Segonzac, 1970). The chlorite peak ratio method was also used to estimate the faulting temperature.

Experimental Techniques

The sieved/unseived grain-size fractions (after chemical pretreatments described above in Section 3.5.1) were powdered and placed on a glass slide. The XRD measurements were done using a RIGAKU D Max II VC XRD system operated at 50kV, 25mA, at a scan speed of 1′/second. The intensity, d-value, half peak widths and peak areas were computed using standard software. The measurements were performed on host rocks, fault gouges, æolian deposits and alluvium. All XRD measurements were carried out in the Deccan College, Pune by Dr. V. Gogte.

Results and Discussion

Table 3.2 and 3.3 represent the illite Hb_{rel} values and chlorite peak area ratios for the various samples. All samples contain mostly illite, chlorite and quartz. Some samples (TLV−3, TLV−2 etc.) also contained dolomite. The illite Hb_{rel} values indicate that both fault gouges and host rocks were heated beyond 200°C. On the basis of V. Gogte's unpublished results, the chlorite peak ratios were 1.6 ± 0.2, 2.0 ± 0.2 and ~0 for the temperature ranges 0−250°C and 250−400°C and 400−500°C, respectively. However, the errors associated with the chlorite peak ratios are underestimates due to exclusion of errors arising from (i) aliquot to aliquot variations and (ii) calculation of peak areas. The suggested peak ratios (based on estimation of chlorite peak ratios for a minimum of 4 aliquots and repeated calculation of peak areas) are 1.6 ± 0.7 and 0 ± 0.7 for the temperature ranges 0−400°C and > 400°C. Thus, presently, the peak ratio method can only indicate if a sample is heated above/below 400°C. The chlorite peak ratios (see table 3.3) indicate that besides fault gouges, host rocks, alluvium and aeolian deposits were also heated beyond 250°C. This result is untenable since host rocks or sedimentary deposits should not depict any heating signatures. This apparent discordance perhaps arises due to the fact that illites and chlorites examined from various samples were derived from a common metamorphic provenance. Further, an additional complication arises due to masking of the 10 A° illite and 7 A° chlorite peaks by the 10 A° muscovite and the 7 A° kaolinite peaks. It thus appears that at the present time, the mineralogical studies cannot unequivocally establish if the heating event corresponds to recent faulting/earlier metamorphic events.

3.5.5 Summary of results concerning zeroing of the luminescence signal during faulting

A combination of various criteria were examined to test the assumption of zeroing of the TL signal during faulting: (i) grain size dependence of TL ages, (ii) comparison of

Table 3.2: Illite Hb_{rel} values for fault gouges and host rocks

Sample	Type	Location	Illite Hb_{rel}	Inferred thermal excursion
KU91-4	Fault Gouge	Nainital Fault	134	>370°C
KU91-5	Fault Gouge	Nainital Fault	144	>370°
KU93-1	Fault Gouge	Nainital Fault	155	200-370°C
KU93-3	Host Rock	Nainital Fault	155	200-370°C
KU93-7	Fault Gouge	Sleepy Hollow Fault	124	>370°C
KU93-8	Rocky Material	Sleepy Hollow Fault	181	200-370°C
S-I	Host Rock	Nainital Fault	120	>370°C
K-I	Host Rock	Nainital Fault	120	>370°C

Table 3.3: Chlorite peak area ratios and inferred thermal excursions for fault gouges and host rocks

Sample	Type	Location	Chlorite+ Peak ratio	Inferred Thermal excursion
KU91-4	Fault Gouge	Nainital Fault	2.0	<400°C
KU91-5	Fault Gouge	Nainital Fault	1.5	<400°C
KU93-1	Fault Gouge	Nainital Fault	1.6	<400°C
KU93-2	Rocky Material	Nainital Fault	2.0	<400°C
KU93-3	Host Rock	Nainital Fault	2.0	<400°C
KU93-4	Host Rock	Nainital Fault	0.8	>400°C
KU93-6	Host Rock	Sleepy Hollow Fault	0.6	>400°C
KU93-7	Fault Gouge	Sleepy Hollow Fault	0.8	>400°C
KU93-8	Rocky Material	Sleepy Hollow Fault	1.9	<400°C
S-I	Host Rock	Nainital Fault	1.7	<400°C
K-I	Host Rock	Nainital Fault	1.7	<400°C
TLV-1	Fault Gouge	Main Boundary Thrust	0.5	>400°C
TLV-3	Fault Gouge	Nainital Fault	2.2	<400°C
TLV-5	Fault Gouge	Main Boundary Thrust	0.6	>400°C
TLV-6	River Terrace Deposit	Nr. Kaladhungi	0.7	>400°C
CNF-2	Aeolian Sands	Ghaggar Flood Plain	0.5	>400°C
CNF-9	Alluvial Sands	Chautang Flood Plain	0.3	>400°C

+ Ratio of the chlorite 7.1A° and 14.2A° peak areas.

host rock and fault gouge paleodoses, (iii) mechanoluminescence and (iv) mineralogical studies. The grain size dependence studies suggest that a plateau in TL ages for grains smaller than a certain critical size is perhaps a good indicator of complete resetting of the TL signals (of these smaller grains) from faulting. Observation of substantially higher host rock luminescence paleodoses and Mechanoluminescence intensities compared to fault gouges will also be consistent with the idea of a definite resetting event. The mineralogical studies are unable to provide a unique association of the heating event indicated by the chlorite and illite data with faulting.

3.6 Stability of the TL signal : Determination of trap parameters and mean life estimation

In thermoluminescence dating, it is important to establish that the TL signals of the minerals constituting the sample remain stable over timescales spanning the event that is being dated. As no luminescence data was available on fault gouges/host rocks (to the best of the author's knowledge), it was considered appropriate to examine the trap parameters and mean lives for host rocks and fault gouges besides looking at the age plateaus. The probability of electron escape (per second) from a trap with depth E below the conduction band is given by the expression

$$\lambda = s \cdot e^{-E/kT} \tag{3.5}$$

where s is the frequency factor, k is the Boltzmann's constant and T is the absolute storage temperature. In Randall and Wilkins' (1945) theory, retrapping of electrons is assumed to be negligible and the rate at which electrons escape is given by the expression

$$\frac{\delta n}{\delta t} = -\lambda n \tag{3.6}$$

where n is the number of electrons trapped at time t. Integrating, one gets

$$\int \frac{\delta n}{n} = -\int_o^t s \cdot e^{-E/kT} \delta t \tag{3.7}$$

If the temperature increase occurs at a constant rate, say β (the heating rate), then

$$n = n_o \cdot \exp - \left(\int_o^T se^{-E/kT} \cdot \frac{\delta T}{\beta}\right) \tag{3.8}$$

The thermoluminescence intensity (I) is proportional to the rate of supply of electrons to the luminescent centres. Thus

$$I = c \cdot \frac{\delta n}{\delta t} = cn_o s \cdot e^{-E/kT} \cdot \exp - \left(\int_o^T se^{-E/kT} \cdot \frac{\delta T}{\beta}\right) \tag{3.9}$$

This relationship only holds for first order kinetics when trapping of electrons is negligible. For any general kinetic order b, the TL intensity (I) is

$$I = c \cdot n^b \cdot s' \cdot e^{-E/kT} \tag{3.10}$$

where s' is the pre-exponential factor in second^{-1} $\text{cm}^{3(b-1)}$ and c is the proportionality constant. For the initial portion of the TL glow curve, for any kinetic order,

$$\ln(\text{Intensity}) = \text{Constant} \cdot \frac{-E}{kT} \tag{3.11}$$

Thus, if ln (Intensity) is plotted as a function of 1/kT, the slope gives the value of the activation energy E. This method is termed as the initial-rise method. This method can be applied to overlapping peaks using the fractional glow technique (Gobrecht and Hofmann, 1966). The lifetime (τ) of electrons in a particular trap of depth E and frequency factor s at the storage temperature T is expressed as

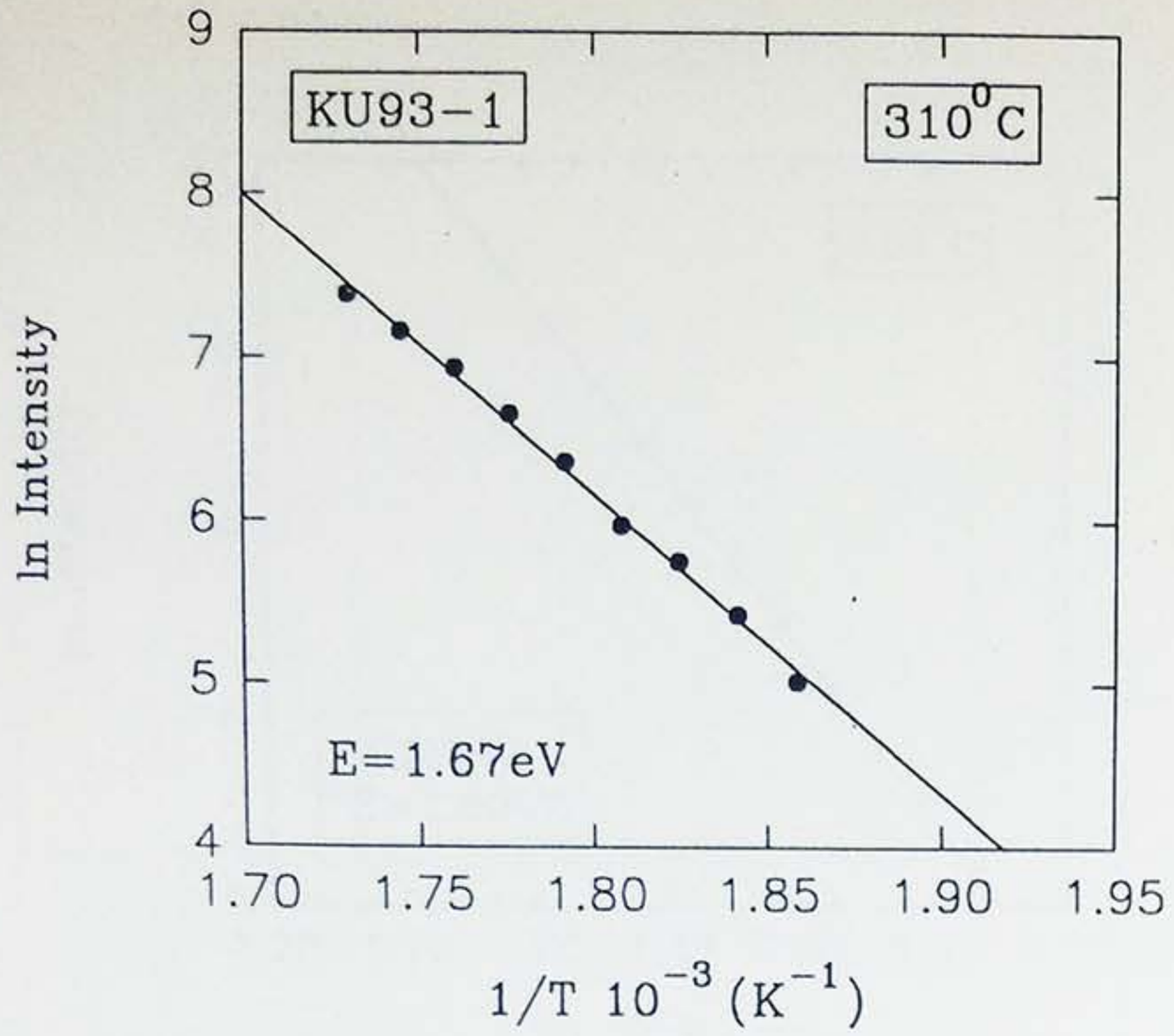
$$\tau = \frac{1}{s} \cdot e^{E/kT} \tag{3.12}$$

Experimental Technique

Representative samples of the fault gouges and host rocks were used to determine their activation energy values. The fractional glow technique was utilized on the 106−150 μm fraction of the samples. The samples were directly placed on the heater plate to ensure a better heat conduction and precise temperature measurements. Several incremental (10°C) cycles of heating and cooling were performed in the temperature range from 200−380°C.

Results

Figures 3.7 and 3.8 represent typical plots of ln (Intensity) versus 1/T for fault gouges. The dependence of E values on temperature is also shown in Figs. 3.7 and 3.8. Tables 3.4 presents the trap parameters evaluated for the fault gouges and host rocks. The spectrum of activation energies for fault gouges determined using the initial rise method are 1.37 eV (210°C), 1.56 eV (280°C), 1.67 eV (310°C) and 1.71 eV (350°C). For the host rock from Sleepy Hollow Fault, the E values were 1.61 eV and 1.67 eV for 310°C and 350°C respectively. These values closely correspond to E values of quartz and K-feldspar as quoted in the literature (Aitken, 1985). The activation energy values were used to calculate the lifetime of the TL signal (at 15°C) assuming first order kinetics and frequency factors taken from Aitken (1985). Since thermal quenching can affect E



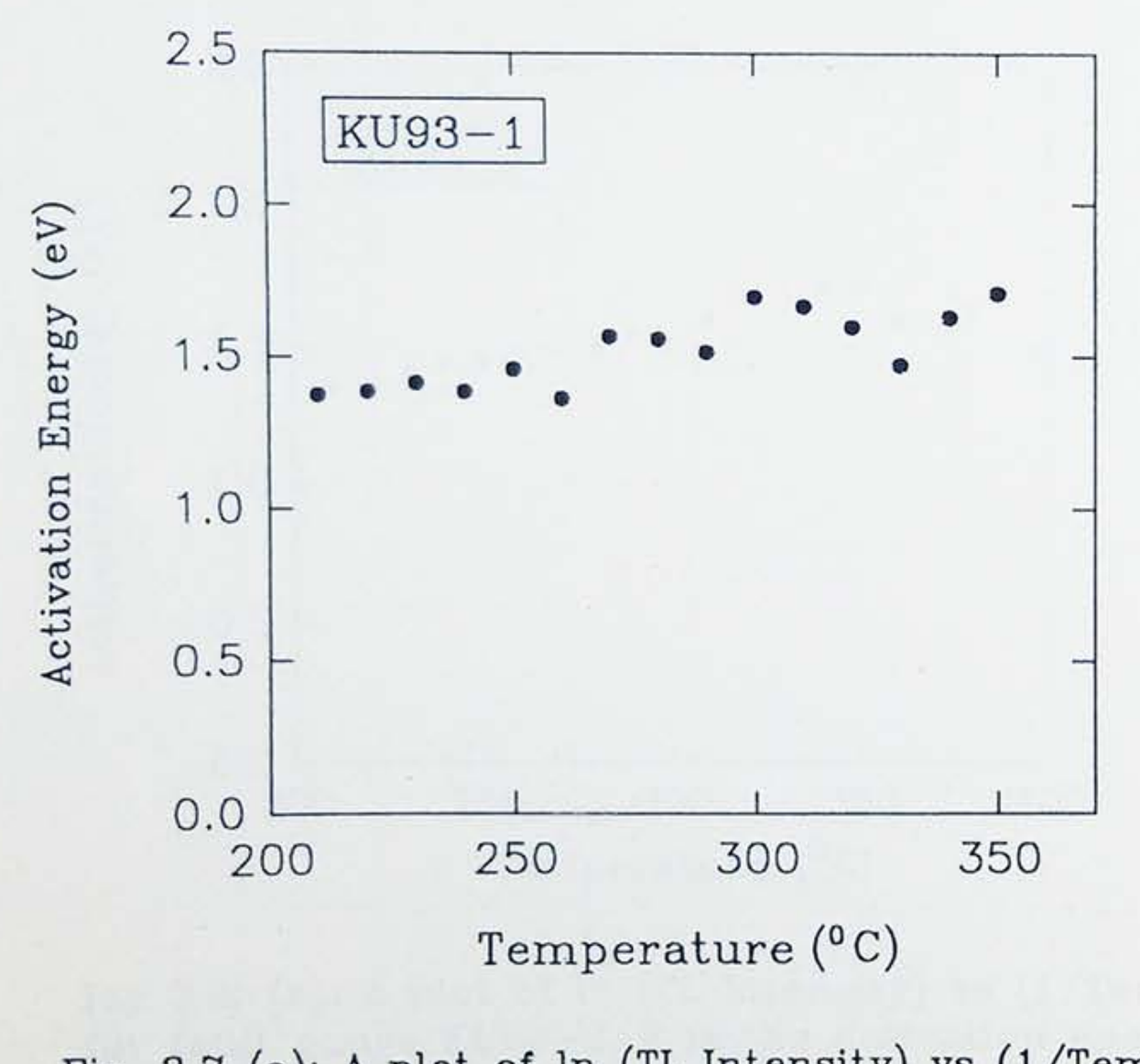
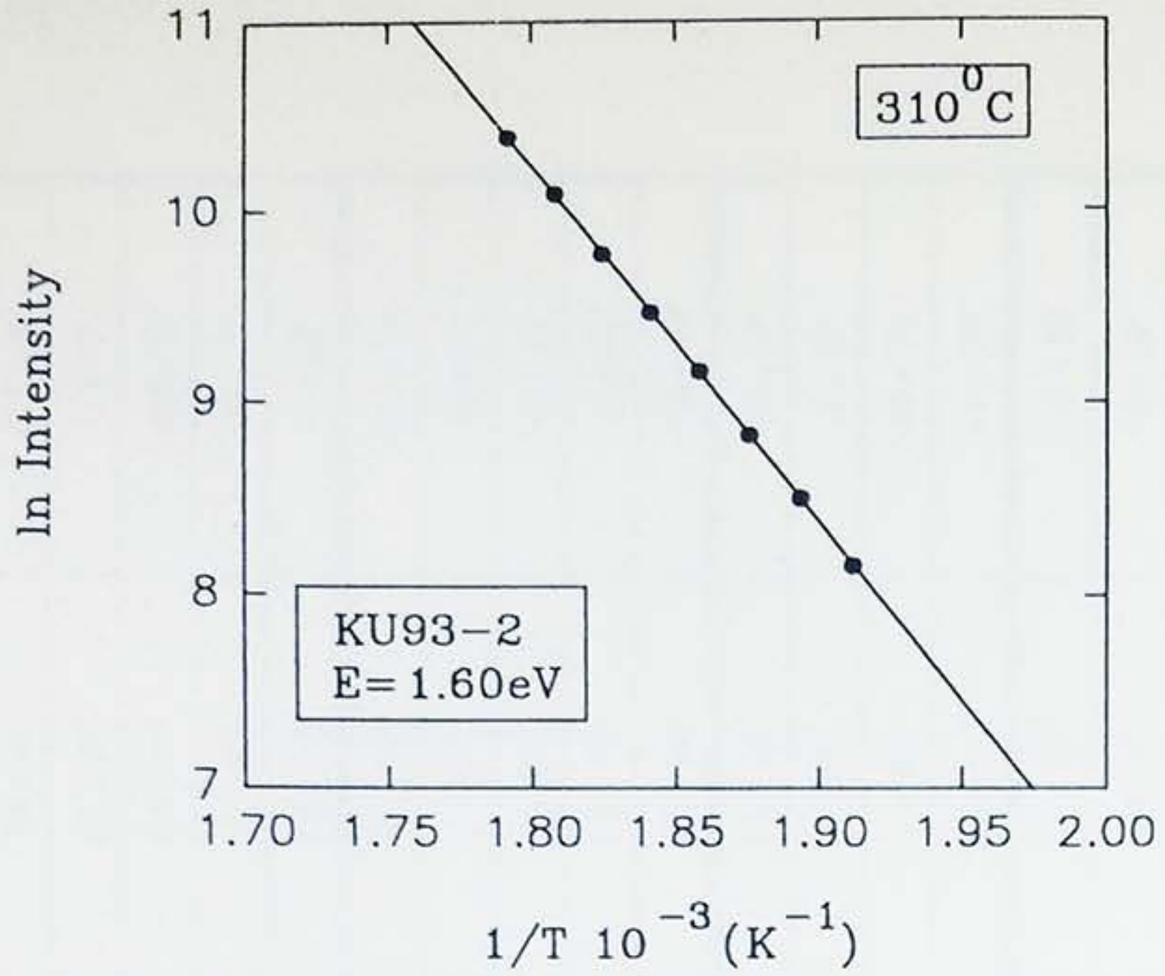


Fig. 3.7 (a): A plot of ln (TL Intensity) vs (1/Temperature) for fault gouge KU93-1. E is the activation energy.
Fig. 3.7 (b): Variation of activation energy with glow curve temperature for the fault gouge KU93-1.



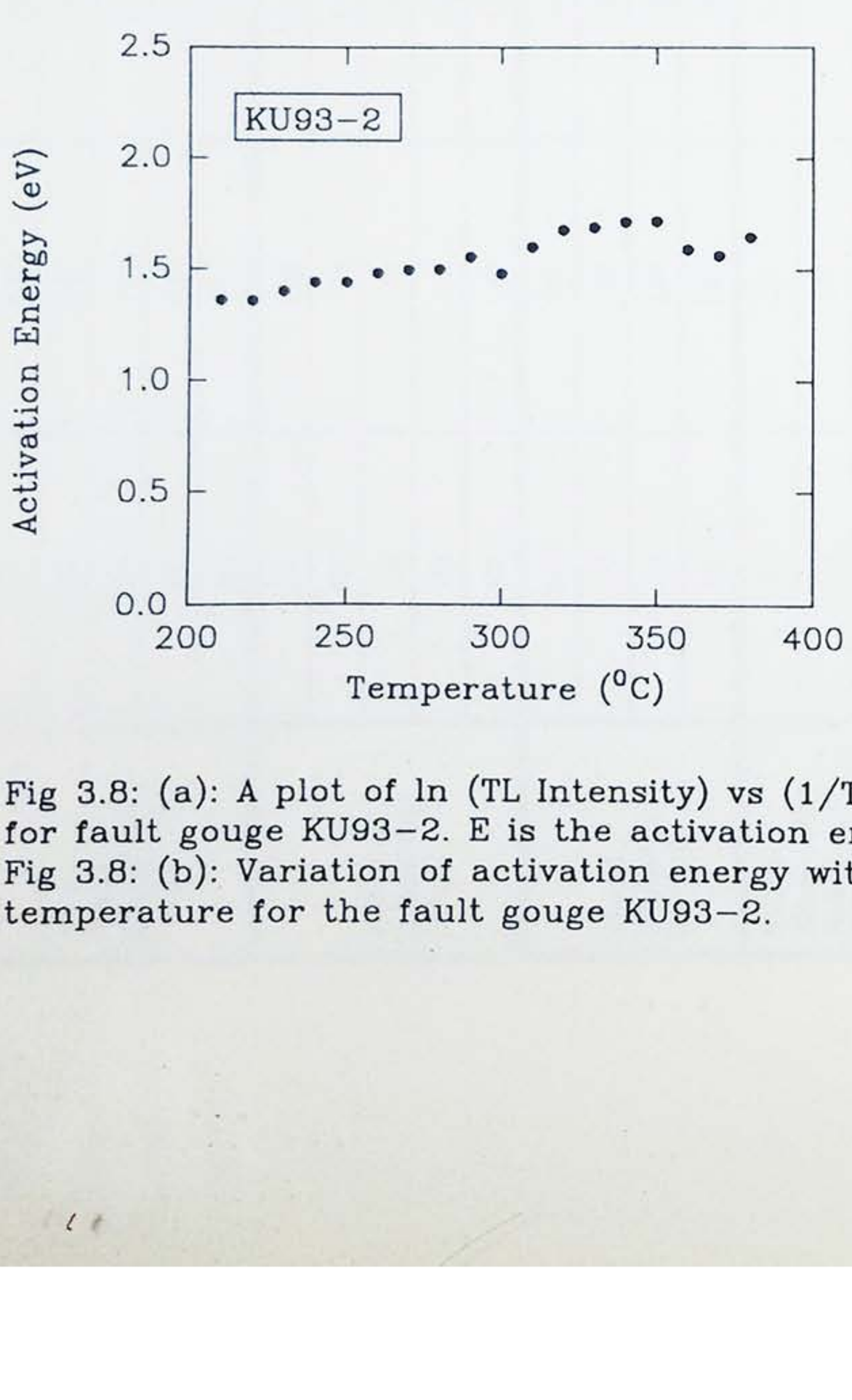


Fig 3.8: (a): A plot of ln (TL Intensity) vs (1/Temperature) for fault gouge KU93-2. E is the activation energy.
Fig 3.8: (b): Variation of activation energy with glow curve temperature for the fault gouge KU93-2.

Table 3.4 : Activation energies, frequency factors and lifetimes for fault gouges and host rocks

Sample	Glow Curve Temperature (°C)	Sample E Value+ (eV)	E Value* (eV)	Frequency** Factor (s^{-1})	Lifetime# (years) at 15°C
KU93-1 (Nainital Fault Gouge)	210	1.37	1.40	2.8×10^{13}	$\sim 0.7 \times 10^{3}$
	280	1.56	1.62	4.1×10^{13}	$\sim 1 \times 10^{6}$
	310	1.67	1.68	1.8×10^{13}	$\sim 200 \times 10^{6}$
	320	1.60	1.60	1×10^{13}	$\sim 20 \times 10^{6}$
	350	1.71	1.68	2.8×10^{12}	$\sim 6 \times 10^{9}$
KU93-2 (Nainital Fault Gouge)	210	1.36	1.40	2.8×10^{13}	$\sim 0.5 \times 10^{3}$
	310	1.60	1.60	1×10^{13}	$\sim 20 \times 10^{6}$
	320	1.68	1.69	1×10^{14}	$\sim 50 \times 10^{6}$
	350	1.72	1.68	2.8×10^{12}	$\sim 9 \times 10^{9}$
	380	1.65	1.66	1.5×10^{13}	$\sim 100 \times 10^{6}$
KU93-5 (Sleepy Hollow Host Rock)	310	1.61	1.68	1.8×10^{13}	$\sim 20 \times 10^{6}$
	320	1.55	1.60	1×10^{13}	$\sim 3 \times 10^{6}$
	330	1.69	1.69	1×10^{14}	$\sim 80 \times 10^{6}$
	350	1.67	1.68	2.8×10^{12}	$\sim 1 \times 10^{9}$
KU93-7 (Sleepy Hollow Fault Gouge)	220	1.36	1.40	2.8×10^{13}	$\sim 0.5 \times 10^{3}$
	320	1.57	1.60	1×10^{13}	$\sim 6 \times 10^{6}$
TLV-3 (MBT Fault Gouge)	210	1.45	1.40	2.8×10^{13}	$\sim 20 \times 10^{3}$
	320	1.55	1.60	1×10^{13}	$\sim 3 \times 10^{6}$
	370	1.61	1.66	1.5×10^{13}	$\sim 2 \times 10^{7}$

+ Calculated using the Initial-Rise Method. Random error in E value is ~5%. Heating rate is 2°C/second.

* Quoted from Aitken (1985).

** At a glow-curve temperature T°C, the estimated sample E value was compared with E values for minerals (at ~T°C) quoted in Aitken (1985). The frequency factor for the E value nearest to the sample E value at ~T°C was assumed to be the sample's frequency factor.

Lifetimes have been calculated using sample E values (column 3) and S values (column 5) assuming first order kinetics.

values determined using the initial rise method (Wintle, 1975), the computed lifetimes must be treated as minimum estimates. The lifetimes indicate that the TL signal from the 250–400°C region of the glow curve is stable over timescales of $\geq$ 1 Ma.

3.7 Anomalous Fading Studies

The loss of luminescence from the high temperature (> 250°C), stable region of the glow curve is termed 'anomalous fading'. Wintle (1973) first reported anomalous fading for various types of feldspars from volcanic lava flows. Luminescence ages affected by anomalous fading will be underestimates of the true age. In the present studies, the fault gouges were imparted a beta dose of $\sim$ 340 Gy and subsequently stored for a period of three weeks at $\sim$ 23°C after irradiation. No fading of the TL signal was observed (Fig. 3.9 and 3.10) from the 250–400°C region of the glow curve. Wintle (1978) demonstrated that fading does not display a strong dependence on the type of ionising irradiation used. Thus no fading of the laboratory beta irradiation generated TL signal should imply that anomalous fading of the fault gouge TL signal did not occur during antiquity.

3.8 Results of TL Dating of fault gouges

Fig. 3.11 and 3.12 provide typical TL glow curves and growth curves for fault gouges. Fig. 3.13 provides IRSL growth curve and shine plateau for a fault gouge. Tables 3.5 and 3.6 present radioactivity data and luminescence ages of fault gouges and host rocks. Fig. 3.14 and 3.15 provide age plateaus for fault gouges.

Methodology

The radioactivity data indicates that annual dose for the fault gouges from Nainital and its vicinities is $\sim$ 6–9 mGy/a. However, the annual dose for a fault gouge

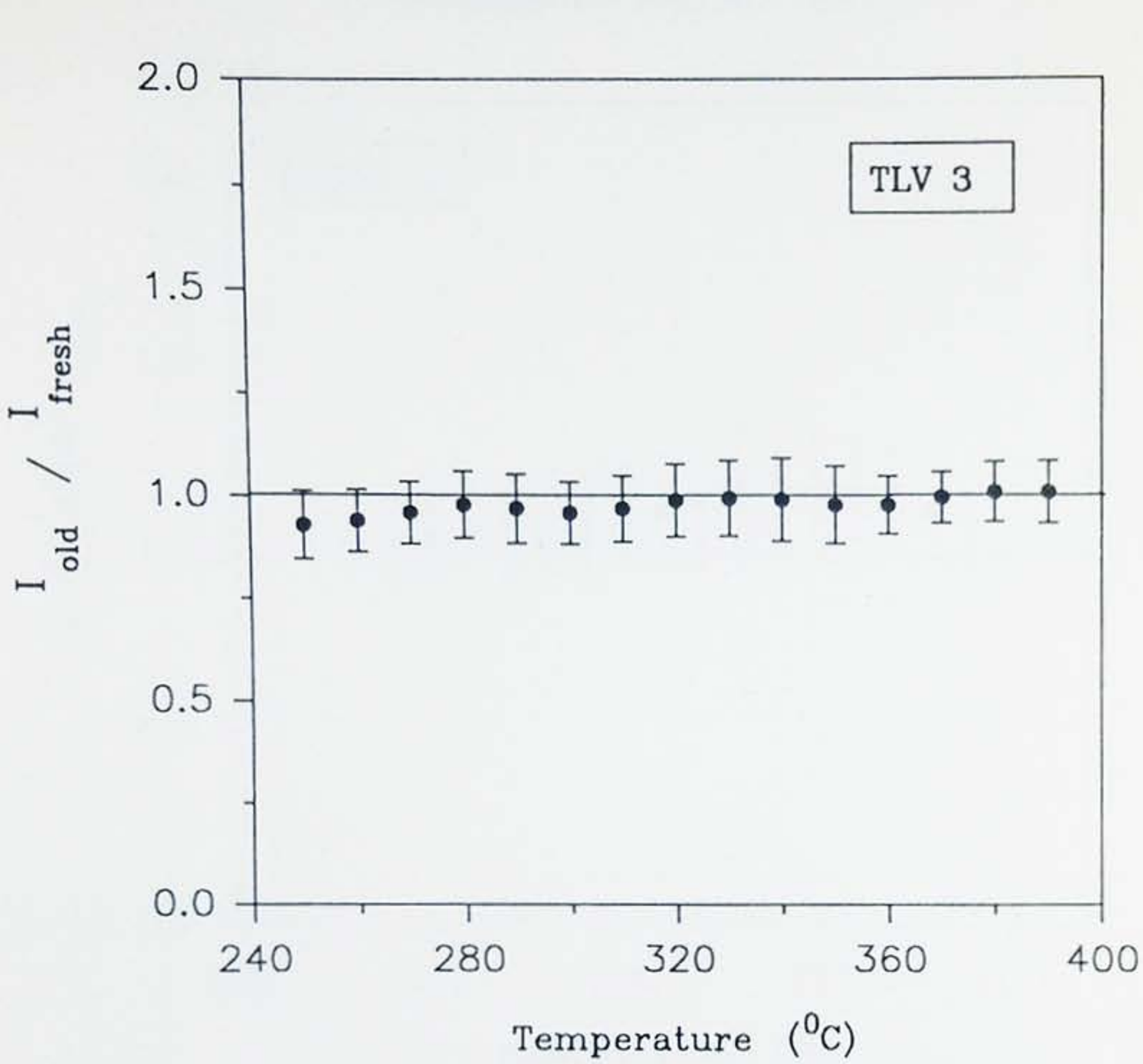


Fig 3.9: Anomalous Fading test for fault gouge TLV–3. I_{fresh} represents the mean value of TL intensity of five aliquots which were recorded within 2–3 days after beta exposure. I_{old} is the mean TL intensity for aliquots which were stored for three weeks at 23^0C after beta exposure before TL readout was performed.

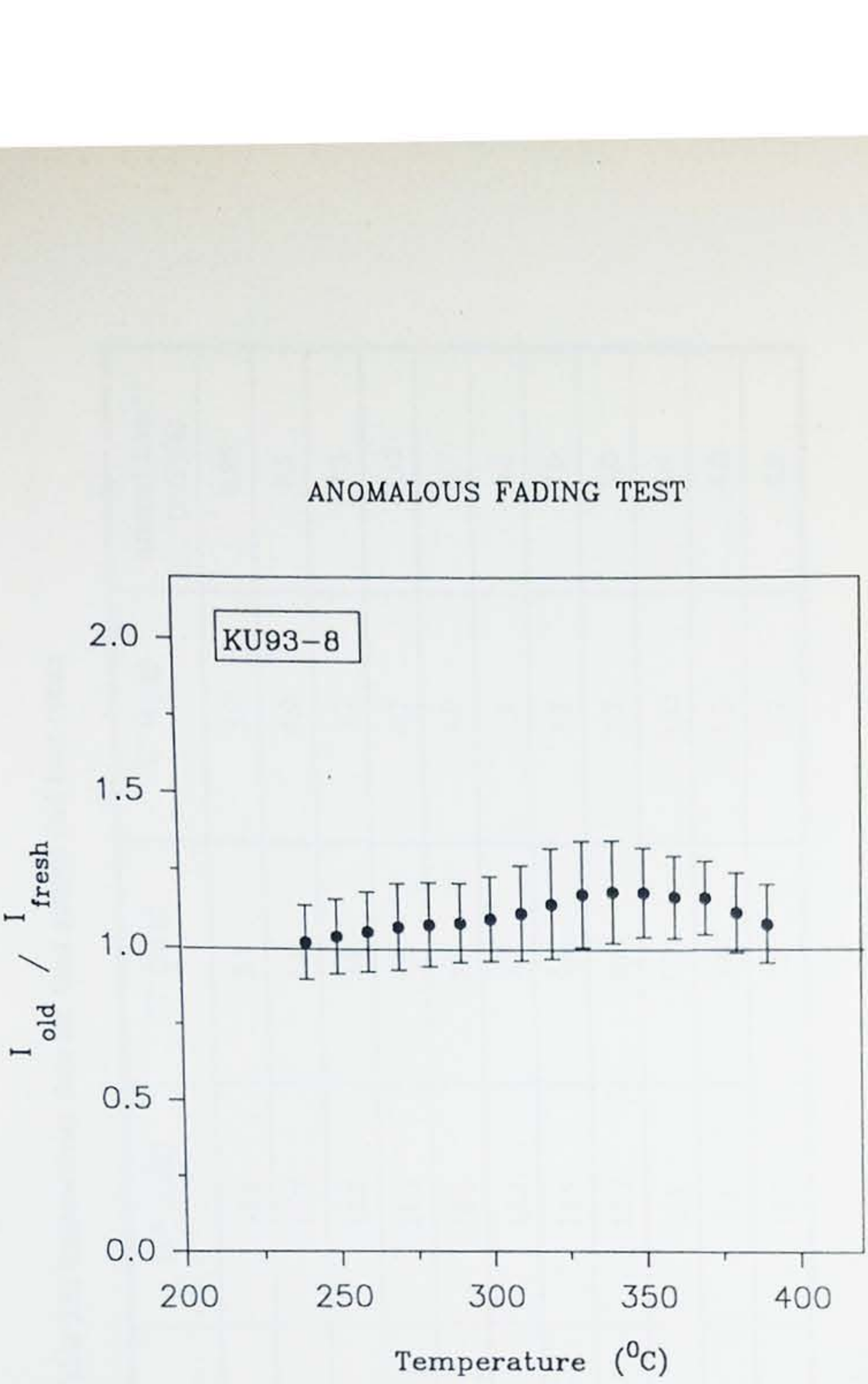
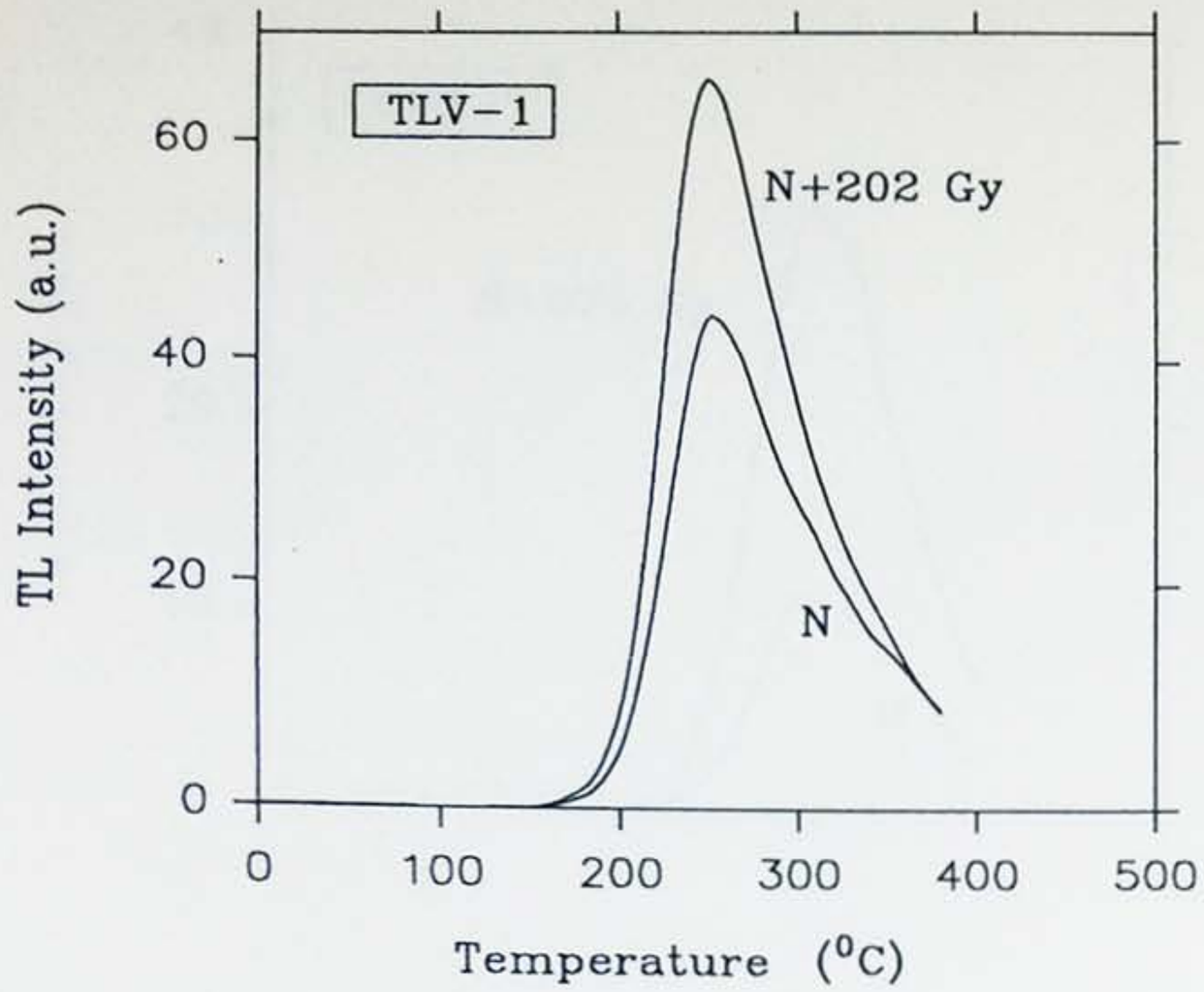


Fig 3.10: Anomalous Fading test for sample KU93-8. I_{fresh} represents the mean value of TL intensity of five aliquots which were recorded within 2-3 days after beta exposure. I_{old} is the mean TL intensity for aliquots which were stored for three weeks at 23^{0}C after beta exposure before TL readout was performed.

Table 3.5: Radioactivity data for fault gouges and host rocks

Sample	Type	Th* (µg/g)	U* (µg/g)	K+ (cg/g)	Annual Dose** (mGy/a)
KU91-4	Fault Gouge	12.4	5.1	3.0	6.95
KU91-5	Fault Gouge	11.7	6.2	4.0	8.5
KU93-1	Fault Gouge	13.6	3.9	3.7	7.6
KU93-2	Rocky Material	21.3	6.2	4.7	9.15
KU93-7	Fault Gouge	18.6	5.4	4.9	8.7
KU93-8	Rocky Material	12.7	3.7	3.7	6.3
TLV-1	Fault Gouge	18.5	5.4	3.7	7.9
TLV-3	Fault Gouge	20.7	6.1	2.7	7.0
TLV-5	Fault Gouge	2.4	0.7	0.85	1.4
MOH-1	Fault Gouge	9.1	2.6	1.3	4.0
MOH-3	Fault Gouge	12.3	3.6	1.2	4.9

* Error in Th and U concentrations is typically ~10%
** Water content (assumed) = 20% ± 6%
\+ Error in K concentration is typically ~5%



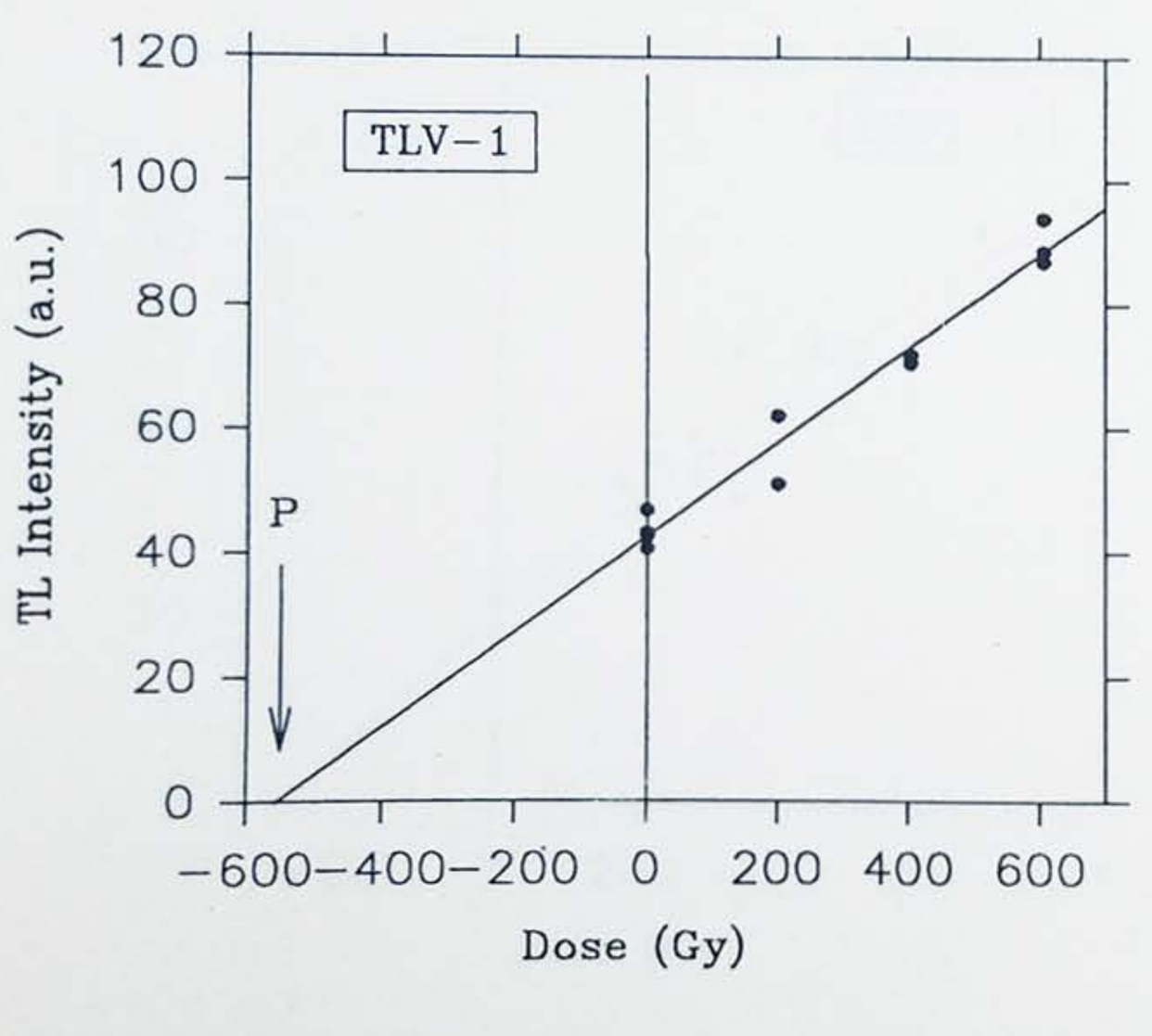
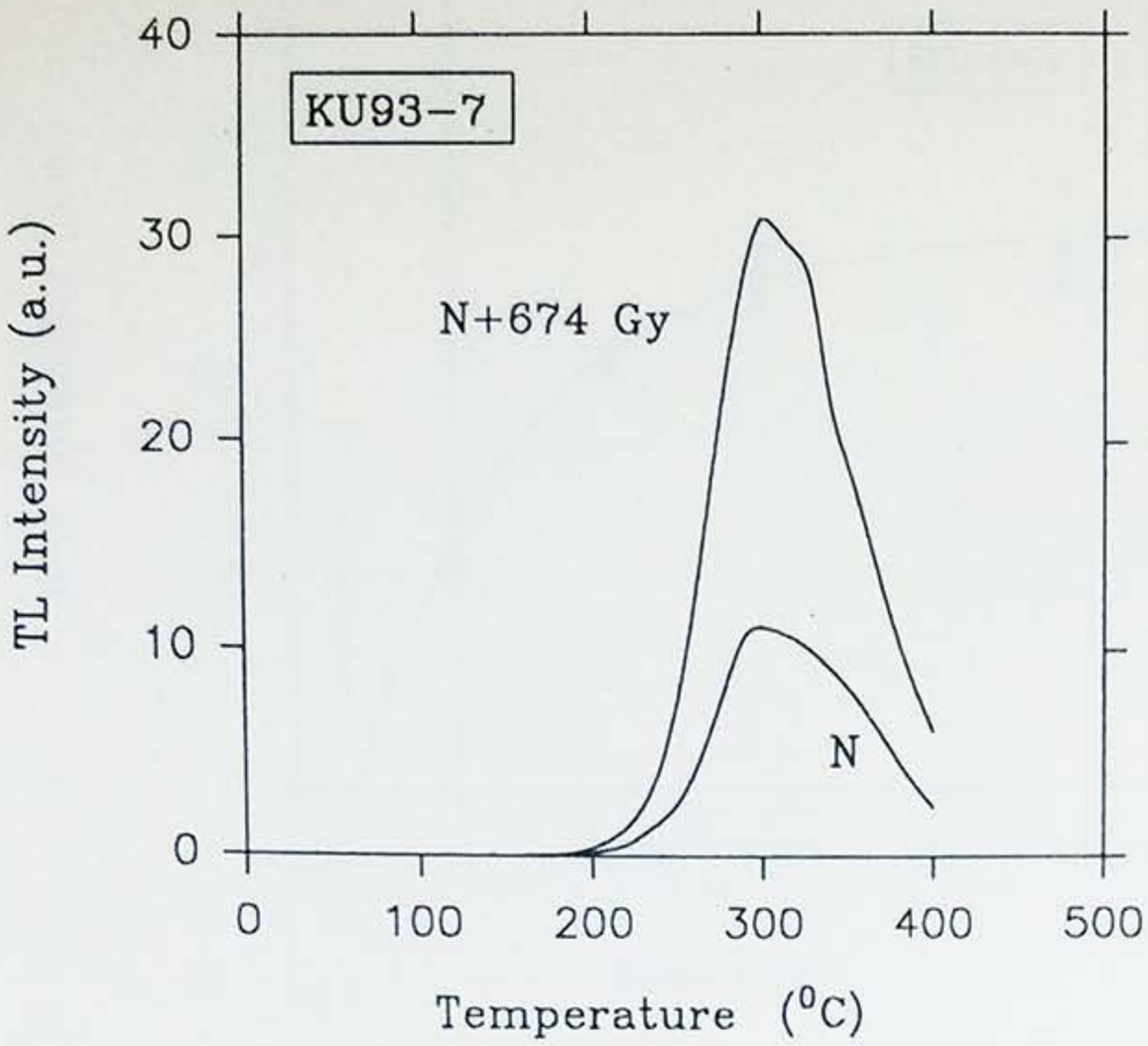


Fig. 3.11: TL glow and growth curves for fault gouge TLV−1 (4−11μ m). P indicates the paleodose.



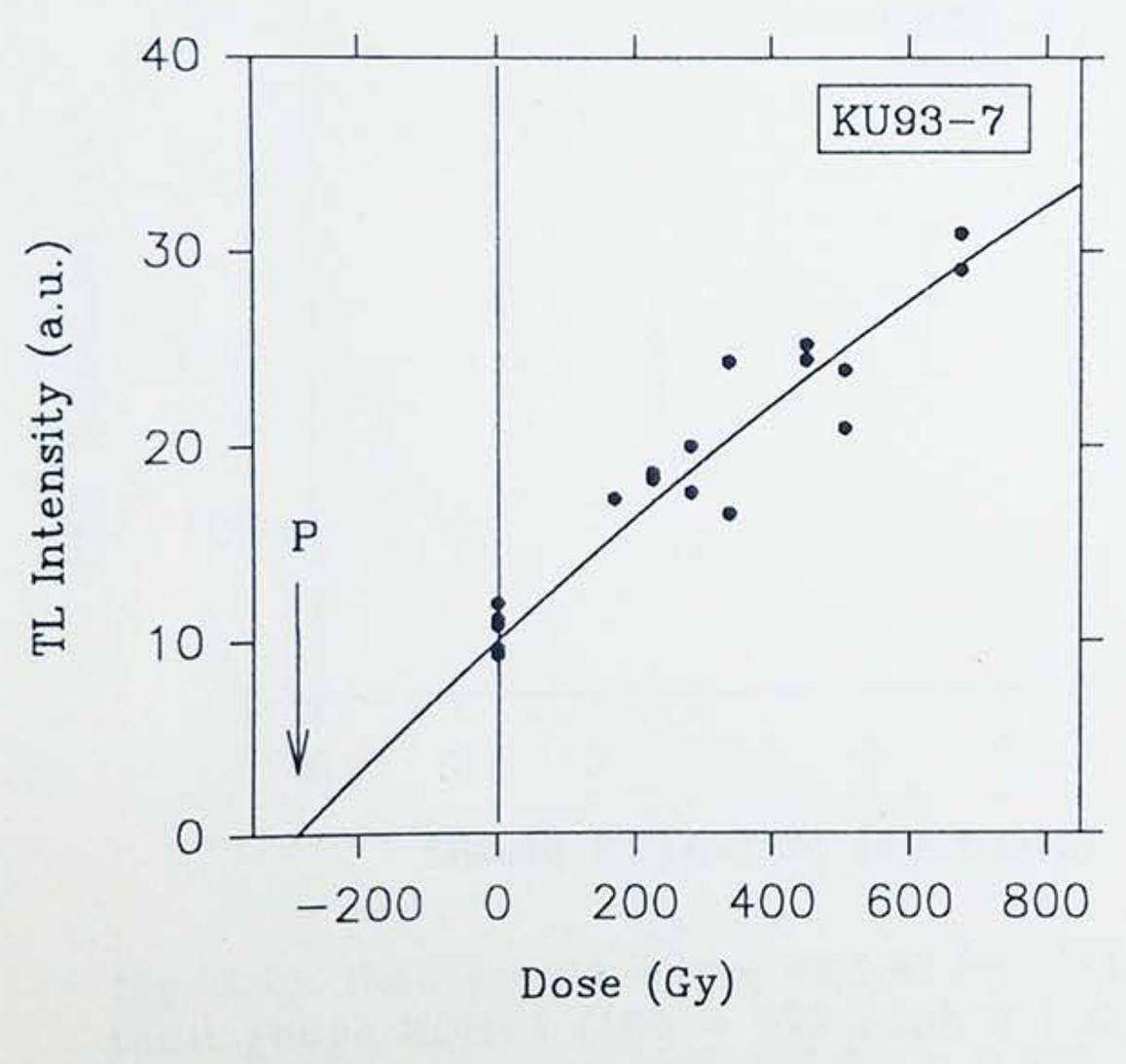


Fig. 3.12: TL glow and growth curves for fault gouge KU93-7 (106-150 μm). P indicates the paleodose.

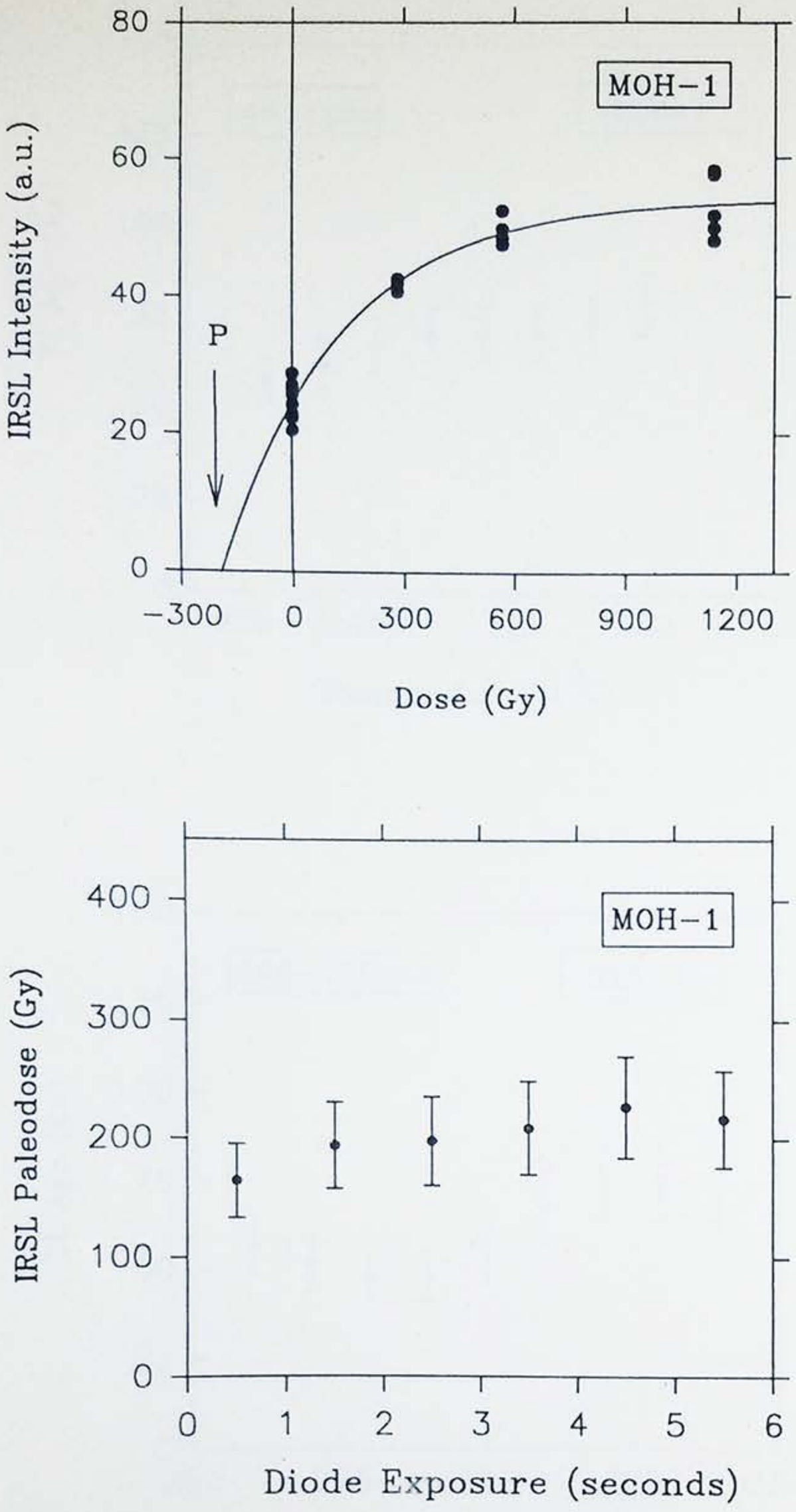
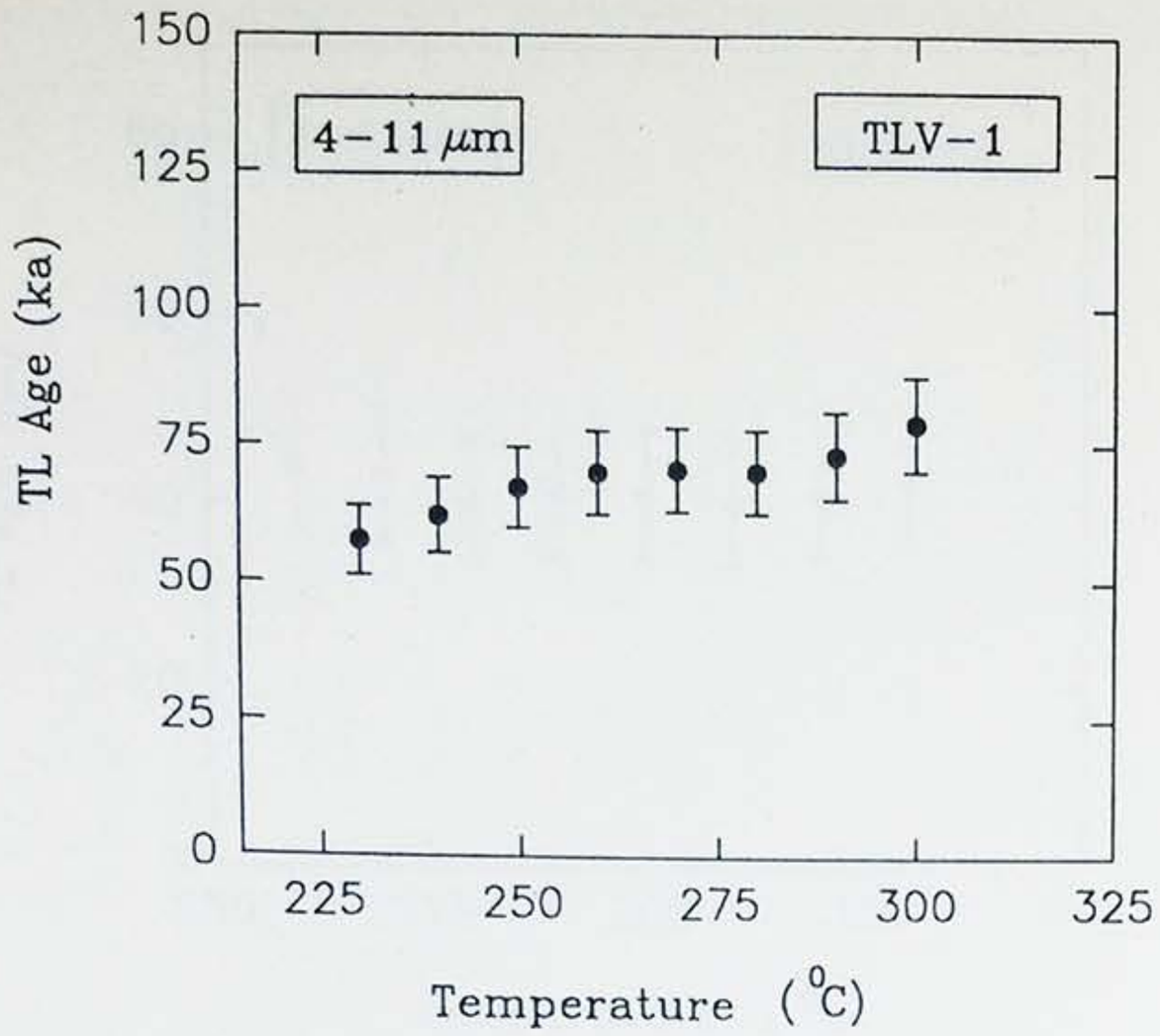


Fig. 3.13: IRSL growth curve and shine plateau for fault gouge MOH−1 (106 − 150 μ m). P indicates the IRSL paleodose.



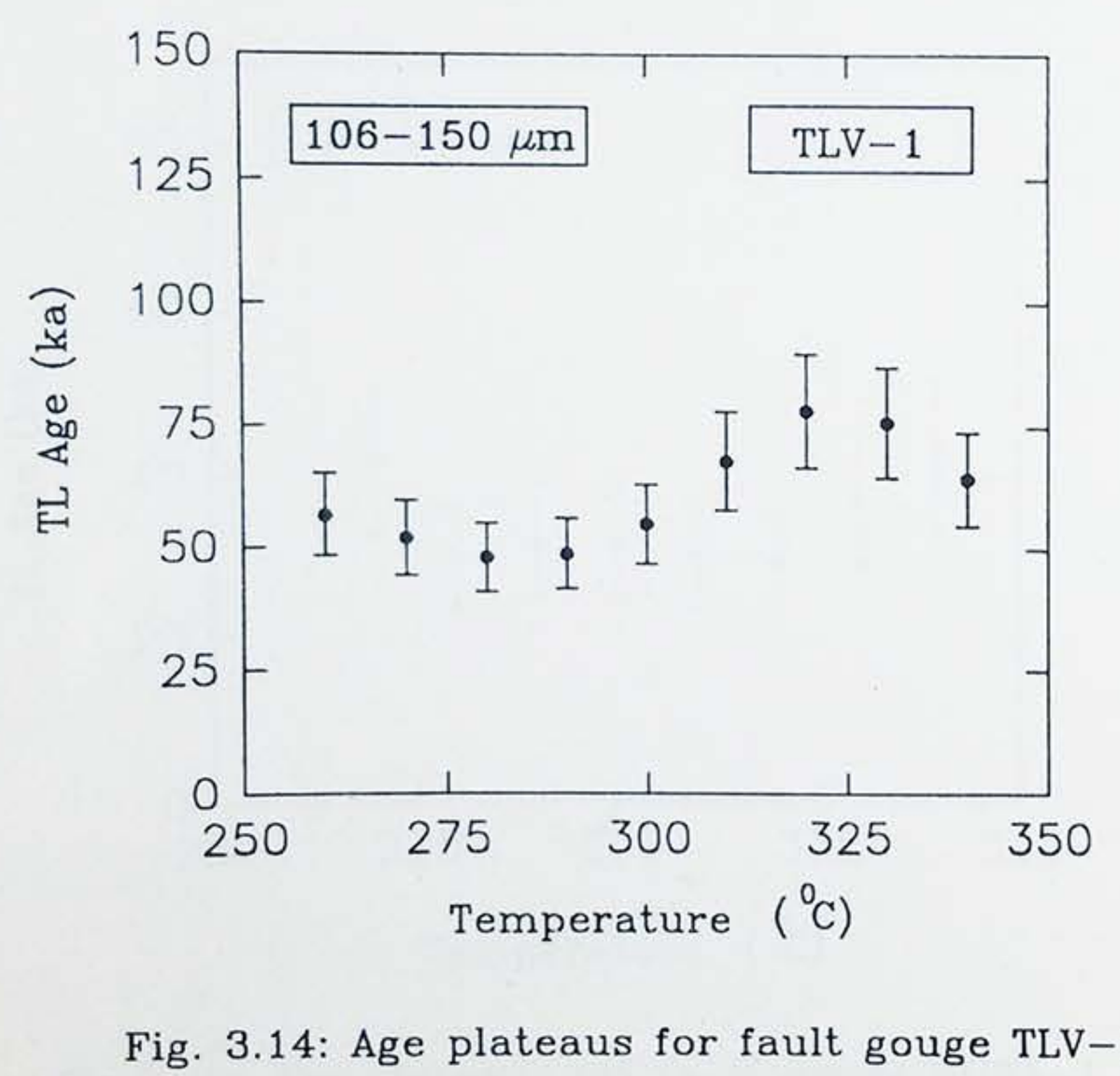
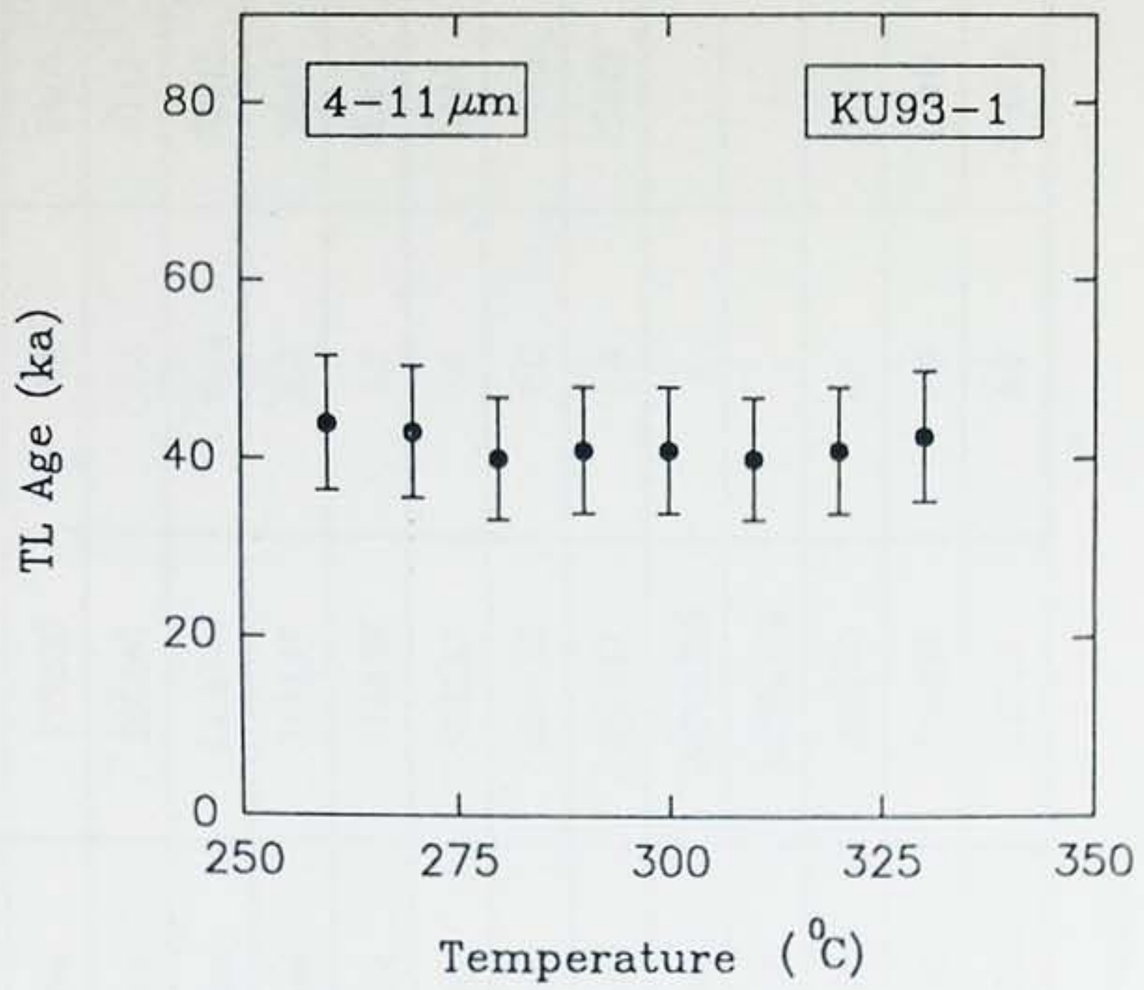


Fig. 3.14: Age plateaus for fault gouge TLV–1.



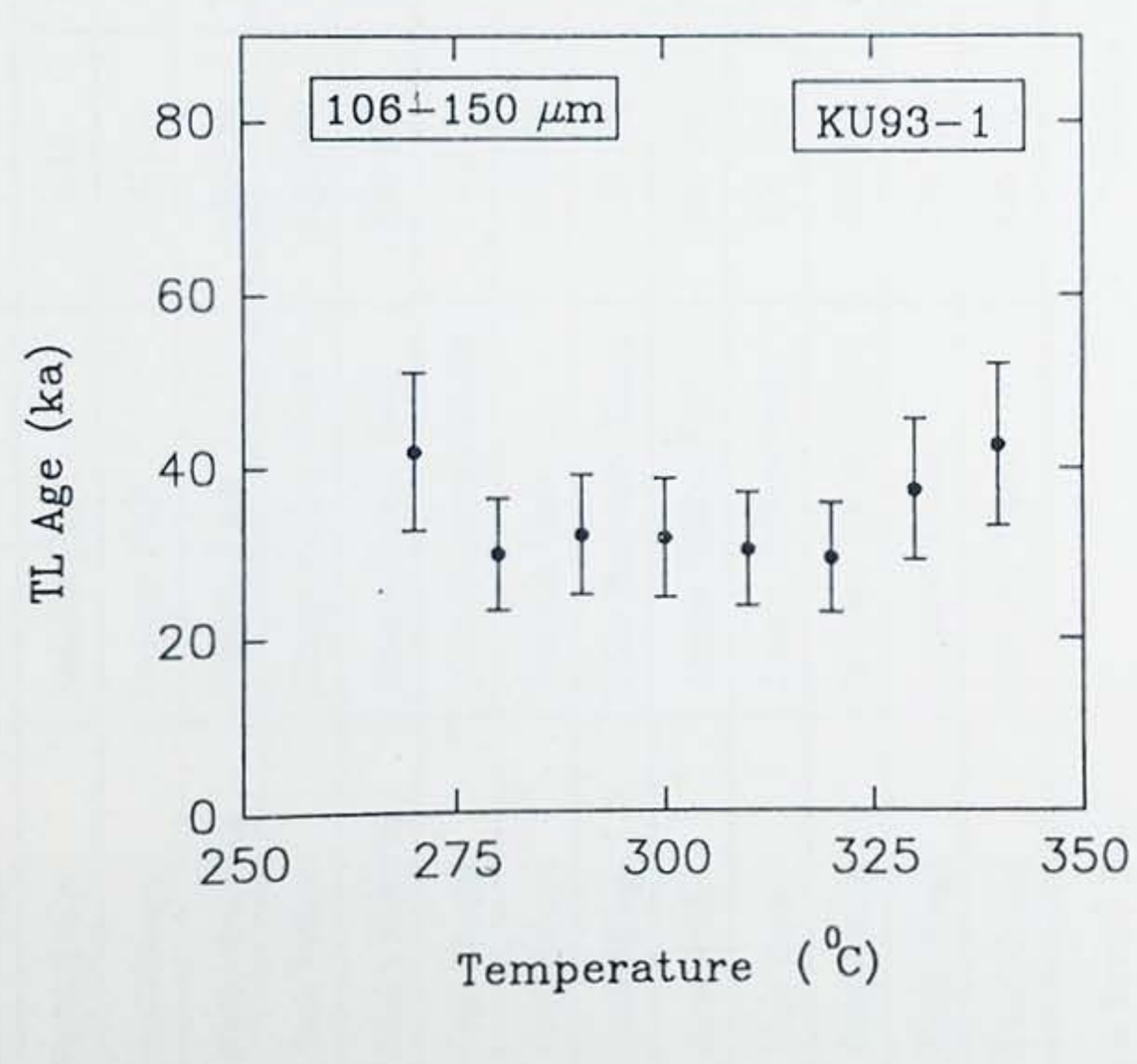


Fig 3.15: Age plateaus for fault gouge KU93–1.

Table 3.6: Luminescence dating results for fault gouges and host rocks

Sample	Type	Location	Grain Size (μm)	Technique	Paleodose* (Gy)	Annual Dose (mGy/a)	Age (ka)
KU91-4	Fault Gouge	Nainital Fault	106-150	TL, Additive Dose	264±50	6.95	38±8
KU91-5	Fault Gouge	Nainital Fault	4-11	TL, Additive Dose	375±30	8.5	44±4
KU93-1	Fault Gouge	Nainital Fault	4-11	TL, Additive Dose	308±61	7.6	41±7
KU93-2	Rocky Material	Nainital Fault	106-150	TL, Additive Dose	827±141	9.15	90±15
KU93-7	Fault Gouge	Sleepy Hollow Fault	106-150	TL, Additive Dose	311±31	8.7	36±5
KU93-8	Rocky Material	Sleepy Hollow Fault	106-150	TL, Additive Dose	518±39	6.3	82±10
TLV-1	Fault Gouge	Main Boundary Thrust	4-11	TL, Additive Dose	542±33	7.9	68±8
TLV-3	Fault Gouge	Nainital Fault	150-250	TL, Additive Dose	290±30	7.0	41±5
TLV-5	Fault Gouge	Main Boundary Thrust	106-150	TL, Additive Dose	102±17	1.4	72±12
KU93-5	Host Rock	Sleepy Hollow Fault	106-150	TL, Additive Dose	≥850±255	-	-
KU93-6	Host Rock	Sleepy Hollow Fault	106-150	TL, Additive Dose	≥650±128	-	-
MOH-1	Fault Gouge	Mohand Thrust (HFF)	106-150	IRSL, Additive Dose	202±40	4.0	51±9
MOH-3	Fault Gouge	Mohand Thrust	106-150	TL, Additive Dose	316±44	4.9	64±9
MOH-3	Fault Gouge	Mohand Thrust	106-150	IRSL, Additive Dose	310±26	4.9	63±7.4

HFF = Himalayan Frontal Fault

* Includes Supralinearity Correction

The mean of fault gouge TL ages from the Main Boundary Thrust is 70 ka.
The mean of fault gouge TL ages from the Nainital Fault is ~41 ka.
The mean luminescence age of fault gouges from the Mohand Thrust is ~59 ka.

(TLV−5) from Bajyun, MBT is extremely low (∼ 1.4 mGy/a) in comparison to other fault gouges. This sample was counted thrice to ensure the authenticity of the alpha count rate and the potassium concentration. The low annual value of annual dose could be due to the presence of larger amounts of calcium carbonate in the gouge matrix. This hypothesis is plausible considering the presence of limestones in this area. The U and Th concentrations of the fault gouges are generally high as fault zones often serve as sites of mineralization.

The aliquot-to-aliquot scatter in TL intensity for coarse-grained fractions is generally higher than the 4−11 μm fraction. This is probably due to the use of the weight normalization procedure for normalising TL intensities of coarse fractions. Weight normalization is based on the premise that TL emission from an aliquot is proportional to the number of grains in the aliquot, in effect assuming that (i) each grain is luminescent and (ii) TL emission per grain is constant over the entire aliquot. These assumptions will not be satisfied if only a few of the grains comprising the sample emit thermoluminescence. The 4−11 μm fraction was normalised using the natural normalisation (∼ 1 second shortshine IRSL intensities) technique, which being a luminescence based technique should be more effective in reducing aliquot-to-aliquot scatter.

The samples KU91-4 and TLV-3 were collected near Jeolikot, Nainital Fault, in 1991 and 1993. KU91-5 and KU93-3 were also sampled near Deopatta, Nainital Fault, in 1991 and 1993. The TL ages for these fault gouges (Table 3.6) indicate that the TL ages are reproducible.

Chronology

The results of luminescence dating provide evidence for neotectonic activity at the Nainital and Sleepy Hollow Fault at 41 ± 8 ka and 36 ± 5 ka respectively. The Mohand Thrust fault gouge is dated to 59 ± 10 ka. Fault gouge in the Main Boundary

Thrust gave an age of around 70 ± 12 ka ago. Absence of organic material at the fault gouge sites precluded any comparisons between ^{14}C and luminescence ages. However, radiocarbon analysis of lake sediments from lakes contemporary to Nainital Lake give a ~ 50 ka formation age of Nainital Lake which is believed to have been created by movement along Nainital Fault. Along the North Almora Thrust and South Almora Thrusts (~ 30 km from Nainital), faulting resulted in the blocking of rivers and formation of lakes (Valdiya, 1996). ^{14}C dating of charcoal from L.Wadda (~ 30 km from Nainital) indicates that the L. Wadda was formed 44 ka BP by movements along Kotli Fault, which runs parallel to North Almora Thrust (Valdiya, 1996). Thus, the agreement between formation age of Nainital Lake, L. Wadda and the TL faulting age lends some credence to the applicability of the luminescence dating techniques. IRSL dating was also performed along with TL dating on Mohand Thrust fault gouges. IRSL (63 ± 7 ka) and TL ages (64 ± 9 ka) of faulting along Mohand Thrust concur with experimental errors. This also suggests that IRSL dating can be developed for reliable dating of heated objects. IRSL ages could not be determined on the other fault gouges since the total photon counts obtained under stimulation were insufficient for evaluation of a proper age.

For host rocks from the Sleepy Hollow Fault, paleodose estimates evaluated using a saturating exponential fit have been presented in Table 3.6. Since the TL intensities exhibit a saturating behaviour over a large dose range of 0–800 Gy, the host rock paleodoses are minimum estimates and have a large error associated with them.

The samples (KU93-2 and KU93-8) collected ~ 3–4 metres away from fault gouges gave higher TL ages (90 ± 15 ka, 82 ± 10 ka) compared to the ages obtained at the fault. This is probably a consequence of (i) partial zeroing of the TL signal during faulting at 40 ka or (ii) an older faulting event (possibly contemporaneous with the 70 ± 12 ka MBT event) at ~ 86 ka since the possibility of repeated faulting events in the same zone cannot be ruled out. Scholz (1987) has demonstrated that recurrence

of faulting (increasing slip) results in increasing thickness of the gouge zone produced during faulting. Further dating work is necessary to resolve this issue.

Chapter 4

Chronology of Paleoseismic/Neotectonic Events : Luminescence dating of seismites, river terraces and soils developed on colluvium

Deformation structures in soft sediment overbank/shallow water deposits (seismites) formed during/immediately after deposition are potentially important indicators of past seismic activity (Sims, 1973; Allen, 1975). Uplifted fluvial terraces are geomorphic expressions of neotectonic activity and can be used for estimating the rates of tectonic activity (Lensen and Vella, 1971; Vhora, 1987). Buried soils within fault scarp derived colluvium can provide constraints on the time of faulting (Forman et al., 1988). This chapter begins with a description of the first attempt to date seismites using the IRSL and TL dating techniques. Subsequently, luminescence dating of soils developed on colluvium and uplifted river terraces is discussed.

4.1 Luminescence Dating of Seismites : Zeroing of the Luminescence signal

The luminescence methods are based on the premise that a short duration of predepositional sun exposure can reduce the geologically acquired IRSL/TL signals of the minerals constituting the sediment to a low value. This resets the IRSL/TL clock (Huntley et al., 1985). On burial, sun exposure ceases and a fresh acquisition of luminescence (IRSL/TL) is initiated through irradiation from ambient natural radioactivity (viz., ^{238}U, ^{232}Th and ^{40}K). This reaccumulation continues unabated until excavation. The luminescence age is then given by the expression

$$\mathsf{Age} = \frac{\mathsf{EquivalentDose}}{\mathsf{AnnualDose}} \tag{4.1}$$

Various field and laboratory studies have previously shown that the deformed sediments were present at the sediment-water interface during the deformation event (Kuenen, 1958; Sims, 1973, 1975; Allen, 1975), suggesting that the time interval between the deposition of the sediment and its deformation is small compared to the deformation age of the sediment. It has also been previously demonstrated that the IRSL/OSL signals of shallow lacustrine/fluvial sediments is well bleached at the time of deposition (Stokes, 1992; Balescu and Lamothe, 1994). In the present studies on the feasibility of using luminescence methods for dating seismites, the applicability of the zeroing assumption was ascertained by examining the bleachability of IRSL signal with sunlight. In view of the rapid bleaching rate of IRSL of sediments (Fig. 4.1) and their transport duration of 10-200 hours before deposition, it is reasonable to assume that these sediments have indeed undergone a predepositional optical bleaching. The seismites would thus have a near zero IRSL signal at the time of deformation and thus satisfy the basic assumption of zeroing in luminescence dating.

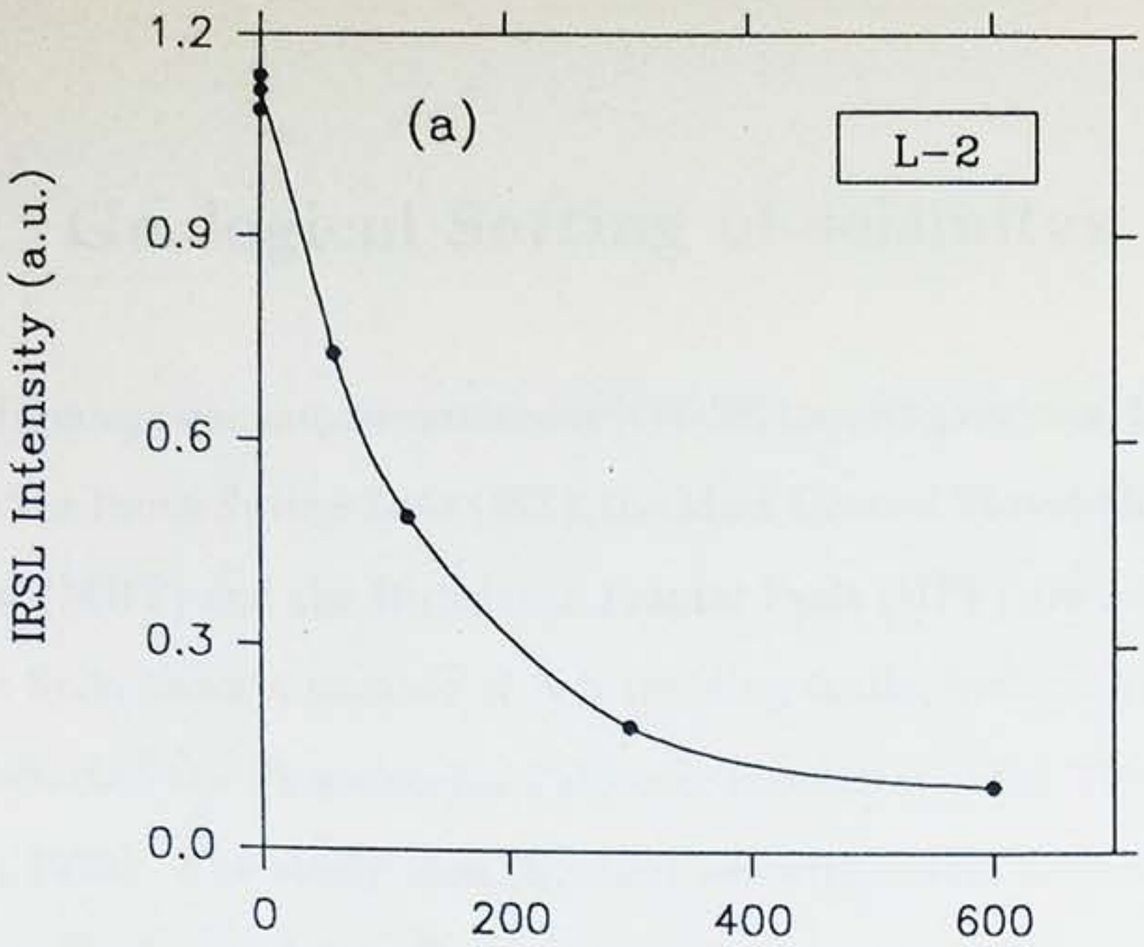


Fig. 4.1a: IRSL bleaching curve for a typical seismite. The IRSL intensity reduces to 8% of its initial value after exposure to natural sunlight filtered through a 4 mm thick transparent window glass for ~10 minutes.

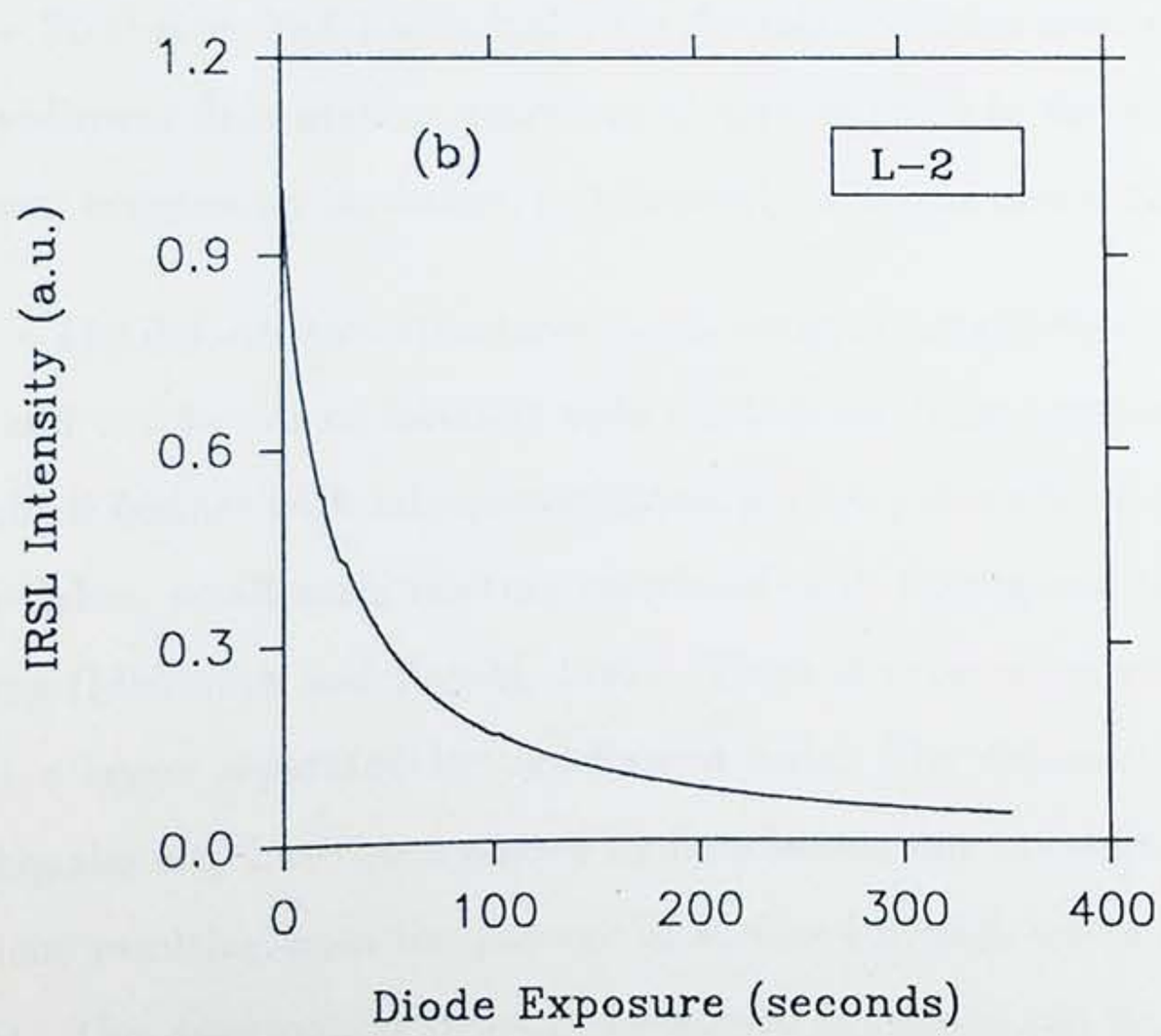


Fig 4.1b: Decay of IRSL with time for the seismite on exposure to LED emitting at 880 nm. Comparison with fig. 4.1a above shows that diode exposure for ~200 s is equivalent to an exposure for about 600 s of filtered natural sunlight in reducing IRSL intensity to 8%.

4.2 Geological Setting of seismites

The Himalaya encompass numerous NW-SE trending regional thrusts/faults (Fig. 4.2) of which the Indus Suture Zone (ISZ), the Main Central Thrust (MCT), the Main Boundary Thrust (MBT) and the Himalayan Frontal Fault (HFF) are noteworthy (Valdiya, 1992). In the Spiti basin a number of N-S trending faults, including the Kaurik-Chango Fault have affected the Precambrian-Paleozoic succession of the Tethys Himalaya (Gupta and Virdi, 1975). The study area (Sumdo) lies within 4km from the active zone of Kaurik-Chango Fault and has suffered at least 9 major earthquakes of magnitude greater than 6 on the Richter scale including the 1975 Kinnaur earthquake which caused widespread damage, landslides and ground rupturing (Mohindra and Bagati, 1996).

The Late Pleistocene-Holocene sedimentary basin in the cold-arid Sumdo region (3200 m above MSL) is represented by fluvio-lacustrine deposits. At the confluence of the Spiti river and Padra Nala, the fluvial/lacustrine sediments are associated with soft sediment deformation structures at various levels in the 120 m thick stratigraphic column, comprising sandstone, conglomerate, siltstone and mudstone (Fig. 4.3).

The deformation structures S_1-S_8 occur at irregularly spaced stratigraphic intervals and can be traced laterally upto a kilometre. These structures include a ruptured anticlinal feature with intrusive sediment plumes / dune-like feature, a flame structure, sand dykes, small scale faulting associated with folding and large scale soft sediment folding (Mohindra and Bagati, 1996). These structures are restricted to single stratigraphic layers separated by undeformed beds. The deformation of sediments during earthquake may have been caused by liquefaction due to cyclic loading and undulatory motions resulting from the passage of surface Rayleigh waves (Seed 1968; Sims, 1973, 1975). The deformation structures observed in Sumdo can be associated with seismic

1 (90)

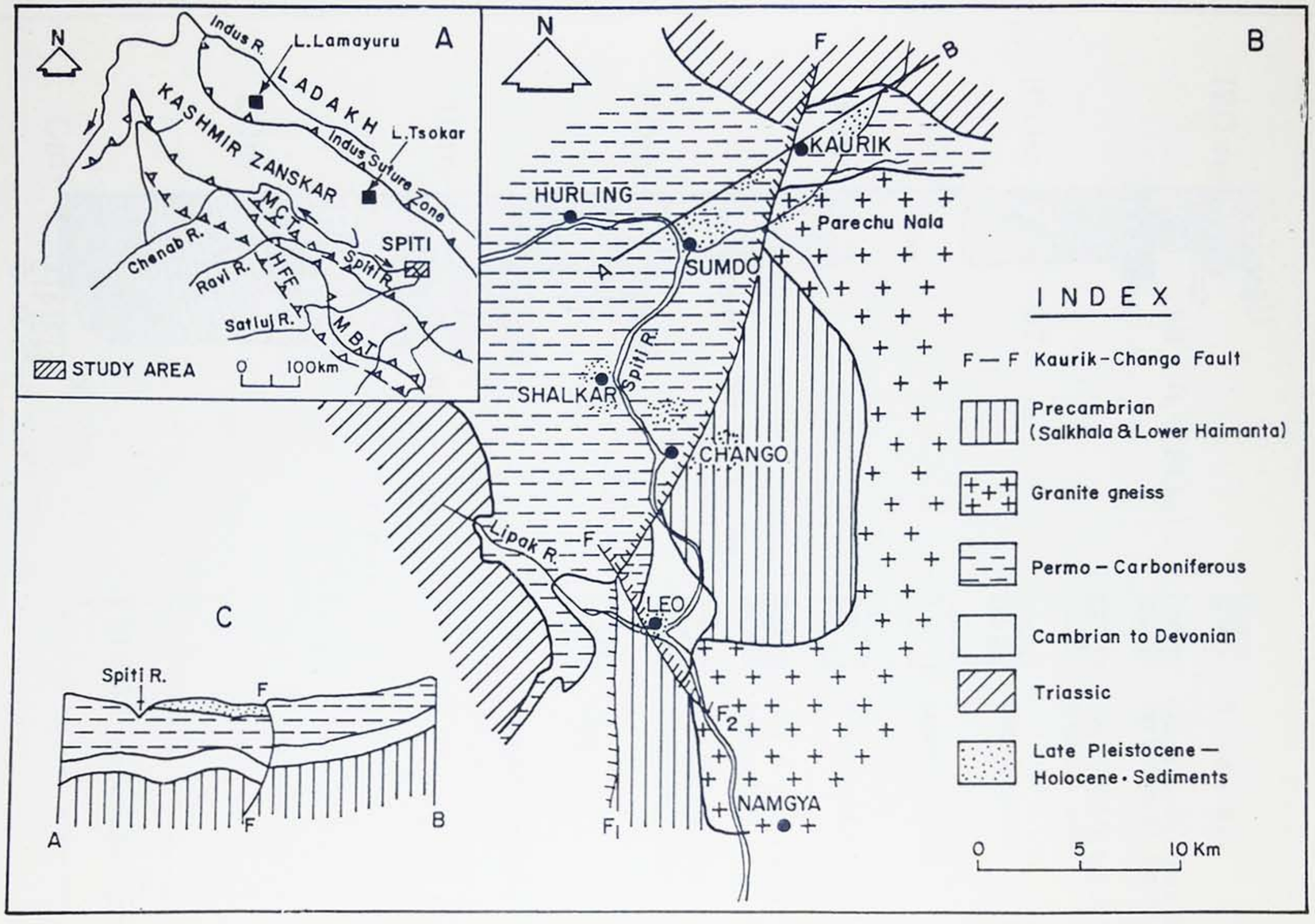


Fig. 4.2 (a) Index map showing general tectonic trend in the northwestern Himalaya and location of the study area, (b) Geological map around Sumdo (after Mohindra and Bagati, 1996), (c) Cross-section along A-B.

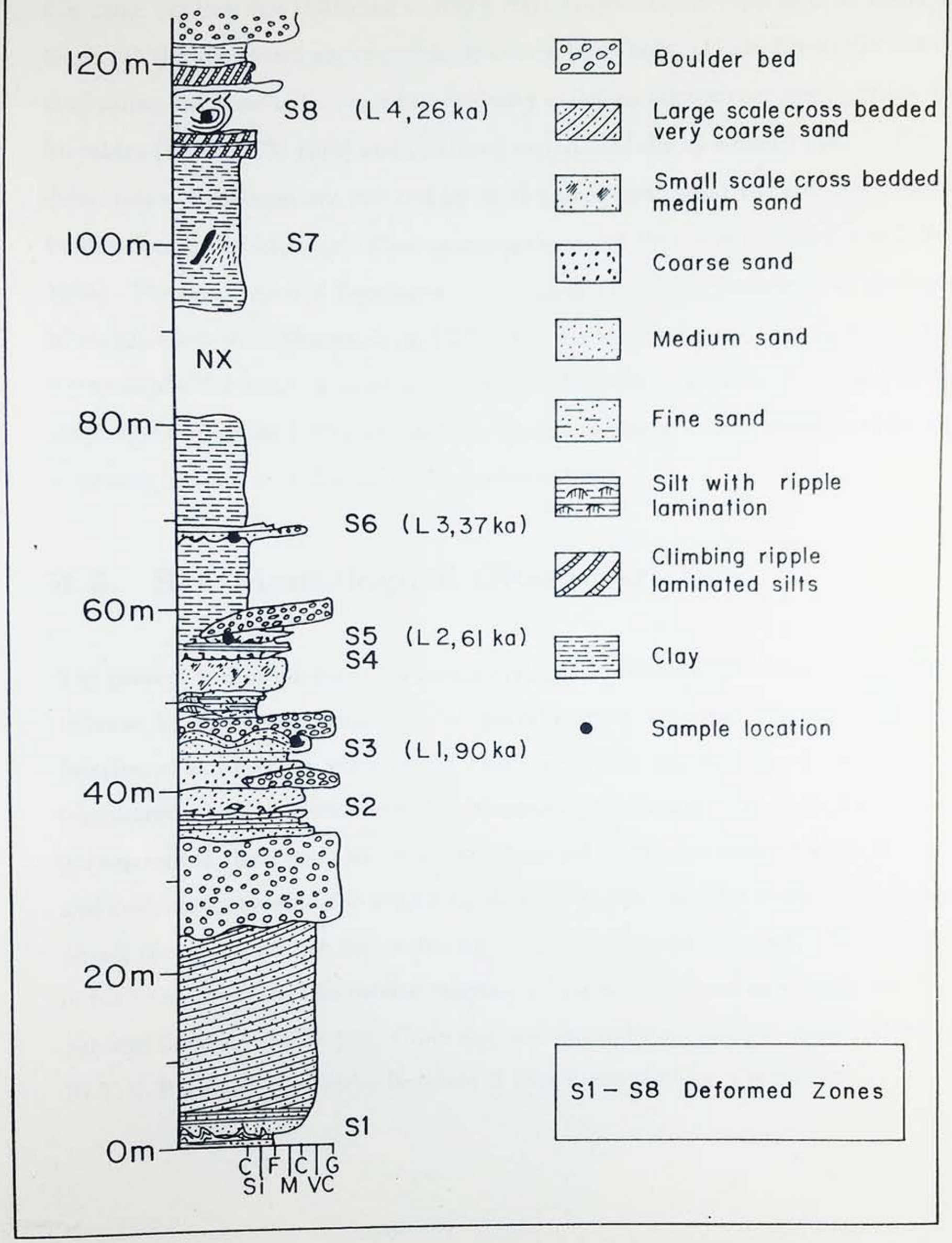


Fig. 4.3. Composite lithostratigraphic column showing deformed zones (S_1-S_8) and facies variation in Sumdo area. Note the location of samples analyzed for dating.

events as they satisfy Sims' (1973; 1975) criteria : (1) they lie close to a seismically active zone; (2) they are restricted to single stratigraphic layers separated by undeformed beds; (3) the structures are correlatable over a large area; (4) the layers are flat-lying, thus ruling out slope failure and (5) similarity to deformation structures described in the literature (Sims, 1973; 1975) and produced experimentally by Kuenen (1958). Thus, the deformation structures are induced by earthquakes and depict the combined effects of fluidization, liquefaction and sheer stress as discussed elsewhere (Mohindra and Bagati, 1996). The occurrence of liquefaction in sediments has been correlated to earthquakes of magnitude > 6.5 (Morgenstern, 1967). The deformation structures S_3, S_5, S_6 and S_8 were sampled for luminescence dating. Since no lake fills existed near the Kaurik-Chango fault zone during the 1995 earthquake, a modern analogue of soft-sediment deformation structure was not available for luminescence dating.

4.3 Sedimentological Characteristics

The present samples represent a fluvial cycle with overbank sediments upto 58 m level followed by lacustrine sediments with periodic sandy influxes. The lithology and the location of samples are given in Fig. 4.3. The grain size analysis of the samples for luminescence dating show bimodal to polymodal distribution (Fig. 4.4). The statistical parameters of these samples show that these sediments are moderately to well sorted and are near symmetrical to negatively skewed. At the transition of fluvial to lacustrine phase, the sediments are well sorted and negatively skewed (Fig. 4.4). The mineralogy of both the fluvial and lacustrine sediments show dominance of quartz followed by calcite and feldspar (Table 4.1). Grain size and mineralogical analysis were performed by Dr.T.N. Bagati at the Wadia Institute of Himalayan Geology, Dehradun.

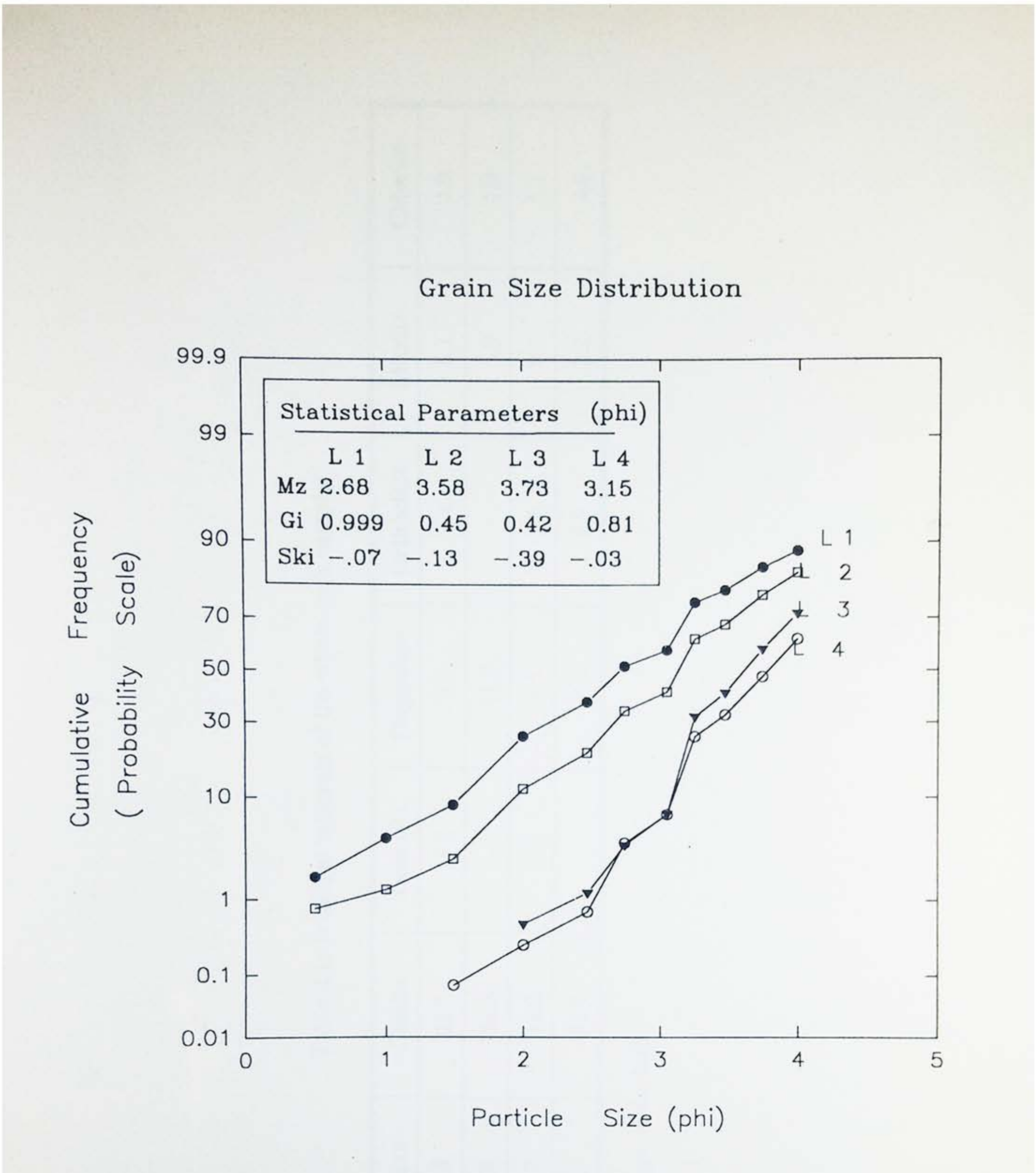


Fig. 4.4: Grain Size distributions for the seismites. MZ, SKI and GI indicate mean size, sorting index and skewness of the distributions.

Table 4.1: Principal minerals of the whole rock sample+

Sample No.	Quartz	Calcite	Dolomite	Plagioclase	Orthoclase	Micrite	Chlorite
L-1	38.8	22.7	11.3	8.6	7.4	6.1	4.9
L-2	38.7	38.5	-	11.9	-	5.9	5.0
L-3	47.7	18.2	7.8	8.6	3.6	8.7	5.1
L-4	47.7	31.6	-	7.6	6.9	2.2	4.9

+ Expressed as % by weight of the bulk

4.4 Climatic Attributes

The Sumdo region forms part of the cold arid desert. The humidity is maximum (85.5%) during summer and minimum (49%) during winter. The average rainfall during winter-spring transition is 14 mm, 23 mm during summer and 440 mm during winter. Snowfall of 17–20 m is common during winter.

The sediment transport with maximum water discharge occurs during April-August and is minimum during winter. No quantitative data on the river discharge and sediment transport from the basin was available. However, field observations show that the amount of water is about 50 times more in summer in comparison to winter. The transport from the catchment is about 5–300 km and implies a transport duration of 10–200 hrs and thus it is reasonable to infer that most of the sediments did get exposed to finite daylight during weathering and transportation prior to deposition.

4.5 Experimental Details

The experimental analysis was carried out using the infra-red stimulated luminescence (IRSL) (Hutt et al., 1988) and the TL dating methods (Aitken, 1985; Berger, 1988). The extraction of K-feldspar was made using a sequential pretreatment of the sample using 1N HCl, 30% H_2O_2, sieving 75–106 μm and density separation using Na polytungstate (density = 2.58 g/cm^3). In view of limited sample availability, no HF etching of these grains was done, and an alpha dose corrected for attenuation was considered in the estimation of the annual dose. Attenuation in beta dose was also taken into account in annual dose calculations (Mejdahl, 1979). Monolayers of the grains were deposited on stainless steel discs. The irradiations were made using a 25 mCi $^{90}Sr-^{90}Y$ beta source. The IRSL intensities of the natural and the irradiated discs were normalized using 1

11045

second shortshine glows. The optics channel comprised a EMI 9635 QA coupled to Corning 5-58 + 7-59 blue filters and a Daybreak photon counting system interfaced to an IBM/PC with an Ortec Accuspec multi−scaling card. Sixteen IRSL diodes (TEMT 454) with peak emission at 880 ± 80 nm (operated with a programmable constant current supply) were used for shinedown curves. In one case (L−4) the 75−106 μm K-feldspar yield was negligible and hence the fine grain method was used and a R−β TL analysis was done. The low photon yield of green light stimulated luminescence (GLSL) from quartz precluded a GLSL analysis. Fine grains (4−11 μm) were extracted after pre-treatment of 1N HCl, 30% H_2O_2, 0.01N Na-oxalate and Stokes separation in acetone.

The TL measurements were performed using two Schott UG-11 filters, a quartz ND-1 filter and Chance Pilkington HA-3 filter coupled to an EMI 9635 QA photomultiplier tube and a photon counting system. Alpha irradiations were made in vacuum using a six seater 0.22 mCi ^{241}Am vacuum alpha irradiation system (Singhvi and Aitken, 1978). The sample aliquots were sunbleached under (i) clear sun for 30 minutes and (ii) shaded sun for 5 minutes and the equivalent dose was calculated using the partial bleach method. Second glow normalisation was used. Linear and saturating exponentials were fitted for α and β growth curves respectively. The inverse variance method was used for calculation of error in equivalent dose. An alpha-efficiency factor of 0.15 ± 0.075 was assumed for coarse-grained K-feldspars. U and Th concentrations were estimated using thick source ZnS (Ag) alpha counting method and NaI(Tl) gamma ray spectrometry was used for potassium estimation. A radioactive equilibrium in the decay series of U and Th was assumed in the dose rate calculations. The cosmic ray dose rate was assumed to be 150 μGy/a. Error estimation was carried out following the prescription of Aitken (1985).

4.6 Results and Discussion

Table 4.2 provides luminescence data for the four seismites. Figure 4.5 provides a typical IRSL experimental data set. The luminescence (IRSL/TL) dates (Table 4.2) of the seismic events S_3, S_5, S_6 and S_8 are 90 ka, 61 ka, 37 ka and 26 ka respectively. The analysis of the sample L–4 proved to be enigmatic. In contrast to the other samples, L–4 did not yield an appreciable amount of fine-sand sized K-feldspar. Consequently, the fine grain method was used. Although the fine grain discs were sensitive to IRSL, the total photon counts were far too low enough to carry out a reasonable analysis. Accordingly, a TL analysis was done for L–4 and the partial bleach (clear sun, 30 minutes) method gave an age of 26 ka. A preliminary analysis with a sun exposure of 5 minutes under a shaded sun was also carried out for this sample and the reduction in thermoluminescence intensity due to bleaching was used for evaluating an age of $\sim$ 20 ka. This implied that an age of 26 ka is a reasonable estimate for S_8. Quartz extracted from L–4 was also used for the evaluation of a TL age. The slide method (Prescott et al., 1993) equivalent dose was used along with the fractional reduction in TL intensity after a 2 minute bleaching (shaded sunlight) to estimate an age for L–4. The quartz (35 $\pm$ 9 ka) and fine-grain (26 $\pm$ 4.3 ka) TL ages appear concordant within experimental errors despite their varying bleaching behaviour. However, the slow growth of the quartz TL signal in a dose range of 0-600 Gy results in a large error in the extrapolation of the growth curve for determining the equivalent dose. Thus, TL dating of quartz extracts was not attempted on the remaining samples.

It may be apposite to consider the possibility of radioactive disequilibrium in such a fluvial/lacustrine environment. This could not be attempted in the present case due to limited sample availability. However, in view of the fact that upto $\sim$ 55% of the total dose is contributed by potassium, the material being transported by water over short durations and a general concordance of radioactivity data derived assuming an

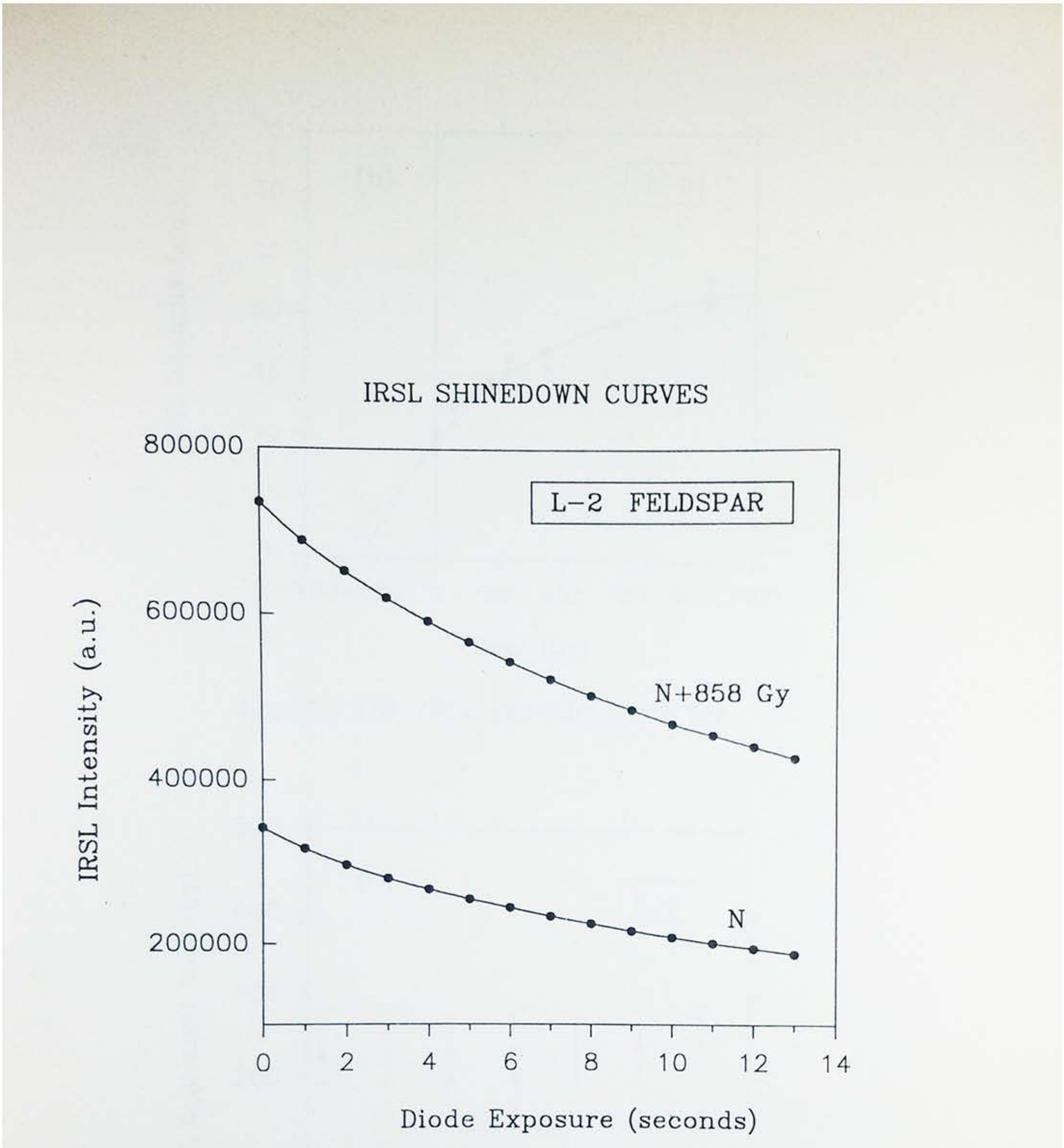


Fig. 4.5(a): IRSL shinedown curves for feldspar extracts from seismite L-2.

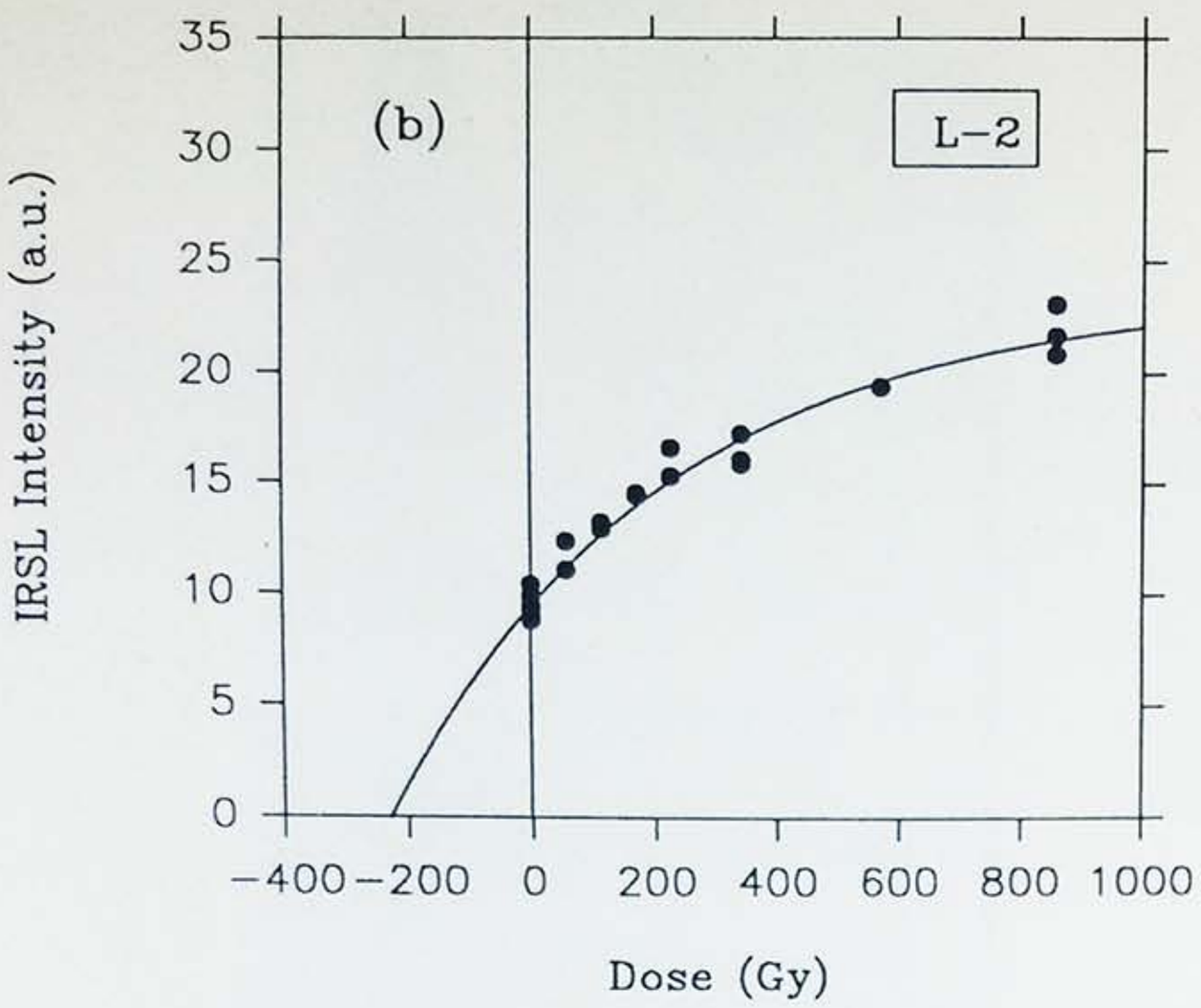


Fig. 4.5 (b): IRSL growth curve for L–2.

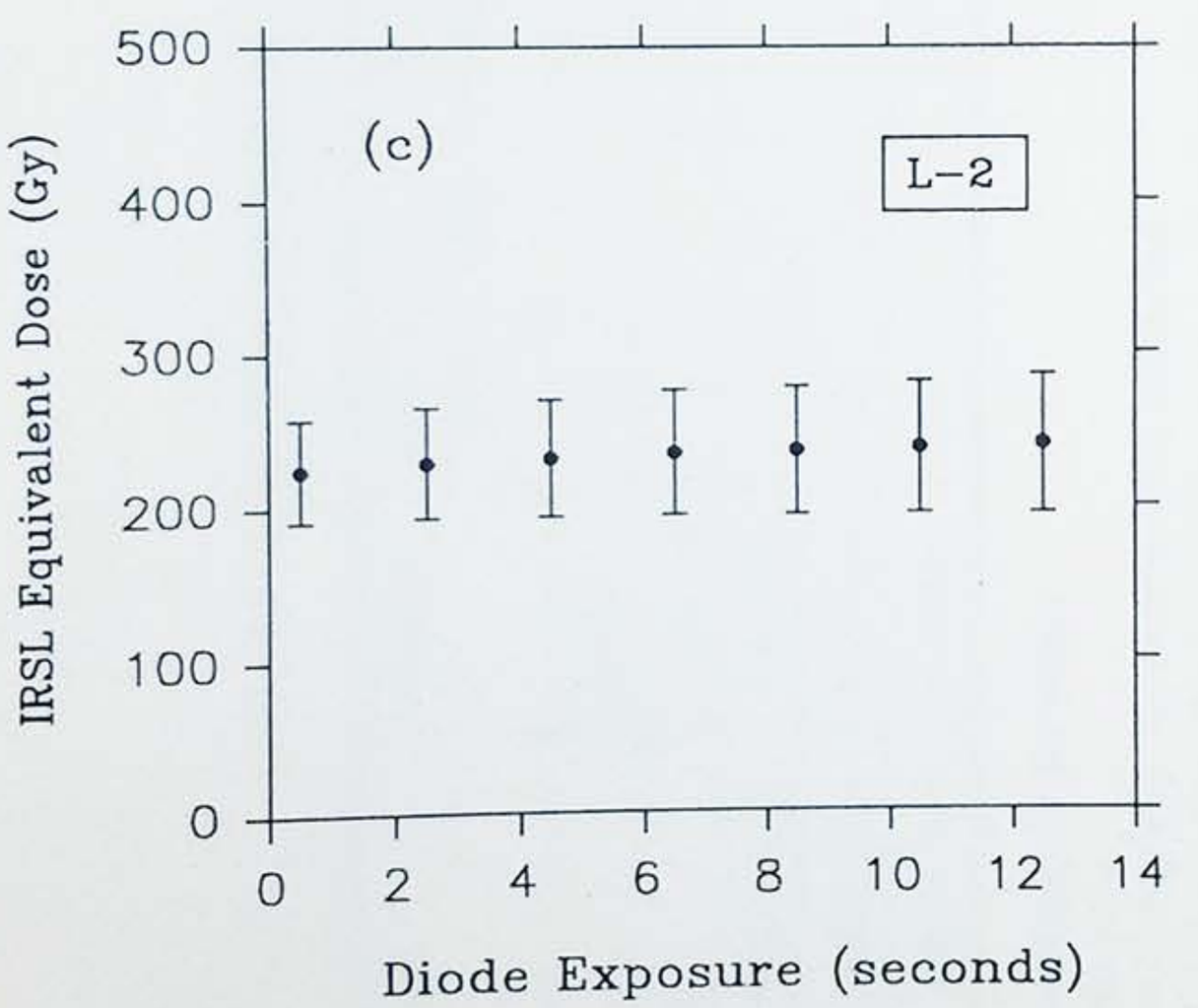


Fig. 4.5 (c): IRSL shine plateau for L–2.

Table 4.2 : Luminescence Dating Results for Seismites from Spiti Valley, India

Sample	Technique	Mineral	Th (µg/g)	U (µg/g)	K (cg/g)	*a* value	Water content* (%)	Annual Dose (mGy/a)	Equivalent Dose (Gy)	Age (ka)
L-4	TL[+]	Quartz	5.4	1.6	0.8	-	0.3	1.9	66±14	35±9
L-4	TL, R-ß	Fine grains	5.4	1.6	0.8	0.12[#]±0.06	0.3	2.9	74±15	26±4.3
L-3	IRSL, Additive Dose	K-feldspar	12.6	3.7	1.6	0.15[$]±0.075	0.5	4.5	165±21.4	37±5.2
L-2	IRSL, Additive Dose	K-feldspar	8.9	2.6	1.75	0.15[$]±0.075	0.3	3.8	232±34.2	61±9.5
L-1	IRSL, Additive Dose	K-feldspar	9.4	2.7	1.96	0.15[$]±0.075	0.2	4.1	372±33.4	90±10.5

* Water content as percentage of dry weight
\+ See discussion in the text
\# The a value for L-4 (fine-grains) was experimentally determined.
$ The a-values for K-feldspars from samples L-3, L-2 and L-1 was assumed to be 0.15±0.075.

equilibrium of the decay series in three samples suggest that radioactive disequilibrium may not be a serious problem and that the age estimates are realistic.

The interval between the seismites S_3-S_5, S_5-S_6 and S_6-S_8 is 29, 24 and 11 ka respectively (Fig.4.3). The presence of few more seismites in Sumdo area are not ruled out as the exposures at places are covered by debris. The erosion in the few fluvial cycles at different stratigraphic levels may have eroded some seismites and it may also be possible that at times seismites do not get preserved due to lack of prerequisite conditions. The higher duration of 29 ka (S_3-S_5) and 24 ka (S_5-S_6) in the fluvial part of the section may be due to periodic non-deposition and at places due to erosion. Ideally, it would have been desirable to obtain ages on all available seismites. However, due to logistical problems, collection of four seismites was possible. Nonetheless, the rate of sedimentation in the lacustrine fill has been considered for estimation of the seismic interval between S_7 and S_8. The calculated rate of sedimentation is $\sim$ 400 cm / 1000 years. On the basis of this sedimentation rate, the minimum interval between the two seismic events S_7 and S_8 is $\sim$ 3,500 years. Further, sedimentological and chronological data suggest a change from fluvial to lacustrine facies at $\sim$ 40–45 ka implying that at $\sim$ 45 ka, lacustrine sedimentation started in Sumdo area. This may be contemporary to the formation of lakes in parts of Spiti and Ladakh due to damming (Bagati and Thakur, 1993) by a major earthquake. ^{14}C ages on gastropod shells found within lacustrine sediments in Lamayuru ($\sim$ 350 km from Spiti) show that Lake Lamayuru formed at least 35 $\pm$ 0.6 ka (radiocarbon years) ago (Fort et al., 1989). Interestingly, the activation of Nainital Fault and formation of Naini Lake (about 450 km across from Sumdo) is dated to 41 ka (Singhvi et al., 1994). Also, ^{14}C ages on charcoal (Valdiya et al., 1996) within lake sediments from Wadda Lake (30 km from Nainital) indicates that Wadda Lake formed at 44 ka ago due to movement along Kotli Fault (parallel to the North Almora Thrust). Luminescence ages on fault gouges from Main Boundary Thrust (in Nainital) and Mohand Thrust (Dehradun) provide evidence for tectonic activity at 70 $\pm$ 12 ka and

59 ± 10 ka which may be coeval with the ~ 61 ka seismic event at Spiti. Thus, the above results provide some indication of the possibility of regionally extended tectonism in the Himalaya at ~ 40 ka and ~ 60 ka ago. However, additional dating work is essential to establish this idea on a firm footing.

4.7 Luminescence dating of river terraces and soils developed on colluvium

Dating of fluvial terraces in seismically active regions is important for determining slip-rates along a fault and the potential seismic risk associated with the particular area. Lensen and Vella (1971) examined a flight of terraces along the Waiohine River, New Zealand which were offset by movements along the Wairarapa Fault. The fault produced a major earthquake in 1855 and caused vertical and horizontal displacements at the Waiohine River. Similar studies were performed on Kiso River terraces produced by movements along Atera Fault, Japan (Yoshikawa et al., 1981), Wanganui River, (near Alpine Fault), New Zealand where a recurrence interval of large earthquakes was deduced using ^{14}C dating of wood from the river terraces (Adams, 1980) and on Ventura River, Ojai, California (Clark and Kellar, 1979). Vhora (1987) established the feasibility of dating river terraces from Solani River, Roorkee using the thermoluminescence dating technique and indicated faulting at ~ 1.6 ka. Proszynska-Bordas et al., (1992) observed a good concordance between ^{14}C and TL ages (19 ± 0.3 ka BP and 20 ± 4 ka) of fossil soils and sediments from river terraces in Po Plain, Italy and Cova Negra, Spain.

Buried soils developed on fault derived colluvium represent periods of tectonic quiescence (Amit et al., 1995). Thus, dating soils buried between colluvial layers constrains the time of faulting. Forman et al., (1989; 1991) established the feasibility of dating soils (A-horizon) developed on colluvial debris using TL technique. For the present studies, soils developed on colluvium were sampled from Bhawali river terraces

(Figs. 3.1 and 4.6) along with the uplifted river terrace sediments at Kaladhungi and Garjiya (Fig. 4.6).

4.8 Experimental Techniques

The luminescence techniques for dating soils are based on the assumption that faunal pedoturbation at the surface (A-horizon) causes resetting of the luminescence signal (Wintle and Catt, 1985; Berger, 1988; Huntley, 1985). Thermoluminescence dating of soils (KU91−1 and KU91−2) was performed using the fine-grain technique. The soil samples were sunbleached for 30 minutes within a quartz tube under natural sun and the partial bleach method was used to estimate the equivalent dose. After the development of the IRSL system during 1994 in PRL, both TL and IRSL dating of 75−106 μm feldspars were attempted on river terrace sediments (TLV−6 and TLV−8) and the buried soil sample KU93−10. The experimental techniques used in IRSL dating have been described previously in section 4.5 of this chapter. Equivalent doses for terrace sediments were estimated using the additive dose method, the R-β method. A short exposure (2 minutes) to natural sunlight (in a cloudy day) filtered through a 4 mm thick transparent window glass was used to estimate the residual signal level which was then used to calculate the equivalent doses and ages using the total bleach method.

4.9 Results and Discussion

Figure 4.7 provides a typical TL data set for a buried soil. Fig. 4.8 provides the IRSL growth curve and the shine plateau for a terrace sediment. Table 4.3 presents the radioactivity data for the soil and river terrace samples. Table 4.4 provides the luminescence dating results for the terrace sediments and soils. The soil samples (KU91−1 and

1 (104)

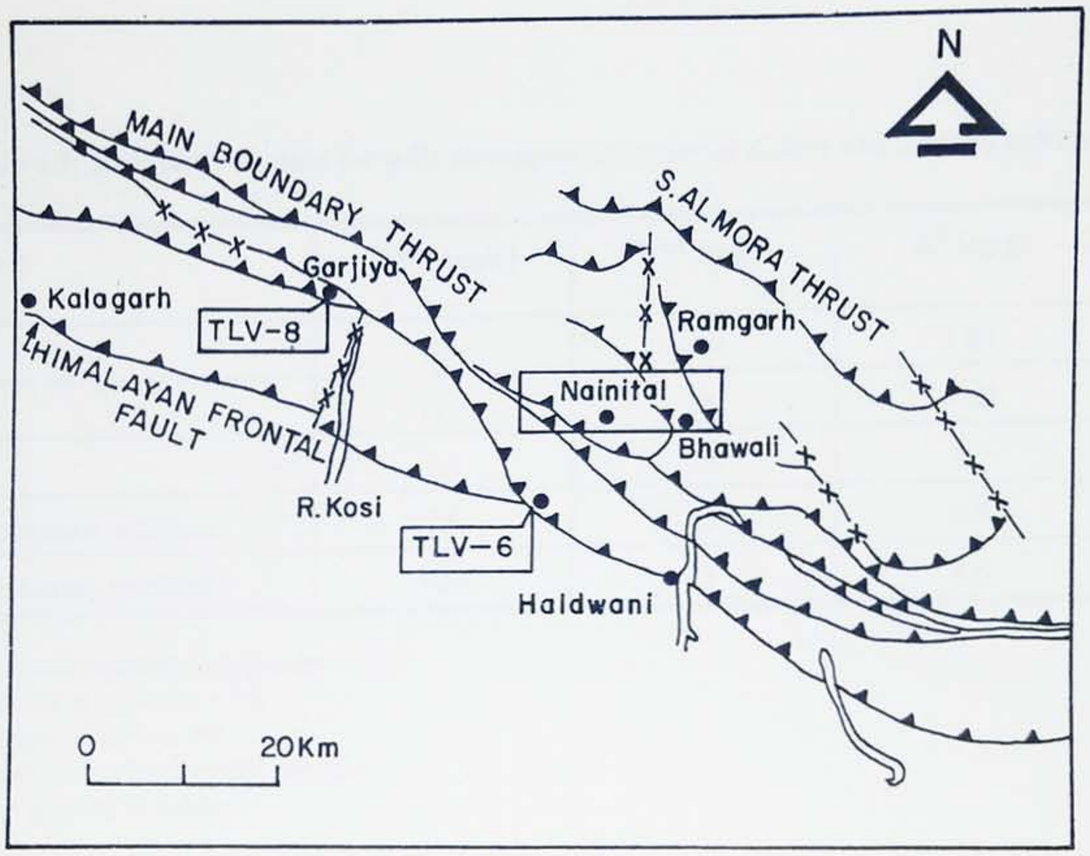
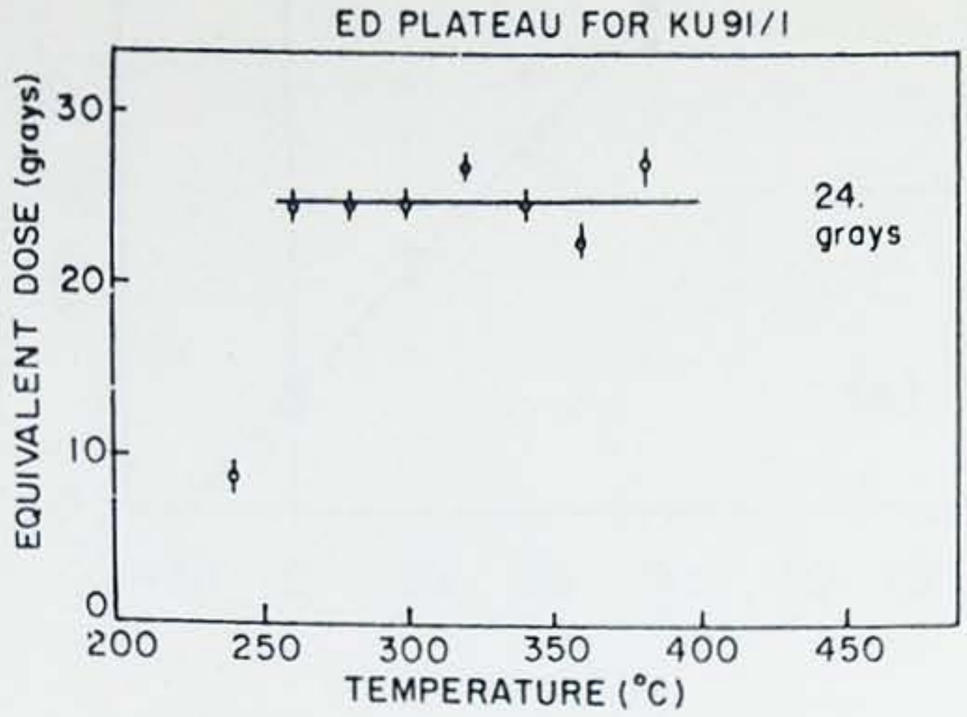


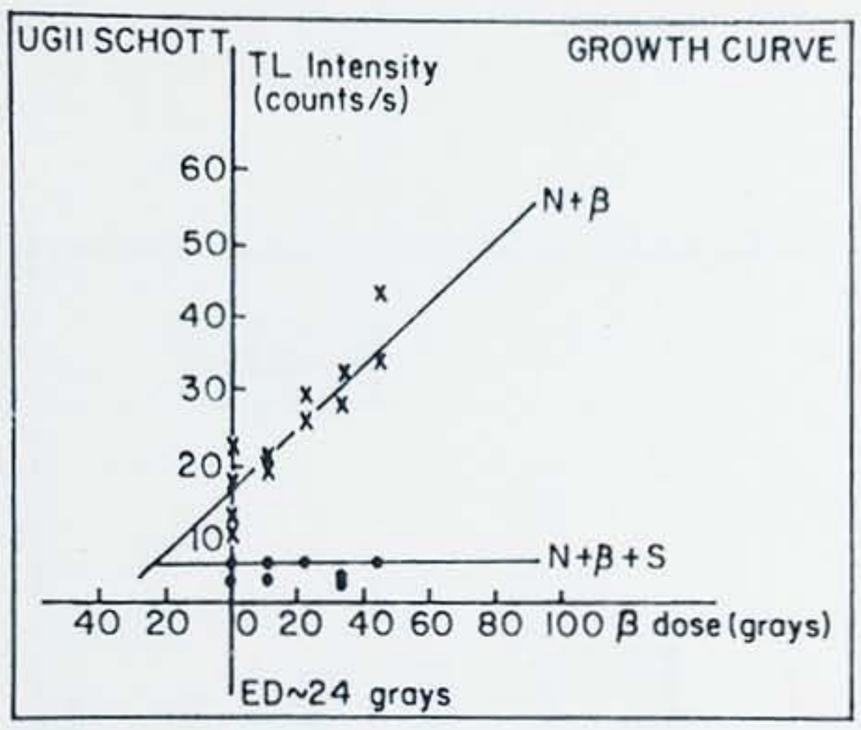
Fig. 4.6: Location map showing uplifted river terraces sites around Nainital where samples were collected for luminescence dating (modified after Valdiya, 1990).

Table 4.3: Radioactivity data for soils developed on colluvial debris and terrace sediments

Sample	Type	Th** (µg/g)	U** (µg/g)	K$ (cg/g)	Annual Dose* (mGy/a)
KU91-1	Soil	9.1	4.9	1.95	5.5#
KU91-2	Soil	12.3	2.9	1.65	4.75#
KU93-10	Soil	8.8	2.6	1.7	3.0+
TLV-6	River terrace sediment	7.6	2.25	0.9	2.2+
TLV-8	River terrace sediment	10.4	3	1.6	3.2+

** Error in U and Th concentrations in typically ~10%
$ Error in K concentration is typically ~5%
* Water content (assumed) = 20% ± 6%
Calculated for fine grained polyminerallic sample
+ Calculated for coarse grained K-feldspar





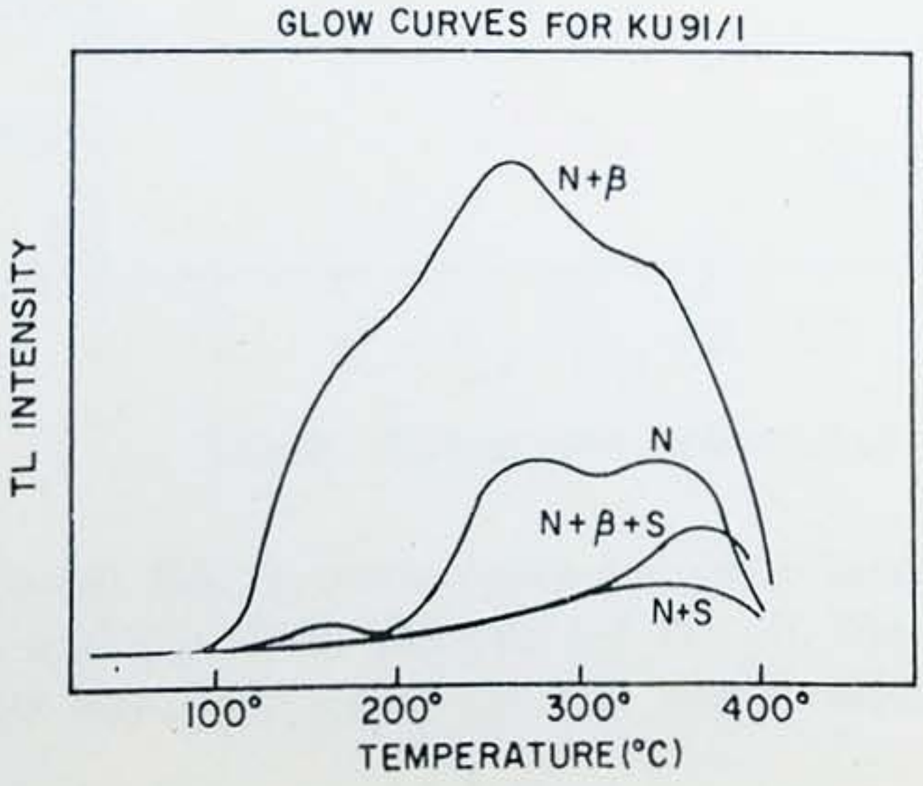


Fig. 4.7. TL glow curve, growth curve and equivalent dose plateau for a typical buried soil, KU91-1.

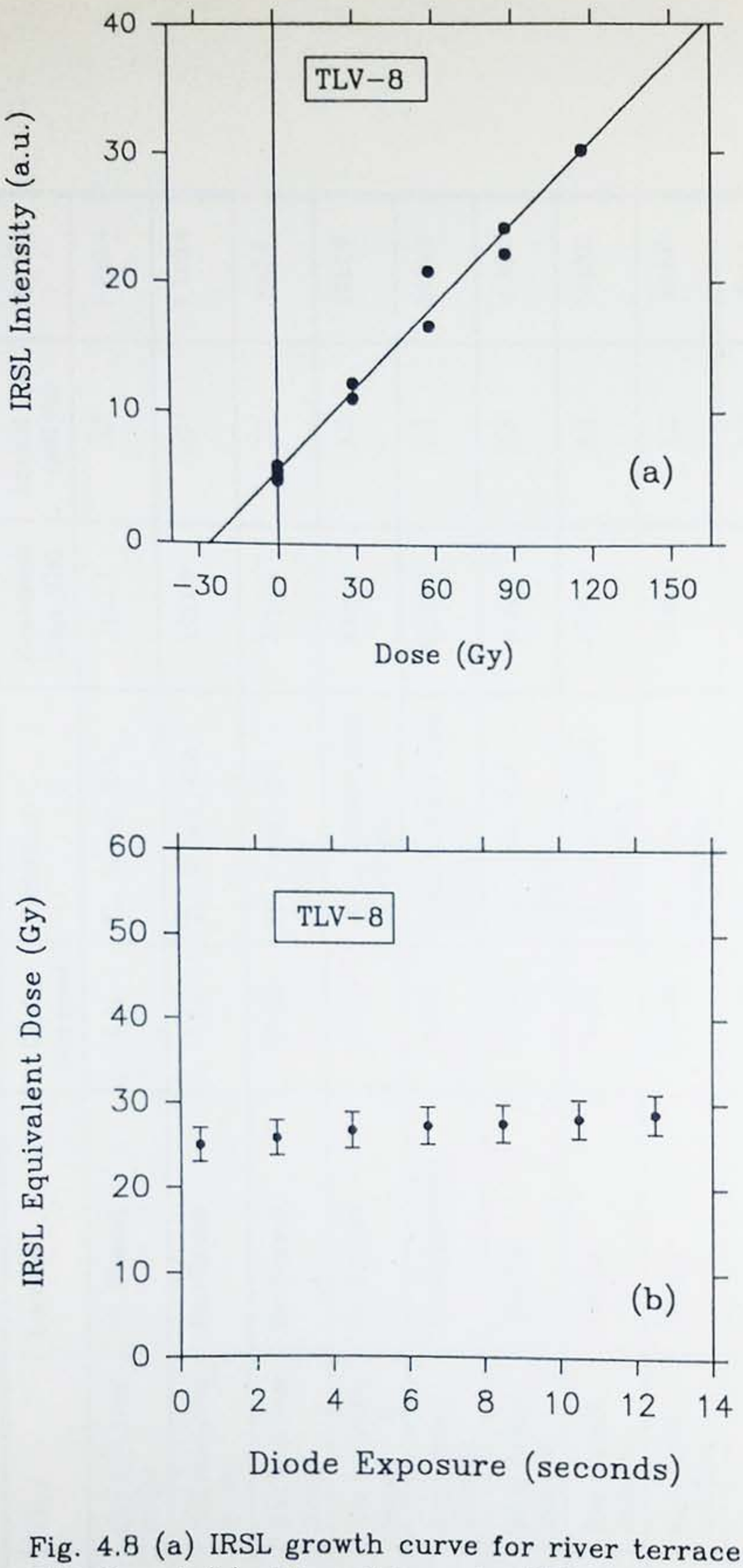


Fig. 4.8 (a) IRSL growth curve for river terrace TLV−8 and (b) shine plateau for TLV−8. The IRSL analysis was done using 75−106 μm K−feldspars.

Table 4.4: Luminescence Dating results for soils developed on colluvial debris and river terrace sediments

Sample	Type	Location	Grain Size (μm)	Technique	Equivalent Dose (Gy)	Annual Dose (mGy/a)	Age (ka)
KU91-1	Soil from river terrace	Nr. Bhawali	4-11	TL, 30 min. R-ß	24±2.4	5.5	4.4±0.4
KU91-2	Soil from river terrace	Nr. Bhawali	4-11	TL, 30 min., R-ß	19±1.9	4.75	4.1±0.4
KU93-10	Soil from river terrace	Nr. Bhawali	75-106	TL, 2 min., FSE (Quartz)	21±5.0	2.7	8±2.1
KU93-10	Soil from river terrace	Nr. Bhawali	75-106	IRSL, Additive Dose (K-feldspar)	37±5.4	3.0	12±1.9
TLV-6	River terrace sediment	Nr. Kaladhunghi	75-106	IRSL, Additive Dose (K-feldspar)	52±17.0	2.2	24±6.8
TLV-8	River terrace sediment	Garjiya	75-106	TL, 1 min., R-ß (Quartz)	< 32.0	2.8	< 12.0
TLV-8	River terrace sediment	Garjiya	75-106	TL, Additive Dose (K-feldspar)	45±5.4	3.2	14±2.0
TLV-8	River terrace sediment	Garjiya	75-106	TL, 2 min., FSE (K-feldspar)	25±6.0	3.2	8±1.8
TLV-8	River terrace sediment	Garjiya	75-106	IRSL, Additive Dose (K-feldspar)	27±3.0	3.2	8±1.2

FSE: Sunlight filtered through a 4mm thick transparent window glass (for a short duration of time indicated above) was used to evaluate the residual signal in the determination of TL age (see text).

KU91−2) from the terraces at two different locations near Bhawali gave stratigraphically concordant partial-bleach ages. These ages agree with ^{14}C ages (K.S. Valdiya, pers. commn.), suggesting that some neotectonic activity took place at $\sim$ 4 ka ago in Bhawali. It is also interesting to note that Bhargava (1990) on the basis of folded river terraces in S.E. Ladakh (near TsoMorari-Puga Fault) suggests that the area south of the Indus Suture Zone (Fig. 4.2) experienced neotectonic activity at $\sim$ 4 ka ago.

The IRSL (8 $\pm$ 2.1 ka) age of soil sample KU93−10 agreed with the FSE TL age (12 $\pm$ 1.9 ka) on quartz extracts within errors. Although this sample (KU93−10) was also collected from almost the same spot as KU91−1 (2 years after KU91−1 was collected), its age is more than two factors higher compared to KU91−1's age (4.4 $\pm$ 0.4). The implication of the luminescence age ($\sim$ 10 ka) is not yet known. A possible explanation could be that larger grains ($\sim$ 125 μm) used in dating KU93−10 will be suspended in water for shorter intervals of time in comparison to fine grains (4−11 μm) utilized for dating KU91−1. Bleaching is thus more efficient for fine grains. Clumping of the silt fraction can also result in overestimation of the depositional age.

The ages on sediments from uplifted river terraces at Garjiya and Kaladhungi are stratigraphically consistent. TL age determined on quartz extracts from the terrace TLV−8 using the partial-bleach method agreed with FSE TL ages on feldspar extracts. The TL ages (8 $\pm$ 1.8ka) are also concordant with IRSL age (8 $\pm$ 1.2 ka). But, as expected, the additive dose TL age overestimates the true depositional age. Concordance between quartz TL and feldspar IRSL/TL ages suggests that the feldspar ages are not affected by anomalous fading as it is now reasonably well established that quartz does not exhibit anomalous fading. However, the luminescence ages represent only maximum estimates of the true faulting age since the possibility of erosion of the upper horizons of the river terraces cannot be ruled out. The luminescence ages on river terraces (TLV−6 and TLV−8) suggest neotectonism in Kaladhungi and Garjiya at $\leq$ 31 ka and $\leq$ 9 ka.

Chapter 5

Thermoluminescence and Infra-red Stimulated Luminescence dating of Pedogenic Carbonates

5.1 Introduction

Calcretes are defined as terrestrial materials which consist primarily (but not exclusively) of calcium carbonate and occur in different forms from powdery to highly indurated ones (Goudie, 1983). Pedogenic carbonates occur in a variety of sedimentary sequences and soil profiles and may be present as kankar nodules, rhizoconcretions, pedotubules etc. In soil profiles, they often form several distinct horizons (e.g., calcic or petrocalcic horizons). Machette (1985) has recognised six stages of development of such carbonates depending upon the amount of calcium carbonate and gravel content present within the horizon. Generally, formation of pedogenic carbonates takes place when carbonates derived mostly from dust, rainfall, vegetation litter, shells and chemical weathering of Ca^{2+} bearing minerals are leached downwards in a profile and precipitate in the lower soil horizons (Goudie, 1983). The chemical reactions involved in the dissolution and reprecipitation of calcium carbonate are :

$$CaCO_3 + H_2CO_3 \rightleftharpoons Ca^{2+} + 2HCO_3^- \tag{5.1}$$

$$H_2CO_3 \rightleftharpoons CO_2(aq) + H_2O \tag{5.2}$$

$$CO_2(aq) \rightleftharpoons CO_2(g) \tag{5.3}$$

where (aq) and (g) denote the aqueous and gaseous phases respectively. Carbonate precipitation occurs if there is decrease in the CO_2 partial pressure, evaporation, common ion effect or biological activities. Evaporation results in a rapid loss of vadose water and could lead to rapid carbonate precipitation and causing the formation of small calcite crystals. Evapotranspiration can also result in carbonate precipitation.

The basic importance of pedogenic carbonates stems from the fact that they have long been considered as important stratigraphic markers as also paleoclimatic and paleovegetational indicators. They generally form in regions of net annual moisture deficit and net annual precipitation of less than 400 mm. It has also been suggested that the presence of pedogenic carbonates implies landscape stability (Callen et al., 1983). Present estimates indicate that pedogenic carbonates cover $\sim$ 20 million km^2 or about 13% of the total land surface (Yaalon, 1981). In Arizona, the depths of occurrence of carbonates have been related to the annual precipitation (Cooke et al., 1993). The rates of soil carbonate accumulation have also been correlated with modern mean annual precipitation (Marion et al., 1985). Pedogenic carbonates also constitute a significant part of the global carbon budget. Thus, it is essential to understand the timescales of carbon fixation as carbonates in the arid zones of the world and examine their correlation with global climatic events (Adams et al., 1990). After a brief review of the existing methods for dating carbonates, this chapter describes the new luminescence method

to date pedogenic carbonates. Luminescence ages of carbonates from Thar Desert and their implications are also presented at the end of this chapter.

5.2 Dating of Pedogenic Carbonates: Earlier work

Radiocarbon dating of carbonates has been attempted by many workers (Godwin, 1951; Williams and Polach, 1969; 1971; Chen and Polach, 1986). Comparisons between ^{14}C ages on carbonates with coexisting organic materials have generally indicated that: (a) relative ages agree suggesting that the radiocarbon ages have some stratigraphic implications; (b) arid zone carbonate ages are typically a $\sim$ few ka older than the true carbonate age due to incorporation of 'dead' carbon (containing little/no ^{14}C) and (c) ages on carbonates from semi-arid to humid regions are mostly younger than the age on the coexisting organics. The latter result has been attributed to post-formation contamination by atmospheric ^{14}C dissolved in meteoric waters (Williams and Polach, 1969). However, Callen et al., (1983) obtained stratigraphically inconsistent ^{14}C carbonate ages from Strzelecki Desert, South Australia. The ages from the rim of nodules were found to be much younger (29 ka BP) than those from the centre of the nodule ($>$ 44 ka BP). Thus, Callen et al. (1983) suggested that ^{14}C carbonate ages from arid zones are often unreliable and have little or no stratigraphic significance.

$^{230}Th-^{234}U$ disequilibrium dating has also been attempted on pedogenic carbonates (Ku et al., 1979). However, the method needs correction for the detritral Th/U component and also assumes that after their formation, the carbonates act as closed systems in respect of exchange of thorium and uranium isotopes. Incorporation of older crust material or limestone particles can also result in erroneous ages. The Electron Spin Resonance dating method (Radtke et al., 1988) has also been used to date calcretes. However, many of the ESR ages obtained by Radtke et al., (1988) were not

consistent with the $^{230}Th-^{234}U$ ages on the same calcretes. Also, the g = 2.45 ESR signal used for dating is associated with humic acids and thus might not remain stable over geological timescales. It is also not apparent whether the ESR method can be applied for ascertaining the chronology of young calcrete profiles.

Thermoluminescence (Nambi and Hedge, 1982; May and Machette, 1984) techniques have also been utilized to date calcretes but are open to criticism on various aspects: isolation of carbonate luminescence from quartz and feldspar luminescence, opacity and TL sensitivity changes on heating and diagenetic changes (Berger, 1988).

Recently, an attempt has been made to use the in situ production of ^{36}Cl by cosmic rays for dating pedogenic carbonate nodules (Liu et al., 1994). This method at best provides model ages as it crucially depends on several factors such as the changes in the calcrete burial depth, constancy of cosmic ray fluxes through time and negligible erosion. Liu et al., (1994) reported ages from 200-700 ka for a calcrete profile from Ajo Mountains, southern Arizona. However, the leachable fraction ^{36}Cl ages were generally larger than the carbonate fraction and the silicate residual ^{36}Cl ages. An age inversion is also observed in the silicate residual ^{36}Cl ages. Thus, additional dating work is necessary to test the validity of the ^{36}Cl method for dating carbonates.

The present studies involved the development of a new luminescence dating technique for dating pedogenic carbonates, which (unlike other radiometric methods discussed above) is less susceptible to post-depositional changes and is also immune to variability of cosmic ray fluxes. This approach exploits subtle changes in the natural radiation field of a luminescent mineral after being trapped in a carbonate precipitate. Thus, the proposed method utilizes the 'dirt' of a nodule to date a carbonate precipitation event. In principle, the methodology should allow us to apply it to a large variety of terrestrial carbonate deposits ranging from root casts, kankar nodules and loess dolls.

5.3 The Luminescence dating method

The proposed method is based on the same premise as used in luminescence dating of sunlight bleached sediments (Aitken, 1985). Sunlight exposure of the minerals constituting the sediment stratum during their pre-depositional transport optically bleaches the geological luminescence to a residual value (I_o). On burial, a fresh acquisition of luminescence is initiated due to irradiation arising from the decay of U, Th, K in the ambient strata. This reacquisition of luminescence continues unabated till the sample is excavated and a laboratory analysis of this sample provides a signal I_{nat} , such that

$$I_{nat} = I_o + I_d \tag{5.4}$$

where I_d is the TL acquired since sedimentation. In terms of equivalent radiation doses, the above equation can be functionally expressed as $P_s = P_o + Q_s$ where P_s is the total paleodose in a sample. P_o is the initial dose corresponding to TL intensity I_o and Q_s is the dose acquired since burial and corresponds to I_d . The luminescence age equation can be written as:

$$t_s = \frac{Q_s}{aD_{\alpha,s} + D_{\beta,s} + D_{\gamma,s} + D_{cos,s}} \tag{5.5}$$

where t_s is the age of the sedimentation episode of the host stratum (e.g., a sand dune). D_s is the total annual radiation dose whereas $D_{\alpha,s}$, $D_{\beta,s}$ and $D_{\gamma,s}$ are the components of gamma dose rates provided by the decays of ^{238}U, ^{232}Th and ^{40}K. $D_{cos,s}$ is the cosmic ray dose rate and a is the sample dependent alpha efficiency parameter. In the case of carbonate formation, some of the mineral grains that are trapped in the carbonate matrix suffer a change in their dose rate due to dilution (or enrichment) of the radioactivity of sediment matrix by carbonate. If the dose rate experienced by a grain in a carbonated

matrix is D_c, then the total paleodose P_c of a mineral grain trapped in the carbonate matrix can be expressed simply as (Fig. 5.1),

$$P_c = P_o + Q_c \tag{5.6}$$

where Q_c , the calcrete equivalent dose is given by the equation

$$Q_c = (t_s - t_c)D_s + t_c D_c \tag{5.7}$$

Here t_c is the age of carbonate formation event. Realizing that,

$$P_s = P_o + Q_s = P_o + t_s D_s \tag{5.8}$$

using equation (5.7) and equation (5.8) one obtains,

$$t_c = \frac{P_s - P_c}{D_s - D_c} \tag{5.9}$$

Since both P_s and P_c have identical predepositional bleaching (i.e. P_o),

$$P_s - P_c = Q_s - Q_c \tag{5.10}$$

$$t_c = \frac{Q_s - Q_c}{(aD_{\alpha,s} + D_{\beta,s} + D_{\gamma,s} + D_{cos,s}) - (aD_{\alpha,c} + D_{\beta,c} + D_{\gamma,c} + D_{cos,c})} \tag{5.11}$$

The above equation simplifies if one considers 100–150 μm mineral separates which have negligible internal radioactivity. Also, the alpha dose contribution from the host matrix can be ignored by etching the outer alpha-dosed skin of the mineral. The large range

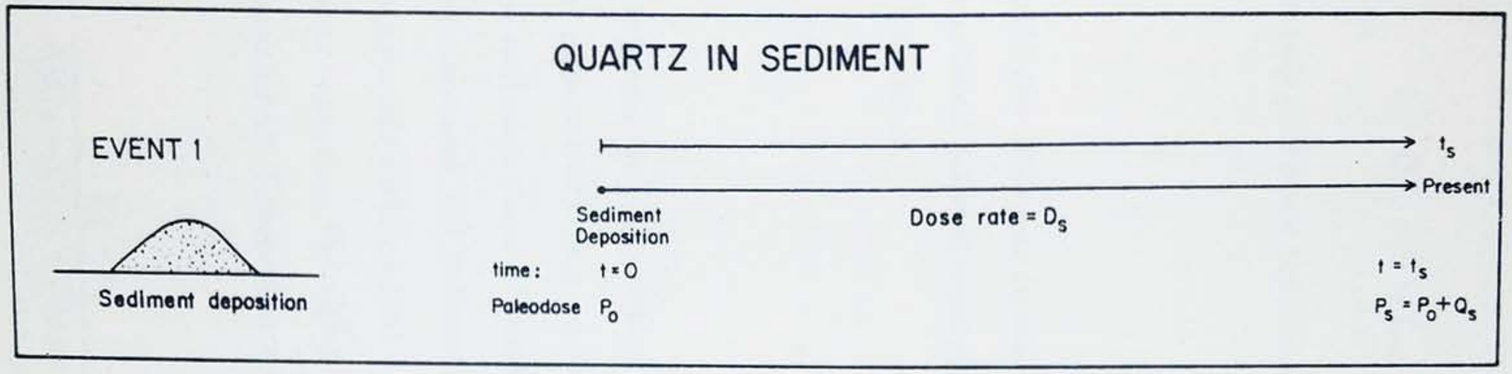


Fig. 5.1. Schematic representation of basic principles involved in luminescence dating of a carbonate. The symbols used have been explained in the text.

of gamma rays further implies that the γ dose and cosmic ray contribution from the host matrix (< 30 cm) when compared to typical size of 1–3 cm of a carbonate nodule remains essentially unaltered even after carbonate precipitation. Setting,

$$D_{\alpha,s} = 0 = D_{\alpha,c} \quad D_{\gamma,s} = D_{\gamma,c} \quad \text{and} \quad D_{cos,s} = D_{cos,c} \tag{5.12}$$

the dose rate difference reduces to

$$D_s - D_c = D_{\beta,s} - D_{\beta,c} \tag{5.13}$$

Thus, only the difference in the total annual beta dose from U, Th, K in uncarbonated and carbonated mineral separates needs evaluation. The age equation in its final form can be written as,

$$t_c = \frac{Q_s - Q_c}{D_{\beta,s} - D_{\beta,c}} \tag{5.14}$$

which suggests that the dating of carbonates for mineral separates having negligible internal radioactivity (e.g. quartz) requires estimation of the differences in (i) accumulated radiation doses of mineral separates from both the carbonate matrix and the host sediment and, (ii) radioactivity content (i.e. the difference in the net annual beta dose to minerals within a host matrix and a carbonate nodule). However, for unetched K-feldspar separates, the alpha dose contribution also needs to be considered and the expression for the luminescence age becomes

$$t_c = \frac{P_s - P_c}{a(D_{\alpha,s} - D_{\alpha,c}) + (D_{\beta,s} - D_{\beta,c})} = \frac{Q_s - Q_c}{a(D_{\alpha,s} - D_{\alpha,c}) + (D_{\beta,s} - D_{\beta,c})} \tag{5.15}$$

5.4 Methodological Aspects of the luminescence dating method

This section discusses some methodological aspects of the dating method, viz., dosimetric changes due to loss/gain of radionuclides, change in the luminescence age as a result of redissolution and reprecipitation and estimation of error in the calcrete age.

5.4.1 Dosimetric changes due to loss of ^{238}U and/or ^{232}Th

The calcrete age equation can be written as

$$\mathsf{Age} = \frac{\mathsf{Q_s} - \mathsf{Q_c}}{\beta_{\mathsf{Th,s}} + \beta_{\mathsf{U,s}} + \beta_{\mathsf{K,s}} - \beta_{\mathsf{Th,c}} - \beta_{\mathsf{U,c}} - \beta_{\mathsf{K,c}}} \tag{5.16}$$

Now if $\beta_{Th,c}$ and $\beta_{U,c}$ change to $\beta'_{Th,c}$ and $\beta'_{U,c}$ after precipitation of the nodule, the expression for the new age is given by

$$\mathsf{Age'} = \frac{\mathsf{Q_s} - \mathsf{Q'_c}}{\beta_{\mathsf{Th,s}} + \beta_{\mathsf{U,s}} + \beta_{\mathsf{K,s}} - \beta'_{\mathsf{Th,c}} - \beta'_{\mathsf{U,c}} - \beta_{\mathsf{K,c}}} \tag{5.17}$$

Using the two equations above and assuming $Q'_c \sim Q_c$ (a reasonably good assumption since $\sim$ 80 % of the β dose comes from K), one gets the relative change in age

$$\frac{\triangle\mathsf{Age}}{\mathsf{Age}} = \frac{\mathsf{Age} - \mathsf{Age'}}{\mathsf{Age}} \tag{5.18}$$

given by the expression

$$\frac{(\beta_{\mathsf{Th,c}} + \beta_{\mathsf{U,c}}) - (\beta'_{\mathsf{Th,c}} + \beta'_{\mathsf{U,c}})}{(\beta_{\mathsf{Th,s}} + \beta_{\mathsf{U,s}} + \beta_{\mathsf{K,s}} - \beta_{\mathsf{Th,c}} - \beta_{\mathsf{U,c}} - \beta_{\mathsf{K,c}}) + ((\beta_{\mathsf{Th,c}} + \beta_{\mathsf{U,c}}) - (\beta'_{\mathsf{Th,c}} + \beta'_{\mathsf{U,c}}))} \tag{5.19}$$

Now $(\beta_{Th,s} + \beta_{U,s} + \beta_{K,s} - \beta_{Th,c} - \beta_{U,c} - \beta_{K,c})$ is the original annual beta dose difference between the host sand and the calcrete. For the calcrete sample CAL-3, this difference is 0.56 mGy/a whereas $\beta_{Th,c}$ and $\beta_{U,c}$ are $\sim$ 0.086 mGy/a and 0.084 mGy/a respectively. Calculations using these values show that (i) if 50 % loss of either ^{238}U or ^{232}Th occurs, the change in the age will be 7 % while (ii) if 50 % loss of both ^{238}U and ^{232}Th occurs, the age changes by 13%.

5.4.2 The interpretation of luminescence ages for multiple carbonate precipitation events in a single profile

After the carbonate precipitation event, if redissolution and reprecipitation occurs, it is most likely that the new carbonate will form at a different depth. Assuming this to be so, we now consider two situations and the interpretation of the luminescence age in each case.

Scenario A

We assume that the new carbonate forms at a lower depth and incorporates only those mineral grains which were present within the adjacent host sand. Therefore, the carbonate does not contain any mineral grains present within the original carbonate. Under these circumstances, the procedure indicated in Section 5.3 can be applied to evaluate a carbonate age. The estimated carbonate age denotes the time of the new precipitation event and will be lower than the age of the earlier carbonate formation event. If such events repeatedly occur, i.e., each time the new carbonate forms at a new horizon and contains grains only from the adjacent sands, the estimated carbonate age will represent the age of the latest precipitation event.

Scenario B

If the new carbonate formed comprises of grains having different irradiation histories, i.e., grains originating from the older carbonate and from the adjacent host sand, the above approach cannot be applied to estimate the carbonate age since the paleodose P_c for carbonate minerals cannot be expressed in a unique way. Also, the resulting inhomogeneity in radioactivity within the carbonate implies that the infinite matrix assumption breaks down and the annual dose cannot be calculated in the usual manner. Additional assumptions regarding the rate of deposition and the annual dose D_s need to be made to evaluate a proper age. In such situations, the single grain dating method can perhaps be used to obtain a meaningful age.

5.4.3 Estimation of errors

If f is a function dependent on n parameters x_i each with a standard deviation σ_i, then the variance in f, σ_f^2 is defined as

$$\sigma_f^2 = \sum_{i=1}^{n} \sigma_i^2 (\frac{\delta f}{\delta x_i})^2 \tag{5.20}$$

If σ_{Q_c}, σ_{Q_s}, σ_{D_c}, σ_{D_s} and σ_{Age} are the standard deviations for Q_c, Q_s, D_c, D_s and the calcrete age respectively then using equation (5.15) and simplifying, we get

$$\sigma_{Age}^2 = Age^2 (\frac{\sigma_{Q_s}^2}{(Q_s - Q_c)^2} + \frac{\sigma_{Q_c}^2}{(Q_s - Q_c)^2} + \frac{\sigma_{D_s}^2}{(D_s - D_c)^2} + \frac{\sigma_{D_c}^2}{(D_s - D_c)^2}) \tag{5.21}$$

Thus an evaluation of the standard deviation in age involves use of five quantities σ_{Q_c}, σ_{Q_s}, σ_{D_c}, σ_{D_s} and the calcrete age. Using equation (5.16), it can be shown that if $Q_s - Q_c$ is < 5 Gy and $D_s - D_c < 0.5$ mGy/a, measurement errors of Q and D values must be

less than 5% for achieving a reasonable error limit (< 20%) on the calcrete age. Another implication of equation (3) is that the luminescence method is most suitable for dating pedogenic carbonates which have (i) formed at least a few thousand years after the sand depositional event and (ii) a large annual beta dose difference between the host sand and the carbonate ($| D_s - D_c | > 2$ mGy/a).

5.5 Samples and procedures

5.5.1 Luminescence Measurements

For the present study, carbonates were sampled from various sites viz., Budha Pushkar, Chamu, Amarsar and Jalore in a transect across Thar Desert (Fig. 5.2). Presently, the mean annual precipitation in Chamu is ~ 300 mm. Jalore passes through the ~ 350 mm isohyet whereas Budha Pushkar and Amarsar receive ~ 450 mm and ~ 500 mm rainfall annually. For TL measurements, 105-150 μm quartz mineral separates were extracted by a sequential pretreatment of the original sand sample by HCl, H_2O_2 and HF. The extraction of quartz from carbonates was done by first dissolving (and discarding) the outer 0.5−1 cm of the carbonate and then fully dissolving the remaining carbonate. The residue was then treated identically as described above. The extracted quartz was tested for purity using an 880 nm infra-red stimulated luminescence system. K-feldspar extraction was performed by treating the sample with HCl, H_2O_2, sieving the 75−106 μm fraction and using the density separation technique (density = 2.58 mg/cm^3) with sodium polytungstate. No HF etching was done during feldspar separation due to the possibility of grain rupture and limited sample availability. Thus, alpha dose (attenuated) was also taken into account in the calculation of the annual dose for K-feldspar ages. The α-efficiency factor was assumed to be 0.15 ± 0.075 for K-feldspar grains.

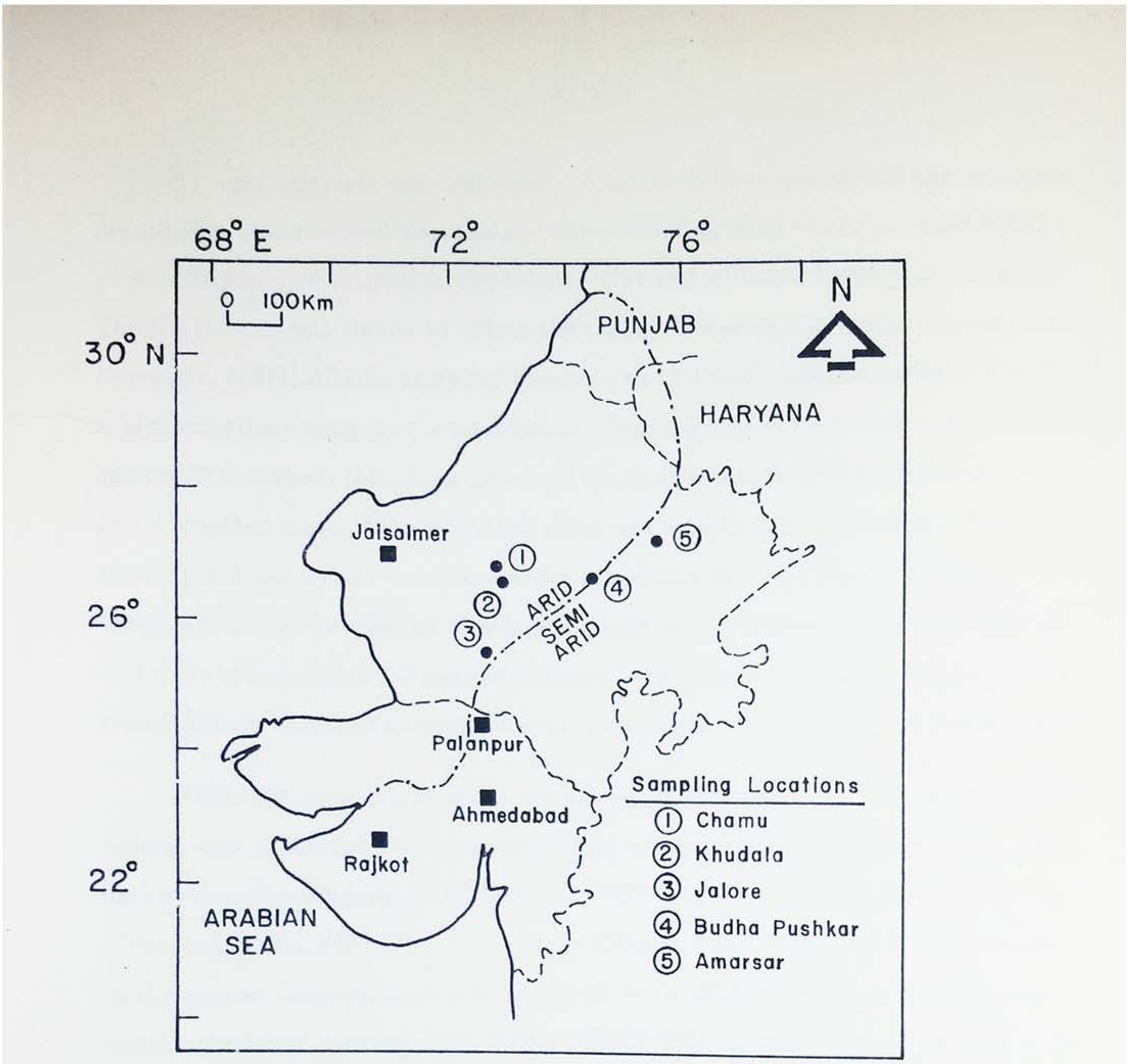


Fig. 5.2. Locality map of North-west India. Pedogenic carbonate sites sampled for luminescence dating are presented in the diagram (modified after Kar, 1995). Khudala was only sampled for aeolian sands (results are discussed elsewhere).

TL measurements were done on ~ 5 mg monolayer quartz/feldspar separates deposited on stainless steel discs using a photon counting setup comprising EMI 9635QA photomultiplier tube coupled to two Schott UG11 and a Chance Pilkington HA3 filters. The UG11 filter was chosen to isolate the rapidly bleaching 325° peak (Prescott and Purvinskis, 1991). All laboratory sun-bleaching was done using natural sunlight. The TL analysis was done using the the total-bleach (bleaching time ~ 7 hrs. and ~ 30 minutes) and the R-β methods (bleaching time ~ 30 minutes) generally used for sediment dating and a weighted mean of the equivalent doses was used in estimation of age. However, the weighted mean error was not used for calculating the error (σ_Q) in Q values since the growth curves for different bleaching methods are not independent of each other (N + β curve is common for all methods). Instead, the error in the equivalent dose (from a typical growth curve) at a certain plateau temperature was used as σ_Q for the samples.

IRSL dating was carried out on K-feldspar extracts. The IRSL intensities of natural and irradiated discs were normalized using 1 second shortshine glows. The optics channel comprised a EMI 9635 QA PMT coupled to corning 5-58 + 7-59 blue filters, one quartz ND-1 filter and a chance Pilkington HA-3 filter. The PMT operated in the photon counting mode was interfaced to an IBM/PC with an Ortec Accuspec multi-scaling card. Sixteen IRSL diodes (TEMT 454) with peak emission at 880 ± 80 nm (operated with a programmable constant current supply) were used for shinedown curves. Beta irradiations were performed using a 25 mCi $^{90}Sr-^{90}Y$ beta source.

Since the K-feldspar separates from host sands and carbonates have identical pre-depositional bleaching histories, $P_s - P_c = Q_s - Q_c$ and thus the additive dose method can be used in the determination of luminescence ages. In principle, the paleodoses and ages obtained using this method should have a lower error compared to partial bleach and the total bleach techniques. TL and IRSL ages on K-feldspar extracts were evaluated using equation 5.15.

The carbonate nodules kept for α-counting and γ-spectrometry were first cleaned with a brush to remove loose sandy grains and then powdered in an agate pestle. For both sands and calcretes, thick source ZnS(Ag) alpha counting was used for determining thorium and uranium concentrations and γ-ray spectrometry (NaI) was used for the determining K concentration. Secular equilibrium was assumed in the calculation of annual doses.

5.5.2 X-ray Diffraction Studies

An important methodological aspect involving dating is the mobility of potassium. X-ray diffraction studies were performed to ascertain the possibility of post-formation movement of radionuclides and validity of the annual dose estimates. X-ray diffraction analysis of the samples were also carried out by Dr. V. Gogte at the Deccan College, Pune, using a RIGAKU D Max II VC XRD system, operated at 50 kV, 25mA at scan speed of 1′/sec. The peak intensities, peak positions, half widths were computed using standard software. The X-ray diffraction analysis indicated that the potassium-bearing phases are microcline, richterite, albite and muscovite. The presence of minerals such as microcline, the semi-arid nature of the region and low water exchangeable potassium ($<$ 50 ppm) suggest that K-mobility is low, and the potassium largely remains locked up in silicate phases. Consequently the dose rate estimates can be taken as realistic. The β-range of $\sim$ 2mm further suggests that with respect to β-doses the luminescence dating system closes over scale lengths of a few mm, an aspect that could allow examination of growth rates of carbonate nodules based on sequential leaching of grains from the core to its centre. The dominance of the beta dose from potassium ($\sim$ 83-70%) for etched quartz separates (Table 5.2a) also indicates that the effect of a possible mobility of uranium also gets substantially diluted. However, for unetched 75-106 μm K-feldspars (Table 5.2b), the contribution of potassium ($\sim$ 80-45%) towards the annual alpha and

Table 5.1 : Radionuclide Data for carbonates and host sands from Thar Desert

Location	Calcrete	Th+ (µg/g)	U+ (µg/g)	K* (cg/g)	Host Sand	Th+ (µg/g)	U+ (µg/g)	K* (cg/g)
Jalore	JAL-I/17C	1.9	0.50	0.75	JAL-I/17S	2.15	0.6	1.0
	JAL-II/2C	1.9	0.55	1.0	JAL-II/2S	2.40	0.7	1.05
Chamu	TR-11C	5.2	1.5	0.6	TR-11S	5.7	1.7	1.4
	TR-13C	3.7	1.1	0.8	TR-13S	5.8	1.7	1.5
Amarsar	TR-29C	4.2	1.2	0.5	TR-29S	9.7	2.8	1.1
	TR-31C	4.6	1.3	0.7	TR-31S	10.3	3.0	1.2
Budha Pushkar	CAL-0	3.7	1.4	0.90	PSH 92-1	4.75	0.8	1.5
	CAL-1	2.2	0.9	0.75	PSH 92-1	4.75	0.8	1.5
	CAL-3	3.2	0.6	0.9	PSH 92-1	4.75	0.8	1.5
	CAL-2	1.85	0.8	0.9	PSH 92-2	6.10	2.4	1.5
	CAL-4	4.0	0.65	0.9	PSH 92-3	5.05	0.8	1.5

+ Error in U and Th concentration is typically ~10%
* Error in K concentration is typically ~5%

Table 5.2a: ß dose fraction from potassium to 106-150 µm quartz extracts from host sands and calcretes

Calcrete	Fraction of beta dose+ from potassium	Host sand	Fraction of beta dose+ from potassium
CAL-0	0.71	PSH 92-1	0.83
CAL-1	0.76	PSH 92-1	0.83
CAL-3	0.80	PSH 92-1	0.83
CAL-2	0.82	PSH 92-2	0.70
CAL-4	0.78	PSH 92-3	0.83

+ Alpha dose is negligible since 106-150 µm quartz extracts were used for TL dating of these calcretes and host sands (see Section 5.3 of text)

Table 5.2b: Fraction of annual alpha and beta dose from potassium to 75-106 µm K-feldspars within host sands and calcretes

Location	Calcrete	$ß_K^*/(\alpha+ß)$	Host sand	$ß_K^*/(\alpha+ß)$
Jalore	JAL-I/17C	0.74	JAL-I/17S	0.76
	JAL-II/2C	0.80	JAL-II/2S	0.76
Chamu	TR-11C	0.46	TR-11S	0.63
	TR-13C	0.60	TR-13S	0.65
Amarsar	TR-29C	0.46	TR-29S	0.45
	TR-31C	0.52	TR-31S	0.46

* $ß_K^*/(\alpha+ß)$ is the fraction of the annual alpha and beta dose to 75-106 µm K-feldspars from ^{40}K. Since no HF etching was performed in the extraction of K-feldspars used for TL and IRSL dating of these calcretes and sands, alpha dose (attenuated) contribution has also been taken into account in estimating this ratio.

beta dose decreases by ~ 20-30% in situations where the sand and the carbonate matrix contain higher U and Th concentrations and low potassium concentrations.

5.6 Results and Discussion

Table 5.1 provides radioactivity data for carbonates and host sands from the various sites. Table 5.3 provides the TL ages, carbon and oxygen isotopic values of the calcretes from Budha Pushkar, Thar Desert. Tables 5.4 and 5.5 presents luminescence data for calcretes and host sands from other sites in Thar Desert. Fig. 5.3, 5.4 and 5.5 present TL glow curves, growth curves and plateaus for quartz and feldspar extracts from host sands and calcretes. Fig. 5.6, 5.7 and 5.8 provide IRSL shinedown curves, IRSL growth curves and shinedown plateaus for K-feldspar extracts from host sands and calcretes. Fig. 5.9 presents the stratigraphy, TL ages and stable isotopic data for carbonates from Budha Pushkar, Thar Desert.

A comparison of thermoluminescence and calibrated (Stuiver and Reimer, 1993) ^{14}C ages on carbonates from Budha Pushkar (Table 5.4) indicate that the TL ages are significantly higher compared to their radiocarbon counterparts. This is expected in view of the likelihood of post-depositional contamination of the radiocarbon samples by modern carbon. Absence of coexisting organic materials in the carbonate horizons sampled for the present studies meant that comparisons between luminescence ages of carbonates and ^{14}C ages on coexisting organic material was not possible. However, some clues on the plausibility of luminescence ages can be found from isotopic data and the regional paleoclimatic reconstruction. Oxygen isotopic ratios of the Budha Pushkar carbonates ranging from -4.82 ‰ to -6.57 ‰ (relative to PDB) can be compared with the oxygen isotopic composition of -5 to -6 ‰ (relative to SMOW) of modern meteoric waters (Sarkar et al., 1990). This suggests that the carbonates analysed were formed primarily from leaching and thus are related to monsoonal precipitation. The

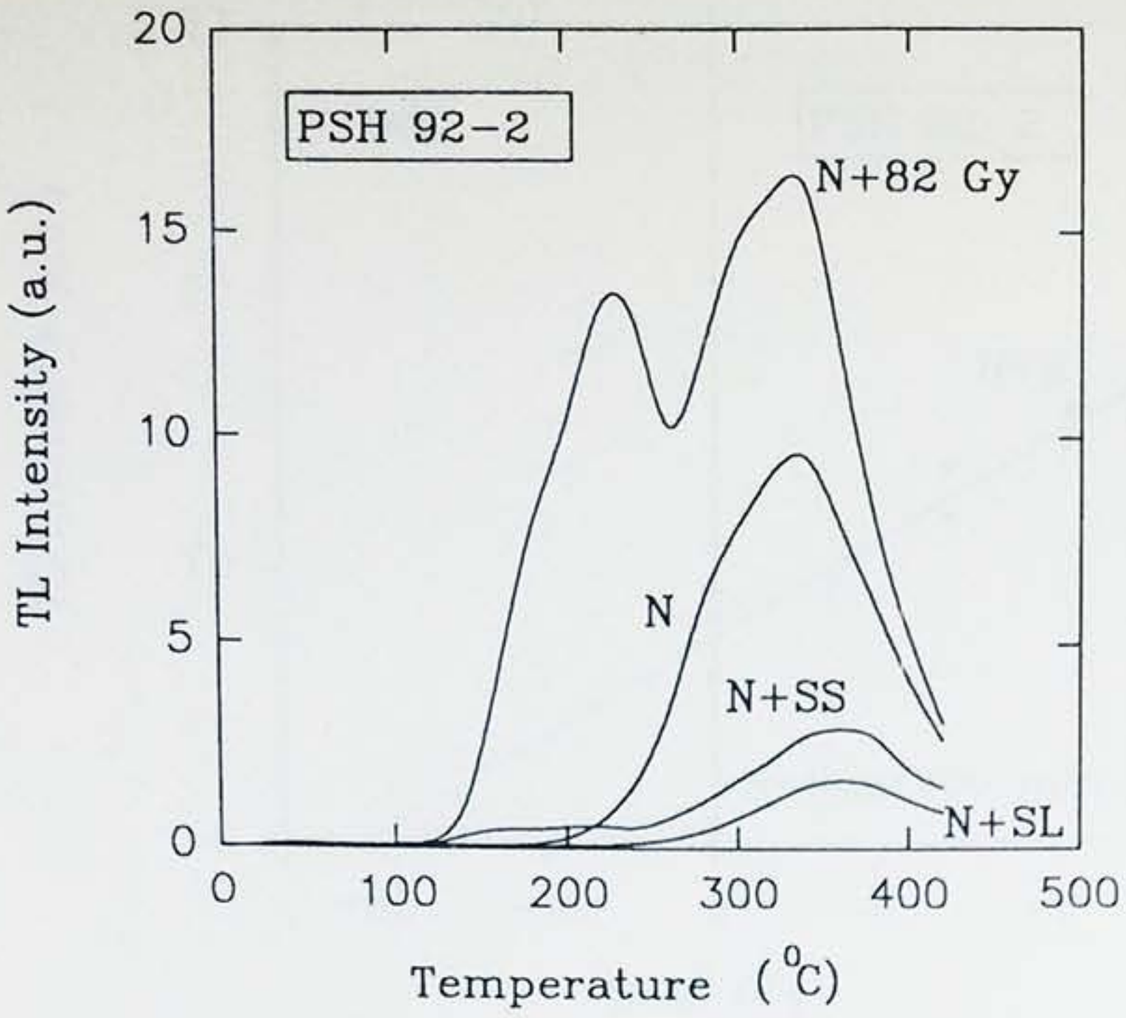


Fig. 5.3 (a): TL glow curves for quartz separates from host sand, PSH 92–2. SL and SS are bleaching times of 700 and 30 minutes under natural sun.

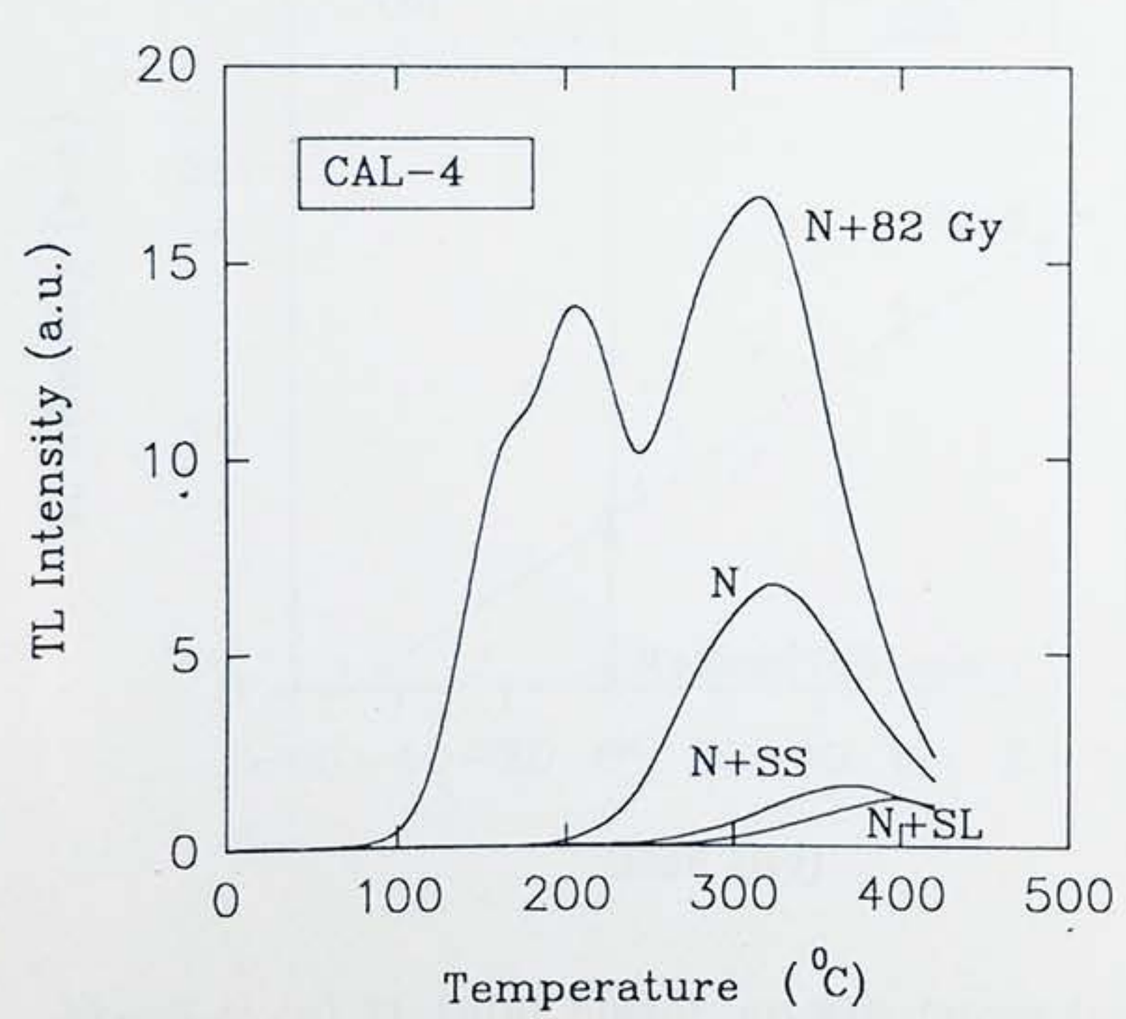
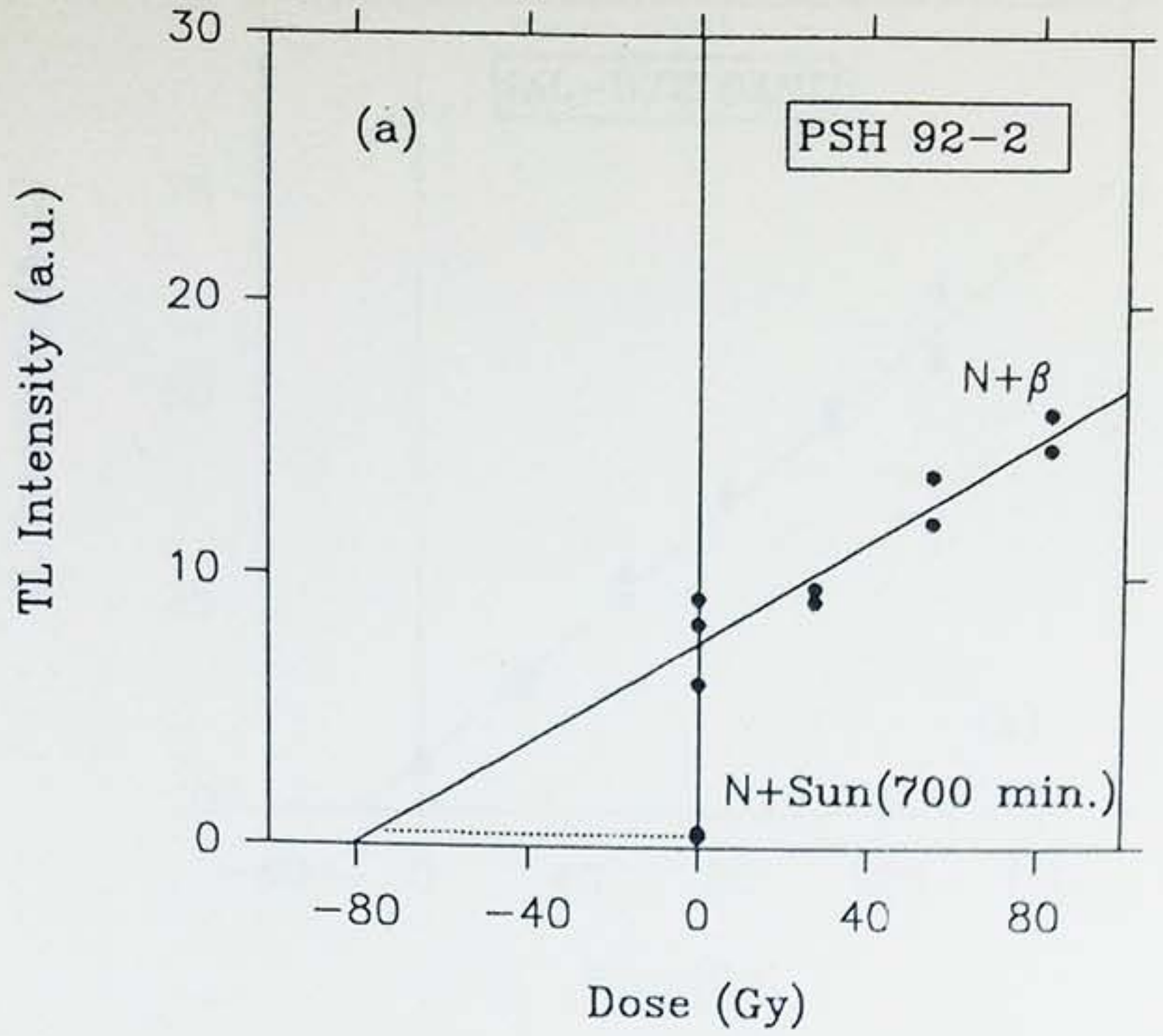


Fig 5.3 (b): Glow curves for quartz separates from carbonate CAL–4. SL and SS carry the same meaning as in fig. 5.3 (a)



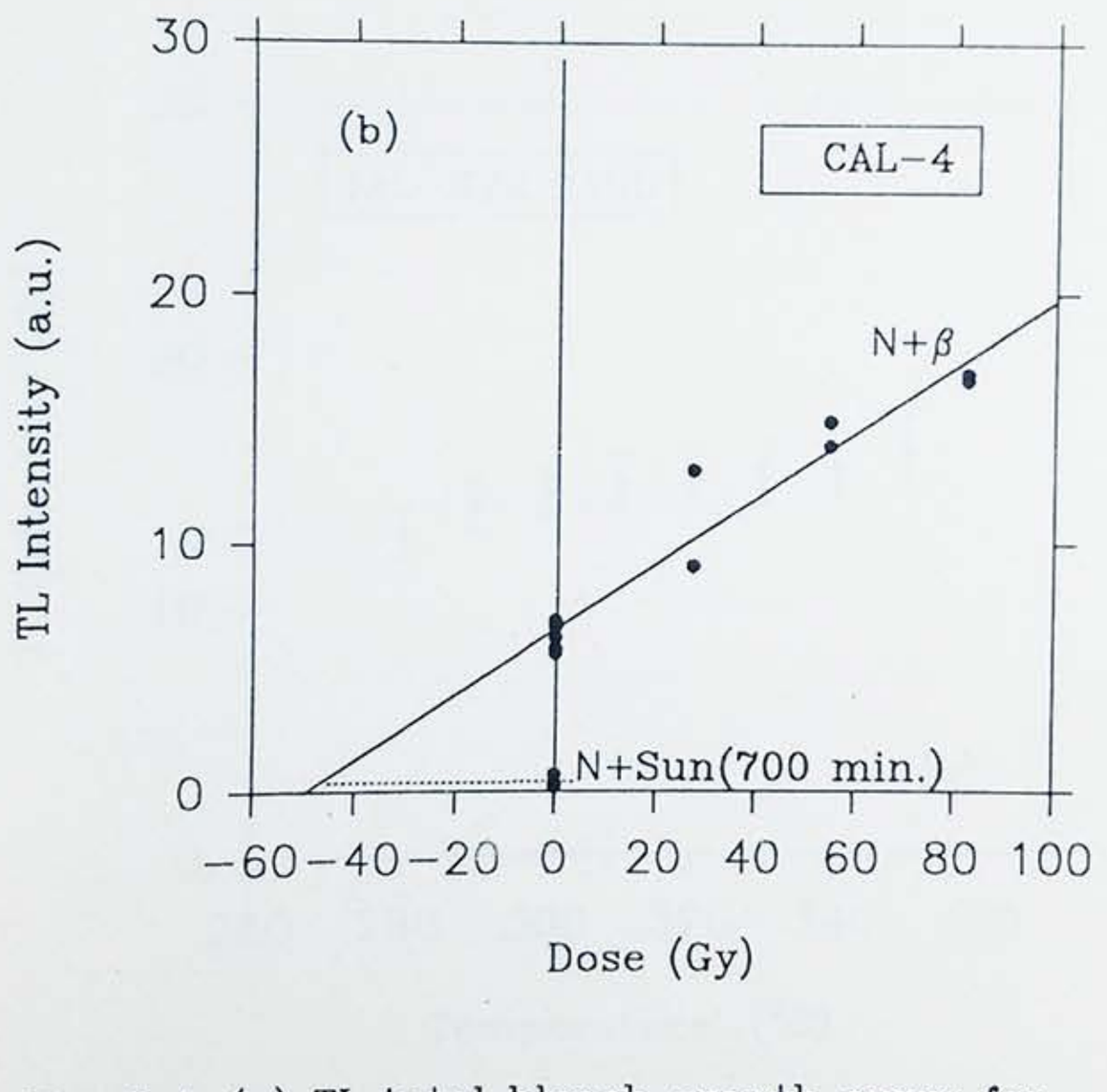


Fig. 5.4: (a) TL total bleach growth curve for quartz separates from host sand, PSH 92-2 and (b) TL total bleach growth curve for quartz separates from carbonate CAL-4.

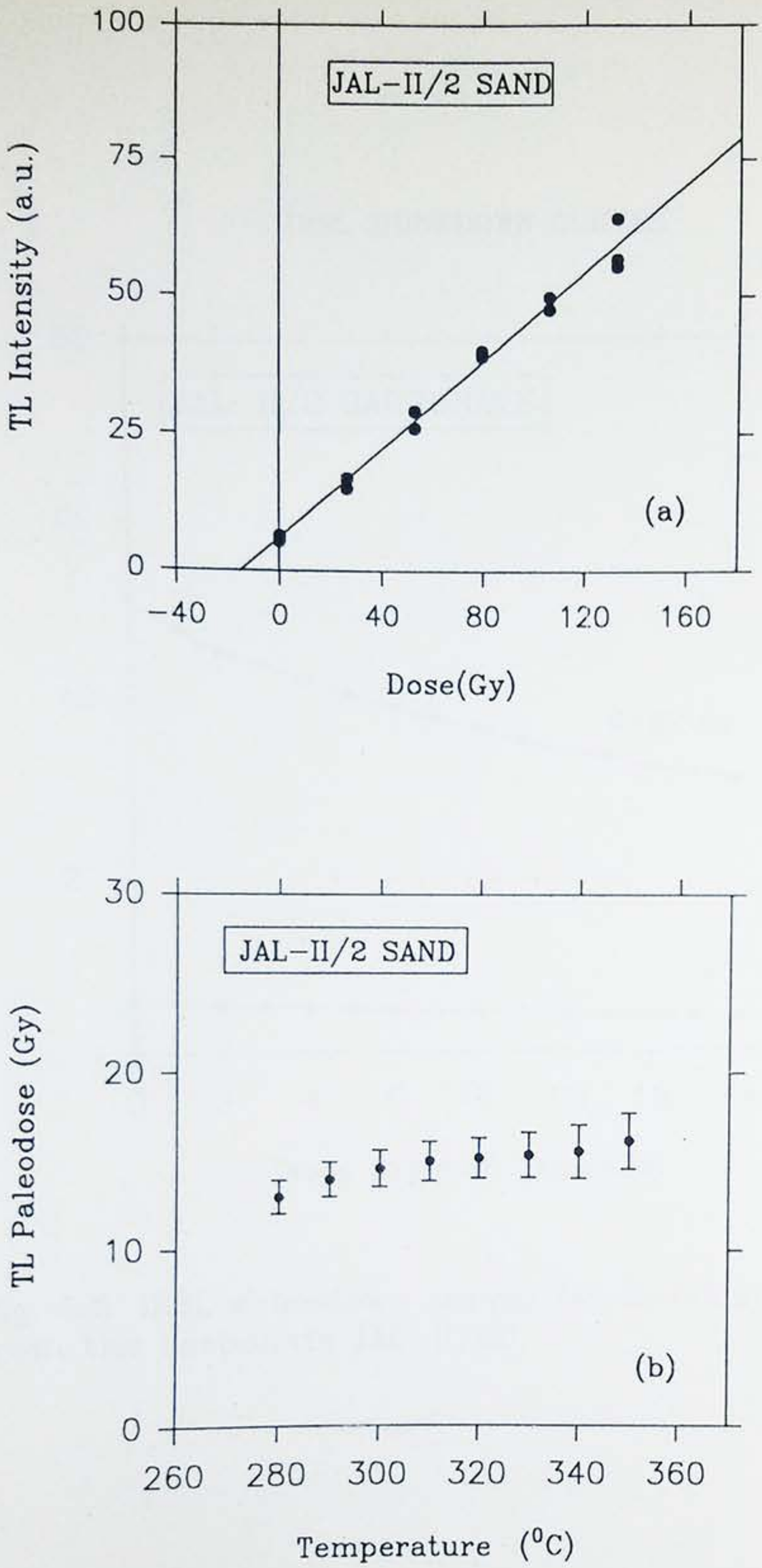


Fig. 5.5: (a) TL growth curve for K-feldspar extracts from host sand JAL-II/2S and (b) TL paleodose plateau for the host sand JAL-II/2S.

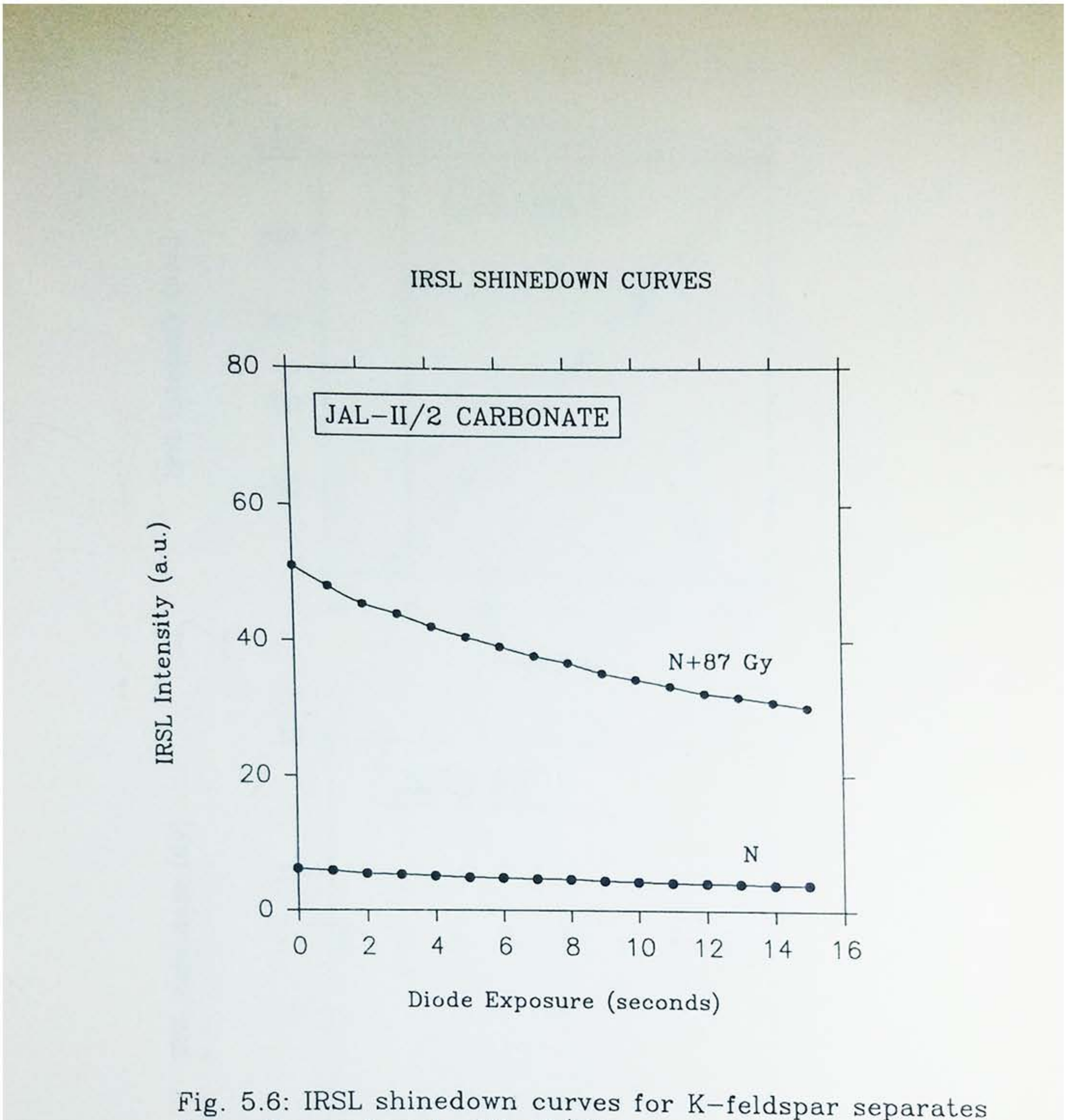


Fig. 5.6: IRSL shinedown curves for K–feldspar separates from the carbonate JAL–II/2C.

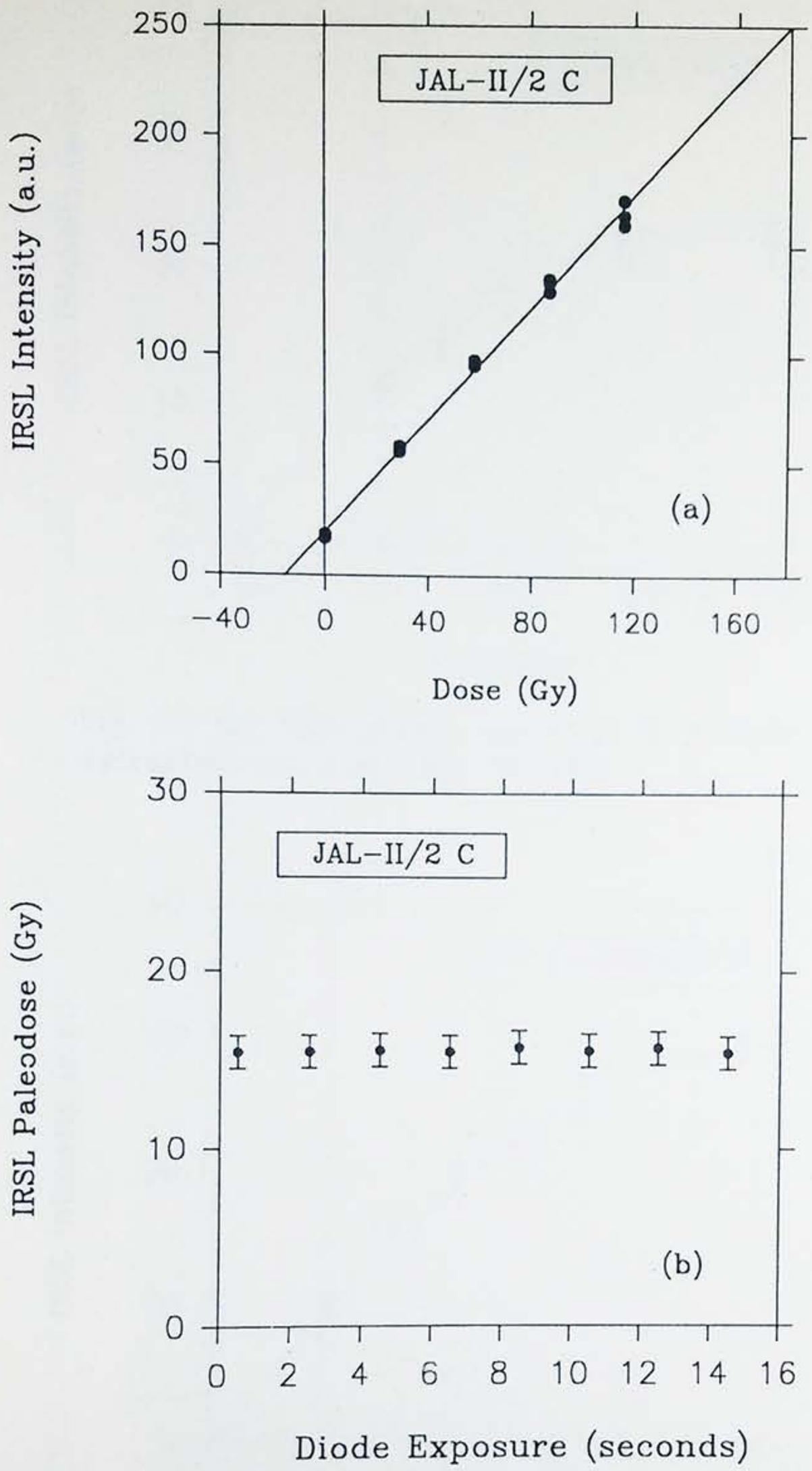


Fig. 5.7: (a) IRSL growth curve for K–feldspar separates from carbonate JAL–II/2C and (b) IRSL shine plateau for JAL–II/2C.

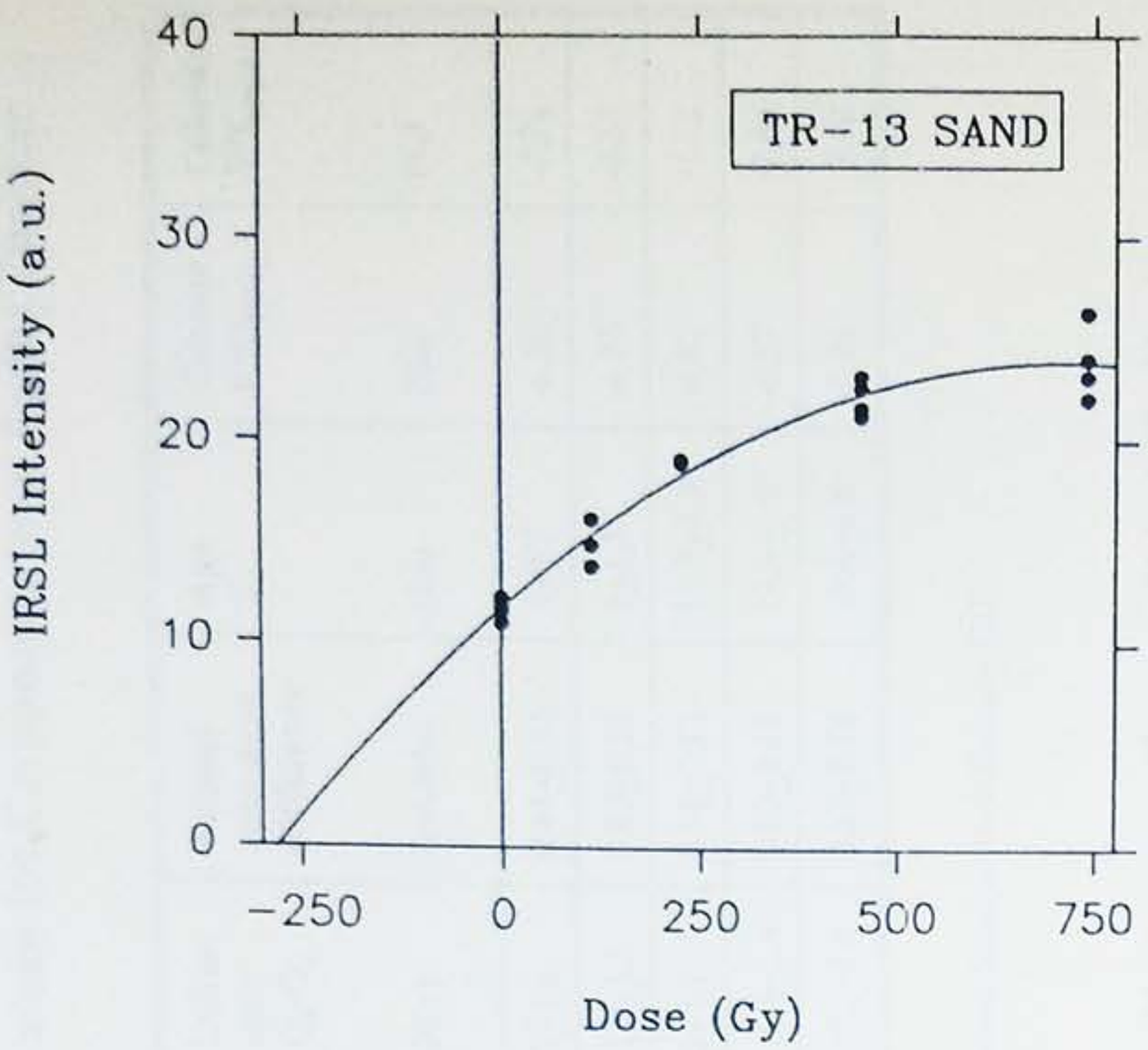


Fig. 5.8 (a): IRSL growth curve for K-feldspar extracts from host sand TR-13S.

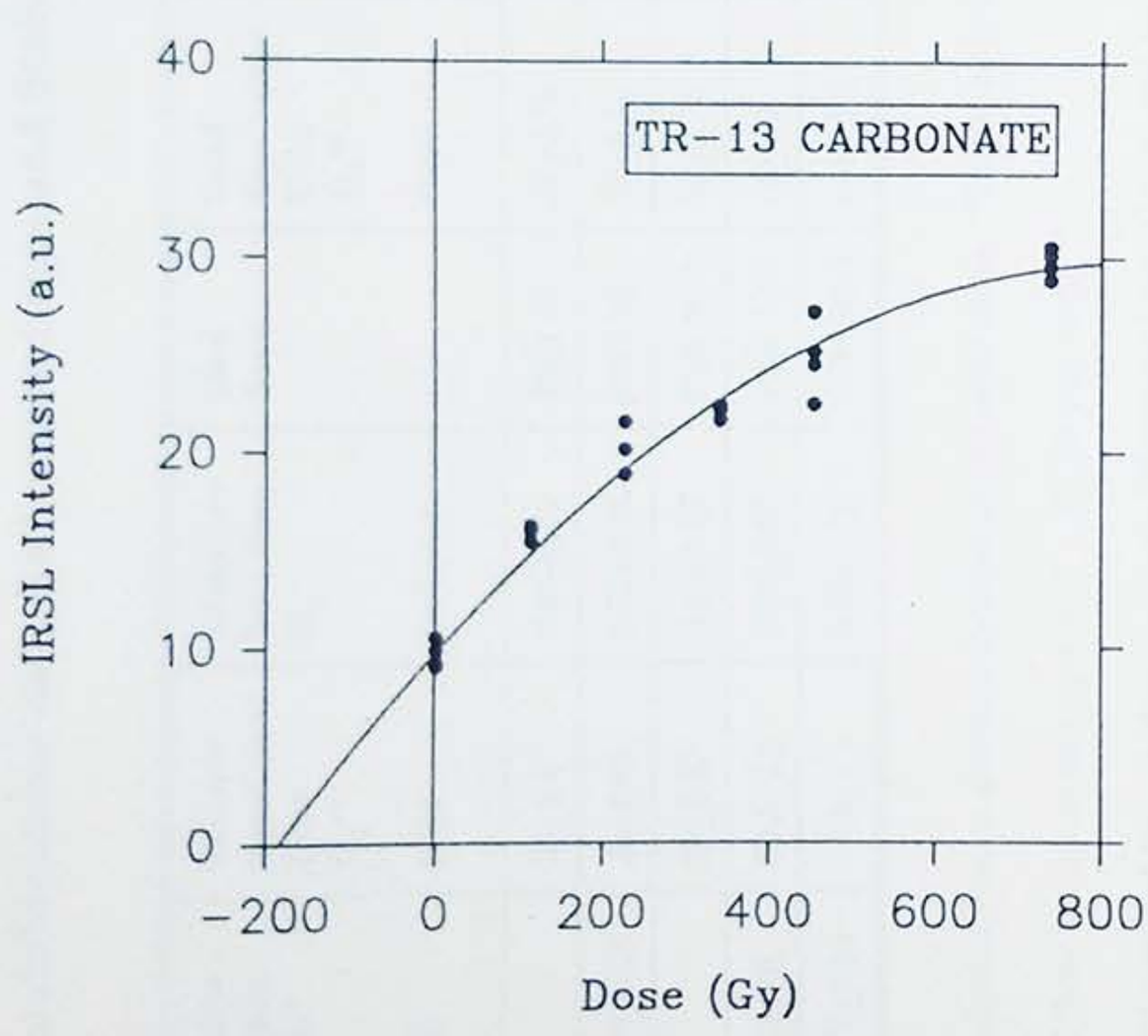


Fig. 5.8 (b): IRSL growth curve for K-feldspar extracts from carbonate TR-13C.

Table 5.3 : Thermoluminescence data, Radiocarbon ages and Stable Isotopic Values for Carbonates from Budha Pushkar

Calcrete Sample	Average depth (cm)	Radio-carbon ages* (ka)	Calcrete Equivalent Dose Q_c** (Gy)	Annual++ beta dose D_c (mGy/a)	Host Sand	Sand Equivalent Dose Q_s** (Gy)	Annual++ beta dose D_s (mGy/a)	Differ-ence Q_s-Q_c (Gy)	Annual beta dose difference (mGy/a)	Age T_c (ka)	Calcrete $\delta^{18}O_{PDB}$ (‰)	Calcrete $\delta^{13}C_{PDB}$ (‰)
CAL-0	55	-	35±1.4	0.99±0.09	PSH 92-1	37±0.75	1.40±0.13	2±1.6	0.41±0.13	5±3.7	-6.20	-7.74
CAL-1	78	7.38±0.20	36±0.86	0.77±0.07	PSH 92-1	37±0.75	1.40±0.13	1.0±1.1	0.63±0.13	2±1.3	-6.25	-8.57
CAL-3	125	-	29±0.87	0.85±0.07	PSH 92-1	37±0.75	1.40±0.13	8±1.1	0.56±0.13	14.3±4.3+	-4.82	-7.02
CAL-2	145	7.22±20	50.5±2.0	0.88±0.08	PSH 92-2	66±1.3	1.68±0.15	15.5±2.4	0.80±0.15	19.4±5.0+	-6.57	-7.84
CAL-4	195	3.78±0.31	51.3±1.3	0.89±0.08	PSH 92-3	61.6±1.2	1.42±0.14	10.3±1.8	0.53±0.14	19.4±6.8+	-5.24	-7.42

* These samples were collected from a different location in the same dune. ^{14}C ages have been calibrated using Stuiver and Reimer [20].

\+ The weighted mean of these three calcrete ages is 17 ± 2.9 ka (see text)

** Estimated as a weighted mean of partial bleach analysis (bleaching time 30 min) and total bleach analysis (bleaching time 30 min. and 7 hrs.). The bleaching was done under natural sunlight and both the sand and calcrete samples were exposed simultaneously. Typical bleached fractions were ~10-18% (after 30 min. bleaching) and reduced only marginally (~few %) thereafter. This is attributed to the selection of easily bleachable quartz signal using a UG11 filter.

++ Includes beta dose contribution from U, Th and K.

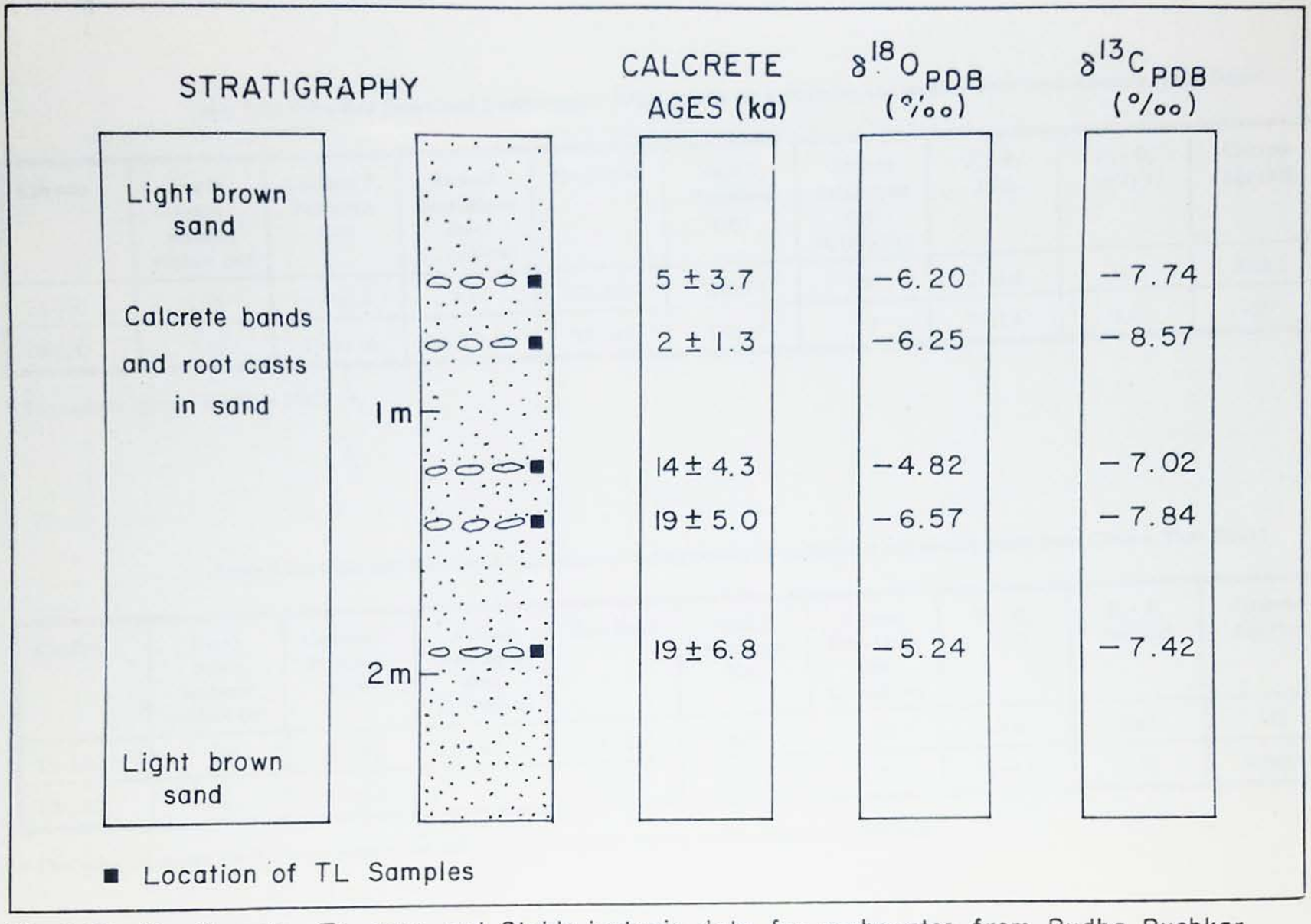


Fig. 5.9: Stratigraphy, TL ages and Stable isotopic data for carbonates from Budha Pushkar, Thar Desert.

Table 5.4a: Infra-Red Stimulated Luminescence dating results for carbonates and aeolian sands from Amarsar, Thar Desert

Calcrete	Depth below ambient surface (m)	Calcrete P_c Paleodose (Gy)	Annual beta+alpha dose D_c (mGy/a)	Host Sand	Sand P_s Paleodose (Gy)	Annual beta+alpha dose D_s (mGy/a)	$P_s - P_c$ (Gy)	$D_s - D_c$ (mGy/a)	Calcrete Age (ka)	Host Sand Age (ka)
TR-29C	1.65	107±3.4	0.84	TR-29S	128±7.7	1.89	21±1.4	1.05	20±8.2	42±3.4
TR-31C	3.10	196±17.6	1.0	TR-31S	210±14	2.0	14±1.6	1.0	<36*	64±6.0

* The calcrete age of TR-31C is 14±22 ka.

Table 5.4b: Infra-Red Stimulated Luminescence dating results for carbonates and aeolian sands from Chamu, Thar Desert

Calcrete	Depth below ambient surface (m)	Calcrete P_c Paleodose (Gy)	Annual beta+alpha dose D_c (mGy/a)	Host Sand	Sand P_s Paleodose (Gy)	Annual beta+alpha dose D_s (mGy/a)	$P_s - P_c$ (Gy)	$D_s - D_c$ (mGy/a)	Calcrete Age (ka)	Host Sand Age (ka)
TR-11C	3.0	164±6.2	1.02	TR-11S	160±7.4	1.66	<9.6+	0.64	<15	62±5.5
TR-13C	5.0	194±8.5	1.0	TR-13S	273±11.4	1.77	79±4.8	0.77	100±23	100±8.4

+ This value represents the maximum value of the difference between the calcrete and the host sand paleodoses

Table 5.5: Luminescence data for carbonates and aeolian sands from Jalore, Thar Desert

Sample	Tech-nique+	Calcrete P_c Paleodose (Gy)	Annual beta+alpha dose D_c (mGy/a)	Host Sand	Tech-nique+	Sand P_s Paleodose (Gy)	Annual beta+alpha dose D_s (mGy/a)	ΔP (Gy)	$D_s - D_c$ (mGy/a)	Calcrete Age (ka)	Host Sand Age (ka)
JAL-I/17C	TL	10.14±1.37	0.70	JAL-I/17S	TL	9.85±2.7	0.90	3.78	0.2	<7.0	7±2.0
JAL-I/17C	IRSL	10.05±1.40	0.70	JAL-I/17S	IRSL	9.61±0.7	0.90	1.66	0.2	<7.0	7±0.7
JAL-II/2C	TL	13.6±1.3	0.92	JAL-II/2S	TL	14.82±1.32	1.02	3.84	0.1	<9.0	9±0.9
JAL-II/2C	IRSL	15.52±0.93	0.92	JAL-II/2S	IRSL	15.46±0.7	1.02	1.57	0.1	<10.0	10±0.7

Water content (assumed) = 5% ± 1.5%
a value (feldspar) = 0.15 ± 0.075
* ΔP represents the maximum value of the difference between the host sand and the calcrete paleodoses.
Since the calcrete ages estimated by the expression $\Delta P/(D_s - D_c)$ are higher than the host sand ages (which is physically unrealistic), only upper limits can be provided on the calcrete age. The host sand ages represent maximum age of calcrete formation.
+ The additive dose method was used for both TL and IRSL dating.

carbon isotopic values range from $-$ 7.02 to $-$ 8.57 ‰ which (Cerling, 1984) implies a contribution of 28–35 % from C_4 type plants and upto 65 % from C_3 type, indicating somewhat wetter conditions. Marine records from the Indian Ocean show that during the last glacial maximum (LGM) at 21.5 ka (calendar years), the monsoon circulation over the Indian subcontinent weakened significantly, resulting in marked aridity. The reestablishment of the monsoon began at around 18 ka (Van Campo, 1986) reaching its full vigour by $\sim$ 11 ka. Similarly, on land, palynological studies (Singh et al., 1974) and ^{14}C dating of the organic fraction of the sediments of a saline lake (L. Didwana) in the Thar Desert indicate hyper-arid conditions from LGM to $\sim$ 16 ka. In the period 16–11 ka, the monsoon circulation reestablished itself and the annual precipitation reached twice its present value by $\sim$ 7 ka. Assuming that carbonates will be only formed when precipitation is $<$ 400 mm (Cooke et al., 1993), the paleomonsoonal reconstruction in Thar Desert (Bryson, 1989) suggests that during the last $\sim$ 20 ka, carbonates could have only formed in Thar Desert between $\sim$ 17 ka–10 ka, $\sim$ 6.8–4.8 ka and $<$ 2.5 ka. The luminescence age estimates thus agree well with these estimates.

For the carbonate TR–11C from Chamu, Thar Desert, only an upper age limit could be estimated due to a small difference between paleodoses P_s and P_c. This suggests that only maximum age limits can be estimated for young carbonates (few thousand years old) which precipitate in much older host sands. Even in Jalore, only maximum ages of carbonate formation could be obtained since the differences between the calcrete and host sand paleodoses is $<$ 1.5 Gy. The apparent IRSL ages (estimated by dividing the maximum value of the difference between P_s and P_c by the difference in annual doses D_s and D_c) for the carbonates JAL–I/17 and JAL–II/2 are $<$ 8.5 ka and $<$ 16 ka and are higher than the host sand ages, 7 $\pm$ 0.7 and 10 $\pm$ 0.7. Since the calcrete cannot be formed before the deposition of the host sand, only upper limits can be provided on the luminescence ages for the calcretes JAL–I/17 and JAL–II/2, viz., $<$ 7 $\pm$ 0.7 and $<$ 10 $\pm$ 0.7 respectively. These results imply that presently, the luminescence dating

method is best suited for dating carbonates which formed a few ka after the deposition of the host matrix. For young carbonates, the host sand age will constrain the age of the carbonate.

The luminescence ages on carbonates and host sands are stratigraphically consistent and suggest that carbonate formation occurred in Thar Desert at 100 ± 23 ka, 17 ± 3 ka and 2.3 ± 1.3 ka ago. The 100 ± 23 ka event is only observed at Chamu, whereas the 2.3 ± 1.3 event is indicated at Budha Pushkar and Jalore. The 17 ± 3 ka episode is observed at Chamu, Budha Pushkar and Amarsar, a west-east transect spanning ~ 300 km in Thar Desert. Thus, the luminescence data provides a possibility that a major carbonate formation episode took place in Thar Desert at ~ 17 ka. However, these inferences are based on limited data and are only suggestive and not conclusive. Further dating work remains to be done to make a more definitive statement about the 17 ka event.

Chapter 6

Thermoluminescence and Infra-Red Stimulated Luminescence dating of alluvial sediments

6.1 Introduction

Alluvial sediments form an important part of the Indian Quaternary in that they provide a testimony to both paleoseismic events and paleoclimatic changes. The application of alluvial sediments in paleoseismology has already been presented in the fourth chapter. This chapter discusses the application of TL and IRSL techniques for dating alluvial deposits for paleoclimatic reconstruction.

6.1.1 Alluvial sediments in Paleoclimatology

The response of river systems to the changing climate can be understood by studying the alluvial depositional history of the river. Striking differences have been observed in the form of rivers and the character of the sediments they carry in the arid and humid zones of the world (Schumm, 1977). Geomorphological studies in the rivers, Nile (Africa),

Murray-Darlington (South-eastern Australia) and Son (India) suggest that rivers 'metamorphose' with changing climatic conditions (Williams et al., 1993). Establishment of a chronology of paleoclimatic changes necessitate development of reliable dating techniques. Organic materials (e.g. wood, charcoal) necessary for radiocarbon dating are rarely preserved in arid/semi-arid zone alluvium and may not always represent the true depositional age (Ely et al., 1992). Thus, a need arises for a reliable technique for providing chronology to alluvium, a role which optical dating techniques promise to fulfill in the coming years. A necessary condition for luminescence dating is the complete resetting of the luminescence signal of the sediment at deposition. Many attempts have been made by luminescence dating workers to test this assumption. The following section gives an overview of these studies and other studies related to bleaching of water-borne sediments. This review includes earlier studies described in Berger (1988), Berger (1990), Duller et al., (1995) and some recent ones.

6.1.2 Earlier studies on zeroing of the luminescence signals of water-borne sediments

The zeroing studies can be effectively divided into two categories: (i) laboratory characterization of bleaching processes and (ii) comparison of luminescence ages with independent ages.

1. Laboratory characterization of bleaching processes

The shorter wavelengths of the visible region of the electromagnetic spectrum are attenuated in cloudy/turbid water due to absorption and scattering by suspended particles. Berger (1990) reports measurements of downwelling spectral irradiances for a Canadian lake and at a river delta amongst other depositional environments. In both these environments, light of wavelengths $\lambda < 550$ nm and $\lambda > 650$ nm were considerably attenuated at depths ≥ 2 m below the surface (irradiances at these depths were $\leq 3\%$ of the surface

irradiance). Thus, most workers recommend the use of passband filters with negligible transmission below 550 nm for laboratory bleaching of waterlaid sediments. Huntley (1985) obtained TL equivalent doses of 2-4 Gy on modern Canadian river silts with the partial bleach method and a Corning 3-67 filter (cutoff at 540 nm) for laboratory sun-bleaching. A striking contrast is provided if these results are compared with those of Belperio et al., (1984): large equivalent doses were estimated for zero-age deposits due to the application of shorter wavelengths and long sunlight exposures.

Other interesting issues which have been discussed previously are: (i) the time of sunbleaching and (ii) use of different bleaching signals for dating. It has been suggested (Berger et al., 1987; Mejdahl, 1988) that two or more bleaching times should be used to estimate the TL age for water-borne sediments. The appearance of an equivalent dose (Q) plateau for various bleaching times implies that the sediments have been well bleached at deposition. For poorly bleached sediments receiving attenuated sunlight for short durations, a decrease in Q values is expected with decreasing bleaching time. Berger et al., (1987) propose that in such situations, the Q value for the shortest bleaching time represents a maximum TL age for the sediment. Mejdahl (1988) suggests that the luminescence residual signal level should be determined for various bleaching times at different temperatures. The residual level which provides the best equivalent dose plateau should represent an accurate estimate of the equivalent dose value. As regards bleaching signals, Bailiff (1992) and others propose that two luminescence signals from the same sample be used for luminescence dating of poorly bleached samples.

With the advent of optical dating, the focus of luminescence dating workers has shifted to bleaching of the sediment OSL and IRSL signals. Godfrey-Smith et al., (1988) has reported comparisons between bleaching of the TL and OSL signals for quartz and feldspar (Fig. 6.1). Whereas it took 20 hours of sunlight (clear sky) for quartz TL to be bleached to 17% of its initial level, the quartz OSL signal was bleached to 1% of the

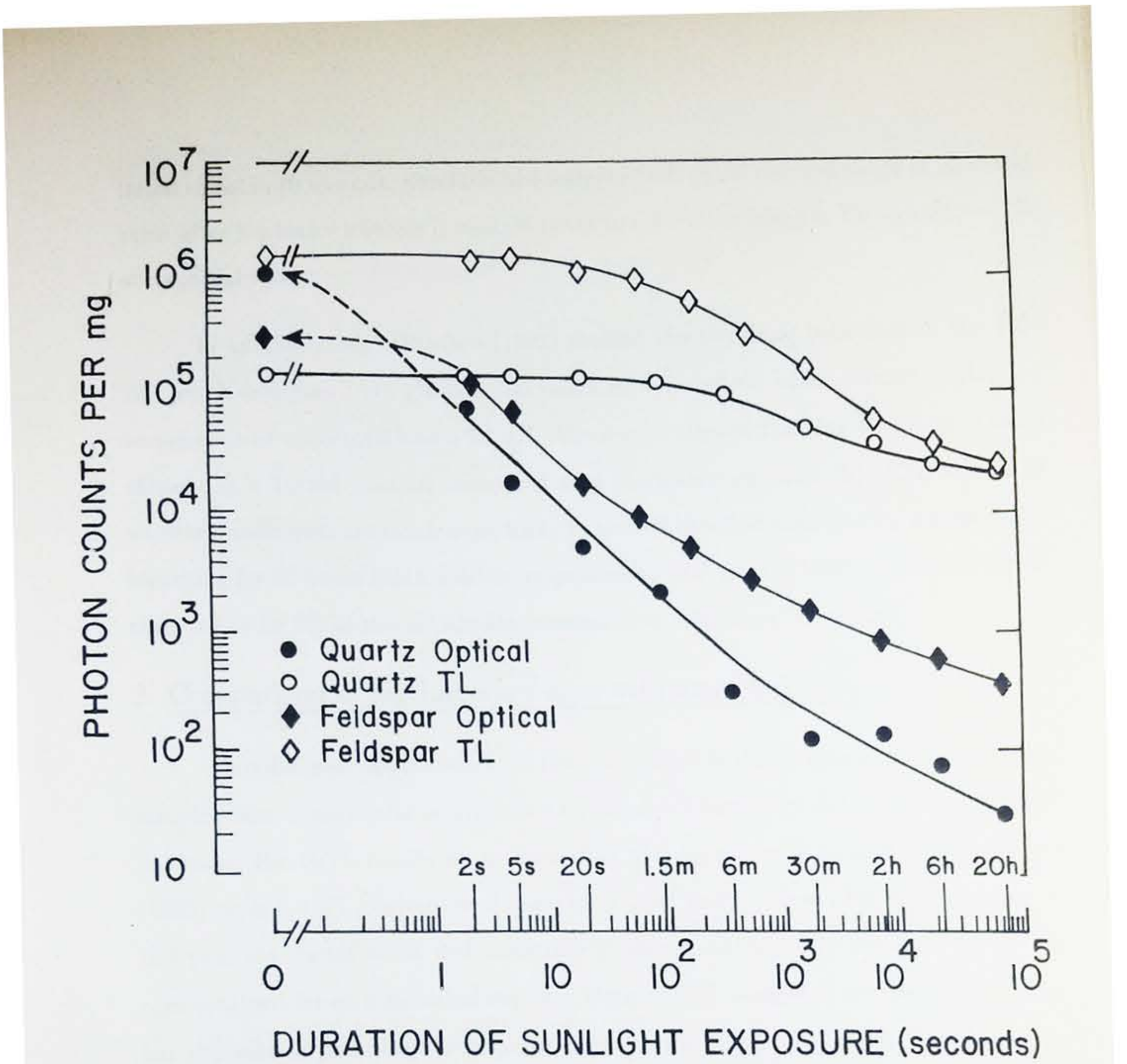


Fig. 6.1. Effect of sunlight exposure on OSL and TL signals of quartz and feldspars. Optical signal is for 1 second after laser is switched on (10 mW/cm^2: Quartz; 15mW/cm^2: feldspar). The 514 nm was the exciting wavelength (after Godfrey-Smith et al., 1988).

initial signal in 10 seconds. Similarly, the feldspar OSL signal reduced to 1% of its initial value after 9 minutes whereas it took 20 hours to reduce the feldspar TL signal to $\sim$ 2% of its initial value.

In another study, Ditlefsen (1992) studied the bleaching behaviour of the 100-200 μm K-feldspars from glaciofluvial sands in a turbulent water column containing suspensions of concentrations 0-0.1 g/l. His results showed that (a) bleaching is more efficient in a turbid medium compared to a stationary one and (b) IRSL signals of waterlaid sediments are much more likely to be well bleached than the TL signals: after bleaching for 20 hours below a dilute suspension of 0.02 g/l, the IRSL residual level was observed to be 5% of the initial value compared to $\sim$ 50% for TL signals.

2. Comparison of luminescence ages with expected ages.

Two different approaches have been developed in these studies. Firstly, zero-age samples from a particular sedimentary environment have been dated by luminescence methods. Huntley's results on modern river silts have been discussed above. Berger (1990) reported TL partial-bleach ages of $\sim$ 1000 years and $\sim$ 1000-2000 years on $<$ 100 year old fluvial sands and lacustrine muds respectively. On the basis of the TL ages obtained for such historical deposits, Berger (1990) suggested the use of sandy river bar deposits in preference to silty bar deposits and thin clayey layers from lacustrine rhythmites compared to silt bearing laminae for TL dating. In another study, Stokes (1992) reported OSL equivalent doses of 0.05-0.3 Gy for modern deposits from aeolian and fluvial environments. Recently, Rao (1996) has obtained IRSL ages of $\sim 200 \pm 100$ years on modern river terrace sediments from Kanpur, India.

These studies have been complemented by determination of luminescence ages on samples where some age control was available. The following discussion gives a description of some of these case studies.

Rendell et al., (1991) obtained TL ages on the quartz (Q) and feldspar (F) components from alluvial sands lying above and below a peat horizon in Cheshire, U.K. The TL ages were 82 ± 8.2 ka (F) and 74 ± 8.1 ka (Q) for sands above the organic horizons. The lower alluvial sand horizon gave TL ages of 84 ± 8.2 ka (F) and 99 ± 12 ka (Q). The TL ages are consistent with (i) a U-series age of 86 ka on the peat horizon and (ii) amino-acid analyses results which suggested that the peat representing the Chelford Interstadial should be correlated with the Oxygen Isotope Stage 5c, ~ 100 ka.

In an inter-comparison study, Nanson and Young (1987) observed a general agreement between TL ages on the fine-grain fraction from sandy Australian fluvial sediments and available ^{14}C ages on associated wood and charcoal. Murray et al., (1992) have also obtained TL ages on Northern Australian fluvial sands ranging from 0-6000 years. These ages were consistent stratigraphically and with ^{14}C chronology.

Balescu and Lamothe (1994) have reported TL and IRSL ages on 150-250 μm alkali feldspars from a variety of water-borne environments (shallow marine, estuarine, shallow lacustrine and sublittoral). The ages obtained were in the range 10-200 ka and were consistent with independent ages based on ^{14}C, ESR and Amino-Acid dating within experimental errors. Balescu and Lamothe (1994) concluded that beach, estuarine and shallow lacustrine sediments are well bleached at deposition and are suitable for luminescence dating.

IRSL ages on floodloams from South Germany were reported by Lang (1994). An IRSL equivalent dose of 3.5 ± 0.1 Gy was obtained from a 1990 flood deposit. The high equivalent dose was attributed to recuperation and incomplete bleaching. IRSL floodloam ages from lower depths of the profile were in agreement with the ^{14}C ages. However, some IRSL ages from the upper part of the profile gave overestimates of the true depositional age. The possible reasons suggested by Lang to explain these higher ages were: (i) incomplete bleaching of the IRSL signal and (ii) absence of real sandy

fraction due to coagulation of clay and silt, resulting in incomplete bleaching of the interior of the coagulate.

Recently, Fuller (1996) has performed detailed IRSL dating of Spanish alluvium sites and obtained ages in the range $\sim$ 1-200 ka. A single ^{14}C age was also available for cross-checking the IRSL ages. A few IRSL ages were stratigraphically inconsistent: the occurrence of anomalously low ages was explained by Fuller as a result of anthropogenic disturbance. Anomalously high ages occurred due to incomplete bleaching of the IRSL signal at deposition.

6.1.3 Present Studies

Stratigraphical and sedimentological changes (Courty, 1990) in the Ghaggar and Chautang flood plains (near Hissar), Haryana (Fig. 6.2) demonstrate the response of the river systems to a changing climatic/monsoonal regime. However, paucity of ^{14}C datable materials meant that extremely few absolute ages could be provided to constrain the time frame for the paleoenvironmental changes. The present work involved TL and IRSL dating of Ghaggar, Chautang and Southern Chautang flood plain deposits (Fig. 6.3) to furnish additional data to test the validity of the luminescence methods for dating alluvium besides providing a well-constrained paleoclimatic record for this region.

6.2 Experimental Techniques

TL dating was performed on 106-150 μm quartz extracts whereas 75-106 μm K-feldspar extracts were used for both TL and IRSL dating. The extraction of K-feldspar was performed in a similar manner as described in Section 4.5. In view of limited sample availability, no HF etching of these grains was done. Thus, an alpha dose contribution

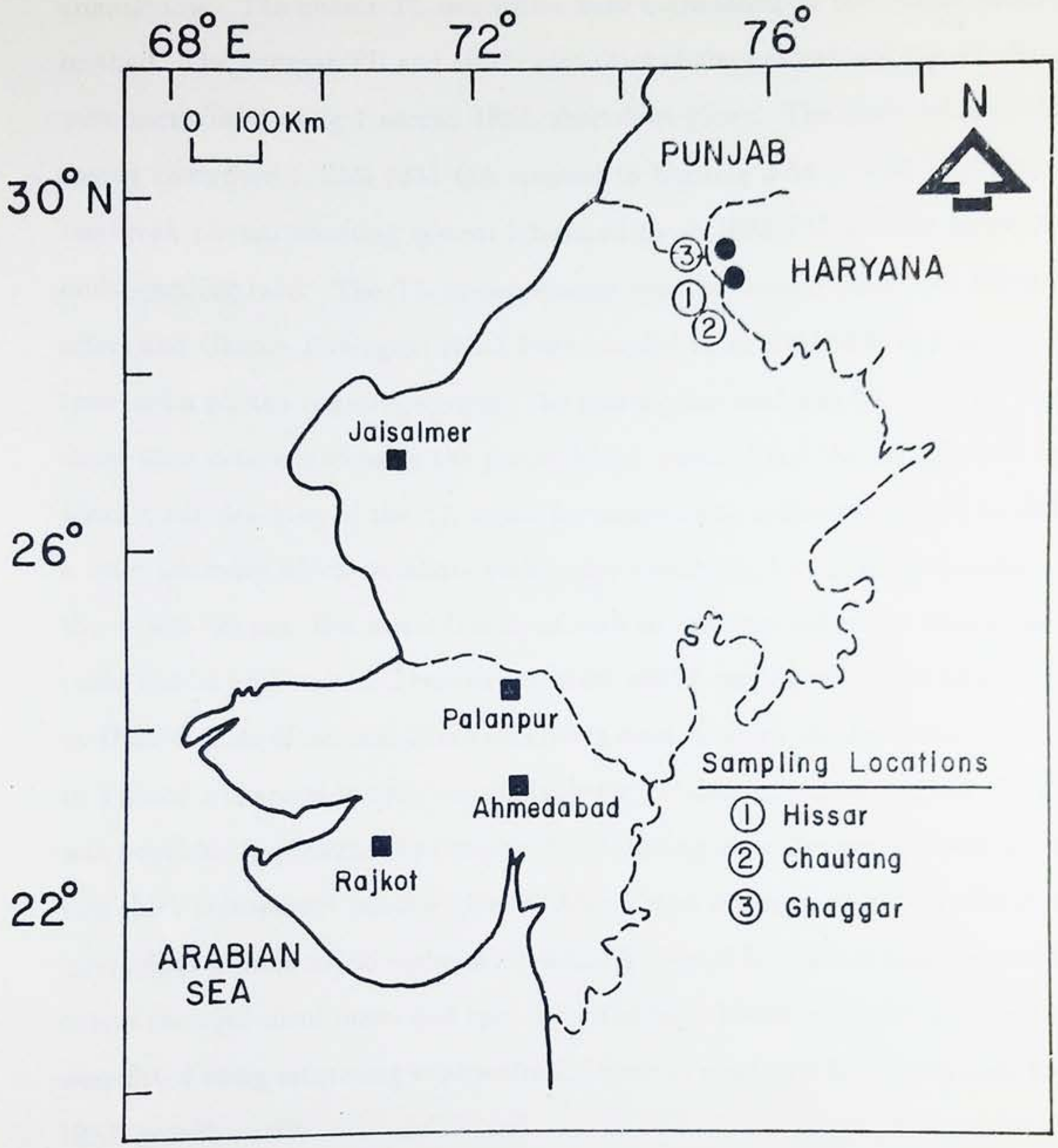


Fig. 6.2: Locality map of North–West India showing Chautang and Ghaggar flood plain sites sampled for luminescence dating.

corrected for attenuation was also considered in the estimation of annual dose. Attenuation in beta dose (Mejdahl, 1979) was also taken into account while calculating the annual dose. The quartz TL intensities were normalized by the weight normalization method. The feldspar TL and IRSL intensities of the natural and the irradiated discs were normalized using 1 second IRSL shortshine glows. The optics channel for IRSL dating comprised a EMI 9635 QA coupled to Corning 5-58 + 7-59 blue filters and a Daybreak photon counting system interfaced to an IBM/PC with an Ortec Accuspec multi–scaling card. The TL measurements were performed using two Schott UG-11 filters and Chance Pilkington HA-3 filter coupled to an EMI 9635 QA photomultiplier tube and a photon counting system. The heating rate used was 2°C s^{-1}. TL Equivalent doses were determined using the partial bleach method and the total bleach methods. Ideally, sunbleaching of the TL signal for water-borne sediments should be done with a filter assembly which simulates underwater conditions, i.e., peak transmission only in the $\sim$ 550-700 nm. But unavailability of such an arrangement meant that these studies could not be undertaken. These experiments will be carried out in the future. However, as IRSL signals of sediments are effectively reset in much shorter durations compared to TL and a charcoal sample was available for ^{14}C dating, a cross-check of the TL dates was possible. Representative samples for TL dating were also sun-exposed through a 4 mm thick transparent window glass in Ahmedabad during a cloudy day for short time intervals (1-4 minutes) to evaluate a residual TL signal level which was then used to calculate the equivalent doses and ages using the total bleach method. TL growth curves were fitted using saturating exponentials. Linear or quadratic fitting was used for fitting IRSL growth curves.

In the estimation of annual dose, an α–efficiency factor of 0.15 $\pm$ 0.075 was assumed for the coarse-grained K-feldspars. U and Th concentrations were estimated using thick source ZnS (Ag) alpha counting method and NaI(Tl) gamma ray spectrometry was used for potassium estimation. A radioactive equilibrium in the decay series of

U and Th was assumed in the dose rate calculations. The beta dose contribution due to the presence of internal potassium within 75-106 μm K-feldspars is comparable to the experimental error (2σ) in the annual dose and was not considered in the annual dose calculations. The cosmic ray dose rate was assumed to be 150 μGy/a. The water content was assumed to be 5% $\pm$ 1.5% in the evaluation of TL/IRSL ages. Error estimation was carried out following the prescription of Aitken (1985).

6.3 Results and Discussion

Fig. 6.3 provides a schematic of the three sections sampled for luminescence dating. Fig. 6.4 provides IRSL shine-down curves. Figs. 6.5 and 6.6 present IRSL growth curves and shine down plateaus for K-feldspar extracts from flood plain deposits. Tables 6.1 and 6.2 present TL and IRSL luminescence data for the samples.

Initially in TL analysis, the total bleach (7 hours natural sunlight exposure) and the partial bleach (R-β) methods (30 minutes natural sunlight exposure) were used to determine the equivalent dose. The total bleach and the R-β ages agree within experimental errors. However, the R-β and the total bleach ages (27 $\pm$ 11 ka, 31 $\pm$ 10 ka) for CNF-16 are much higher in comparison to the available calibrated ^{14}C age of 14.3 $\pm$ 1.0 ka for the charcoal sample CNF-17 located $\sim$ 0.5 m above CNF-16. Thus, it became apparent that even a natural sunlight exposure of 30 minutes overestimates the depositional age. This is due to partial resetting of the TL signal of these sediments at deposition. Disequilibrium in the U and Th series (although possible in the case of waterlaid sediments) was ruled out as an explanation for the higher TL ages since (i) typically, $\sim$ 75% of the annual dose is contributed by potassium, thus limiting the change in TL age as a result of disequilibrium to $< 10\%-15\%$ and (ii) it would lead to lower annual doses and even higher TL ages.

Fig. 6.3. Stratigraphic summary of Ghaggar, Chautang and South Chautang flood plain sections. ^{14}C and IRSL ages on various units sampled for luminescence dating are also provided.

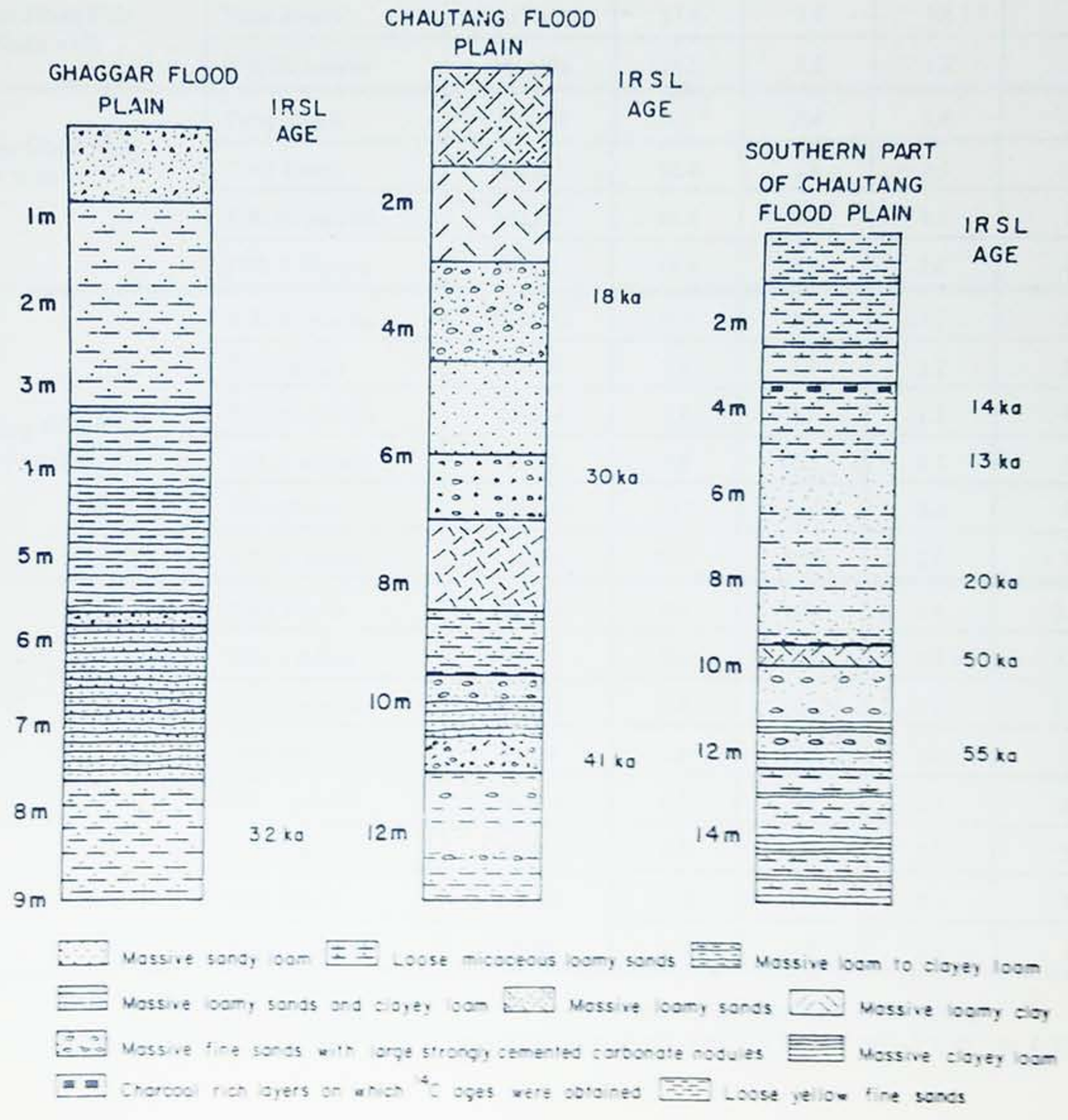


Table 6.1: Results of Thermoluminescence dating of alluvial and aeolian sands from Ghaggar and Chautang flood plains

Sample	Depth# (m)	Location	Technique*	Equivalent Dose (Gy)	Th (µg/g)	U (µg/g)	K (cg/g)	Annual Dose** (mGy/a)	Age (ka)
CNF-1	13.5	Ghaggar Flood Plain (Hjat Singh well)	Total Bleach	317±43	13.1	3.8	1.8	3.9	81±12
CNF-1	13.5		R-ß, 30 minutes	341±120	13.1	3.8	1.8	3.9	87±30
CNF-3	8.3	Ghaggar Flood Plain (Nakta well)	Total Bleach	293±50	8.2	2.4	1.6	3.0	98±19
CNF-6	2.1		Total Bleach	166±63	12.4	3.6	1.6	3.4	49±18
CNF-6	2.1		R-ß, 30 minutes	161±65	12.4	3.6	1.6	3.4	47±19
CNF-7	1.0		FSE, 2 minutes	80±13	15.4	4.5	1.6	4.0	20±3.6
CNF-8	10.7	Chautang Flood Plain (Siswal village)	R-ß, 30 minutes	553±133	11.6	3.4	1.7	3.6	154±38
CNF-10	6.5		Total Bleach	234±41	7.8	2.3	1.7	3.0	78±14
CNF-10	6.5		R-ß, 30 minutes	279±64	7.8	2.3	1.7	3.0	93±21
CNF-10	6.5		FSE, 2 minutes	53±12	7.8	2.3	1.7	3.0	18±4.3
CNF-11	3.5		Total Bleach	158±44	10.5	3.05	2.0	3.7	43±12
CNF-11	3.5		R-ß, 30 minutes	178±71	10.5	3.05	2.0	3.7	48±19
CNF-14	8.0	Southern part of Chautang Flood Plain	Total Bleach	235±22	8.4	2.4	1.4	2.75	85±12
CNF-14	8.0		FSE, 1 minute	68±12	8.4	2.4	1.4	2.75	25±4.8
CNF-14	8.0		FSE, 3 minute	103±13	8.4	2.4	1.4	2.75	37±5.6
CNF-15	5.0		Total Bleach	91±11	6.3	1.8	1.5	2.6	35±5.2
CNF-15	5.0		FSE, 1 minute	36±8.5	6.3	1.8	1.5	2.6	14±3.5
CNF-15	5.0		FSE, 4 minute	38±8.6	6.3	1.8	1.5	2.6	15±3.6
CNF-16	4.0		Total Bleach	116±37	10.0	2.9	2.1	3.7	31±10
CNF-16	4.0		R-ß, 30 minutes	99±40	10.0	2.9	2.1	3.7	27±11

** Water content = 5% ± 1.5% # below ambient surface * Quartz extracts were used for TL dating

FSE: Sunlight filtered through a 4mm thick transparent window glass (for a short time interval indicated above) was used for evaluating the residual in the determination of TL age.

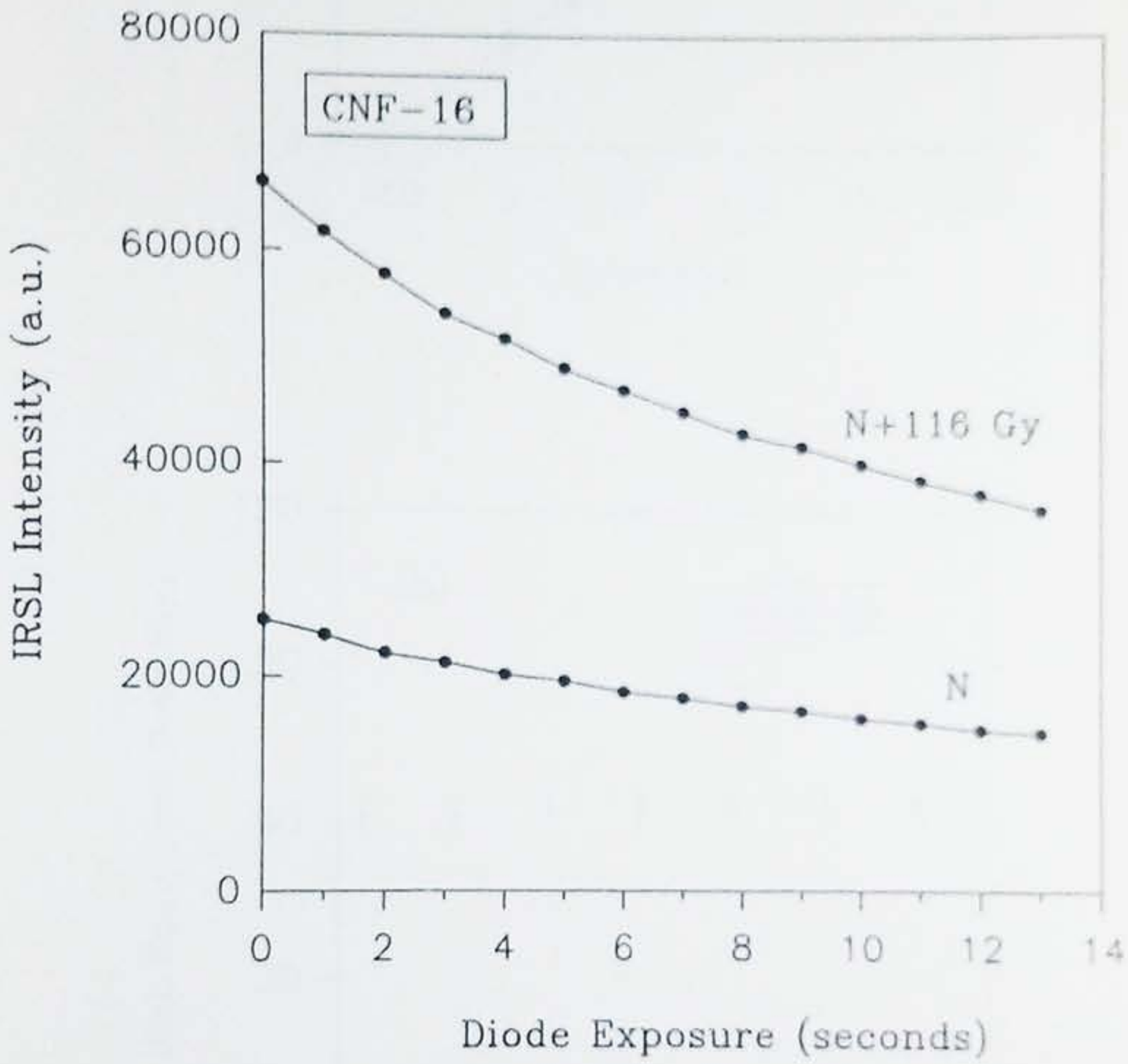
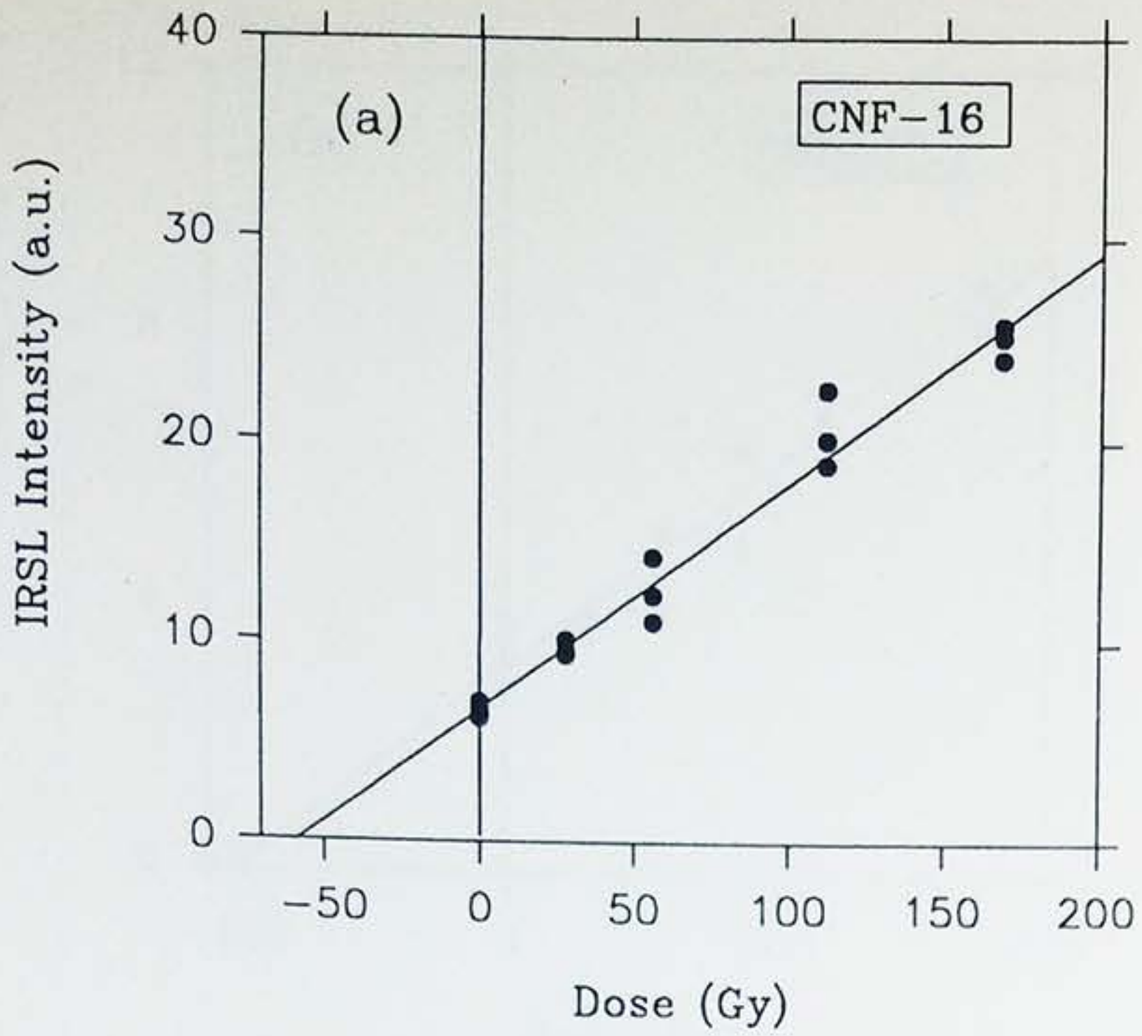


Fig. 6.4: IRSL shinedown curves for K-feldspar separates from the sample CNF-16.



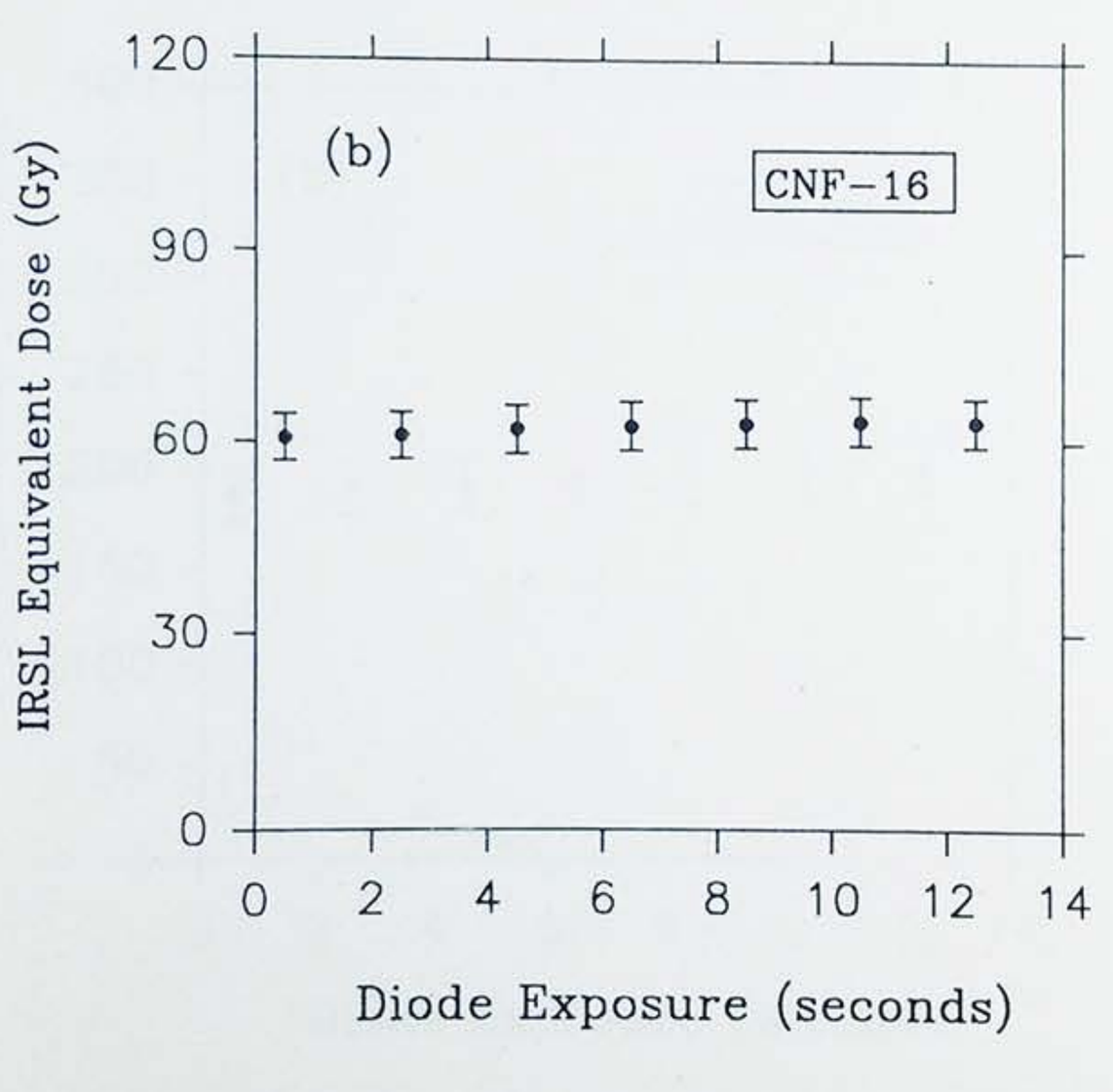


Fig. 6.5: (a) IRSL growth curve for K−feldspar separates from CNF−16 and (b) IRSL shine plateau for CNF−16.

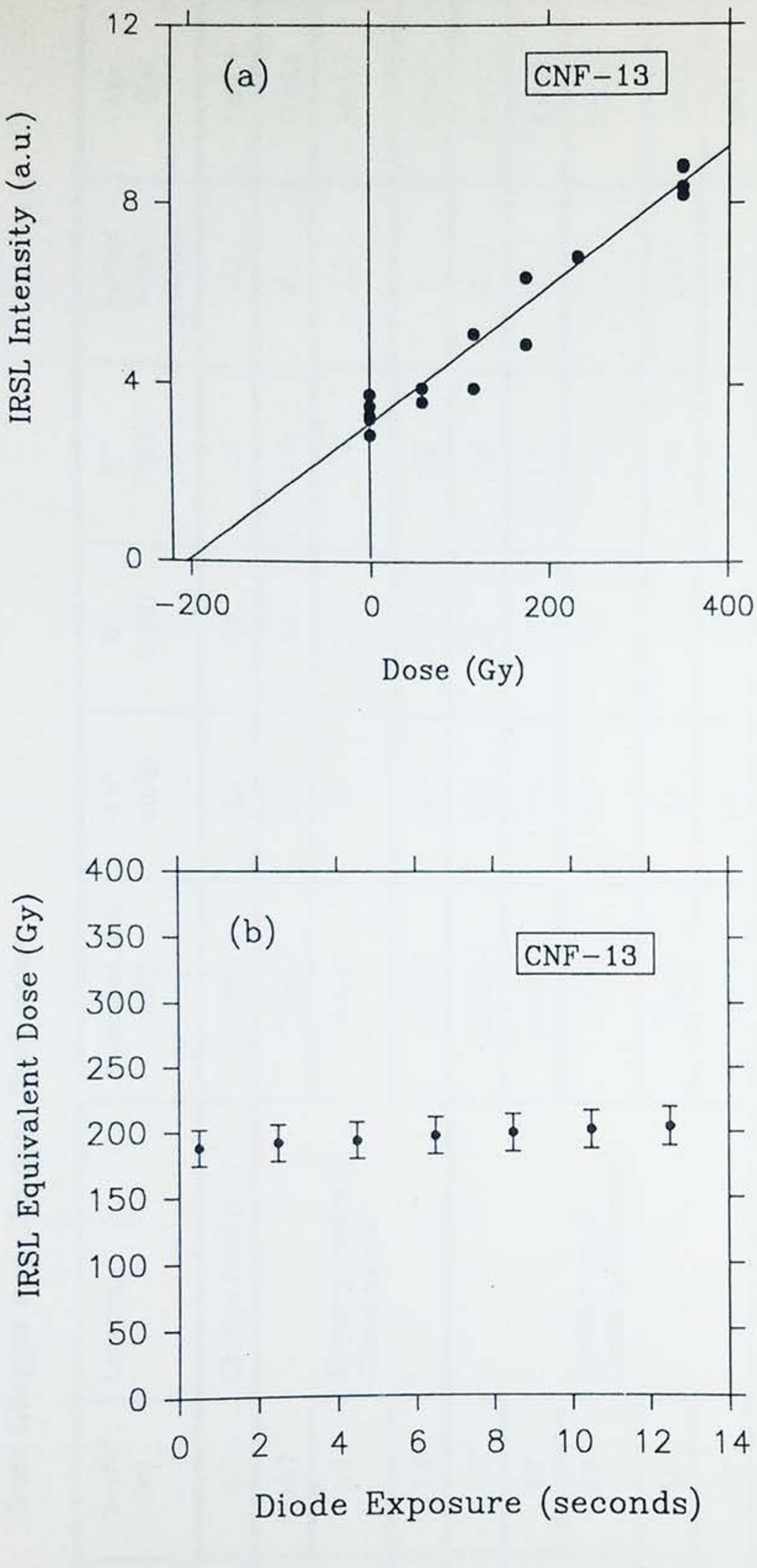


Fig. 6.6: (a) IRSL growth curve for K−feldspar separates from CNF−13 and (b) IRSL shine plateau for CNF−13.

Table 6.2: Results of Infra-Red Stimulated Luminescence Dating of alluvial and aeolian sands from Ghaggar and Chautang flood plains

Sample*	Depth# (m)	Location	Equivalent Dose (Gy)	Th$ (µg/g)	U$ (µg/g)	K++ (cg/g)	Annual Dose+ (mGy/a)	Age (ka)
CNF-3	8.3	Ghaggar flood plain	104±4	8.2	2.4	1.6	3.3	31±2.6
CNF-8	10.7	Chautang flood plain (Siswal village)	167±8.4	11.6	3.4	1.7	4.1	41±3.5
CNF-10	6.5		101±9.1	7.8	2.3	1.7	3.3	30±3.3
CNF-11	3.5		75±8.2	10.5	3.05	2.0	4.1	18±2.2
CNF-12	11.7	Southern part of Chautang flood plain	252±34.8	12.8	3.7	2.0	4.6	55±7.8
CNF-13	9.7		196±14.8	11.0	3.2	1.6	3.9	50±4.9
CNF-14	8.0		63±10	8.4	2.4	1.4	3.1	20±3.2
CNF-15	5.0		38±2.2	6.3	1.8	1.5	2.85	13±1.2
CNF-16	4.0		61±4.5	10.0	2.9	2.1	4.2	14±1.4

+ Water content (assumed) = 5% ± 1.5%
Feldspar a value (assumed) = 0.15 ± 0.075
below ambient surface
* 75-106 µm K-feldspar extracts were used for IRSL dating. The additive dose method was used to evaluate the equivalent dose.
$ Error in Th and U concentrations is typically ~10%
++ Error in K concentration is typically ~5%

Next, as alluded to above, the samples were exposed to various filtered sunlight exposures (4 mm thick window glass, sample kept at a distance of 2 m away from glass) to determine which sun-exposures would result in the evaluation of a correct residual TL level and TL ages concordant with the available ^{14}C age. Also, keeping in mind the suggestions made by earlier workers regarding the use of two or more bleaching signals and the efficient and rapid bleaching of the IRSL signal in comparison to the TL signals (Aitken, 1994), IRSL dating was taken up for some representative samples.

The IRSL age for the sample CNF-16 is consistent with the ^{14}C age for the charcoal layer located 0.5 m above CNF-16. The IRSL ages are also stratigraphically consistent. Their is good agreement between the IRSL ages and the TL ages of CNF-15 and CNF-14 using a residual level determined by filtered sunlight exposure of $\sim$ 1 minute (Table 6.3). This signifies that the sediments were exposed to sunlight for very short intervals of time. It also suggests that the IRSL signal was presumably completely reset for these sediments at deposition. However, different sediments respond to similar filtered sunlight exposures (FSE) in a different manner. This is illustrated by the comparison of FSE-TL ages for samples CNF-15 and CNF-14. The 1 minute and 4 minute FSE-TL ages (and therefore the likelihood of the 3 minute FSE age also) for CNF-15 are similar within errors (14 $\pm$ 3.5 ka and 15 $\pm$ 3.5 ka), whereas for CNF-14, the 1 minute and 3 minute FSE ages are 25 $\pm$ 4.8 ka and 37 $\pm$ 5.6 ka. The explanation for this behaviour is as yet unknown. Another interesting observation is that the FSE (2 minute) TL age for CNF-10 is much lower compared to the respective IRSL age. Since no ^{14}C ages exist for this unit, it is difficult to state whether the FSE TL age underestimates the depositional age. However, it needs to be stated that only IRSL ages (for all sections) were used for ascertaining the climatological implications of the luminescence ages. The discussion below relates to the paleoclimatic scenario which emerges on the basis of earlier sedimentological studies by Courty (1990) and the luminescence ages.

Table 6.3 : Comparison of available ^{14}C, FSE TL and IRSL ages for Chautang and Ghaggar flood plain deposits

Sample	Location	^{14}C age (ka)	FSE+ TL age (ka)	IRSL age (ka)
CNF-10	Chautang Flood Plain	-	18# ± 4.3	30 ± 3.3
CNF-14	Southern part of Chautang Flood Plain	-	25* ± 4.8	20 ± 3.2
CNF-15		-	14* ± 3.5	13 ± 1.2
CNF-16		14** ± 1.0	-	14 ± 1.4

+ FSE : Sunlight filtered through a 4mm thick transparent window glass (for a short time interval indicated below) was used for evaluating the residual signal in the determination of TL ages
2 minute sun exposure used for estimating the residual signal
* 1 minute sun exposure used for evaluating residual signal
** Calibrated

Paleoclimatic Scenario

Courty's (1990) stratigraphical and sedimentological studies of many deep sections in this region (including the present ones) reveal at least four distinct sedimentation periods. The IRSL and radiocarbon chronology establish a time-frame for these paleoenvironmental changes. Phase 1 is a period of regular alluvial activity which began earlier than 55 ka. This phase, observed in the Southern Chautang flood plain section (Fig. 6.3), is succeeded by a period of intermittent fluvial and aeolian activity which began around 50 ka and extended till $\sim$ 20 ka. This phase is prominent in the Chautang flood plain section. After Phase 2, a period of intense aeolian activity set in around 20-14 ka (Phase 3). $\delta^{13}C$ values on peat from Nilgiri Hills, India have previously been used to infer the occurrence of an arid phase in Southern India at $\sim$ 20-12 ka ago (Sukumar et al., 1993). Dust fluxes to the Arabian Sea have been used by Shimmeld et al., (1990) to suggest that Arabia registers an arid episode between 22 and 18 ka ago. Phase 3 was followed by a humider period and an increase of alluvial activity. The present luminescence ages imply the initiation of this phase (Phase 4) at around $\sim$ 13 ka ago. Sukumar et al., (1993) and Wasson et al., (1984) also report the beginning of humid phases in the Indian sub-continent at around 13 ka. The luminescence ages cannot prescribe a limit on the time when this phase ended.

The luminescence chronology are thus consistent with the available radiocarbon age and proxy paleoclimatic records of the Indian sub-continent. The results demonstrate the potential of the IRSL technique for dating alluvial sediments to reconstruct paleoclimatic changes.

Chapter 7

Conclusions

7.1 Summary of Results

In the present thesis, an attempt was made to develop thermoluminescence and infra-red stimulated luminescence techniques for providing a chronology to: (i) neotectonic and paleoseismic events comprising development of luminescence dating methodology for dating fault gouges, seismites, soils developed on colluvium and uplifted river terraces and (ii) climate related sequences by developing luminescence dating methodology for dating pedogenic carbonates and alluvial sediments. Dating of neotectonic/paleoseismic events is important for ascertaining the seismic risks associated with a particular region and in predicting their likely occurrence in the future. Pedogenic carbonates which represent landscape stability are good indicators of climate and are also used as important stratigraphic markers. They have also been identified as important sources and sinks of the global carbon budget. Alluvial deposits are important both in paleoseismological and paleoclimatological studies. Conventional radiometric methods have often been found to be inapplicable and occasionally unreliable. Thus, the present thesis explored the possibilities of utilizing thermoluminescence and infra-red stimulated luminescence dating methods for dating these events.

7.1.1 Dating of Neotectonic/Paleoseismic Events

The feasibility of dating various geomorphic features created in response to neotectonic/paleoseismic events was examined using luminescence techniques. A thermoluminescence method for dating fault gouges was suggested which assumes that faulting in the history of the sample resets its geologically acquired thermoluminescence. Various criteria were explored to test the assumption of zeroing of the TL signal during faulting: (i) grain size dependence of TL ages, (ii) comparison of host rock and fault gouge paleodoses, (iii) mechanoluminescence and (iv) mineralogical studies. The grain size dependence of fault gouge TL ages suggest that a plateau in TL ages for grains smaller than a certain critical size is probably a good indicator of complete resetting of the TL signals (of these smaller grains) from faulting. This can be explained as a result of the development of large stresses at the grain boundaries. The fraction of grain volume experiencing such high stresses increases with decreasing grain size and hence the TL signals of smaller grains will be completely reset. The low value of paleodoses for fault gouges originating from old rocks of the Siwaliks and the concordance of faulting ages for fault gouges derived from rocks of different age and types was suggested to imply a definite TL resetting event. The Mechanoluminescence studies showed that the host rock ML intensities were upto five times higher than the fault gouges, since they have not been recently reset as in the case of fault gouges. However, the mineralogical studies based on chlorite and illite were unable to unequivocally establish whether the heating event indicated corresponds to recent faulting/earlier metamorphic events.

The stability of the TL signal was investigated by kinetic and anomalous fading studies on the fault gouges. The spectrum of activation energies for fault gouges determined using the initial rise method were 1.37 eV (210°C), 1.56 eV (280°C), 1.67 eV (310°C) and 1.71 eV (350°C). These values closely resemble E values of quartz and K-feldspar quoted in the literature. Lifetimes calculated assuming first order kinetics

and frequency factors appropriate for quartz and K-feldspar indicate that the TL signal from the 250°–400°C region of the glow curve is stable over timescales of $\geq$ 1 Ma. No fading of the fault gouge TL signal from the 250°–400°C region of the glow curve was observed over a storage period of 3 weeks.

Absolute dating of fault gouges using luminescence techniques was attempted for the first time. Fault gouges were collected from Nainital Fault, Main Boundary Thrust, Mohand Thrust and the Sleepy Hollow Fault for TL/IRSL dating. The results suggest that neotectonic activity took place at the Nainital Fault and the Sleepy Hollow Fault at 41 ± 8 ka and 36 ± 5 ka respectively. The Mohand Thrust was tectonically active at 59 ± 10 ka ago while tectonic activity along the Main Boundary Thrust (Nainital region) is indicated at ca. 70 ± 12 ka. The TL age of faulting along the Nainital Fault agrees with the ^{14}C age (~ 50 ka) of formation of L.Naini which is considered to have been created by a major faulting event (Valdiya, 1988). ^{14}C dating of charcoal from L. Wadda (~ 30 km from Nainital) indicates that the L. Wadda was formed 44 ka BP by movements along Kotli Fault, which runs parallel to North Almora Thrust (Valdiya, 1996). IRSL (63 ± 7 ka) and TL ages (64 ± 9 ka) of faulting along Mohand Thrust concur within experimental errors. Absence of any organic material at the fault gouge sites precluded any comparisons between ^{14}C and the luminescence ages. However, the agreement between the formation age of L.Naini, L. Wadda and the TL faulting age, concordance between the IRSL and TL ages of Mohand Thrust fault gouges and substantially higher paleodoses for host rocks compared to fault gouges lends some credence to the applicability of the luminescence techniques for dating fault gouges.

Another approach adopted towards dating paleoseismic events was to date soft sediment deformation structures (seismites) produced by seismic events. In this thesis, an attempt was made for the first time to date paleoearthquakes by luminescence dating of seismites. Deformation structures observed in fluvio-lacustrine sediments exposed in

the Sumdo area of the Spiti Valley, Himachal Pradesh, were dated using sediment dating luminescence techniques. The luminescence ages of the seismic events in Spiti Valley are 90 ± 10 ka, 61 ± 9 ka, 37 ± 5 ka and 26 ± 4 ka. A correlation between the seismite ages with ^{14}C ages of lake formation in the region and luminescence ages of fault gouges in Nainital (450 km from Spiti) and Mohand suggests the possibility of regionally extended tectonism in the Himalaya around 40 ka and 60 ka. However, additional dating work is necessary to establish this hypothesis.

The present studies also involved luminescence dating of soils developed on colluvium and sediments from unpaired river terraces around Nainital. The soil samples from the terraces at two different locations in the vicinity of Bhawali gave stratigraphically concordant partial bleach TL ages. The ages possibly suggest that at ~ 4 ka, some neotectonic activity occurred in this region. On the basis of field evidences such as folded river terraces, Bhargava (1990) argued that the area south of the Indus Suture Zone has experienced major tectonic activity at around 4 ka. IRSL ages on terrace deposits from Kaladhungi and Garjiya are stratigraphically consistent and imply that neotectonic activity took place around ≤ 31 ka and ≤ 9 ka respectively in these regions.

7.1.2 Dating of Climate related sequences

1. Pedogenic Carbonates

A new luminescence method was proposed for dating pedogenic carbonates which utilizes subtle dosimetric changes to a mineral on being carbonated. The age of the carbonate can be estimated by determining the differences between (i) the paleodoses (or equivalent doses) of the mineral being dated from the host sand and the carbonate matrix and (ii) the annual dose imparted to the mineral by the host sand and the carbonate matrix. Dosimetric considerations suggest that the luminescence dating methods are

less susceptible to post-depositional changes. The propagation of errors was used for developing a scheme for calculating the error in the calcrete age. For the present studies, carbonates were collected from four sites in Thar Desert viz., Chamu, Jalore, Budha Pushkar and Amarsar to test the validity of the luminescence dating method. The luminescence ages on carbonates are stratigraphically consistent and suggest that a regionally extended episode of carbonate formation probably took place in Thar Desert at around 17 ± 3 ka. This episode is observed at Chamu, Budha Pushkar and Amarsar, a west-east transect spanning ~ 300 km in Thar Desert. However, more dating work is needed at other sites in Thar Desert to make a more definitive statement about the regional extent of this event. The other carbonate formation episodes in Thar desert are suggested to be 100 ± 25 ka and 2 ± 1.3 ka ago. The luminescence ages of carbonate formation epochs in Thar Desert concur with available paleoclimatic data.

2. Alluvium

Sedimentological characteristics of alluvial sequences in the Ghaggar and Chautang flood plains, Haryana, demonstrate the response of river systems to a changing paleoenvironment (Courty, 1990). However, non-availability of reliable ^{14}C datable materials in most of the stratigraphic horizons rendered the chronology of these events illusive. TL and IRSL dating of flood plain deposits from Ghaggar and Chautang basins were performed to test the validity of the luminescence methods for dating alluvial deposits along with a possible reconstruction of the paleoclimatic record. Concordance between IRSL and ^{14}C ages implies that even though the sediments were sun-exposed for very short time intervals, their IRSL signals were well bleached at deposition. The luminescence, ^{14}C ages and sedimentological studies provide evidence for at least four distinct depositional periods: (i) regular alluvial activity terminating at ~ 50 ka, (ii) alluvial activity interposed with irregular aeolian activity between 50–20 ka, (iii) strong aeolian activity and low or absent alluvial discharge between 20–13 ka and (iv) increase

in alluvial activity at ~ 13 ka. These results demonstrate the potential of the IRSL technique for dating alluvial sediments for paleoclimatic reconstruction and also provide a basic methodological framework for future studies on the dating of pedogenic carbonates in alluvial environments.

Thus, the present thesis work pursued new directions to the application of luminescence techniques in Earth Sciences. These studies contribute significantly towards methodological establishment of the applications of luminescence dating techniques and will provide a basis for routine application of the methods. Although the luminescence ages presented in this thesis generally could not be compared with reliable independent chronology, being in most cases the very first attempt, the ages are observed to be generally consistent with available evidence on regional tectonics or on climatic aspects. It is considered that precision in luminescence ages will improve in the future and the luminescence techniques will address many questions related to paleoseismology and paleoclimatology and realize the hopes expressed in the present thesis.

7.2 Future Studies

7.2.1 Dating of Neotectonic/Paleoseismic Events

The luminescence methods for dating paleoseismic/neotectonic events needs to be applied to (i) faults where reliable independent ages of paleoseismic events are available (e.g., Sieh et al., 1989) to provide an inter-comparison between the luminescence and the ^{14}C ages and (ii) faults in continental regions which have been normally considered to be stable in respect of large earthquakes but are susceptible to destructive earth movements at any time in the future (e.g., Latur, India).

Theoretical modelling of fault zones (realistically) accompanied by laboratory experiments on Himalayan rocks are necessary for an accurate determination of the temperatures and displacement (slip) required for perfect resetting of the luminescence signals during faulting. The effect of shearing stresses on the TL signals of minerals such as quartz/feldspars should be investigated.

An attempt to reduce the error in the paleodose and in TL ages of fault gouges can be made by using other normalisation techniques such as zero-glow and second-glow normalisation. The single aliquot method can also be used for determining luminescence ages of faulting. This technique does not require normalization of the luminescence intensity and should therefore result in reducing the error in luminescence ages. The amount of sample required for single aliquot dating is comparatively less than that of conventional multiple aliquot methods. The radiation dependence of ML intensity also needs to be examined. An interesting attempt can also be made to determine fault gouge thermoluminescence ages using various TL emission bands.

The activation energy values determined in this thesis can be affected by thermal quenching. The isothermal decay method should be used to determine s-values (frequency factors), lifetimes and compare the activation energy values and electronic lifetimes obtained using the two different methods.

Verification of 'zeroing' of the TL/IRSL signal during the paleoseismic event can be furnished if a modern seismite can be dated to give a near zero age. Future studies on water-borne sediments should check for disequilibrium in the U and Th series. An estimate of the magnitude of paleoearthquakes can also be made by examining similar ages along a single fault associated with a paleoearthquake to determine the faulting length and then using a calibration curve of faulting length versus paleoearthquake magnitude.

Another possibility of dating paleoseismic events will be to devise procedures for dating mylonites found in fault zones. Of late, an attempt has also been made to date tsunami sands (Huntley and Clague, in press) using IRSL dating. Dating of tsunami deposits can provide information on earthquake hazards. Huntley and Clague reported an IRSL age of 1300 ± 95 years for tsunami sand at Cultus Bay, Washington. This age is consistent with ^{14}C ages on organic material recovered from the tsunami sands (1030-1100 years BP). Modern tidal flat and tidal-channel sands which act as a source for the tsunami deposits gave equivalent doses of 0-0.06 Gy. Tsunami sands at Tofino and Port Alberni, Vancouver Island, British Columbia were dated to ~ 300 years and were consistent with historical records and ^{14}C ages, suggesting that a large earthquake took place on the Cascadia Subduction Zone at ~ 300 years ago which caused the tsunami.

7.2.2 Dating of Climate related sequences

The luminescence methods for dating carbonates need to be applied to carbonates which have been independently dated using the radiocarbon technique on organic material from the same strata or by phase-constrained TIMS ^{230}Th-^{234}U dating. Concordance between the luminescence and ^{14}C/^{230}Th-^{234}U ages will further validate the luminescence techniques. Also, single grain dating (McFee, 1995) of carbonates needs to be developed in the near future to decipher the effects of redissolution/reprecipitation on the luminescence age in a semi-arid/humid environment.

Precise dating of young carbonates using luminescence techniques will also be possible once the random errors on the TL/IRSL equivalent doses can be limited to ~ 1%. Single grain and single aliquot methods should again help in improving the precision on carbonate ages. The luminescence methods for dating pedogenic carbonates can also be attempted in an alluvial context. Availability of a large database of carbonate ages in arid zones can be utilized to correlate the rates of carbonate formation (Marion et

al., 1985) with the average annual precipitation.

In respect of alluvium dating, TL ages presented in this thesis were estimated using residual signals determined by bleaching aliquots in conditions which did not simulate a perfect under-water environment. Only the 550-700 nm portion of the spectrum should be allowed during solar bleaching of the samples for determining the residual TL signal and TL ages. Also, more alluvial profiles with independent age control need to be dated using luminescence methods.

Bibliography

1. Adams, J. (1980). Paleoseismicity of the Alpine fault seismic gap, New Zealand, Geology, 8, 72-76.

2. Adams, J.M., Faure, H., Faure-Dencard, L., McGlade, J.M. and Woodward, F.I. (1990). Increases in terrestrial carbon storage from the Last Glacial Maximum to the present, Nature, 348, 711-744.

3. Aitken, M.J. (1985). Thermoluminescence dating, Academic Press, London, 359 pp.

4. Aitken, M.J. (1992). Optical Dating, Quaternary Science Reviews, 11, 127-131.

5. Aitken, M.J. (1994). Optical Dating : A Non-Specialist Review, Quaternary Geochronology, 13, 503-508.

6. Aitken, M.J. and Bowman, S.G.E. (1975). Thermoluminescence dating : assessment of alpha particle contribution, Archaeometry, 17, 132- 138.

7. Aitken, M.J., Tite, M.S. and Reid, J. (1964). Thermoluminescent dating of ancient ceramics, Nature, 202, 1032-1033.

8. Aitken, M.J. and Xie, J. (1992). Optical Dating Using Infrared Diodes : Young Samples, Quaternary Science Reviews, 11, 147-152.

9. Allen, C.R. (1975). Geological criteria for evaluating seismicity : Bulletin of the Geological Society of America, 86, 1041-1057.

10. Amit, R., Harrison, J.B.J. and Enzel, Y. (1995). Use of soils and colluvial deposits in analyzing tectonic events - The Southern Arava Rift, Israel, Geomorphology 12, 91-107.

11. Ansari, A.R., Chugh, R.S., Sinvhal, H., Khattri, K.N. and Gaur, V.K. (1976). Geodetic determination of earth strain and creep on the Krol Thrust in the Dakpathar area, Dehradun District, U.P., Himalayan Geology, 323-337.

12. Ariyama, T. (1985). Conditions of resetting the ESR clock during faulting. In : M.Ikeya and T.Miki (Eds.), ESR Dating and Dosimetry, Ionics, Tokyo, 249-256.

13. Bagati, T.N. and Thakur, V.C. (1993). Quaternary basins of Ladakh and Lahaul Spiti in northwestern Himalaya, Current Science, 64, 898-903.

14. Bailiff, I.K. (1992). Luminescence dating of alluvial deposits. In: S. Needham and M.G. Macklin (Eds.), Alluvial archaeology in Britain, Oxbow, Oxford, 27-35.

15. Balescu, S. and Lamothe, M. (1994). Comparison of TL and IRSL age estimates of feldspar coarse grains from water-lain sediments, Quaternary Geochronology, 13, 437-444.

16. Bar, M., Kolodny, Y. and Bentor, Y.K. (1974). Dating Faults by Fission Track Dating of Epidotes - An Attempt, Earth and Planetary Sciences, 22, 157-162.

17. Belperio, A.P., Smith, B.W., Polach, H.A., Nittrouer, C.A., DeMaster, D.J., Prescott, J.R., Hails, J.R. and Gostin, V.A. (1984). Chronological studies of the Quaternary marine sediments of northern Spencer Gulf, South Australia, Marine Geology, 61, 265-296.

18. Berger, G.W. (1984). Thermoluminescence dating studies of some glacial silts from Ontario, Canadian Journal of Earth Sciences, 21, 1393-1399.

19. Berger, G.W. (1988). Dating Quaternary events by luminescence, Geological Society of America, Special Paper, 227, 13-49.

20. Berger, G.W. (1990). Effectiveness of natural zeroing of the thermoluminescence in sediments, Journal of Geophysical Research, 95, 12375-12397.

21. Berger, G.W. and Eyles, N. (1994). Thermoluminescence chronology of Toronto-area Quaternary sediments and implications for the extent of midcontinent ice sheets, Geology, 22, 31-34.

22. Berger, G.W., Clague, J.J. and Huntley, D.J. (1987). Thermoluminescence dating applied to glacio-lacustrine sediments from central British Columbia, Canadian Journal of Earth Sciences, 24, 425-434.

23. Bhargava, O.N. (1990). Holocene tectonics south of the Indus Suture, Lahaul-Ladakh Himalaya, India : a consequence of Indian Plate Motion, Tectonophysics, 174, 315-320.

24. Blenkinsop, T.G. (1988). Definition of low-grade metamorphic zones using illite crystallinity : Journal of Metamorphic Petrology, 6, 623-636.

25. Bryson, R.A. (1989). Modelling the NW India monsoon for the last 40000 years, Climate Dynamics, 3, 169-177.

26. Bucknam, R.C. and Anderson, R.E. (1979). Estimation of fault-scarp ages from a scarp-height-slope-angle relationship, Geology, 7, 11-14.

27. Buhay, W.M., Schwarz, H.P. and Grun, R. (1988). ESR Dating of Fault Gouge : The Effect of Grain Size, Quaternary Science Reviews, 7, 515-522.

28. Bull, W.B. (1996). Dating San Andreas fault earthquakes with lichenometry, Geology, 24, 11-114.

29. Calderoni, G. and Petrone, V. (1993). Radiocarbon dating of paleoseismicity along an earthquake fault in Southern Italy, Radiocarbon, 35(2), 287-293.

30. Calderoni, G., Lorenzoni, P., Ortolani, F., Pagliuca, S. and Serva, L. (1990). Ren. Geological Society of Italy, 13, 27-32.

31. Callen, R.A., Wasson, R.J. and Gilespie, R. (1983). Reliability of radiocarbon dating of pedogenic carbonate in the Australian arid zone, Sedimentary Geology, 35, 1-14.

32. Cardwell, R.K., Chinn, D.S., Moore, G.F. and Turcotte, D.L. (1978). Frictional heating on a fault zone with finite thickness, Geophysical Journal of the Royal Astronomical Society, 52, 525-530.

33. Carslaw, H.S. and Jaeger, J.C. (1959). Heat conduction in solids, Clarendon Press, Oxford.

34. Cerling, T.E. (1984). The stable isotopic composition of modern soil carbonate and its relationship to climate, Earth and Planetary Science Letters, 71, 229-240.

35. Chandra, B.P. (1985). Squeezing Light out of Crystals : Triboluminescence, Nuclear Tracks, 10, 225-241.

36. Chen, R. and Bowman, S.G.E. (1978). Superlinear growth of TL due to competition during irradiation, PACT 2, 216-230.

37. Chen, Y. and Polach, H. (1986). Validity of ^{14}C ages of carbonates in sediments, Radiocarbon, 28(2A), 464-472.

38. Clark, M.N. and Kellar, E.A. (1979). Newly identified zone of potentially active reverse faulting, Western Transverse Ranges, California, Geological Society of American Abstracts Program, 11(7), 402-403.

39. Cooke, R., Warren, A. and Goudie, A.S. (1993). Desert Geomorphology, University College of London Press, 525 pp.

40. Courty, M.A. (1990). Environments geologiques dans le nord-ouest de l'Inde. Contraintes geodynamiques au peuplement protohistorique (Bassins de la Ghaggar - Saraswati - Chautang), Ph.D. Thesis, Bordeaux University, France, 328 pp.

41. Crone, A.J. (1987). Introduction to Directions in Paleoseismology. In : Crone, A.J. and Omdahl, E.M. (Eds.), Directions in Paleoseismology, U.S. Geological Survey Open - File Report 87-673, 1-6.

42. Daniels, F., Boyd, C.A. and Saunders, D.F. (1953). Thermoluminescence as a research tool, Science, 117, 343-349.

43. Debenham, N.C. and Walton, A.J. (1983). TL properties of some wind- blown sediments, PACT 9, 531-538.

44. Deer, W.A., Howie, R.A. and Zussman, J. (1962). Rock forming minerals, Volume 3 : Sheet Silicates, Longmans, London, 270 pp.

45. Ditlefson, C. (1992). Bleaching of K-feldspars in turbid water suspensions: A comparison of photo- and thermoluminescence signals, Quaternary Science Reviews, 11, 33-38.

46. Duller, G.A.T., Wintle, A.G. and Hall, A.M. (1995). Luminescence dating and its applications to key pre-late Devensian sites in Scotland, Quaternary Science Reviews, 14, 495-519.

47. Dunoyer de Segonzac (1970). The transformation of clay minerals during diagenesis and low grade metamorphism : a review, Sedimentology, 15, 281-346.

48. Edwards, R.L., Taylor, F.W. and Wasserburg, G.J. (1988). Dating earthquakes with high precision thorium-230 ages of very young corals, Earth and Planetary Science Letters, 90, 371-381.

49. Ely, L.L., Webb, R.H. and Enzel, Y. (1992). Accuracy of post- bomb ^{137}Cs and ^{14}C in dating fluvial deposits, Quaternary Research, 38, 196-204.

50. Eyal, Y., Kaufman, A. and Bar-Matthews, M. (1992). Use of $^{230}Th/U$ ages of striated carnotites for dating fault displacements, Geology, 20, 829-832.

51. Forman, S.L., Jackson, M.E., McCalpin, J. and Maat, P. (1988). The potential of using thermoluminescence to date buried soils developed on colluvial and fluvial sediments from Utah and Colorado, U.S.A. : Preliminary results, Quaternary Science Reviews, 7, 287-293.

52. Forman, S.L., Machette, M.N., Jackson, M.E. and Maat, P. (1989). An evaluation of thermoluminescence dating of paleoearthquakes on the American Fork segment, Wasatch Fault Zone, Utah, Journal of Geophysical Research, 94 (B2), 1622-1630.

53. Forman, S.L., Nelson, A.R. and McCalpin, J.P. (1991). Thermoluminescence dating of fault scarp derived colluvium : Deciphering the timing of paleoearthquakes on the Weber segment of the Wasatch Fault zone, North Central Utah, Journal of Geophysical Research, 96(B1), 595-605.

54. Fort, M., Burbank, D.W. and Freytet, P. (1989). Lacustrine sedimentation in a semi-arid alpine setting : An example from Ladakh, NW Himalaya, Quaternary Research, 31, 332-350.

55. Fukuchi, T., Imai, N. and Shimokawa, K. (1985). Dating of the fault movement by various ESR signal in quartz-cases of the faults in the south Fossa Magna, Japan. In : Ikeya, M. and Miki, T. (Eds.), ESR Dating and Dosimetry, 211-218.

56. Fukuchi, T., Imai, N. and Shimokawa, K. (1986). ESR dating of fault movement using various defect centres in quartz; the case in the western South Fossa Magna, Japan, Earth and Planetary Science Letters, 78, 121-128.

57. Fukuchi, T. (1989). Increase of radiation sensitivity of ESR centres by faulting and criteria of fault dates, Earth and Planetary Science Letters, 94, 109-122.

58. Fukuchi, T. (1992). ESR studies for absolute dating of fault movements, Journal of the Geological Society, London, 149, 265-272.

59. Fuller, I.C. (1996). Luminescence dating of late Quaternary alluvium: the Guadalope and Regallo basins, NE Spain. In: Programs and Abstracts, 8th International Conference on Luminescence and ESR Dating, 185-189.

60. Geyh, M. and Schleicher, H. (1990). Absolute Age Determination, Springer Verlag, Berlin, 530 pp.

61. Gobrecht, H. and Hofmann, D. (1966). Spectroscopy of traps by fractional glow technique, Journal of Physics and Chemistry of Solids, 27, 509-522.

62. Godfrey-Smith, D.I., Huntley, D.J. and Chen, W.H. (1988). Optical dating of quartz and feldspar sediment extracts, Quaternary Science Reviews, 7, 373-380.

63. Godwin, H. (1951). Comments on Radiocarbon Dating for samples from the British Isles, American Journal of Science, 249, 301-307.

64. Goudie, A.S. (1983). Calcrete, In : Chemical Sediments and Geomorphology, Goudie, A.S. and Pye, K. (Eds.), Academic Press, London, 93-132.

65. Grun, R. (1992). Remarks on ESR dating of fault movements, Journal of the Geological Society, 149, 261-264.

66. Gupta, V.J. and Virdi, N.S. (1975). Geological aspects of the Kinnaur earthquake, Himachal Pradesh, Journal of the Geological Society of India, 16(4), 512-514.

67. Hase, K., Masumoto, S., Oyama, A., Masuda, H. and Miono, S. (1983). Active Fault and Thermoluminescence, Fiscal Meeting of Seismological Society of Japan, 213.

68. Huntley, D.J. (1985). On the zeroing of the Thermoluminescence of sediments, Physics and Chemistry of Minerals, 12, 122-127.

69. Huntley, D.J. and Clague, J.J. (1996). Optical Dating of Tsunami-laid sands, Quaternary Research, in press.

70. Huntley, D.J., Godfrey-Smith, D.J. and Thewalt, M.L.W. (1985). Optical Dating of Sediments, Nature, 313-105-107.

71. Huntley, D.J., Godfrey-Smith, D.J., Thewalt, M.L.W. and Berger, G.W. (1988). Thermoluminescence spectra of some mineral samples relevant to thermoluminescence dating, Journal of Luminescence, 39, 123-136.

72. Hutt, G., Jaek, I. and Tchonka, J. (1988). Optical Dating : K- feldspars Optical Response Stimulation Spectra, 7, 381-385.

73. Hutton, J.T., Prescott, J.R., Bowman, J.R., Dunham, M.N.E., Crone, A.J., Machette, M.N. and Twidale, C.R. (1994). Thermoluminescence Dating of Australian Paleoearthquakes, 13, 143-147.

74. Ikeya, M., Miki, T. and Tanaka, K. (1982). Dating of a fault by electron spin resonance on intrafault materials, Science, 215, 1392-1393.

75. Ikeya, M., Tani, A. and Yamanaka, C. (1995). Electron Spin Resonance Isochrone Dating of Fracture Age: Grain-size Dependence of Dose Rates for Fault Gouge, Japanese Journal of Applied Physics, 34, 334-338.

76. Ivanovich, M., Vita-Finzi, C. and Hennig, G.J. (1983). Uranium- series dating of molluscs from uplifted Holocene beaches in the Persian Gulf, Nature, 302, 408-410.

77. Jacoby, G.C. (1987). Potential and limits for dating prehistoric earthquakes using tree-ring analysis. In : Directions in Paleoseismology, Crone, A.J. and Omdahl, E.M. (Eds.), Open-File Report, 87-673, 18-22.

78. Khattri, K.N. (1996). A call for paleoseismic investigations to constrain the repeat time of great earthquakes in the Himalaya, Current Science, 70(12), 1039-1041.

79. Kralik, M., Klima, K. and Riedmuller, G. (1987). Dating fault gouges, Nature, 327, 315-317.

80. Kranz, R.L. (1983). Microcracks in rocks : a review, Tectonophysics, 100, 449-480.

81. Ku, T.L., Bull, W.B., Freeman, S.T. and Knauss, K.G. (1979). ^{230}Th-^{234}U dating of pedogenic carbonates in gravelly desert soils of Vidal valley, Southeastern California, Bulletin of the Geological Society of America, 90, 1063-1073.

82. Kuenen, P.H. (1958). Experiments in geology, Transactions of the Geological Society of Glasgow, 23, 1-28

83. Lang, A. (1994) Luminescence dating of holocene reworked silty sediments, Quaternary Geochronology, 13, 525-528.

84. Lee, H.K. and Schwarz, H.P. (1994). Criteria for complete zeroing of ESR signals during faulting of the San Gabriel Fault Zone, Southern California, Tectonophysics, 235, 317-337.

85. Lensen, G.J. and Vella, P. (1971). The Waiohine River faulted terrace sequence: Recent crustal movements, Bulletin of the Royal Society of New Zealand, 9, 117-119.

86. Lyons, J.B. and Snellenburg, J. (1971). Dating Faults, Bulletin of the Geological Society of America, 82, 1749-1752.

87. Liu, B., Phillips, F.M., Elmore, D. and Sharma, P. (1994). Depth dependence of soil carbonate accumulation based on cosmogenic ^{36}Cl dating, Geology, 22, 1071-1074.

88. Machette, M.N. (1985). Calcic soils of the southwestern United States. In : Soils and Quaternary Geology of the Southwestern United States, Geological Society of America Special Paper, 203, 1- 21.

89. Marion, G.M. (1985). Correlation between long-term pedogenic $CaCO_3$ formation rate and modern precipitation in deserts of the American Southwest, Quaternary Research, 32, 291-295.

90. May, R.J. and Machette, M. (1984). Thermoluminescence dating of soil carbonate, U.S. Geological Survey Open-File Report, 84-083, 25 pp.

91. McCalpin, J. and Forman, S.L. (1991). Late Quaternary faulting and thermoluminescence dating of the East Cache Fault Zone, North- Central Utah, Bulletin of the Seismological Society of America, 81(1), 139-161.

92. McFee, C.J. (1995). The use of Imaging Photon Detector for luminescence dating, Ph.D. Thesis, University of Oxford, 275 pp.

93. McKenzie, D. and Brune, J.N. (1972). Melting on fault planes during large earthquakes, Geophysical Journal of the Royal Astronomical Society, 29, 65-78.

94. Meghraoui, M., Jaegy, R., Lammali, K. and Albarede, F. (1988). Late Holocene earthquake sequences on the El Asnam (Algeria) Thrust Fault, 90, 187-203.

95. Mejdahl, V. (1969). Thermoluminescence dating of ancient Danish ceramics, Archaeometry, 11, 99-104.

96. Mejdahl, V. (1979). Thermoluminescence dating : beta-dose attenuation in quartz grains, Archaeometry, 21, 61-73.

97. Mejdahl, V. (1988). The plateau method for dating partially bleached sediments by thermoluminescence, Quaternary Science Reviews, 7, 347-348.

98. Mohindra, R. and Bagati, T.N. (1996). Seismically induced soft sediment deformation structures (seismites) around Sumdo in the Lower Spiti Valley (Tethys Himalaya), Sedimentary geology, 101, 69- 83.

99. Morgenstern, N.R. (1967). Submarine slumping and the initiation of turbidity currents. In : Marine Geotechnique, Richards, A.F. (Ed.), 3, 189-219.

100. Murray, A., Wohl, E. and East, J. (1992). TL and Excess ^{226}Ra decay dating of Late Quaternary fluvial sands, East Alligator River, Australia, Quaternary Research, 37, 29-41.

101. Nambi, K.S.V. and Hegde, K.T.M. (1982). Thermoluminescence dating of $CaCO_3$ nodules from buried soils of the Lower Narmada Valley. In : Natural Radiation Environment, Vohra, K.G., Mishra, U.C., Pillai, K.C. and Sadasivan, S. (Eds.), Wiley Eastern, 664-669.

102. Nanson, G.C. and Young, R.W. (1987). Comparison of thermoluminescence and radiocarbon age determinations from late Pleistocene alluvial deposits near Sydney, Australia, Quaternary Research, 27, 263-269.

103. Nanson, G.C., Price, D.M. and Short, S.A. (1992). Wetting and drying of Australia over the past 300 ka, Geology, 20, 791-794.

104. Pande, I.C. (1974). Tectonic interpretation of the geology of Nainital area, Himalayan Geology, 4, 532-546.

105. Postpischl, D., Agostini, S., Forti, P. and Quinif, Y. (1991). Paleoseismicity from Karst sediments : the 'Grotta del Cervo' cave case study (Central Italy), Tectonophysics, 193, 33-44.

106. Prescott, J.R. and Stephan, L.G. (1982). Contribution of cosmic radiation to environmental dose, PACT 6, 17-25.

107. Prescott, J.R. and Purvinskis, R.A. (1991). Zero thermoluminescence for zero age, Ancient TL, 9, 19-20.

108. Prescott, J.R. and Hutton, J.T. (1995). Environmental dose rates and radioactive disequilibrium from some Australian luminescence dating sites, Quaternary Geochronology, 14, 439-448.

109. Prescott, J.R., Huntley, D.J. and Hutton, J.T. (1993). Estimation of equivalent dose in thermoluminescence dating : the Australian slide method, Ancient TL, 11, 1-5.

110. Proszynska, H. (1983). TL dating of some sub-aerial sediments from Poland, PACT 9, 539-546.

111. Proszynska-Bordas, H., Pronszynska-Stansa, W. and Proszynski, M. (1992). TL Dating of river terraces with fossil soils in the Mediterranean region, Quaternary Science Reviews, 11, 53-60.

112. Radhakrishnan, B.P. and Ramaseshan, S. (1992). A dedicated organization for earthquake studies. In: Seismology in India - An Overview, Special Issue, Current Science, 6-7.

113. Radtke, U., Bruckner, H., Mangini, A. and Hausmann, R. (1988). Problems encountered with absolute dating (U-Series, ESR) of Spanish Calcretes, Quaternary Science Reviews, 7, 439-445.

114. Rajal, B.S., Virdi, N.S. and Hasija, N.L. (1986). Recent crustal uplift in the Doon Valley, Proceedings of the International Symposium on Neotectonics in South Asia, Dehradun, Survey of India, 146-159.

115. Randall, J.T. and Wilkins, M.H.F. (1945). Phosphorescence and electron traps, Proceedings of the Royal Society of London, A 184, 366-407.

116. Rao, M.S. (1996). Studies on physical basis of luminescence geochronology and its applications, Ph.D. Thesis, submitted to Nagpur University.

117. Rieser, U., Krbetschek, M.R. and Stolz, W. (1994). CCD-camera based high sensitivity TL-OSL spectrometer, Radiation Measurements, 23, 523-528.

118. Rendell, H., Worsley, P., Green, F. and Parks, D. (1991). Thermoluminescence dating of the Chelford Interstadial, Earth and Planetary Science Letters, 103, 182-189.

119. Ritz, J.F., Brown, E.T., Bourles, D.L., Philip, H., Schlupp, A., Raisbeck, G.M., Yiou, F., Enkhtuvshin, B. (1995). Slip rates along active faults estimated with cosmic ray exposure dates : Application to the Bogd fault, Gobi-Altai, Mongolia, Geology, 23(11), 1019-1022.

120. Sarkar, A., Ramesh, R. and Bhattacharya, S.K. (1990). Effect of size and pre-treatment on the $\delta^{13}C$, $\delta^{18}O$ of foraminifera from the Arabian Sea sediments, Terra Nova, 2, 489-493.

121. Scholz, C.H. (1987). Wear and gouge formation in brittle faulting, Geology, 15, 493-495.

122. Scholz, C.H. (1990). The mechanics of earthquakes and faulting, Cambridge University Press, New York, 439 pp.

123. Schumm, S.A. (1977). The fluvial system, Wiley, New York.

124. Scott J.S. and Dreever, H.I. (1953). Frictional fusion along a Himalayan thrust, Proceedings of the Royal Society of Edinburgh, 65B(2), 121-141.

125. Seed, H.B. (1968). Landslides during earthquakes due to soil liquefaction, Proceedings of the American Association of Civil Engineering, Journal of Soil Mechanics, 94, 1055-1122.

126. Shimmield, G.B., Mowbray, S.R. and Weedon, G.P. (1990). A 350 ky history of the Indian south-west monsoon evidence from deep-sea cores, north west Arabian Sea, Earth Science, 81, 289-299.

127. Shore, J.S., Bartley, D.D. and Harkness, D.D. (1995). Problems encountered with the ^{14}C dating of peat, Quaternary Geochronology, 14, 373-383.

128. Sibson, R.H. (1975). Generation of pseudotachylyte by ancient seismic faulting, Geophysical Journal of the Royal Astronomical Society, 43, 775-794.

129. Sibson, R.H. (1977). Fault rocks and fault mechanisms, Journal of the Geological Society of London, 133, 191-213.

130. Sieh, K. (1978). Prehistoric large earthquakes produced by slip on the San Andreas fault at Pallet Creek, California, Journal of Geophysical Research, 83(B8), 3907-3939.

131. Sieh, K., Stuiver, M. and Brillinger, D. (1989). A more precise chronology of earthquakes produced by the San Andreas Fault in southern Caifornia, Journal of Geophysical Research, 94, 603-623.

132. Sims, J.D. (1973). Earthquake induced structures in sediments of Van Norman Lake, San Fernando, California, Science, 182, 161-163.

133. Sims, J.D. (1975). Determining earthquake recurrence intervals from deformational structures in young lacustrine sediments, Tectonophysics, 29, 141-152.

134. Singh, G., Joshi, R.D., Chopra, S.K. and Singh, A.B. (1974) Late Quaternary history of vegetation and climate of the Rajasthan Desert, India, Philosophical Transactions of the Royal Society of London, B 267, 467-501.

135. Singhvi, A.K. and Aitken, M.J. (1978). Americium-241 for alpha irradiation, Ancient TL, 3, 2-9.

136. Singhvi, A.K. and Wagner, G.A. (1985). Thermoluminescence dating and its applications to young sedimentary deposits. In: Hurford, A.J., Jaeger, E. and Tencate, L.A.M. (Eds.), Dating Young Sediments, Thailand UNCCOP Technical Secretariat, Bangkok, 159-197.

137. Singhvi, A.K., Sharma, Y.P. and Agrawal, D.P. (1982). Thermoluminescence dating of sand dunes in Rajasthan, Nature, 29, 313-315.

138. Singhvi, A.K., Banerjee, D., Pande, K., Gogte, K. and Valdiya, K.S. (1994). Luminescence studies on neotectonic events in South-Central Kumaun Himalaya : A Feasibility study, Quaternary Geochronology, 13, 595-600.

139. Stokes, S. (1992). Optical dating of young (modern) sediments using quartz : Results from a selection of depositional environments, Quaternary Science Reviews, 11, 153-159.

140. Stuiver, M. and Riemer, P.J. (1993). Extended ^{14}C database and revised calib.3.0 ^{14}C age calibration program, Radiocarbon, 35, 215-230.

141. Sukumar, R., Ramesh, R., Pant, R.K. and Rajagopalan, G. (1993). A $\delta^{13}C$ record of late Quaternary climatic change from tropical peats in southern India, Nature, 364, 703-705.

142. Suzuki, S. and Kennedy, F.E. (1991). The detection of flash temperatures in a sliding contact by the method of tribo-induced thermoluminescence, J. Tribolumineschence, 113, 120-127.

143. Tanaka, K. (1990). Dating of fault movement by the ESR method; basis and application, Ph. D. Thesis, University of Kyushu, Japan, 111 pp.

144. Teufel, L.W. and Logan, J.M. (1978). Effect of displacement rate on the real area of contact and temperatures generated during frictional sliding of Tennassee sandstone, Pure and Applied Geophysics, 116, 840-865.

145. Tuttle, M.P. and Schweig, E.S. (1995). Archaeological and pedological evidence for large prehistoric earthquakes in the New Madrid Seismic Zone, Central United States, Geology, 23(3), 253- 256.

146. Valdiya, K.S. (1976). Himalayan transverse faults and folds and their parallelism with subsurface structures of North Indian plains, Tectonophysics, 32, 353-386.

147. Valdiya, K.S. (1981). Tectonics of central sector of the Himalaya. In : Zagros-Hindukush-Himalaya: Geodynamic evolution, Gupta, H.K. and Delany, F.M. (Eds.), American Geophysical Union, 87-110.

148. Valdiya, K.S., Joshi, D.D., Sanwal, R. and Tandon, S.K. (1984). Geomorphological development across the Main Boundary Thrust, an example from the Nainital Hills in Kumaun Himalaya, Journal of the Geological Society of India, 25, 761-774.

149. Valdiya, K.S. (1988). Geology and Natural Environment of Nainital Hills, Gyan-odaya Prakashan, Nainital, 155 pp.

150. Valdiya, K.S. (1992). The Main Boundary Thrust Zone of the Himalaya, India, Annales Tectonicae, 6, 54-84.

151. Valdiya, K.S., Kotlia, B.S., Pant, P.D., Shah, M., Mungali, N., Tewari, S., Sah, N. and Upreti, M. (1996). Quaternary paleolakes in Kumaun Lesser Himalaya : finds of neotectonic and paleoclimatic significance, 70(2), 157-161.

152. Van-Campo, E. (1986). Monsoon fluctuations in the 20,000 yr. B.P. oxygen isotope/pollen records off southwestern India, Quaternary Research, 26, 376-388.

153. Vhora, S. (1987). Thermoluminescence dating of fluvial terraces : A feasibility study, M. Tech. Dissertation Thesis, University of Roorkee, Roorkee.

154. Vita-Finzi, C. and King, G.C.P. (1985), The seismicity, geomorphology and structural evolution of the Corinth area of Greece, Philosophical Transactions of the Royal Society of London, A 314, 379-407.

155. Vittori, E., Labini, S.S. and Serva, L. (1991). Paleoseismology : review of the state-of-the-art, Tectonophysics, 193, 9-32.

156. Wallace, R.E. (1977). Profiles and ages of young fault scarps, north-central Nevada, Bulletin of the Geological Society of America, 88, 1267-1281.

157. Wasson, R.J., Smith, G.I. and Agrawal, D.P. (1984). Late Quaternary sediments, minerals and inferred geochemical history of Didwana Lake, Thar Desert, India, Paleogeography, Paleoclimatology and Paleoecology, 46, 345-372.

158. Waterbolk, H.T. (1983). Ten guidelines for the archaeological interpretation of radiocarbon dates. In : Mook, W.G. and Waterbolk, H.T. (Eds.), ^{14}C and Archaeology, PACT 8, 57-70.

159. Weaver, C.E. (1960). Possible uses of clay minerals in search of oil, Bulletin of the American Association of Petroleum Geologists, 44, 1505-1518.

160. Weber, K. (1972). Note on the determination of illite crystallinity, Neues Jahrbuch fur Mineralogie Monatshefte, 6, 267- 276.

161. Williams, G.E. and Polach, H.A. (1969). The evaluation of ^{14}C ages for soil carbonate from the arid zone, Earth and Planetary Science Letter, 7, 240-242.

162. Williams, G.E. and Polach, H.A. (1971). Radiocarbon dating of arid zone calcareous paleosols, Bulletin of the Geological Society of America, 82, 3069-3086.

163. Williams, M.A.J., Dunkerley, D.L., DeDeckker, P., Kershaw, A.P. and Stokes, T.J. (1993). Quaternary Environments, Edward Arnold, London, 329 pp.

164. Wintle, A.G. (1973). Anomalous fading of thermoluminescence in mineral samples, Nature, 245, 143-144.

165. Wintle, A.G. (1975). Thermal quenching of thermoluminescence in quartz, Geophysical Journal of the Royal Astronomical Society, 41, 107-113.

166. Wintle, A.G. (1978). Anomalous fading, PACT 2, 240-243.

167. Wintle, A.G. and Aitken, M.J. (1977). Absorbed dose from a source as shown by thermoluminescence dosimetry, International Journal of Radiation Isotopes, 28, 625-627.

168. Wintle, A.G. and Huntley, D.J. (1980). Thermoluminescence dating of ocean sediments, Canadian Journal of Earth Sciences, 17, 348-360.

169. Wintle, A.G. and Huntley, D.J. (1982). Thermoluminescence dating of sediments, Quaternary Science Reviews, 1, 31-53.

170. Wintle, A.G. and Catt, J.A. (1985). Thermoluminescence dating of soils developed in late Devensian loess at Pegwell Bay, Kent, Journal of Soil Science, 36, 293-298.

171. Wybrecht, E., Duplay, J., Pique, A. and Weber, F. (1985). Mineralogical and chemical evolution of white micas and chlorites, from diagenesis to low-grade metamorphism; data from various size fractions of greywackes (Middle Cambrian, Morocco), Mineralogical Magazine, 49, 401-411.

172. Yaalon, D.H. (1981). Pedogenic carbonate in aridic soils - magnitude of the pool and annual fluxes, Abstracts of International Conference on Aridic Soils, Jerusalem, 94 pp.

173. Yoshikawa, T., Kaeyerka, S. and Ota, Y. (1981). The landforms of Japan, Tokyo University Press, Tokyo, 39-72.

174. Zimmerman, D.W. (1971). Thermoluminescent dating using fine grains from pottery, Archaeometry, 13, 29-52.

Appendix A: TL and IRSL Measurement Systems

A.1: TL measurements

The TL measurements were made on a manual Daybreak TL reader system (Fig.A.1). The system comprised a sensitive photon counting system and a digital ramp based temperature controller system with a reproducibility of < 1%. The luminescence was detected by EMI 9635 QA photo-multiplier tube attached to a filter pack normally consisting of HA3 + Corning (5-58 + 7-59) or HA3 + UG11 filters. For brighter samples, fused silica neutral density filters were used and the maximum photon count rate was always kept below 5 x 10^5 counts/s to avoid any pulse pile up effects. The signal from the PMT was routed through a charge sensitive pre-amplifier to a ratemeter and through a computer interface to an IBM-PC. The temperature controller worked on a digital ramp that also provided a channel advance pulse for the IBM/PC, used essentially as a multi-scaling system. Typical heating rates were 2°C/s for mineral inclusions and 5°C/s for fine grains. All the glow curves were recorded in ultra high purity nitrogen atmosphere. Short preheats before recording (220°C/s for 1 minute) were carried out on TL reader itself. For long duration preheats (160°C/s for 360 minutes), the system used

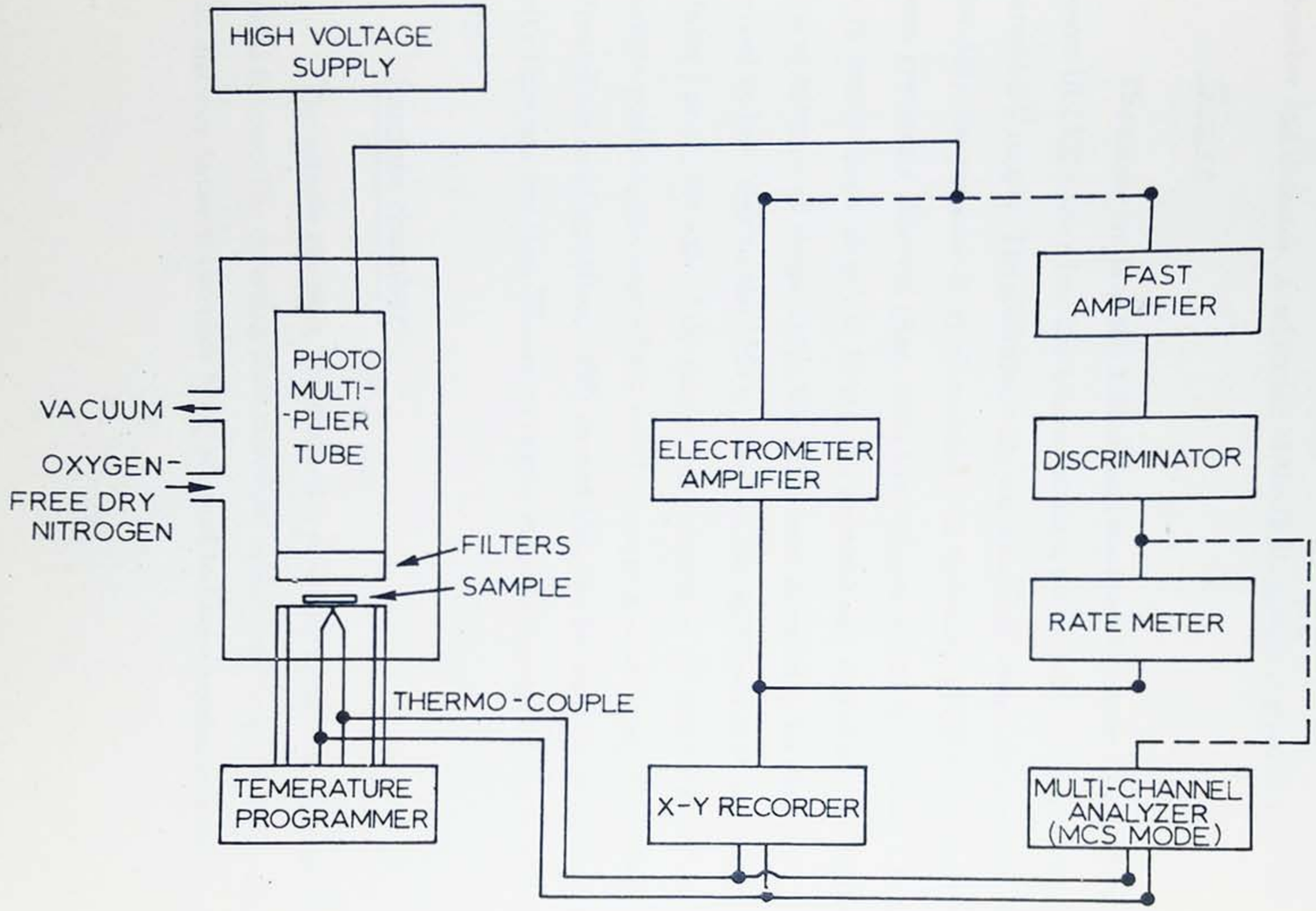


Fig. A.1. Schematic of TL measurement system.

consisted of a brass block (~ 30 kg in weight) with a stainless steel lining such that a copper drawer with samples could be inserted into it. The entire block was enclosed in an oven which was maintained at elevated temperatures (160°C/s).

A.2: IRSL measurements

The system comprised three parts, a source for stimulation, sample mounting chamber and detector. A schematic of the IRSL system is given in Fig. A.2.

Source

The source emits at 880 ± 80 nm and was made by connecting fourteen GaAs high power IR LED's in series. The source output is controlled by a programmable constant current DC supply. The source intensity was monitored using a photo-diode, BPX 65 (RS 304-346), the response of which matches with the source (TEMT 484) spectrum. It has been previously observed (Rao, 1996) that the source output exhibited a linear increase with current from 20 mA to 90 mA. To overcome any degradation of radiant intensity due to increase of temperature, the LEDs were mounted in an aluminum flange which served as heat sink to the LED's. Based on the specification of half angle of emission (fwhm) as 8°, the axis of the diodes were inclined to the normal at 60° so that at the sample position, the source light would converge and uniformly illuminate the sample. Photodiode readings (Rao, 1996) showed that the fluctuations in the source intensity with time was less than 5% and on rapidly switching on and off, the reproducibility was 99%.

Sample chamber

The sample chamber was made of a revolving metal disc enclosed between two metal flanges. The revolving plate contained equidistant sample slots for disc mounting, the distance between two slots being adjusted to have a maximum number of slots on a

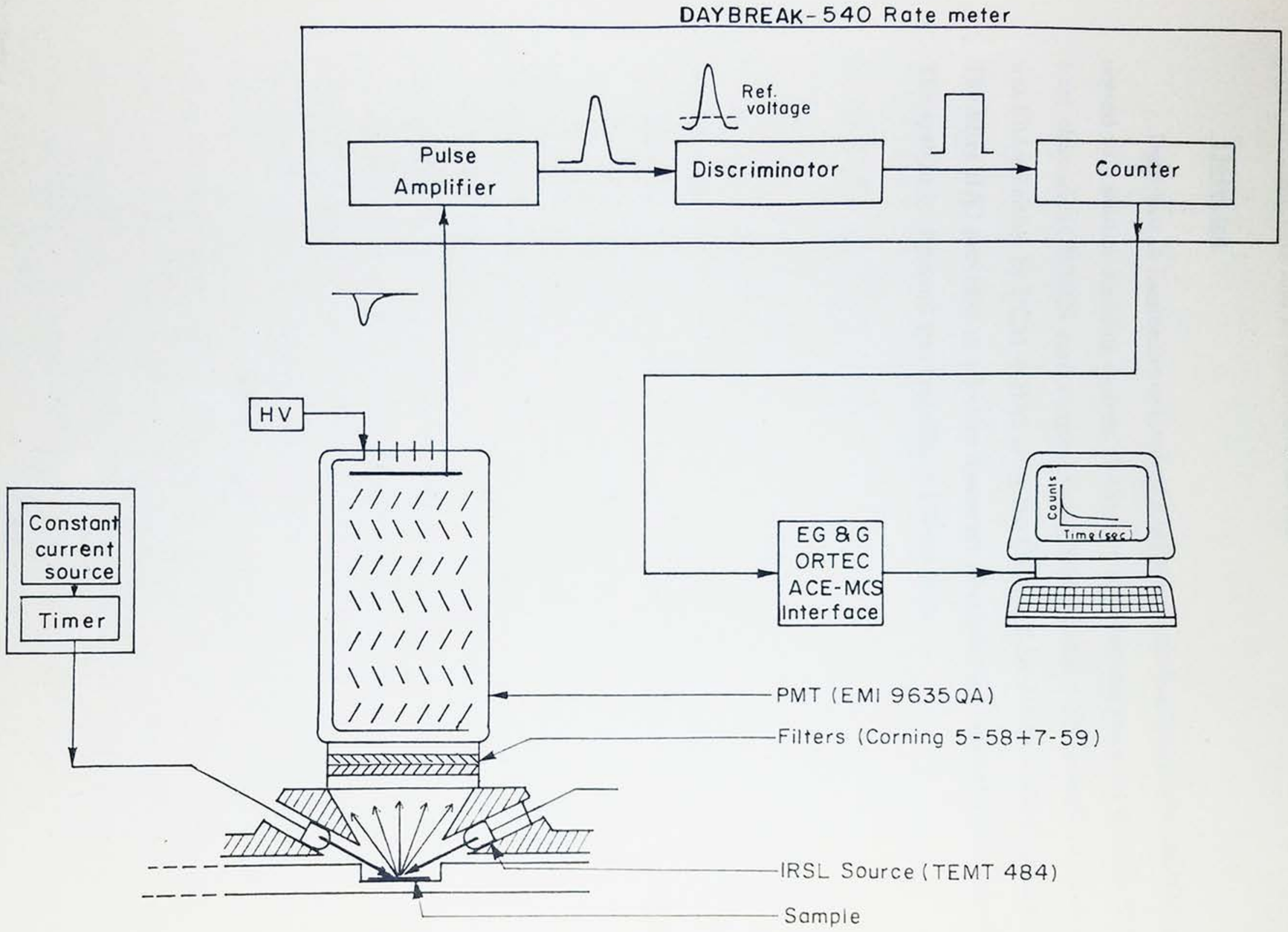


Fig. A.2: Schematic diagram of IRSL measurement system

given circumference and to minimise cross talk.

Detector

Detection of luminescence involved a bialkali photo-multiplier tube 9635QA connected to a photon counting system, the output of which was recorded through EG&G 4096 channel ACE-MCS card coupled to an IBM/PC-486. The sample luminescence was filtered either by UG11 + HA3 or by the Corning 5-58 + 7-59 + HA3 combination. The filter HA3 provided an effective means for discrimination against the source light. The system background was typically < 150 counts/s.

Appendix B: Thermoluminescence Emission Spectra of fault gouges and host rocks

Measurement of TL spectra is important because of various reasons : (i) to enable a better understanding of the bleaching process; (ii) choice of appropriate filters for selecting the portion of the spectrum which maximizes S/N ratio; (iii) to enable discrimination against unwanted minerals (e.g., separation of TL of calcite from that of limestone inclusions). Spectral measurements are also useful in determining special types of recombination centres, i.e., impurities/structural defects. In our studies, TL spectra were measured on 106-150 μm polyminerallic extracts from fault gouges and host rocks. The spectral measurements were performed at the Freiberg Luminescence dating laboratory with a CCD camera based spectrometer (Reiser et al., 1994). Figs. B.1, B.2 and B.3 present TL spectra for the fault gouge TLV-3 and host rocks KU93-5 and KU93-6 respectively. The TL spectra for the fault gouge TLV-3 consists of a single broad band at $\sim$ 600-700 nm. The TL spectra for host rocks is characterized by broad band emissions at 375-600 nm and at 675-750 nm. A comparatively less intense peak is also indicated for the host rocks at $\sim$ 275 nm (Fig. B.3). At present, the difference in spectral characteristics of the host rocks and fault gouges could not be directly attributed to heating.

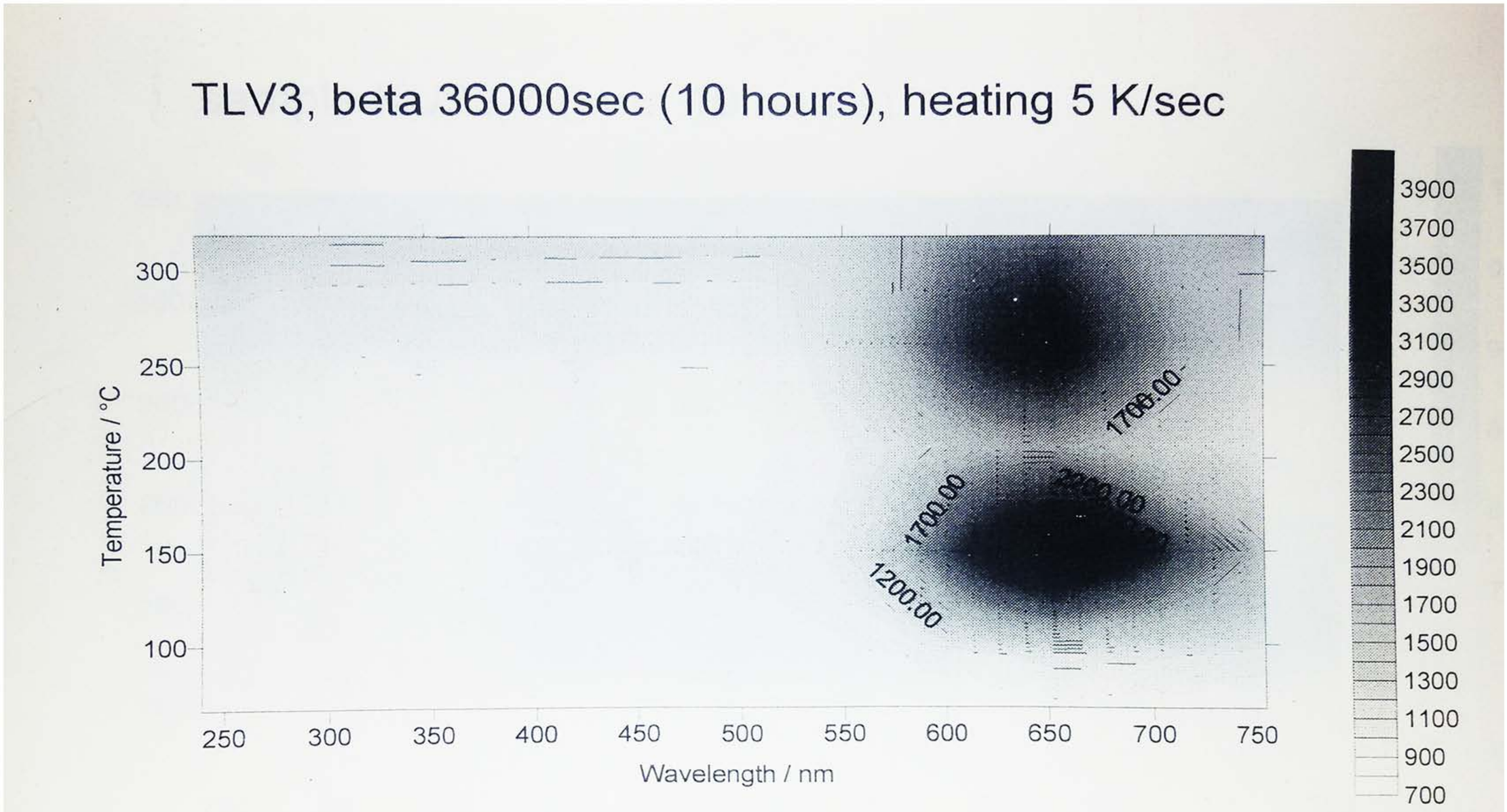


Fig. B.1. TL Emission spectra for fault gouge TLV-3, shown as a contour map.

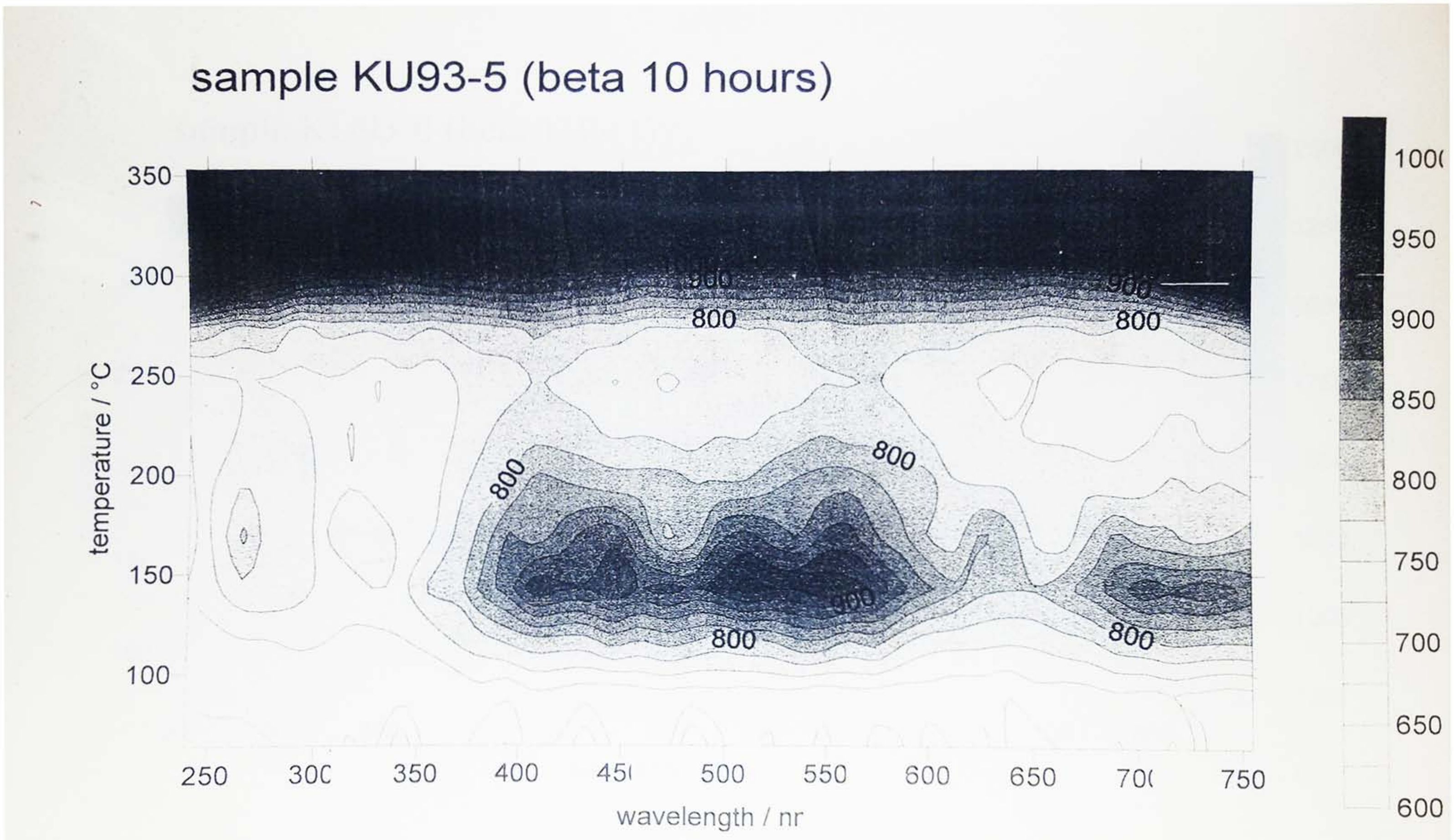


Fig. B.2. TL Emission spectra for host rock, KU93-5.

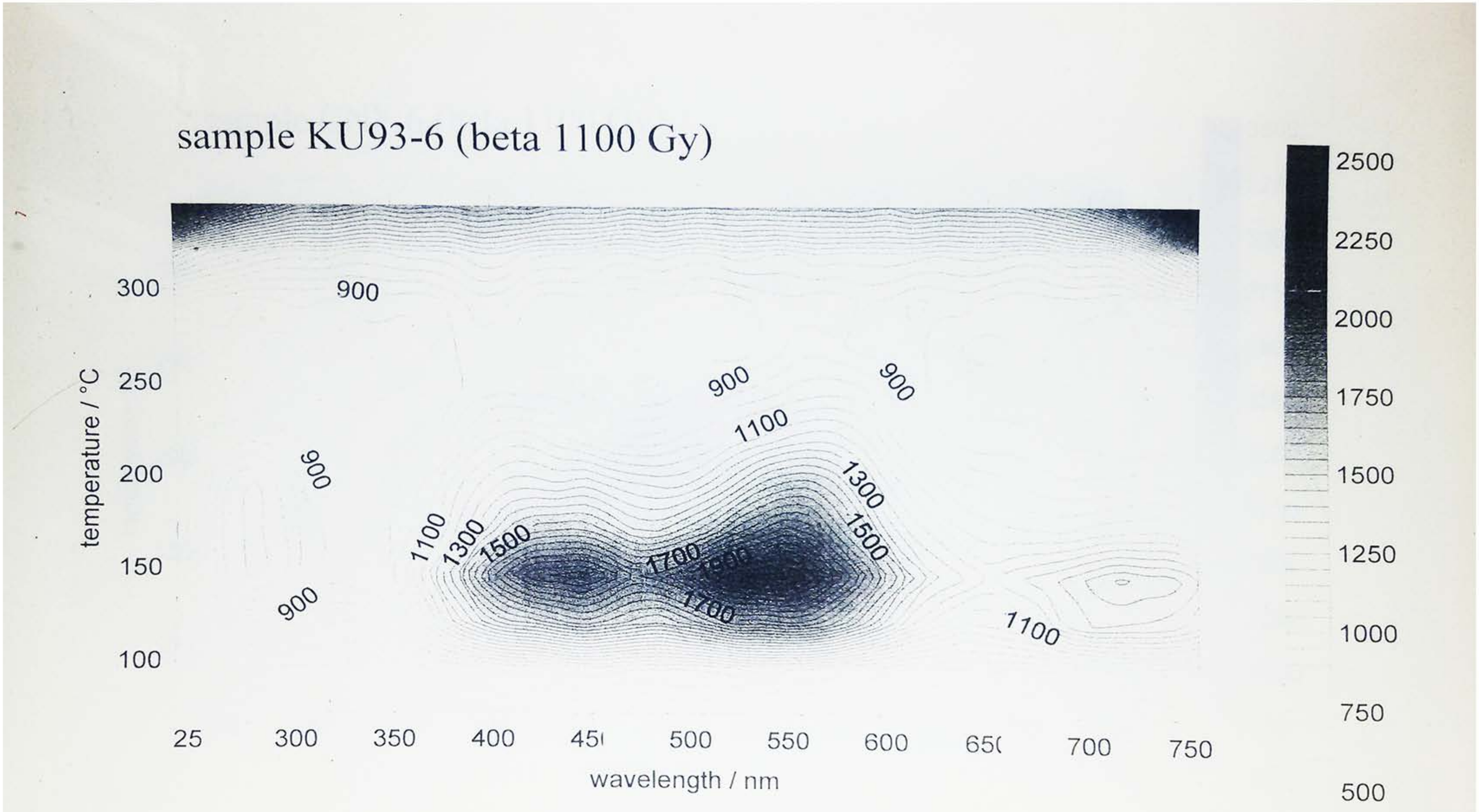


Fig. B.3. TL Emission spectra for host rock, KU93-6.

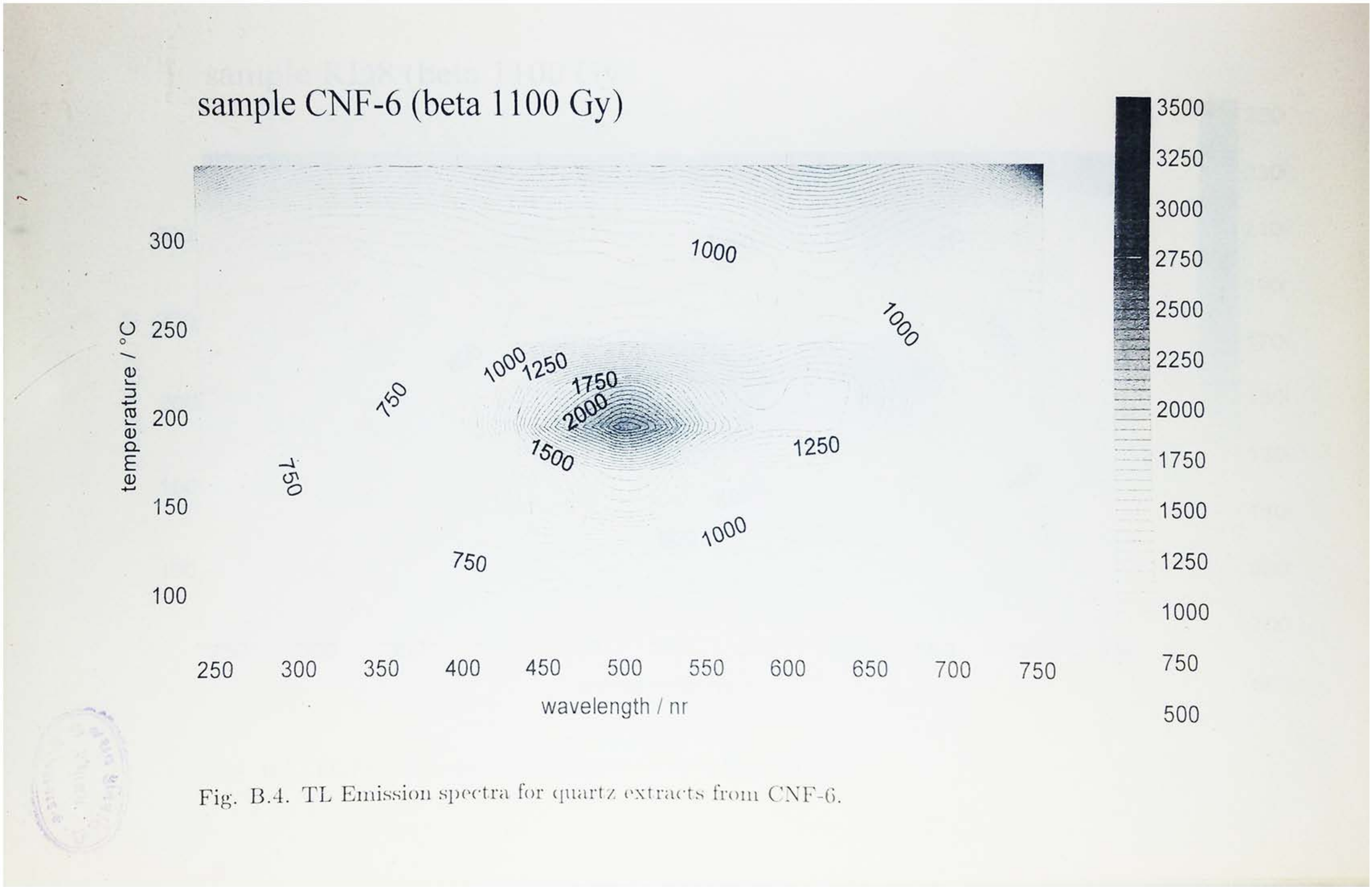


Fig. B.4. TL Emission spectra for quartz extracts from CNF-6.

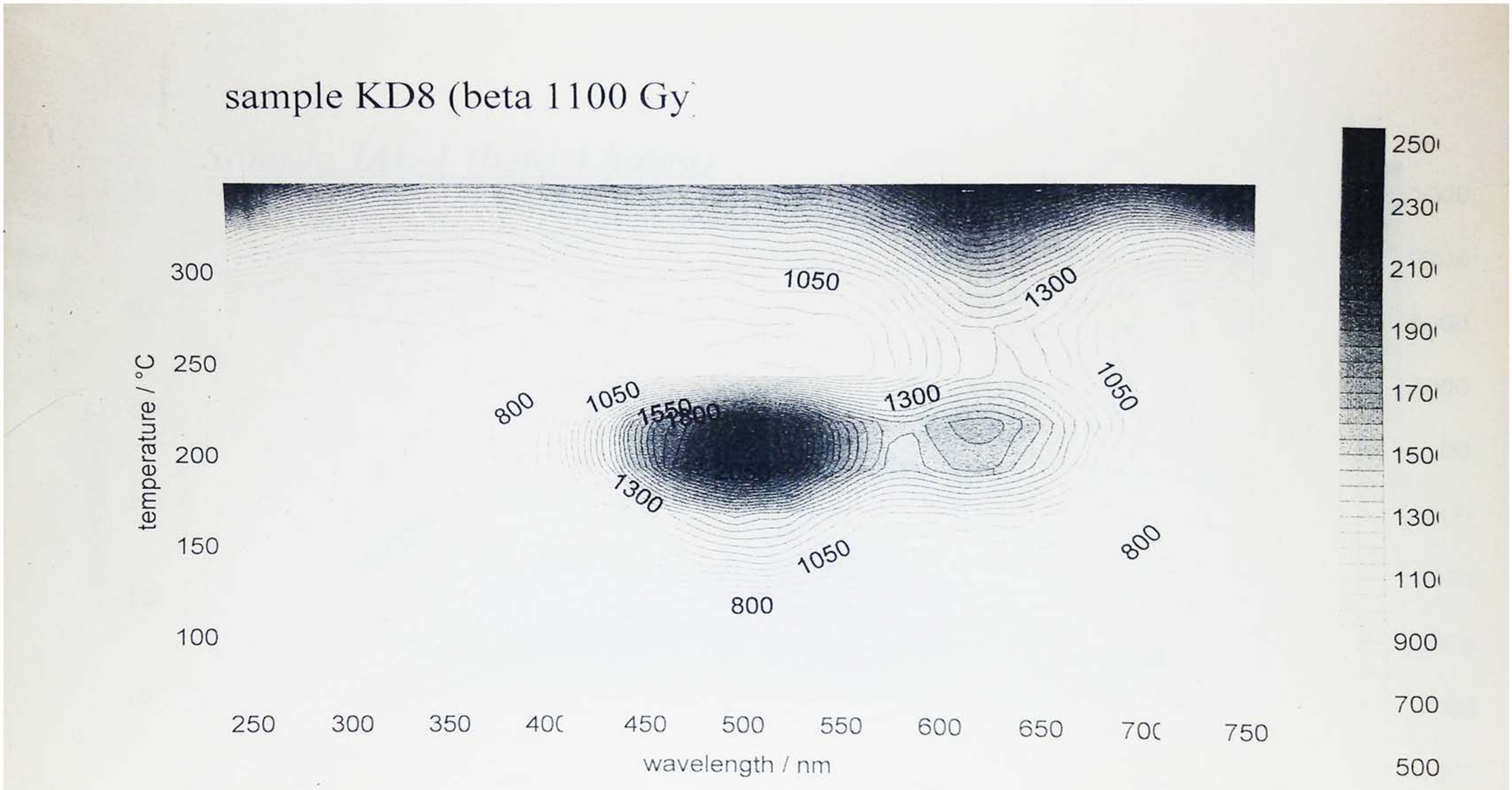


Fig. B.5. TL Emission spectra for quartz extracts from KD-8.

Sample JAL-1 (beta 4 hours)

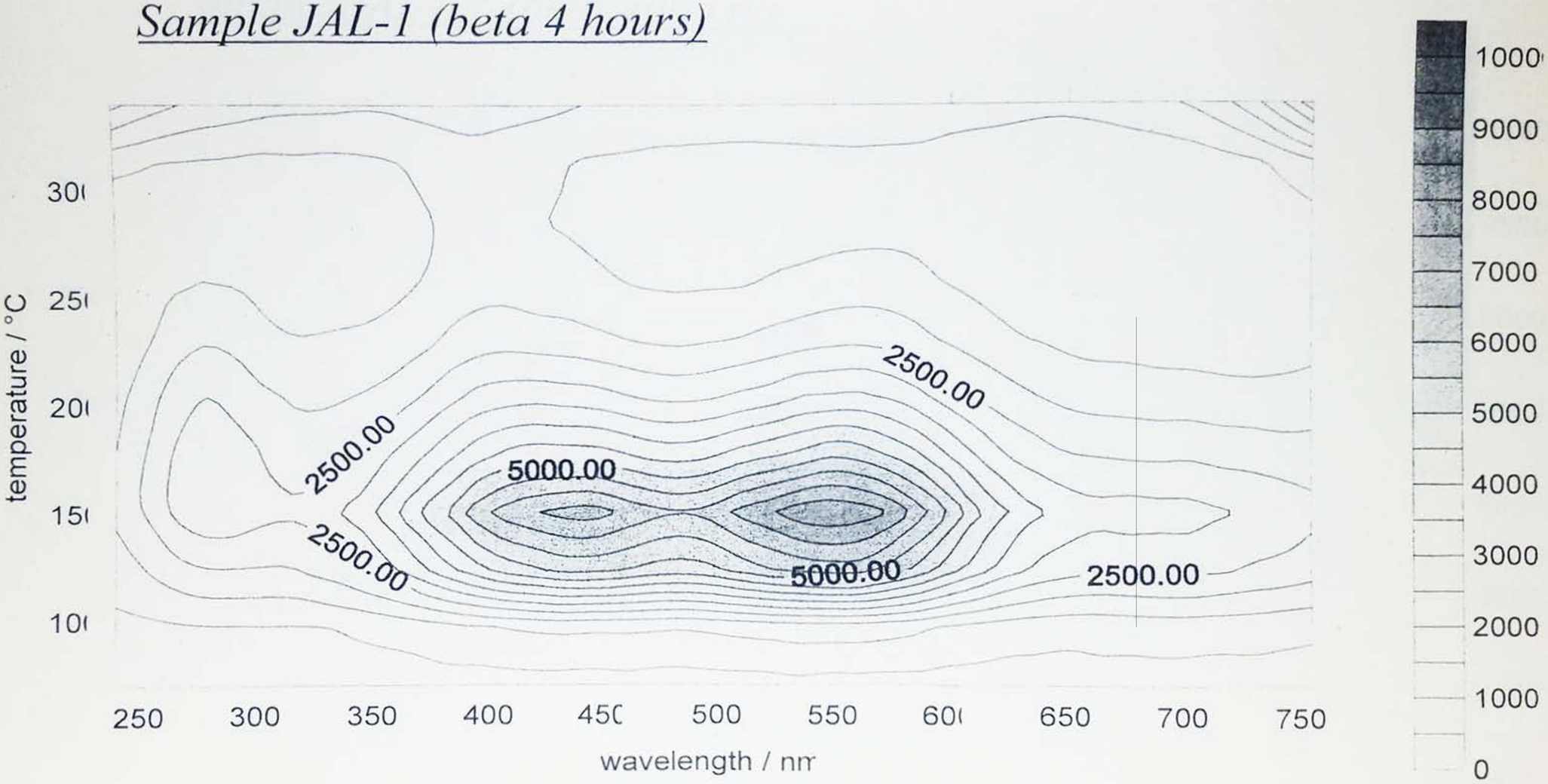


Fig. B.6. TL Emission spectra for alkali feldspar extracts from JAL-I/1.

sample JAL-17 (beta 400 Gy)

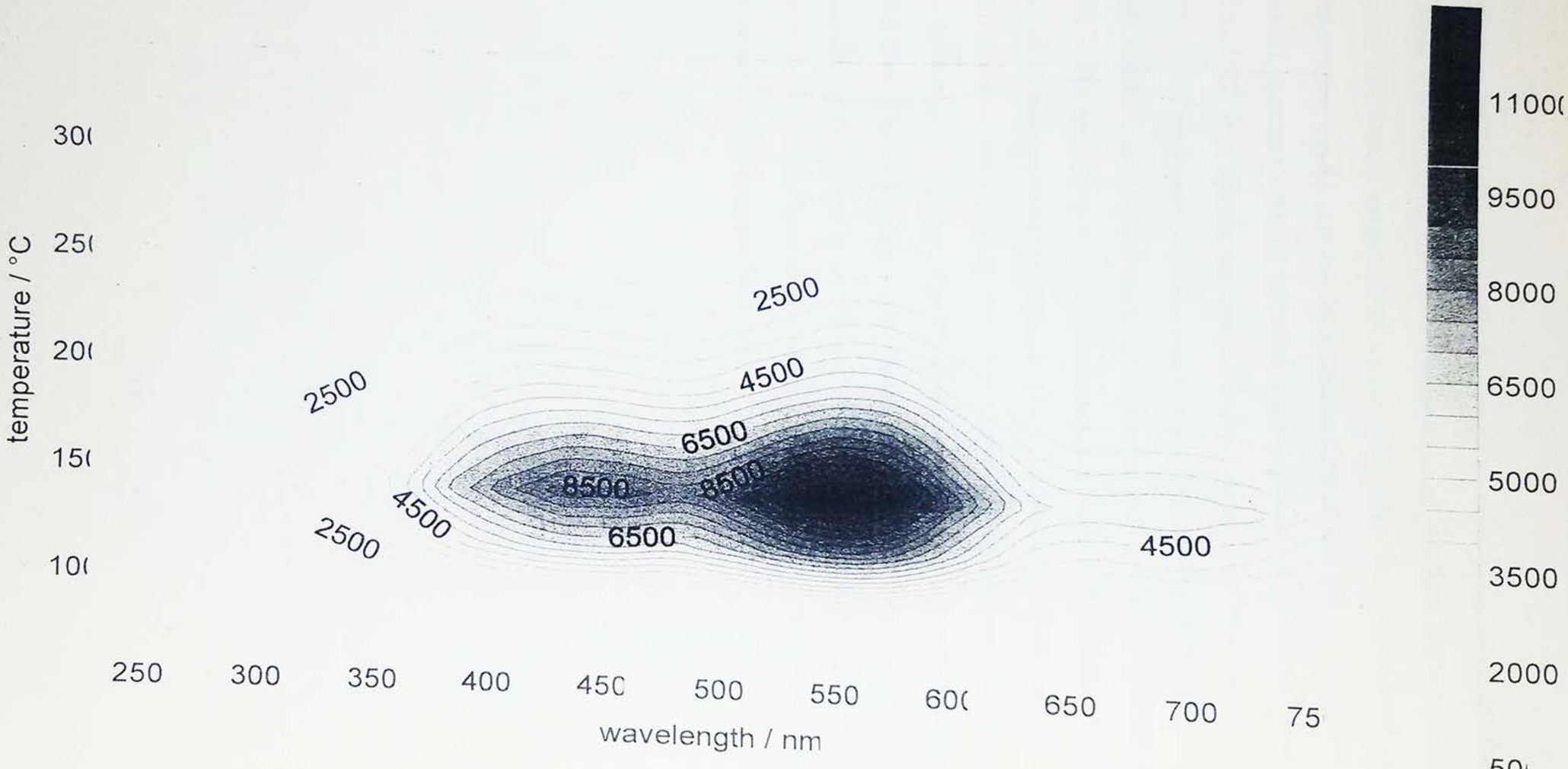


Fig. B.7. TL Emission spectra for alkali feldspar extracts from JAL-I/17.

Since it was possible that these variations could be explained in terms of mineralogical differences, the spectra for host rocks and fault gouge were then compared with spectra for quartz and feldspar extracts from aeolian sands. Figs. B.4 and B.5 show TL spectra for 106-150 μm quartz extracts from samples CNF-6 and KD-8. Figs. B.6 and B.7 present TL spectra for 75-106 μm alkali feldspar extracts from aeolian sands JAL-I/1 and JAL-I/17. The spectra for quartz extracts consists of a broad band emission at 425-525 nm. A less intense emission peak is also indicated at $\sim$ 625 nm (Fig. B.5). The feldspar emission spectra is characterized by broad emission bands centered at $\sim$ 450 nm and $\sim$ 550 nm. These results are consistent with earlier TL spectral data: Huntley et al., (1988) have reported the presence of broad emissions for quartz centred at $\sim$ 470 nm (blue) and $\sim$ 630 nm (red). They also observed feldspar emission bands at $\sim$ 390 nm, $\sim$ 450 nm and $\sim$ 570 nm. The 390 nm emission peak is not observed in the present spectral data. The TL spectra for fault gouges and host rocks suggest that most of their TL emission is dominated by quartz and feldspars. This result is consistent with the inference drawn on the basis of kinetic studies that the E values for fault gouges are characteristic of quartz and K-feldspar.

Appendix C: Estimation of temperatures generated in a fault zone due to frictional heating

During faulting, work done by frictional shear stresses acting on a fault is converted into heat. If η, σ and A represent the efficiency of conversion, shear stress and area of the fault plane along which displacement has taken place, then conservation of energy implies,

$$\eta\sigma \mathsf{Ad} = \mathsf{mc}\theta$$

where θ is the temperature increase, d is the displacement during faulting, c is the specific heat at constant pressure and m is the mass.

$$\text{Thus,} \quad \theta = \eta \, \frac{\sigma \mathsf{Ad}}{\mathsf{mc}}$$

Since $\mathrm{m} = \mathrm{A} \cdot \omega \cdot \rho$ where ω and ρ are the fault width and density, the above equation

can be rewritten as

$$\theta = \frac{\eta\sigma\, d}{\rho c\, \omega}$$

This is the expression for temperature rise during faulting along the fault plane. The derivation assumes that parameters on the right-hand side of the equation are constant with time. If $\eta = 1$, $\rho = 2.7$ g/cm^3, c = 1 J/g K and $\sigma = 100$ bars, the expression for temperature rise is

$$\theta \sim 4°C \cdot \frac{d}{\omega}$$

The ratio d/ω must be as high as possible for producing higher temperatures. So, for large earthquakes (magnitude ≥ 6) when displacement (d) is of the order of a few metres, this expression suggests that temperatures greater than 300°C can be generated in the fault zone.

For determining temperatures away from the fault plane and at different times after the faulting event, we consider the one-dimensional heat conduction equation and its solutions for uniform heating of the fault across its width. The following discussion is based upon the paper by Cardwell et al., (1978). The one-dimensional heat conduction equation is given by the expression

$$k\frac{\delta^2 T}{\delta^2 x} + Q(x,t) = c\rho\frac{\delta T}{\delta t}$$

where k is the thermal conductivity and Q is the heat generation per unit volume and

time. We now assume that $T = T_0$ and $Q = 0$ for $t < 0$ prior to faulting. The solution of the above equation is

$$T(x,t) = T_0 + \frac{1}{2\rho c\sqrt{\pi\kappa}} \int_0^t \int_{-\infty}^{\infty} \exp[\frac{-(x-x_0)^2}{4\kappa(t-t_0)}] \frac{Q(x_0,t_0)}{\sqrt{(t-t_0)}} dx_0 dt_0$$

where $\kappa = k/c\rho$ is the thermal diffusivity. Assuming that the heating is uniform along the width ω of the fault and is independent of time during faulting

$$Q(x_0,t_0) = \frac{\sigma d}{\omega\tau}[H(x_0+\omega/2) - H(x_0-\omega/2)], \quad 0 < t_0 < \tau$$

$$Q(x_0,t_0) = 0 \quad \text{for} \quad t_0 < 0, \quad t_0 > \tau$$

where τ and H represent time of faulting and the Heaviside step function. Using the last two equations and integrating over the space coordinate, we get

$$\text{For} \quad 0 < t < \tau, \quad T = T_0 + \frac{\sigma D}{2\rho c\omega\tau} \int_0^t (\text{erf}[\frac{x+\omega/2}{4\kappa\sqrt{t-t_0}}] - \text{erf}[\frac{x-\omega/2}{4\kappa\sqrt{t-t_0}}])dt_0$$

$$\text{For} \quad t > \tau, \quad T = T_0 + \frac{\sigma D}{2\rho c\omega\tau} \int_0^\tau (\text{erf}[\frac{x+\omega/2}{4\kappa\sqrt{t-t_0}}] - \text{erf}[\frac{x-\omega/2}{4\kappa\sqrt{t-t_0}}])dt_0$$

We now consider two cases: firstly, the situation where $\omega/\sqrt{\kappa\tau} \ll 1$. The maximum temperature (T_m) increase at $t = \tau$ and $x = 0$ is

$$T_m - T_0 = \frac{\sigma d}{\rho c \sqrt{\pi \kappa \tau}}$$

This is the expression for the maximum temperature for a fault of zero width. If $\omega/\sqrt{\kappa\tau} \gg 1$, the maximum temperature at $t = \tau$ and $x = 0$ is

$$T_m - T_0 = \frac{\sigma d}{\rho c \omega}$$

This is the thick fault approximation and is identical to the third equation in this appendix (assuming $\eta = 1$). Here, thermal conduction becomes unimportant and the frictional heat is uniformly distributed across the fault width. Assuming the time of faulting to be 1 second, if $\kappa = 10^{-2}$ cm^2/s, the conduction distance $\sqrt{2\kappa\tau} \sim 0.14$ cm. Thus, if we consider faults whose widths are greater than 1 cm, the thick fault approximation can be used for determing the maximum temperature on the fault.

Both the scenarios presented above are deficient in some respects. It is assumed that heating is uniform across the fault zone. This may not be always be satisfied. Other phenomena which have to be modelled satisfactorily are interaction of fault planes in a fault zone, dissipative losses (in real situations, $\eta < 1$) and the increase in temperature for fault zones containing water.

Guj. Unl. Library
T2168